Current and future state of groundwater in coastal unconsolidated sediment systems worldwide

De huidige en toekomstige toestand van het grondwater in niet-geconsolideerde kustsystemen wereldwijd

(met een samenvatting in het Nederlands)

Proefschrift

ter verkrijging van de graad van doctor aan de
Universiteit Utrecht
op gezag van de
rector magnificus, prof.dr. H.R.B.M. Kummeling,
ingevolge het besluit van het college voor promoties
in het openbaar te verdedigen op

vrijdag 3 september 2021 des middags te 4.15 uur

door

Daniel Zamrsky

geboren op 19 september 1986
te Praag, Tsjechië

Promotor:

Prof. dr. ir. M.F.P. Bierkens

Copromotor:

Dr. ir. G.H.P. Oude Essink

This work was financially supported by the Netherlands Organization for Scientific Research (NWO), under the Water Nexus programme (project no. 14298).

Current and future state of groundwater in coastal unconsolidated sediment systems worldwide

Daniel Zamrsky

Utrecht, 2021

Department of Physical Geography,

Faculty of Geosciences,

Utrecht University

Promotor:

Prof. dr. ir. M.F.P. Bierkens (Utrecht University, The Netherlands)

Copromotor:

Dr. ir. G.H.P. Oude Essink (Utrecht University, The Netherlands)

Examination committee:

prof. H.A. Michael (University of Delaware, USA)

prof. dr. N. Moosdorf (Kiel University, Germany)

dr. V. Post (Federal Institute of Geosciences and Natural Resources (BGR), Germany)

prof. dr. R.J. Schotting (Utrecht University, The Netherlands)

prof. dr. K. Walraevens (Ghent University, Belgium)

ISBN 978-90-6266-605-8

Published by Faculty of Geosciences, Universiteit Utrecht, The Netherlands, in: Utrecht Studies in Earth Sciences (USES), ISSN 2211-4335

Printed by: Ipskamp Printing || https://www.proefschriften.net

The cover page was designed by Dede Nugraha (Neosalamana) - nugraharts@gmail.com.

Contents

Summary

Coastal areas historically attracted human populations due to their relatively flat topography enabling agriculture, fishing resources and trading possibilities. However, settling down at the coast also brings threats in the form of short-term storm events such as coastal surges leading to flooding and long-term sea-level rise that slowly eats away space suitable for human life while also leading to groundwater salinization. The need for coastal populations to constantly adapt to these threats led to technological developments resulting in various adaptation strategies. Additionally, population growth led to increased water demand that in turn forced the coastal populations to look for alternative water sources of domestic, agricultural and industrial use. Large-scale groundwater pumping became accessible during the 20th century thanks to new technologies. However, what might have appeared as a good solution brought along new problems such as increased rates of groundwater salinization. This means that coastal populations are facing serious threats in the near future and are in need for new adaptation strategies and measures to compensate the potential fresh groundwater shortages while facing the natural threats of storm surges and sea-level rise. Therefore, the main goal of this study is to estimate the current state of fresh groundwater resources in coastal areas worldwide while also looking for new potential water sources and analyzing the effects of future sea-level rise.

To achieve this goal a large set of numerical groundwater models have been built in order to estimate groundwater salinity on a global scale. Developments in computational power (and its availability) and computer codes dedicated to simulating groundwater flow and coupled salinity provided the essential tools to carry out such large-scale and complex analysis. Nonetheless, an important gap in geological information on global scale was encountered at the beginning of this study and therefore its improvement formed the essential initial step of this study. First, the thickness of the groundwater bearing geological formations (unconsolidated sediments only) is estimated, as described in **Chapter 2**. While it is an important input parameter into the groundwater models, it is shown that varying thickness has a much lower influence on simulated groundwater salinity compared to geological composition. To this end, **Chapter 3** focuses on defining geological composition and its complex nature. Several proxy parameters are defined which, combined with an approach to create synthetic geological representations, translated into sets of regional coastal geological formations formed by permeable aquifers and low-permeable aquitards.

This new global coastal geological dataset is then applied to simulate groundwater salinity in coastal regions worldwide. Recent studies suggest that large offshore fresh (and brackish) groundwater reserves are located offshore near the current coastline. These could potentially serve as additional source of fresh water for coastal communities and their global distribution is studied in **Chapter 4**. It is assumed that these offshore fresh groundwater reserves were deposited during past low sea-level stands. To account for

these sea-level changes, the groundwater model simulations cover more than 120 000 years which corresponds approximately to one full glacial-interglacial cycle accompanied by fluctuations of sea-level by about 120m. Our findings suggest that large offshore fresh groundwater reserves are present in numerous coastal regions around the world and their exploitation could either serve as input into desalination plants or directly as water source for domestic, high-end agricultural and/or industrial use. While this potential new source of fresh groundwater is yet to be explored and confirmed as suitable and profitable for human usage, rising sea levels are looming over coastal populations in the current century directly threatening current fresh groundwater reserves. In **Chapter 5** the effects of different sea-level rise scenarios on coastal fresh groundwater are studied. Our findings show a large difference between the groundwater salinization severity projected for the different sea-level rise scenarios. Coastal populations would only suffer minor consequences in the most moderate sea-level rise scenario. In contrast, the most severe sea-level rise scenario would lead to a major groundwater salinization in several regions around the globe by the end of the 21st century. If this scenario would continue in the coming centuries as well, a large fraction of all coastal regions would be rendered uninhabitable by the end of the 23rd century. Keeping in mind that sea-level rise is only one of many threats to coastal populations, drastic changes in global environmental policies and behavior have to be made to avoid the worst-case scenarios.

Samenvatting

Kustgebieden trekken sinds mensenheugenis mensen aan. Dit is vanwege de relatief vlakke hoogteligging waardoor handel, visserij en landbouw op vruchtbare grond mogelijk waren. Het leven in een kustgebied brengt echter ook bedreigingen met zich mee. Denk aan korte-termijn gebeurtenissen zoals stormen die leiden tot overstromingen, maar ook aan lange-termijn ontwikkelingen zoals zeespiegelstijging. Langzaam legt deze beslag op de schaarse ruimte geschikt voor menselijk leven en leidt tot verzilting van het grondwater. De noodzaak voor mensen in kustgebieden is om zich voortdurend aan deze bedreigingen aan te passen en dat heeft gaandeweg geleid tot technologische ontwikkelingen en in verschillende adaptatiestrategieën. De bevolkingsgroei leidde bovendien tot een grotere vraag naar voldoende water van voldoende kwaliteit. Dit dwong kustbewoners op zoek te gaan naar alternatieve waterbronnen voor huishoudelijk, landbouwkundig en industrieel gebruik. In de 20e eeuw werd het dankzij nieuwe technologieën mogelijk om op grote schaal grondwater te onttrekken uit grondwatersystemen. Wat een goede oplossing voor watertekorten leek, bracht echter nieuwe problemen met zich mee zoals een toenemende verzilting van het grondwater. In de nabije toekomst wordt de bevolking in kuststreken geconfronteerd met meer natuurlijke bedreigingen, zoals een toename van stormvloeden en zeespiegelstijging. Er is behoefte ontstaan aan nieuwe aanpassingsstrategieën en maatregelen waarmee potentiële tekorten aan zoet grondwater worden gecompenseerd. De belangrijkste doelen van deze studie zijn daarvoor: a. het inschatten van de huidige toestand van zoet grondwater in kustgebieden wereldwijd, b. het zoeken naar nieuwe potentiële zoetwaterbronnen, en tenslotte c. het analyseren van de effecten van een toekomstige zeespiegelstijging op het grondwatersysteem in het kustgebied.

Om deze doelen te bereiken is een groot aantal numerieke grondwatermodellen gebouwd om het zoutgehalte van grondwater in het kustgebied op wereldschaal te schatten. Ontwikkelingen in beschikbare rekenkracht op de Nederlandse supercomputer Cartesius en in computer codes voor het simuleren van grondwaterstroming en gekoppeld zouttransport, leveren de essentiële hulpmiddelen om dergelijke grootschalige en complexe analyses uit te voeren. Desalniettemin werd aan het begin van dit onderzoek een belangrijke leemte in geologische informatie op wereldschaal aangetroffen. De verbetering van geologische informatie in het kustgebied vormde zodoende de essentiële eerste stap in deze studie. In **Hoofdstuk 2** is beschreven hoe de dikte van de geologische formaties (alleen niet-geconsolideerde sedimenten) is geschat. Hoewel de dikte van geologische formaties een belangrijke invoer parameter is in grondwatermodellen, wordt in dit onderzoek aangetoond dat de variërende dikte een veel kleinere invloed heeft op het gesimuleerd zoutgehalte in het grondwatersysteem dan de geologische samenstelling. **Hoofdstuk 3** richt zich op het definiëren van de geologische samenstelling en de complexe aard ervan. Er zijn verschillende indirecte parameters gedefinieerd die, gecombineerd met een specifieke methodiek om synthetische geologische realisaties te

creëren, vertaald worden in sets van regionale geologische verdelingen in het kustgebied. Deze verdelingen bestaan uit goed doorlatende watervoerende pakketten en slecht doorlatende weerstandslagen die elkaar afwisselen.

Deze nieuwe wereldwijde geologische kustdataset wordt vervolgens toegepast om het zoutgehalte van grondwater in kustgebieden over de hele wereld te simuleren. Recente studies suggereren dat vóór de huidige kustlijn ('offshore') grote zoete (en brakke) grondwaterreserves liggen. Deze zouden mogelijk kunnen dienen als een extra bron van zoet water voor de groeiende bevolking in het kustgebied. De wereldwijde verspreiding van deze zoete (en brakke) grondwaterreserves wordt bestudeerd in **Hoofdstuk 4**. Aangenomen wordt dat deze zoete grondwaterreserves op zee zijn afgezet tijdens lage niveaus van de zeespiegel in het verre verleden. Om rekening te houden met de veranderingen in het niveau van de zeespiegel, bestrijken de simulaties van de numerieke grondwatermodellen meer dan 120.000 jaar. Deze periode komt ongeveer overeen met een volledige glaciaal-interglaciale cyclus die gepaard gaat met fluctuaties van het niveau van de zeespiegel met ongeveer 120 meter. Onze bevindingen suggereren dat in tal van kustgebieden over de gehele wereld offshore grote zoete grondwaterreserves aanwezig zijn. Na exploitatie kunnen deze reserves dienen als grondstof voor ontziltingsinstallaties of direct als waterbron voor huishoudelijk, hoogwaardig landbouwkundig en/of industrieel gebruik. Deze potentiële nieuwe bron van zoet grondwater als geschikte en winstgevende bron voor menselijk watergebruik moet nog verder worden onderzocht. Parallel doemt de stijgende zeespiegel in de huidige eeuw op en dit vormt een directe bedreiging voor de huidige zoete grondwaterreserves in de kustzone. In **Hoofdstuk 5** worden de effecten van verschillende scenario's van zeespiegelstijging op het zoete grondwater in het kustgebied bestudeerd. Onze bevindingen laten een groot verschil zien tussen de geprojecteerde intensiteit van de verzilting van het grondwater voor verschillende scenario's van zeespiegelstijging. De bevolking in het kustgebied zal slechts geringe gevolgen ondervinden in het meest gematigde zeespiegelstijgingscenario. Daarentegen zal het meest ernstige scenario van zeespiegelstijging tegen het einde van de 21ste eeuw leiden tot een significante verzilting van het grondwater in verschillende regio's over de hele wereld. Als dit scenario zich ook in de volgende eeuwen voortzet, dan is tegen het einde van de 23ste eeuw de zoetwaterbeschikbaarheid van alle kustgebieden zeer ernstig afgenomen. Rekening houdend met het feit dat zeespiegelstijging slechts één van de vele bedreigingen is voor de bevolking in kustgebieden, moeten om de meest ongunstige scenario's te vermijden drastische veranderingen in het milieubeleid gecombineerd met menselijk gedrag op wereldschaal worden doorgevoerd.

1 Introduction

1.1 Background

1.1.1 Human history and interaction with coastal landscapes

Since the dawn of civilization in the Fertile Crescent (Lev-Yadun et al., 2000), Ancient China (Murowchick, 1994) and India (Feuerstein et al., 2005), human societies chose to settle in coastal areas. The Nile delta in Egypt, the eastern Mediterranean coast and the Euphrates-Tigris delta in Iraq all played (and still play) an essential part in human history. These low-lying, predominantly flat and very fertile landscapes enabled agricultural development by providing an easy access to fresh water sources. Building large-scale irrigation systems was possible due to porous nature of the surficial sediment (i.e., sand, clay, silt), steady supply of fresh water via rivers and a shallow groundwater table. Increased agricultural production facilitated formation of long-distance naval trade networks bringing along the agricultural technologies to new destinations. The bond between humanity and coastal areas was then sealed and was preserved throughout history until present day.

Unfortunately, settlement in coastal areas also brings its risks and dangers, coming from both inland and seaward directions. While river flooding can damage buildings, infrastructures and crop fields, it is less devastating than storm surges (including tsunamis and hurricanes, typhoons, cyclones) resulting in temporary inundation of low-lying coastal areas by seawater. Such events occurred regularly throughout recorded history (Chaumillon et al., 2017) and still do as several recent catastrophes are still fresh in our memories, e.g. the 2005 Hurricane Katrina in Southern USA or the 2004 Tsunami in the Indian Ocean . Human society has tried to adapt to hostile environments and mitigate the negative effects of natural disasters such as coastal storm surges. The first recorded attempts to protect the human settlements from seaborn threats are from 2nd century BC when ancient Romans and Egyptians built protective coastal walls and dikes (Charlier et al., 2005). While on military campaign in what is nowadays the Netherlands, the Caesarian army observed more than a thousand of clay mounds each spanning over few hectares and about 10m above sea-level (Charlier et al., 2005). While similar coastal protection endeavors were taking place around the world, the Dutch lands stayed ahead of the pack and pushed the human boundaries in the fight against natural forces further and further.

The Dutch battle against the sea might seem to be won at this moment with their most densely populated areas positioned relatively safely below current sea-level in the polder areas. This was achieved through organized work and well-planned water management strategies making the Dutch regional waterboard organizations formed in the 13th century one of the oldest local public government bodies in the world. However, a stark reminder of the force of nature took place during the North Sea flood in 1953 which claimed 1836 human casualties in the Netherlands. Unfortunately, this is only one among many tragic coastal flooding events which claim on average more than 8000 human casualties and directly affect 1,5 million people worldwide every year (Bouwer and Jonkman, 2018). As a

reaction to the flood in 1953, the Dutch built huge river locks in most of the estuaries in effort to prevent such catastrophe in the future. The Netherlands, renowned for their creativity and cost-saving desires, is one of many countries (along e.g., Germany, Denmark, Bangladesh, Egypt or Vietnam) that are racing to develop new coastal water management technologies and strategies to fight back at current and future seaborn threats.

However, regardless of the sophistication and level of protection against the rising seas, water management bodies around the world have to deal with countless other problems that occur in heavily populated coastal zones as shown in Figure 1-1. There are many stakeholders with high demands for fresh water (with sufficient quality for domestic, industrial and agricultural water use) whose needs are frequently satisfied by groundwater pumping (Jasechko et al., 2020). These needs were exacerbated during the past decades due to population growth going hand in hand with industrialization and more intensified agricultural production. The increased groundwater pumping as a result of these increasing demands has led to progressive depletion and salinization of groundwater resources in coastal areas (Post et al., 2018c). In recent years additional pressure on local fresh groundwater resources is generated by tourism, further increasing local water demand, and by surface sealing by urbanization limiting recharge of fresh groundwater resources. Providing sufficient fresh water to satisfy a growing demand and keeping groundwater resources fresh is a continuous struggle in coastal areas, and is expected to become even more challenging in the near future due to climate change and sea-level rise (Ferguson and Gleeson, 2012; Giosan et al., 2014; Ingebritsen and Galloway, 2014; Michael et al., 2013; Neumann et al., 2015; Post et al., 2018a; Rahman et al., 2019; Taylor, 2012; UNESCO, 2015).

Changing climate and sea-level fluctuations during the past millions of years formed the current hydrogeological settings in the coastal areas. The focus of this study is solely on unconsolidated sedimentary systems formed by periods of surficial sediment deposition and erosion over time. As a result, the unconsolidated sedimentary systems are a rather complex combination of groundwater bearing permeable layers (called aquifers, of mainly sandy composition) and low-permeable layers (called aquitards, of mainly clayey composition), see Figure 1-1. The groundwater flow pattern is directly related to these geological conditions as different groundwater sources come into play with the geological settings. Surficial aquifers get recharged by precipitation that infiltrates into the soil and a fraction of it reaches the groundwater table and gets drained. Deeper aquifer systems can be either non-renewable, in which case groundwater pumping leads to its depletion, or receive groundwater recharge slowly coming from upland areas located relatively far away from the coastline.

Such variable and complex geological settings can also accommodate equally complex groundwater flow and salinity patterns, see Figure 1-1. Saltwater intrusion takes place as a result of advection and dispersion processes resulting in a mixing zone between saline, brackish and fresh groundwater. This natural process can be disrupted by inland fresh groundwater pumping or surface sealing in urban areas resulting in lower groundwater recharge reaching the coastline as well as saltwater upconing (or even well salinization in extreme cases (Custodio, 2002)). In the offshore area, large fresh (and brackish)

groundwater volumes can be found (Micallef et al., 2021; Post et al., 2013) as a result of past low sea-levels and ensuing surficial groundwater recharge seeping into the aquifer systems that are currently covered by sea.

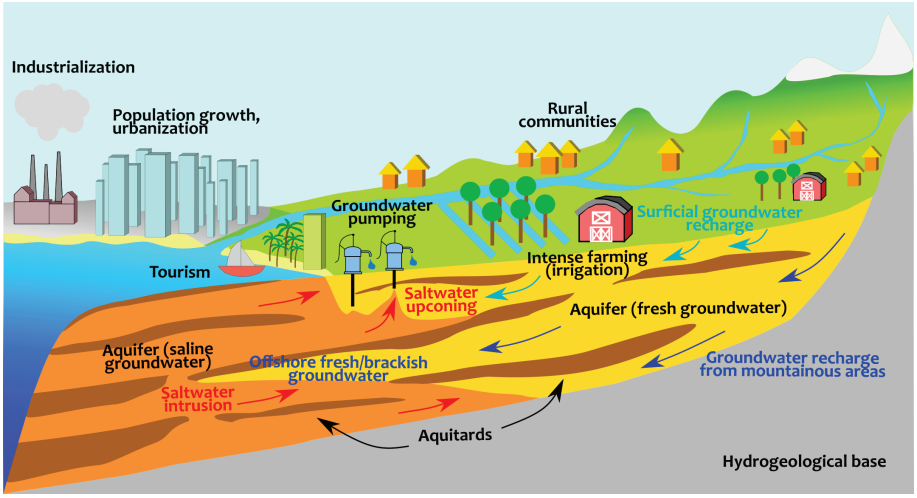

Figure 1-1 Hydrogeological settings in coastal areas (unconsolidated sedimentary systems) bearing both fresh and saline groundwater. The fresh groundwater demand is on the rise due to increased groundwater pumping to satisfy the rising demands stemming from population growth, urbanization, industrialization and intense irrigation farming.

The large-scale groundwater pumping alongside rising sea-levels and an associated increase in coastal flooding frequency forces one to find mitigation and adaptation strategies that ensure human wellbeing in coastal areas in the future. For instance, managed aquifer recharge techniques were studied and implemented in past decades to constrain seawater intrusion effects either by artificially injecting fresh water into the aquifers or by building infiltration structures such as ponds and basins (Dillon et al., 2019; Sprenger et al., 2017). More recently, engineers have explored the potential of depositing large sand quantities in the shallow sea to enhance and accelerate the natural buildup of dunes, acting as natural coastal protection and also increasing fresh groundwater volumes in coastal aquifers (Huizer et al., 2019, 2016). Because these novel techniques are still researched and cannot be applied right away in most cases, adjustments in water management strategies are currently the most effective, efficient and widely applicable ways how to decrease water stress levels (demand vs. supply) in coastal areas. Water management agencies need accurate information and scientific methods to develop their strategies and implement future mitigation and adaptation measures. An introduction to saltwater intrusion and its effects on coastal groundwater is briefly given in the following text.

1.1.2 Introduction to coastal groundwater

First recorded mention of fresh groundwater occurring at the coastline dates back to the times of Caesar's Alexandrine war around 40 BC (Post et al., 2018b). Fresh groundwater remained an important source of drinking water in coastal areas and islands throughout history but its origin was still disputed until early 19th century (Du Commun, 1828). It was believed for a long time that coastal fresh groundwater possibly originates from underground seawater evaporating through the porous media and then condensing on the surface. According to another theory, the driving force in purifying the saltwater was the soil which acted as a natural filtration mechanism. In early 19th century the theory of hydrostatic equilibrium between fresh and salt water in coastal areas was first presented. By late 19th century this theory was expressed as an equation by a German engineer Alexander Herzberg who at that time studied the freshwater lenses in German North Sea islands (Herzberg, 1901). Just a few years earlier, while studying for the city of Amsterdam fresh water sources in a neighboring coastal dune area, Willem Badon Ghijben concluded that groundwater flowing out of the freshwater lenses below the coastal dunes flows both into the sea and towards the low-lying polder areas (Drabbe and Badon Ghijben, 1888). The ensuing Badon Ghijben-Herzberg principle defines the interface position between the saline and fresh groundwater, with saline groundwater having higher density than fresh groundwater. The Badon Ghijben-Herzberg principle is applicable in homogeneous aquifers, e.g., located either in relatively thin dune areas (or coral islands). Even though such conditions are quite rare, the Badon Ghijben-Herzberg principle can provide a good first order approximation of fresh-saline groundwater interface in homogenous aquifers with no vertical flow component (Strack, 1976).

Throughout the second half of the 20th century more analytical approaches were developed (Bear and Dagan, 1964; Dagan and Bear, 1968) alongside numerous case studies and observations of saltwater intrusion in coastal areas worldwide. Initially, most of these studies were performed in countries such as the Spain, Italy, Netherlands, Israel, Germany and USA. Scientists from Germany, the Netherlands and Denmark shared their observations and research in the first Saltwater Intrusion Meeting (SWIM) in Germany in 1968. The interest in saltwater intrusion research slowly spread around the world and eventually became a global research field in late 20th century reaching all continents, see Figure 1-2. This can be attributed to deteriorating groundwater conditions in highly populated and productive coastal areas around the world (Larsen et al., 2017; Mabrouk et al., 2019; Pham et al., 2019).

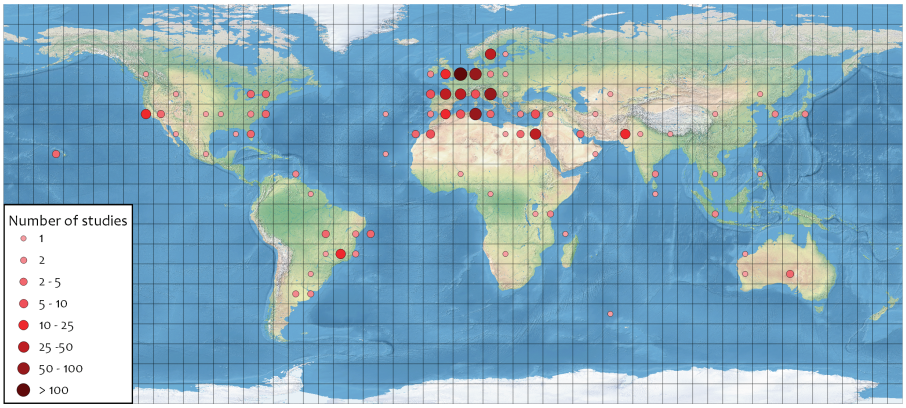

Figure 1-2 Number of studies presented at SWIM meetings (1968-2014) clustered together by location for each UTM zone. Dots located inland are either theoretical studies or national scale studies and are therefore placed inland.

1.1.3 Computer modelling of coastal groundwater

Development and application of analytical formulas and analogue models was the primary research focus before modern powerful computers became easily accessible and made numerical solutions available to the groundwater community. The main strength of analytical models is the calculation speed and reproducibility. However, they can often only be applied to idealized conditions. The most famous example is the so-called Henry case (Cooper, 1964) that calculates the fresh-saline groundwater interface and a mixing zone in an idealized hypothetical porous aquifer. Analytical models are still used nowadays to better understand the processes underlaying saltwater intrusion (Bakker et al., 2013; Knight et al., 2019; Werner et al., 2012; Werner and Simmons, 2009). Despite these advantages, analytical approaches are seldom fit for real-life cases in heterogeneous conditions.

Heterogeneous conditions require more complex models that do not only take into account variable densities (fresh, brackish and saline groundwater in this case) but also solute transport by advection and hydrodynamic dispersion (which includes molecular diffusion); applications using such models started in late 20th century (Sanford and Konikow, 1985; Voss, 1984; Voss and Souza, 1987) and this trend continues until nowadays. These models allow to simulate saltwater intrusion in non-uniform density coastal aquifer environments, upconing near pumping wells and changes in freshwater lenses in island and dune areas (Ghassemi et al., 1990). By using numerical approximations, such models can also simulate solute transport in systems with heterogeneous geological conditions and over large time scales. One of the most popular ways to simulate variable-density groundwater flow and salt transport in heterogeneous conditions is the use of numerical models: dividing the domain (2D or 3D) into a finite number of grid points or volumes (blocks or cells) of either uniform or non-uniform size and assuming the hydrogeological properties within the cells or between the grids to be uniform. The popularity of this

approach led to multiple numerical codes being developed over the past few decades. Amongst the most known and used are for example the SEAWAT code (Langevin and Guo, 2006), FEFLOW (Diersch, 2013) or SUTRA (Voss, 1984). In our study we opted for the SEAWAT code developed by United States Geological Survey (USGS) due to its modularity and implementation possibilities via Python scripting language (Bakker et al., 2016). Combining the SEAWAT code and Python allows for building a large set of independent SEAWAT models representing different hydrogeological systems around the world, as applied in this PhD research.

Several key decisions and parameter inputs are essential in successfully setting up a numerical groundwater model. Two dimensional (2D) models can be used to simulate cross-sectional groundwater flow and solute transport. However, this approach can only be applied if the system that is simulated has no lateral (along the coast) groundwater flow. Such conditions can be assumed when the cross-section is set up perpendicular to the coastline, groundwater extraction rates are limited and the coastline is more or less straight. This simplification largely decreases the computation time of 2D models when compared to three dimensional (3D) models. The latter option is, however, a better suited approach for large-scale models in areas with highly complex and heterogeneous conditions such as deltaic areas as recent 3D model studies show (e.g., Engelen et al. 2019; Oude Essink 2001; Mabrouk et al. 2019). Even though 3D models can provide valuable insight into saltwater intrusion, their setup requires vast amount of input data and substantial computational resources.

Geological information and hydrogeological input data are amongst the most important building blocks of a groundwater model. As mentioned above, coastal areas are often highly geologically heterogeneous and in order to successfully reproduce such conditions in a groundwater model several key inputs are necessary. The spatial variation of aquifers and aquitards and their thicknesses must be assessed, usually by collecting geological borehole data or interpreted geological cross-sections. Countries such as Denmark and the Netherlands have an immense collection of borehole data and are able to build a reliable country scale hydrogeological model (De Lange et al., 2014; Henriksen et al., 2003). In cases where borehole data are either not available or only in limited numbers, simplifying assumptions about the geological heterogeneity need to be made in order to build a groundwater model (e.g., Engelen et al., 2019; Faneca Sànchez et al., 2015). These simplifying assumptions will lead to local discrepancies when validated with local groundwater head and salinity measurements but still provide valuable tools for water management scenarios and overall qualitative understanding of groundwater flow and salinity pattern in the local (or regional) hydrogeological setting. Another key geological parameter is the hydraulic conductivity that is defined as the ability of the fluid to pass through a porous medium (e.g., sand, clay) and fractured rocks. In cases where there are no hydraulic conductivity measurements in-situ, estimated values based on literature and calibration provide ways to overcome the missing local information. Other parameters such as effective porosity and hydrodynamic dispersion parameters are as well often estimated from literature sources in case of lacking information (Dagan et al., 2013; Gelhar et al., 1992; Zech et al., 2019, 2015). It is important to bear in mind that building a detailed

3D hydrogeological model is still an approximation of reality even if extensive hydrogeological datasets are available. Naturally, with decreasing level of local data and information available the uncertainty in groundwater model results rises (Konikow, 2011; Konikow and Bredehoeft, 1992).

Boundary conditions are another key component of every groundwater model and are implemented to control the inflow into and outflow from the groundwater model domain of groundwater and salt. This can be controlled by defining constant groundwater level at the boundary (as groundwater pressure head or fixed concentration) which can be determined based on direct measurement or estimated. Another way is to define constant inflow (or outflow) through the boundary. This parameter should be estimated and calibrated (a no-flow boundary is a special case of this feature). These two boundary condition types are most often used to simulate inflow from inland ("Groundwater recharge from mountainous areas" in Figure 1-1) or in cases where the model domain is at the coastline and constant saltwater groundwater head is assigned. The SEAWAT (and underlying MODFLOW) code provides a third way to define inflow and outflow in the groundwater model domain. The so-called general head boundary calculates the flow through the boundary based on difference in groundwater head pressure between the boundary model cell and its neighboring cells taking into account a user defined resistance in the boundary model cell (McDonald and Harbaugh, 1988). Additionally, salt concentration has to be defined in model boundary cells in groundwater models that take into account variable-density groundwater flow and salt transport.

Surficial groundwater recharge (Figure 1-1) is a result of precipitation, more accurately a fraction of it, reaching the groundwater table through the overlaying unsaturated zone. There are several methods to estimate this groundwater recharge rate, mostly involving soil properties, land use types, evapotranspiration and precipitation (Mohan et al., 2018). In groundwater models the groundwater recharge is usually applied to the upper part of the model domain at either constant rate or varying in time. Surface water bodies such as rivers, canals or lakes interact with the groundwater system by either draining it or recharging it depending on the groundwater head and its position compared to the surface water level. These processes are difficult to add in 2D groundwater models due to their complex nature and lateral as well as vertical flow components. The same applies for groundwater extraction (pumping), which basically requires a 3D groundwater model to be simulated properly.

Gathering all the different input data and information is often lengthy, time demanding and requires a thorough and well-planned organization if carried out on larger scales (e.g., nationwide). On an even larger (global) scale, such issues are even more noticeable. An overview of recent global studies and how they navigate around or contribute to solve this issue is elaborated on in the following chapter.

1.2 Overview of recent global studies in coastal areas

Global models and analyses can help us to better understand the behavior of natural systems and find potential implications of local or regional changes on global scale. Just as a butterfly flapping its wings on one side of the globe can cause a storm on the other side (Lorenz, 2000), changes in local weather pattern, land use or a new river dam being built can affect areas far away. Another important outcome provided by global studies is the possibility to compare how different regions worldwide are affected in a certain scenario. Finding similar characteristics for the most (or least) affected regions can shed new light on how these regions can adapt or serve as an example for adaptation and mitigation in other areas around the world.

In recent years and decades, a growing threat of climate change initiated rapid advancement in global climate models in efforts to better understand potential future impacts. The Intergovernmental Panel on Climate Change (IPCC), established in 1988, periodically provides an overview of most recent scientific advances and climate model outcomes to inform both the scientific community and wider public (e.g., Masson-Delmotte et al. 2018). The overviews cover a wide range of climate change effects, such as current and projected CO_2 emissions, their effects on global warming, land use change impacts or melting of glaciers. In 2019 a special report (H.-O. Pörtner et al., 2019) covered the sea-level rise projections in coming centuries taking into account various CO_2 emission scenarios. The alarming rates at which sea level could rise in the near future under the highest CO_2 emission scenarios is a huge threat to coastal areas worldwide, as well as to their fresh groundwater resources.

Global hydrological models (GHMs) are built to study the potential effects of climate change, among other stress factors, on fresh water availability in the future (e.g., Bierkens et al. 2015; de Graaf et al. 2015; Döll 2009). Development of GHMs has been gaining momentum in recent decades due to developing and more accessible computation power and better global datasets available covering a wider range of necessary parameter inputs. Covering the whole globe means also a lower grid resolution of the model itself, usually in the order of 10*10km grid cell size at the equator. The coarse grid resolution and necessary input parameter simplifications can lead to large uncertainties and mismatch with local measurements. However, GHMs and their predictions provide a valuable source of information about the global hydrological cycle and future fresh water availability. The PCR-GLOBWB model (Sutanudjaja et al., 2018) also implements a groundwater flow model component (De Graaf et al., 2017). Since it does not include variable-density groundwater flow and coupled salt transport modelling it is unable to simulate saltwater intrusion in coastal areas. Moreover, due to lack of global geological data, the two-layer groundwater model setup of PCR-GLOBWB is only suitable for groundwater head simulation and not for plausible/accurate salt transport.

Several recent global studies focusing on geology provide valuable information that helps to build large-scale groundwater models without extensive local information. Estimated hydraulic conductivity (Gleeson et al., 2014; Huscroft et al., 2018) can be used as direct input into GHMs combined with global lithological (Hartmann and Moosdorf, 2012) and

soil type (Hengl et al., 2014; Montzka et al., 2017) information. Another important geological parameter input for groundwater models is the thickness of the aquifer and aquitard layers forming the hydrogeological system. There have been several studies in recent years focused on estimating this thickness, but none specifically aimed at unconsolidated sediment systems. The PCR-GLOBWB groundwater model component does not differentiate between unconsolidated and consolidated geological formations and provides an estimated combined thickness of all groundwater bearing formations (De Graaf et al., 2015). Multiple studies estimated the thickness of the upper most (soil) layer but do not provide a bottom limit estimation of the unconsolidated sediment systems (Montzka et al., 2017; Pelletier et al., 2016). More accurate thickness and heterogeneity (aquifer and aquitard) estimates are necessary in order to build more detailed groundwater models in coastal areas.

Due to this lack of available information and input datasets, the only global studies dealing with coastal groundwater used simplified numerical (or analytical) groundwater models or literature review to map salinity in coastal groundwater reserves. An overview of areas affected by salinity issues worldwide was presented in 2009 (Van Weert et al., 2009) showing salinization as a worldwide issue and serious future threat. Not only groundwater is vulnerable to saltwater intrusion. More than 10 million km^2 of soil is currently under threat of salinization worldwide (Wicke et al., 2011), posing a serious risk for agricultural production. On a more positive note, large fresh (and brackish) offshore groundwater volumes are predicted to be located along the global coastline (Post et al., 2013), potentially providing an unexpected new source of fresh water. The only global numerical groundwater modelling study taking into account variable-density groundwater flow and coupled salt transport (Michael et al., 2013) identified low-elevated (or topography limited) areas as the most vulnerable to saltwater intrusion caused by sea-level rise. The low elevation does not allow the inland fresh groundwater table to move up and match the sea-level rise leading to increased salinization due to both overtopping by seawater and increased seawater head pressure. Michael et al., 2013 conclude that the hydrogeological conditions are the most important determining factor in assessing the saltwater intrusion severity in coastal areas. A similar conclusion was reached by a recent literature review focused on sea-level rise impacts on seawater intrusion in coastal aquifers (Ketabchi et al., 2016), stressing the necessity to include higher level of geological detail in future coastal groundwater models. Obtaining better estimates of aquifer (and aquitard) thickness and their hydraulic conductivity values is a necessary step before more complex coastal groundwater models can be built.

1.3 Research questions and thesis outline

The main ***objective of this PhD study is to assess the current and future state of groundwater resources in coastal areas hosting unconsolidated sediment systems around the world***. New global geological datasets and information are crucial for global model development, and as such need to be focused on before attempting to build a global

groundwater model for coastal areas. Answering the research questions listed below form the steps towards reaching the goal of this thesis:

How to estimate regional coastal unconsolidated sediment aquifer thickness based on available global topographical and geological datasets?

In Chapter 2, a method to estimate coastal aquifer thickness is presented. The underlying assumption is that unconsolidated sediments that form coastal aquifers and aquitards are located on top of hard rock formations. First, a global lithological dataset is used to identify coastal areas where unconsolidated sediment formations are present. Next, the coastal aquifer thickness is estimated by approximating the topographical slope of older rock formations inland and extending it until the coastline. Additionally, the effect of varying coastal aquifer thickness is examined on estimated groundwater salinity by building variable-density groundwater flow and coupled salt transport models. As a final step the results are compared to available literature and borehole data.

How to quantify geological heterogeneity in unconsolidated sediment systems in coastal areas worldwide and what is its influence on offshore fresh groundwater presence?

Chapter 3 provides an overview of available global geological datasets and a methodology designed to estimate geological heterogeneity in coastal areas. Unconsolidated sediments have been deposited over large time scales and the deposition rate and sediment type is dependent on multiple factors (e.g., inland lithology, elevation, climate). Geological heterogeneity is related to three indicators/drivers: the sediment influx from inland; fraction of coarse-grained and fine-grained sediments deposited over time; and the influence of erosion on the deposited sediment formations. The influence of geological heterogeneity on estimated groundwater salinity is assessed by building variable-density groundwater flow and coupled salt transport models spanning far into the offshore domain for several selected coastal regions.

Can offshore fresh groundwater be a viable source of fresh water in coastal areas with high water stress?

In Chapter 4, the groundwater modelling framework developed in Chapter 3 is extended to the rest of coastal regions with unconsolidated sediment aquifer systems. The estimated volumes of fresh (and brackish) offshore groundwater are compared with regional scale literature studies and to current water demands in coastal regions. Furthermore, the renewability of these resources is examined as well as the time scale on

which these fresh offshore groundwater volumes could provide an additional source of fresh water. A paleo-reconstruction simulating more than one full glacial-interglacial period (approx. 125 000 years) is set up to follow the past sea-level fluctuations leading to fresh and brackish groundwater deposition in currently submerged offshore areas.

What are the threats of different sea-level rise scenarios on future coastal fresh groundwater resources?

In Chapter 5, the effects of sea-level rise on coastal fresh groundwater reserves are assessed. Similar groundwater models as in Chapters 3 and 4 are implemented but the global coastline is split into smaller regions allowing to capture better local topography. Three different climate change scenarios are taken into account and the final results show large differences in estimated decrease of fresh groundwater volumes in coastal areas between these three scenarios. Three different global digital elevation models are tested as groundwater model inputs as topography is identified as one of the main factors determining the severity of sea-level rise effects.

The final Chapter 6 provides an overall summary and discussion regarding the main findings in this study as well as suggestions for future research.

2 Estimating the thickness of unconsolidated coastal aquifers along the global coastline

Abstract

Knowledge of aquifer thickness is crucial for setting up numerical groundwater flow models to support groundwater resource management and control. Fresh groundwater reserves in coastal aquifers are particularly under threat of salinization and depletion as a result of climate change, sea-level rise, and excessive groundwater withdrawal under urbanization. To correctly assess the possible impacts of these pressures we need better information about subsurface conditions in coastal zones. Here, we propose a method that combines available global datasets to estimate, along the global coastline, the aquifer thickness in areas formed by unconsolidated sediments. To validate our final estimation results, we collected both borehole and literature data. Additionally, we performed a numerical modelling study to evaluate the effects of varying aquifer thickness and geological complexity on simulated saltwater intrusion. The results show that our aquifer thickness estimates can indeed be used for regional-scale groundwater flow modelling but that for local assessments additional geological information should be included.

The final dataset has been made publicly available at:
https://doi.pangaea.de/10.1594/PANGAEA.880771

Based on: Zamrsky, D., Oude Essink, G. H. P., and Bierkens, M. F. P.: Estimating the thickness of unconsolidated coastal aquifers along the global coastline, Earth Syst. Sci. Data, 10, 1591–1603, https://doi.org/10.5194/essd-10-1591-2018, 2018.

2.1 Introduction

Coastal aquifers provide fresh groundwater for more than two billion people worldwide (Ferguson and Gleeson, 2012). Multiple local and regional studies have shown that these fresh groundwater resources are not only threatened by natural disasters such as storm surges and tsunamis (Cardenas et al., 2015), but also increasingly by climate-induced sea-level rise (Carretero et al., 2013; Rasmussen et al., 2013; Sefelnasr and Sherif, 2014) and urbanization that leads to coastal aquifer over-exploitation combined with reduced groundwater recharge (Custodio, 2002).

Comparing coastal aquifer vulnerabilities worldwide in a consistent manner requires a global scale study (Döll, 2009). However, many necessary input datasets, both physical and societal, are only available on regional or local scales and can therefore only be used in coastal aquifer vulnerability investigations on regional scale. Notable work on global coastal aquifer vulnerability are studies by Ranjan et al. (2009), and Michael et al. (2013) looking at coastal aquifer vulnerability to sea water intrusion and by Nicholls and Cazenave (2010) taking social-economic factors into account. Related observation-based studies are performed by van Weert, F. et al. (2008) on global saline groundwater occurrence assessment and by Post et al. (2013) on the existence of offshore fresh or brackish groundwater. Lacking global information, the few global studies that attempted a modelling approach (i.e., Ranjan et al., 2009 and Michael et al., 2013) used globally or regionally homogenous hydraulic parameters, including aquifer thickness. Indeed, recent reviews concluded that most of the past modelling studies until present day (both on local and global scale) considered a homogeneous aquifer system (Werner et al., 2013; Ketabchi et al., 2016). This pinpoints that there is still a large gap in our knowledge about coastal aquifer hydrogeological settings in many parts of the world. Since the local and regional hydrogeological conditions largely determine the coastal aquifer vulnerability to sea-level rise (Michael et al. 2013) and groundwater pumping (Ferguson and Gleeson, 2012), it is important to improve our insight into the local and regional coastal aquifer hydrogeology worldwide.

The goal of this study is to estimate the unconsolidated aquifer system thickness along the global coastline. This constitutes a first step towards a more complete hydrogeological characterization of coastal aquifers. Our focus is limited to aquifer systems formed by unconsolidated sediments (Table 2-1) that constitute around 25% of the coastal ribbon (200km far or less from coastline) based on the GLIM dataset (Hartmann and Moosdorf, 2012). In contrast, more than 36% is shaped by different types of sedimentary rocks where aquifers can also be expected. These sedimentary rock formations most probably form the coastal aquifer systems that are missed in this study. However, more than 40% of people living in the coastal ribbon (CIESIN, 2017) are located on top of unconsolidated sediment aquifer systems (Table 2-1), while less than 30% live in areas with sedimentary rock aquifers. This means that there is potentially more pressure on fresh water availability in areas with unconsolidated sediment aquifer systems.

Table 2-1 Statistics for individual GLIM classes in the coastal ribbon (200km and less from the coastline). The population numbers are based on the 2015 global population count (CIESIN, 2017).

GLIM class (xx)	GLIM class (name)	Total % in coastal ribbon	Population sum (10^6)	Population % in coastal ribbon
ev	Evaporites	0.27	4.6	0.12
ig	Ice and Glaciers	0.22	0.003	0.00
mt	Metamorphic rocks	20.59	395.6	10.52
nd	No Data	0.03	1.2	0.03
pa	Acid Plutonic rocks	5.66	248.2	6.60
pb	Basic Plutonic rocks	0.74	19.5	0.52
pi	Intermediate Plutonic rocks	0.52	14	0.37
py	Pyroclastics	1.00	39.7	1.06
sc	Carbonate Sedimentary rocks	8.96	268.9	7.15
sm	Mixed Sedimentary rocks	13.69	350.4	9.32
ss	Siliclastic Sedimentary rocks	14.23	487.3	12.95
su	Unconsolidated Sediments	25.78	1562	41.53
va	Acid Volcanic rocks	1.22	60.2	1.60
vb	Basic Volcanic rocks	4.39	166	4.41
vi	Intermediate Volcanic rocks	2.29	128.2	3.41
wb	Water Bodies	0.43	16	0.42
Total		100.00	3 761.6	100

To be globally applicable and comparable, our method of aquifer thickness estimation makes use of already available open-source global datasets (see Table 2-2). These datasets contain information on elevation, surficial lithology, regolith thickness and overall sedimentary thickness. What motivated this study is that none of the globally available thickness datasets are individually suited to represent coastal aquifer thickness Two of these datasets only provide estimated regolith (surficial unconsolidated layer) or soil thickness (Pelletier et al., 2016; Shangguan et al., 2017). The soil or regolith layer is only part of the aquifer system formed by unconsolidated sediments and therefore unfit to use in building a hydrogeological model representing the flow in the whole aquifer system. Conversely, the other two datasets (Whittaker et al., 2013; de Graaf et al., 2015) estimate the total porous media thickness without making a distinction between unconsolidated and consolidated sediments (rocks), and therefore, tend to overestimate the unconsolidated aquifer system thickness.

The resulting dataset consists of 26 968 cross-sections perpendicular to the global coastline with unconsolidated aquifer thickness estimated along each cross-section. Additionally, the uncertainty ranges in aquifer thickness are provided for each cross-section. In order to illustrate how to use the new dataset in a regional groundwater

modelling setting, we will show the results of variable-density groundwater flow and coupled salt transport models for three distinctly different coastal cross-sections. We also show the sensitivity of modelling results to varying the aquifer thickness and geological complexity.

Table 2-2 Summary of global datasets used for aquifer thickness estimation.

Dataset name	***Description***	***Resolution***	***Reference***
GEBCO 2014	Global topography and bathymetry	30 arc-second	*(Weatherall et al. 2015)*
Average soil and sedimentary deposit thickness	A gridded global data set of soil, intact regolith, and sedimentary deposit thicknesses for regional and global land surface modelling, max. estimated depth is 50m	30 arc-second	(*Pelletier et al.* 2016)
PCR-GLOBWB	Thickness of the groundwater layer from the global model (5 arc-minute)	5 arc-minute	(*de Graaf et al.* 2015)
GLIM	Global Lithological Map - Rock types of the Earth surface (16 basic classes), more than 1.2 million polygons	vector	(*Hartmann & Moosdorf* 2012)
Natural Earth coastline	Global coastline	vector	*(Natural Earth, 2017)*

2.2 Materials and Methods

2.2.1 Coastal aquifer unconsolidated sediment thickness estimation

We collected state of the art open source global datasets (Table 2-2) that provide information on topography and bathymetry (Weatherall et al., 2015), regolith thickness estimation (Pelletier et al., 2016), global scale aquifer thickness estimated by de Graaf et al. (2015), lithology (Hartmann and Moosdorf, 2012) and coastline position (Natural Earth, 2017). The core of our aquifer thickness estimation (ATE) method is to combine topographical and lithological information. This enables us to find the topographical slope of outcropping bedrock formations and to determine the coastal plain extent. The latter is defined by a low topographical slope (Weatherall et al., 2015), a lithology consisting of unconsolidated sediments (Hartmann and Moosdorf, 2012) and a regolith thickness thicker than 50m (Pelletier et al., 2016). This is the first study that directly combines

lithology and topographic information to estimate the coastal unconsolidated sediment aquifer systems thickness at global scale.

Given the large variety of coastal environments, ranging from steep cliffs to extensive deltaic flat areas, it is important to develop a robust method that distinguishes between these different coastal types and also takes into account variations of inland bedrock formations. To achieve this, the coastal zones are represented as perpendicular cross-sections to the coastline and are placed equidistantly (5km) along the coastline. The intersections between the cross-sections and the coastline are called coastal points. Along the cross-section, a set of equidistant points (0.5km) are positioned (cross-section points) and mark the locations where values from the datasets listed above are extracted (Figure 2-1a). The cross-sections span 200 km both inland and offshore from the coastal point to capture the bathymetrical and topographical profile. This distance was chosen to safely cover the necessary stretch both landward and offshore for groundwater flow and coupled salt transport modelling. Recent studies dealing with the latter set the landward boundary less than 200km from the coastline even in deltaic areas (Delsman et al., 2013; Larsen et al., 2017; Nofal et al., 2016). Similarly, previous studies showed that submarine groundwater discharge can occur more than 100km offshore (Kooi and Groen, 2001; Post et al., 2013).

Figure 2-1b shows an example of a cross-section running through a coastal point. All the necessary values from the individual datasets are aggregated and used to determine the coastal plain extent and the anchor point position. The inland boundary point of the coastal plain is defined as a cross-section point that has a lithological class different than a water body (to take into account e.g. lagoons, bays) or unconsolidated sediments based on the GLIM dataset. Hartmann and Moosdorf (2012) state that uncertainty in the GLIM dataset is still significant based on the amount of mixed sediment class (~15% of the world area), so it is likely that some unconsolidated sediment coastal areas have been missed in our study.

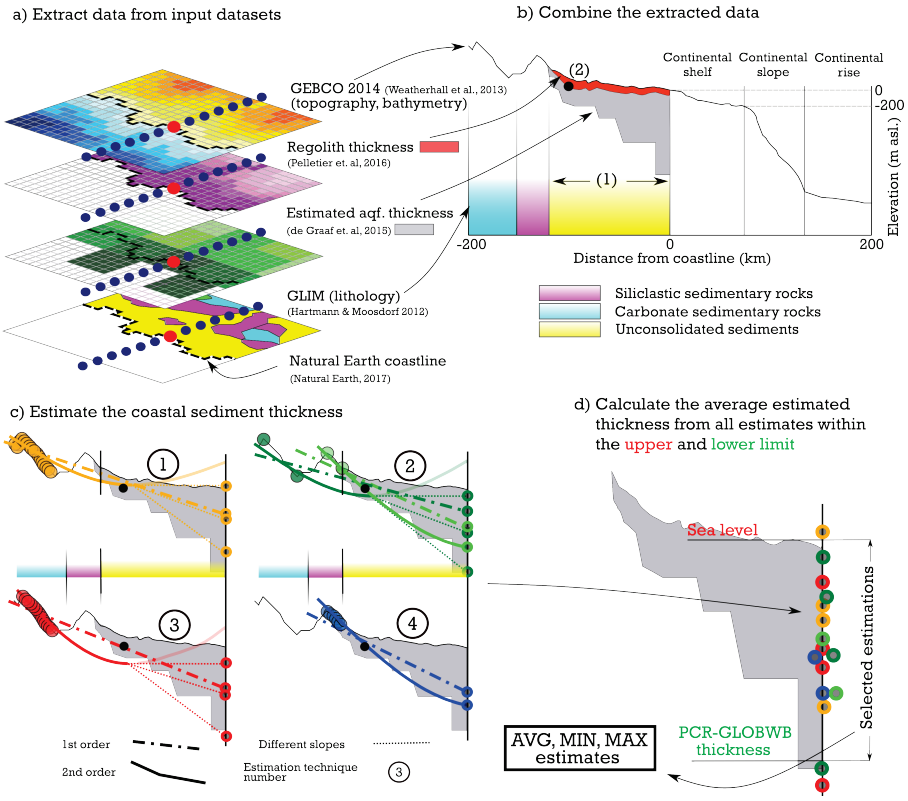

Figure 2-1 Schematization of the ATE method using available open-source global datasets. (a) Combining input datasets and extracting the values at cross-section points along a perpendicular cross-section to the coastline running through a coastal point (red dot), only few are schematized in the figure (in reality 800 per cross-section). (b) Determine the extent of the coastal plain (1) and position of the anchor point (2). Extent of the cross-section is set to 200km landward and offshore, (c) The estimation is performed via topographical points selected based on the coastal plain extent, the position of the anchor points and the lithological classes from the GLIM dataset. The 2nd order estimation line is not used for estimation in case its minimum is reached before the coastline (transparent). (d) Final step of calculating the average, minimum and maximum estimated values.

Once the coastal plain extent is known, the next step is to define the anchor point using the regolith thickness dataset (Pelletier et al., 2016). Taking note of the fact that the Pelletier et al., (2016) dataset generally has increasing thickness values towards the coast in case of unconsolidated sediments and that a thickness larger than 50m is not mapped, we define the anchor point as the last cross-section point (moving from land to coast) with soil and sedimentary deposit thickness smaller than 50m. Pelletier et al., (2016) state that areas with low relief, such as coastal plains, generally have a thicker sedimentary layer (> 50m) than hillslopes so the transition zone between these two relief types is modelled

with acceptable accuracy on global scale. The anchor point represents the last point where soil and sedimentary deposit thickness is known and is located below ground at the indicated depth by this dataset. A histogram of anchor point distances to coastline and of total coastal plain extent values is shown in Figure 2-2. The ATE is then performed for all cross-section points located between the anchor point and the coastline.

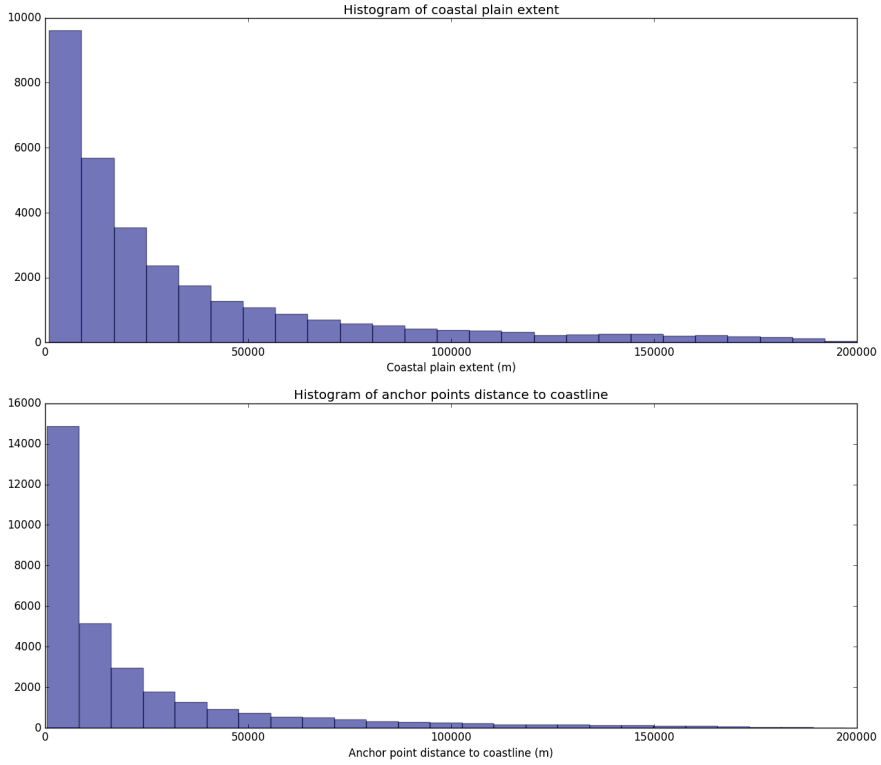

Figure 2-2 Histogram of coastal plain extents and anchor point distance to coastline values.

Due to a large variety in the coastal plain extent, topography and geological diversity of the coastal cross-sections worldwide, four different estimation techniques are proposed to increase the overall estimation method robustness. The differences between these techniques are in the topographical points selection; these points are used to simulate the bedrock slope (Figure 2-1c). The anchor point is added to the set of topographical points in every estimation technique.

The first technique selects all cross-section points elevation values of the first peak located prior to the coastal plain, lithological class regardless. The second technique selects all the cross-section points elevation values of the highest peak located in a bedrock formation

(any different class than unconsolidated sediments). The third selection technique consists of selecting all cross-section points elevations located between the coastal plain end and the bedrock formation end. The last technique selects only the local minimum and maximum points of every peak located behind the coastal plain. This diversity in selecting cross-section points based on lithological and topographical information combinations allows for a more robust method that is fit for various coastal environments.

For each selection techniques described above, a first and second order curve-fitting is performed to simulate the bedrock formation slope (Figure 2-1c). If the minimum point of the second order curve is situated before the coastline, we use three different linear function types to extend the bedrock slope simulation and estimate the sediment thickness by extending it beyond the coastline. All the three lines start at the minimum point of the second order estimation and run through the coastline. The first line is a constant horizontal line, the second simulates the average continental shelf slope (defined as shallower than -200m. bsl.) and the last line simulates the average slope of the whole 200km cross-section offshore segment.

The global scale aquifer thickness estimated by de Graaf et al. (2015) is chosen as the lower boundary since it tends to overestimate the coastal aquifer thickness because its underlying method is more fit to the inland areas and uses river networks and basins as basis for thickness estimates (de Graaf et al. 2015). Finally, all the points are used to estimate the mean, minimum and maximum aquifer thickness at the coastline and the mean coastal profile for the unconsolidated sediment extent. The dataset that is stored contains per coastal cross-section the mean profile as well as the maximum and minimum depth and the depth at the coastline standard deviation. For each coastal cross-section, also the anchor point position and depth are included.

2.2.2 Validation methods

Two different validation approaches are applied to test the fit of our estimated aquifer thicknesses with measured values. First, the results are compared with information from available open-source geological borehole datasets. The second validation method consists of comparing the average estimated aquifer thickness with measured values gathered via a literature review.

A dataset incorporating 168 geological borehole descriptions was collected and sorted out from open-source datasets and web services, mostly located in the Netherlands, USA, Brazil and Australia. After digitizing the borehole reports, we translated the geological information to overall unconsolidated sediment thickness to compare it to our final thickness estimates. This means that all the unconsolidated sediment types such as sand, clay or silt were merged into the same stratigraphic unit and their overall thickness is taken as the final sediment thickness. Figure 2-3 shows the collected borehole location, the data sources are presented in Table A-1. Since some boreholes are not located in direct proximity to the coastline, we chose to extrapolate the estimated sediment thickness by calculating the estimated sediment thickness for each cross-section point. This was done by creating a line between the anchor point depth and the estimated sediment depth at

the coastline (Figure 2-4). Next, the average cross-section point thickness in a circle with radius of 2.5km around the borehole is compared to the thickness in the borehole.

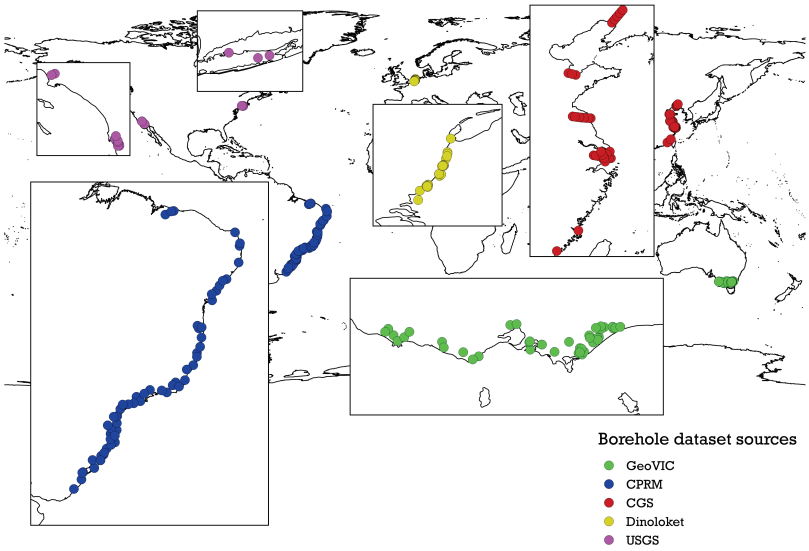

Figure 2-3 Location of the borehole data used as validation dataset; sources are listed in Table A-3. The borehole information in Brazil and Australia was manually digitized while the subsurface information in China was gathered by interpreting the cross-section provided in the hydrogeological maps.

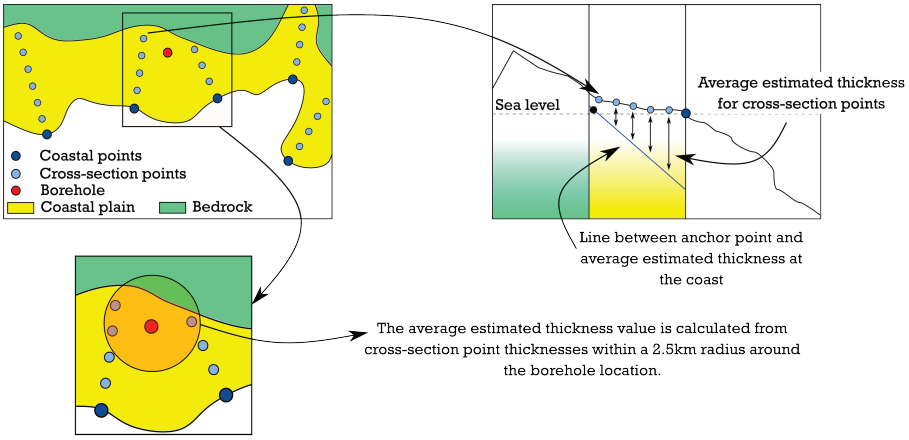

Figure 2-4 Schematization of the borehole validation process. A set of points laying within a given distance is selected for each borehole and their estimated sediment thickness is averaged. The final comparison between these average values and measured values from the boreholes is shown in Figure 2-3.

The final literature validation set is composed of maximum, minimum and/or average aquifer thickness values (unconsolidated sediment) for 64 coastal areas worldwide. However, not all the literature sources provide the average unconsolidated sediment thickness. In the cases where it does not, it is calculated as half the maximum indicated thickness in case only the maximum value is provided. If both maximum and minimum thicknesses are given, the average thickness is set to be halfway between these two values. The table with literature sources references and the sediment thickness values provided by these sources are listed in Tables A-2 and A-3. The final estimated average sediment thickness values were compared with the literature dataset and evaluated based on the relative error and relative improvement compared to the overall average thickness value from all literature sources. The relative error is based on the following equation:

$$RE = \frac{Z_{est} - Z_{lit}}{Z_{lit}} \tag{1-1}$$

where Z_{est} is the ATE by our method and Z_{lit} is the average thickness given by literature. The RE can be either positive or negative which implies that the ATE over or under estimates the aquifer thickness respectively (compared to values indicated by literature). The percentage relative error is calculated as:

$$PRE = \mathrm{RE} * 100 \tag{1-2}$$

The average global aquifer thickness value based on all literature sources was calculated using the equation below:

$$Z_{lit_{avg}} = \frac{1}{N}\sum_{i=1}^{n} Z_i \tag{1-3}$$

where $Z_{lit_{avg}}$ is the overall average value of all literature values Z_i.

The mean absolute error was then calculated for both the overall average value and the estimated average thickness values suggested by our method, see equations below:

$$MAE_{lit} = \frac{1}{N}\sum_{i=1}^{n} |Z_{lit_{avg}} - Z_i| \tag{1-4}$$

$$MAE_{est} = \frac{1}{N}\sum_{i=1}^{n} |Z_{est} - Z_i| \tag{1-5}$$

Subsequently, the relative improvement rate and percentage relative improvement are calculated as follows:

$$RI = \frac{MAE_{lit} - MAE_{est}}{MAE_{lit}} \quad (1\text{-}6)$$

$$PRI = \mathrm{RI} * 100 \quad (1\text{-}7)$$

The same validation criteria are calculated using the borehole data.

2.2.3 Groundwater flow and salt transport modelling

The main motivation behind building numerical models simulating the groundwater flow and salt transport as part of this study is to examine the effects of varying aquifer thickness and its geological complexity (absence or presence of low permeable aquitard layers) on simulated saltwater intrusion. Better understanding of these sensitivities will help create improved large-scale hydrogeological models in coastal areas which in turn will lead to more accurate present and future fresh groundwater volumes predictions. To achieve that, a set of variable-density groundwater flow models with varying aquifer thickness and geological complexity (heterogeneous vs. homogeneous system) is created. To evaluate the sensitivity of saltwater intrusion on aquifer thickness and geological complexity, we compare, at a fixed time, the salinity profiles of all simulations as well as the fresh water cells percentage in the coastal zone.

The models with different parameter settings were set up for three cross-sections located in Italy in the Versilia plain (Pranzini, 2002), the coast of Virginia in the USA (Trapp Jr. and Horn, 1997) and in the Mediterranean aquifer in Israel (Yechieli et al., 2010). We use these studies to build the heterogeneous geological scenarios based on provided cross-sections indicating the exact position of low permeable aquitard layers. This was done to evaluate the relative importance of aquifer thickness to the effect of geological complexity. Since the main motivation of this numerical modelling study is to investigate the sensitivity to aquifer thickness and geological complexity, we kept the both aquifer and aquitard layers hydraulic conductivities constant for all simulations (see Table A-4). The hydraulic conductivity values were based on the GLHYMPS dataset by taking the highest value of the unconsolidated sediment class as hydraulic conductivity of the aquifer and the lowest value (fine grained) as aquitard hydraulic conductivity (Gleeson et al., 2014). To build these steady-state models we use the SEAWAT code (Guo and Langevin, 2002) and the Python Flopy library (Bakker et al., 2016). The model schematizations and input parameter values list are presented in Figure A-3 and Table A-4.

2.3 Results

2.3.1 Sediment thickness estimation

The aquifer thickness is estimated for 26 968 coastal points around the globe, which cover roughly one fifth of the global coastline. The rest of the global coastline is covered by other lithological types than unconsolidated sediments and is not taken into account by the ATE method. The overall estimated aquifer thickness (EAT) results are presented in Figure 2-5a. It shows that the aquifer thickness estimates range between 0.1m and 5145m, with mean value close to 170m. In total 87% out of all the EAT values predict a thickness lower than or equal to 300m (Figure 2-5b). A slightly different result is observed in the literature source analysis, where 69% of the studied areas have aquifer thickness lower than or equal to 300m. This difference is explained by the fact that a disproportionally large number of deltaic areas with thick sediment layers is included in the literature validation dataset. Figure 2-6 shows the areas where there are no EAT results, largely due to the absence of unconsolidated sediments.

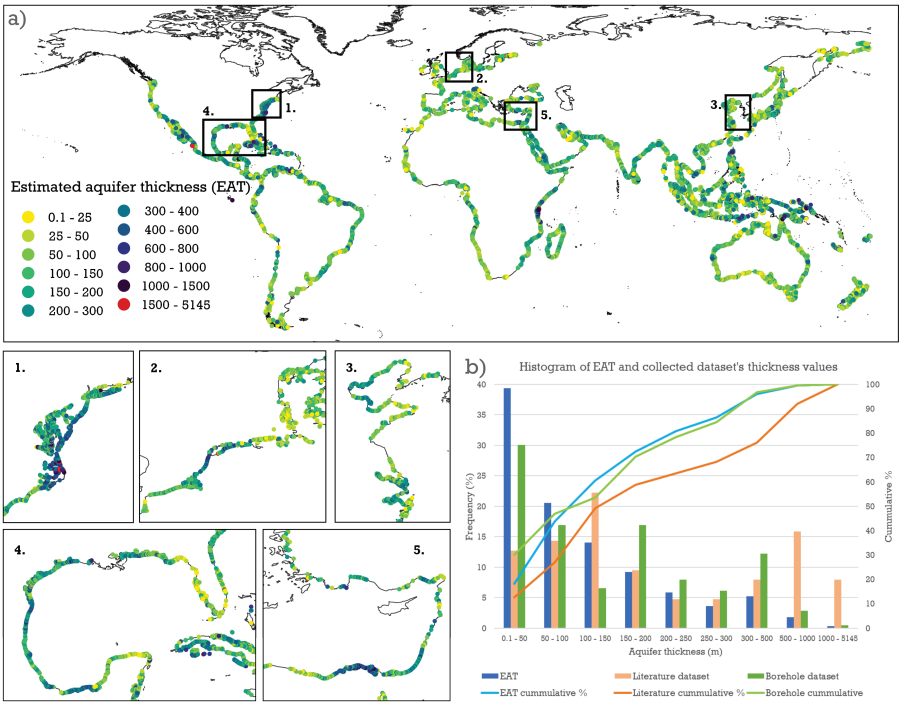

Figure 2-5 (a) Global map of EAT at the coastline and zoomed areas (1–5) showing regional variations of estimated thickness in various coastal zones around the world. The coastal points are magnified, giving the impression that more than the stated 20% of the global coastline is covered, which is not the case (see the plain black line). (b) Histogram of EAT values with cumulative frequency in %.

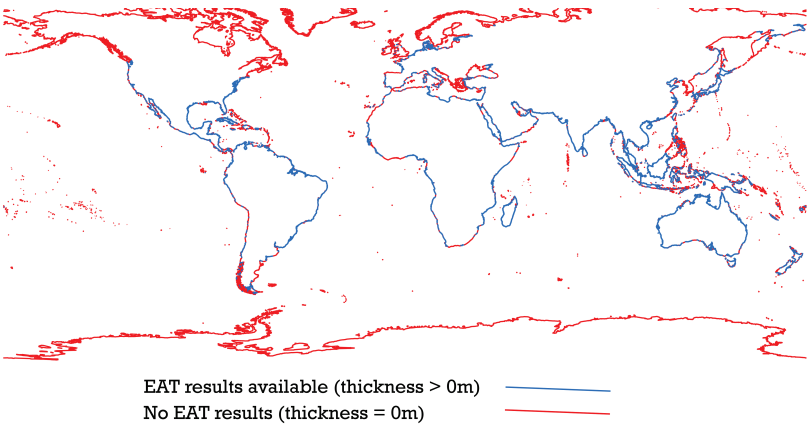

Figure 2-6 Map showing the spatial distribution of EAT values (unconsolidated sediment aquifer thickness > 0 m) and areas where the unconsolidated sediment aquifer thickness is 0 m.

2.3.2 Validation of EAT results

When comparing our EAT with the information collected from the borehole dataset, it is clear that our ATE method provides estimates in right order of magnitude, but it cannot capture local variations of aquifer thickness. Figure 2-7a shows that the majority of EAT have relative error values (Equation 1-1) lower than 100%, meaning that our results are in the same order of magnitude as observed values from the borehole dataset. However, the relative improvement of the EAT, as compared with using the average of the borehole thicknesses as an estimate (Equation 1-6) is inconclusive as the amount of positive values is nearly equal to the total of negative values (Figure 2-7b).

The results of the validation with the coastal sediment thickness values gathered via a literature review show a more positive result compared to the borehole validation. The

Figure 2-7 Overall borehole and literature validation results of the EAT results.

overall average thickness of the literature dataset is 353m, 69% of all studied areas have a sediment thickness of 300m or lower. The relative improvement of sediment thickness estimates using our method is about 22% compared to the overall thickness values average as indicated by the literature (see Table A-3). The relative improvement for individual literature validation areas is shown in Figure 2-8. The majority of the areas show an improvement, while estimates for the large coastal plains of eastern and southern coast of the USA suggest the opposite. This will be discussed further in Section 4. However, in coastal zones that have the average sediment thickness of 300m or less, the relative improvement of our method is around 59%. Since our results suggest that 87% of the global coastline that is composed of unconsolidated sediments has average thickness of 300m or lower, the higher relative improvement achieved by our method gains extra importance.

Overall, about 48% of the validation areas have the absolute relative error percentage below 50%, while 35% of validation areas have the absolute relative error percentage between 50% and 100% (Figure 2-7b). Still, 17% of the validation areas show absolute relative error percentage higher than 100%. A closer look at Figure 2-7b reveals that the majority of these validation areas have the average thickness (based on literature) lower than 100m. However, the overall results for validation areas with average thickness lower than 300m show that 59% have relative error percentage lower than 50%, this is a 11% increase compared to the overall validation dataset.

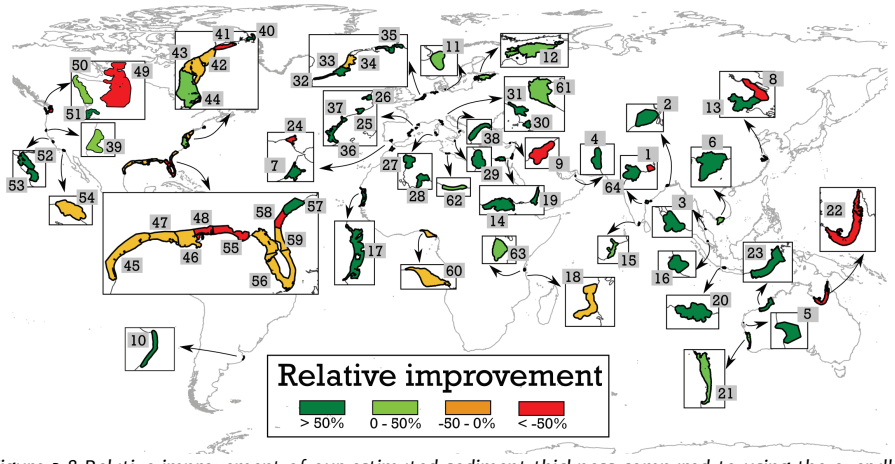

Figure 2-8 Relative improvement of our estimated sediment thickness compared to using the overall average thickness value from all literature sources.

2.3.3 Groundwater flow and salt transport modelling

Figure 2-9 presents a sample of simulated salinity profiles for selected aquifer thickness values for the three test cases. The complete set of the simulated salinity profiles together with the model conceptualization and model parameters and variables is given in Figures A-4 to A-6 and Table A-4. While comparing the salinity profiles for different aquifer thicknesses, it is apparent that aquifer thickness variations for homogenous geological conditions (Figures on the right) do not have large effects on the fresh-saline distribution, except for the lowest aquifer thickness value, (Figures 2-9a, 2-9c). Figure 2-9b shows that the thicker the aquifer at the coastline, the more saline water intrudes inland and, in some cases, upconing under low lying areas can be observed (Figure 2-9c).

The implementation of complex geological conditions based on the literature description that existed about these sites consisted mainly of introducing low conducting layers (aquitards). As Figure 2-9 shows, an aquitard has a substantial effect on the final salinity profile when compared to the salinity profile for homogenous geological conditions with the same aquifer thickness. The aquitard position combined with varying aquifer thickness has a large effect on the salinity profile and potential fresh (or brackish) groundwater offshore reserves (Figure 2-9b left column). In particular the simulations with larger aquifer thickness values show fresh (or brackish) offshore groundwater below the aquitard layer. Similar patterns can be observed in the last test case (Figure 2-9c), where the aquitard layers prevent saline water from intruding inland and show large offshore brackish water volumes.

Comparison of fresh groundwater cells percentage within the coastal zone of all three test cases (Figure 2-9) shows a trend where geological scenario (homogenous versus complex) has a larger effect on the amount of estimated fresh groundwater reserves than varying aquifer thickness. For the same geological scenario, the largest differences are observed between the aquifer thickness extreme values (thinnest vs. thickest).

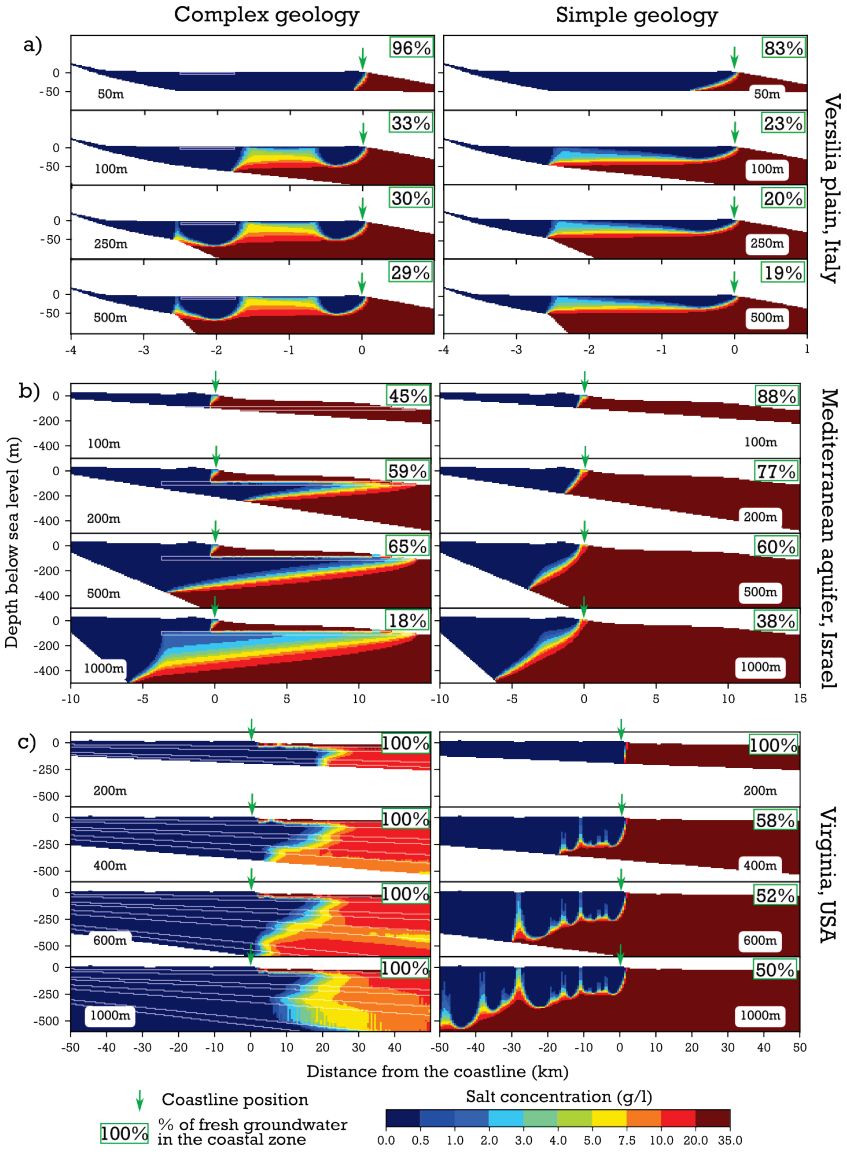

Figure 2-9 Simulation results as salinity concentration profiles for the cross-sections located in the a) Versilia plain, Italy, b) Mediterranean aquifer, Israel and c) Virginia, USA with varying aquifer thickness and 2 geology scenarios. The local geological information for each area (a) (Pranzini 2002) (b) (Yechieli et al., 2010) (c) (Trapp Jr. et al., 1997) was implemented (left column) together with homogeneous aquifer system (right column) to investigate the effects of geological complexity and aquifer thickness on simulated salinity profiles.

2.4 Discussion and conclusion

Although in the right order of magnitude (Figure 2-7a), the ATE validation with borehole measurements is worse than literature dataset validation. The large-scale discrepancy between our global estimated aquifer thickness (EAT) dataset and boreholes is the most obvious cause for this. It shows that our approach is not detailed enough to estimate very local variations in aquifer thickness as picked up by boreholes. Boreholes will generally lie between profile locations, which means that local variation also results in spatial dislocation errors, even though spatial averaging is used to bridge the scale gap (Figure 2-4). Still, even when compare to boreholes, we observe an overall ATE method performance improvement for coastal areas with measured thickness between 100m and 300m. The comparison between literature values comes out more favorably, because the data synthesis in the form of spatial statistics and geological profiles is a spatial aggregation form that better matches the ATE method scale. We have used the validation data that could be collected during the course of this study, but the validation set is far from exhaustive. The validation dataset should be expanded and continuously improved to achieve better EAT along the global coastline.

Our method tends to underestimate the aquifer thickness in deeper systems, such as large complex deltaic sedimentary structures with measured average aquifer thickness larger than 500m (Figure 2-7). This could be due to the limited cross-section length that spans at most 200km inland and offshore from the coastline depending on the coastal plain extent. If the latter exceeds this maximum length, then no bedrock formation is found and thus no aquifer thickness is estimated. In case the bedrock formation is only partially taken into account (e.g., only the foothill of a mountain range), its topographical slope will be lower which leads to lower EAT values at the coastline. The opposite happens for coastal areas with measured average thickness lower than 100m. In these cases, our average EAT values tend to be overestimated (Figure 2-7). This could again be caused by the input datasets resolution (see Table 2-2) which creates larger errors on local scale and for shallow systems which by themselves have a smaller size than more extensive coastal plains. Compared to the other two datasets providing thickness estimates (de Graaf et al., 2015; Pelletier et al., 2016) the lowest EAT values correspond to the range of values provided by Pelletier et al., (2016). The histogram in Figure 2-5b suggests that nearly 20% of coastal areas covered by our study have EAT between 0m and 50m. On the other side of the spectrum, our maximum EAT value is 5145m which is in the order of magnitude of the de Graaf et al., (2015) dataset.

The numerical modelling results show that only the simulations with extreme EAT values give substantially different results from the simulations with average or close to average EAT values. More variation in the fresh groundwater cells fraction in the coastal zone can be observed in the test case with intermediate aquifer thickness (Figure 2-9b). In the other two test cases (Figures 2-9a and 2-9c) the variation in the fresh groundwater cells fraction is very low for both geological scenarios. On the other hand, the model results also show that geological complexity (multi-layering) has a big impact on the results. Thus, for locally meaningful results, the aquifer thickness is but a first result, and a global estimate of multi-

layering (aquifers and aquitards) is a necessary next step. Werner et al., (2013) stresses that accounting for geological heterogeneities is important to accurately simulate the saline groundwater distribution in coastal areas. Previous regional to global scale studies (e.g. Michael et al., 2013; Solórzano-Rivas & Werner, 2018; Knight et al., 2018) considered the geological conditions (permeability and aquifer thickness) to be homogeneous and our EAT dataset could provide a first constraint on unconsolidated sediment thickness for these type of studies.

When comparing our numerical modelling output (with the complex geology incorporated) with the salinity profiles reported from the individual studies (Pranzini, 2002; Yechieli et al., 2010; Trapp Jr. and Horn, 1997) we find that differences for the cases a) and b) are small and a 2D schematization suffices. However, for cross-section c) the differences are considerable. This is most likely due to the presence of strong alongshore flows in the area, a more complex upper hydrological system and the groundwater withdrawals distribution in the area. This shows that 2D-approach modelling approach does not always suffice to estimate coastal groundwater flow.

In conclusion, we showed that it is possible to obtain, at first order, coastal aquifer thickness estimates by using available global datasets and a simple methodology consisting of simulating the bedrock slope from the geological outcrops. Our dataset complements the existing datasets listed in Table 2 by providing an estimate of the complete unconsolidated part of coastal aquifer systems. In such way it is now possible to build more detailed and vertically stratified regional and global scale hydrogeological models based on the herein provided dataset. By combining our dataset with existing sedimentary thickness estimates by e.g. de Graaf et al., (2015) we can distinguish the unconsolidated aquifer system (our dataset) overlaying the sedimentary rocks. However, our dataset is not suitable for building detailed local hydrogeological models, as in such case additional local geological information should be included. Furthermore, the local scale geological complexity seems to play a larger role in simulated salinity concentration profiles than aquifer thickness (except for extreme values). Thus, our EAT dataset provides a satisfactory first step towards a global coastal aquifer characterization that should be followed by the assessment of the coastal aquifers' geological complexity for local application.

Data format and availability

The final output data provides both the EAT at the coastline and the location and depth of the corresponding anchor points. These data are given as shapefile and comma separated value files. The data can be downloaded via:

https://doi.pangaea.de/10.1594/PANGAEA.880771.

Acknowledgements

This research was partially funded by The Netherlands Organization for Scientific Research (NWO) and the Ministry of Infrastructure and Water Management under the TTW Perspectives program Water Nexus (Project no 14298). We thank two anonymous reviewers for their thorough reading and comments that have considerably improved the quality of this paper.

3 Geological heterogeneity of coastal unconsolidated groundwater systems worldwide and its influence on offshore fresh groundwater occurrence

Abstract

Numerous coastal areas worldwide already experience fresh water shortages due to overexploitation and saltwater intrusion. Future climate change and population growth will further intensify this threat in more areas in coming decades. Therefore, it is necessary to explore any potential fresh water source, such as offshore fresh groundwater, that could alleviate this fresh water shortage and provide valuable time for adaptation measures implementation and changes in water management strategies. Recent evidence suggests that a disproportionally large portion of human population living in coastal areas relies on groundwater resources stored in underlying unconsolidated groundwater systems. These systems are often very heterogeneous, combining numerous high permeability aquifers interlaid with low permeability aquitards with varying total thickness. This heterogeneity is a major control on the fresh groundwater volume and groundwater salinity distribution within such systems. Thus, the quantification of geological heterogeneity is often the limiting factor when estimating fresh groundwater volumes, both inland and offshore, along the global coastline. To overcome this obstacle, we combine conceptual geological models with available state-of-the-art global datasets to derive a set of geological heterogeneity parameter distributions quantifying geological heterogeneity of coastal unconsolidated groundwater systems as formed over last 1 Ma. These are then used in an algorithm designed to build synthetic heterogenic parameterizations of coastal unconsolidated groundwater systems along the global coastline. These, in turn, provide key input for modelling variable-density groundwater flow and coupled salt transport to analyze changes in groundwater salinities and offshore fresh groundwater volume. Such an analysis is performed over one full glacial-interglacial cycle (the last 0.13 Ma) to account for oscillating sea-level conditions and shifts in coast-line positions and salinity incursions. Our simulation results show a close match between the modelling scenarios and values presented by literature sources demonstrating the potential of the hereby presented methodology to be applied in similar future studies.

Based on: Zamrsky D, Karssenberg ME, Cohen KM, Bierkens MFP and Oude Essink GHP (2020) Geological Heterogeneity of Coastal Unconsolidated Groundwater Systems Worldwide and Its Influence on Offshore Fresh Groundwater Occurrence. *Front. Earth Sci.* 7:339. doi: 10.3389/feart.2019.00339

3.1 Introduction

Currently more than two billion people live in the coastal areas worldwide (Ferguson and Gleeson, 2012) and are directly dependent on local fresh water resources. Aquifers bearing fresh groundwater are often tapped due to high water quality demands for domestic, industrial and agricultural purposes and thus contribute to the energy and food security (Gleeson et al., 2015). In past decades, an increased pressure is observed on both shallow and deep (modern and fossil) inland fresh groundwater resources which results in depletion and quality deterioration (e.g., due to rising salinity), especially in arid regions (Custodio, 2002; Gleeson et al., 2017). These fragile fresh water sources are also threatened by natural hazards such as seawater-overwash events (Cardenas et al., 2015; Chui and Terry, 2015; Gingerich et al., 2017; Yang et al., 2018, 2013; Yu et al., 2016) and sea-level rise (Costa et al., 2013; Mabrouk et al., 2018; Rasmussen et al., 2013; Sefelnasr et al., 2014), further stressing the need to adjust water management strategies and find potential additional sources of fresh water. According to the latest IPCC report (Masson-Delmotte et al., 2018), the past decade has seen a record-breaking number of such natural disasters (seawater overwash events such as storm surges) while sea-level rise predictions are increasingly alarming (e.g., Pollard and Deconto, 2016). Furthermore, rapidly growing population numbers (e.g., United Nations, 2017) will lead to increased urbanization and consequently to coastal aquifer over-exploitation and lower groundwater recharge rates into the aquifers due to surface sealing (e.g., Custodio, 2002). Michael et al. (2017) stress the need to rapidly improve current water management strategies in coastal areas worldwide to adapt to the threats mentioned above.

Offshore fresh groundwater volumes (OFGVs) could act as an important additional fresh water resource in times with rising water stress in densely populated coastal areas (Cohen et al., 2010). A study by Post et al. (2013) shows that the OFGVs occurrence along the global coastline is higher than previously thought, while they can stretch even hundreds of kilometers offshore (e.g. Edmunds and Milne, 2001; Meisler et al., 1984). It is also important to note that large volumes of brackish groundwater can be found offshore as well. The OFGVs result from recharge that occurred in times of sea-level fall and low stands associated with the Pleistocene ice ages (e.g., Waelbroeck et al., 2002), notably prolonged and deep in the last 1 Ma (e.g., Head and Gibbard, 2005; Pillans et al., 1998), when the shelf groundwater systems interacted with surficial fresh water bodies like rivers and lakes. Additionally, a lower sea-level position also leads to higher groundwater gradient tilted towards the offshore domain. It can be assumed that the fresh groundwater flux coming from the landward direction is therefore increased and contributes to the OFGV creation. Sudden sea-level rise during glacial terminations produced low permeable aquitards deposited on top of the former coastal floodplains (Kooi and Groen, 2001; Pham et al., 2019). The sea-level rise led to deposition of shelf mud belts and estuarine-deltaic low-permeable deposits that rapidly trapped the formerly deposited fresh water. Inner and middle shelf regions went through these geomorphological cycles with each Pleistocene ice age (e.g., Cohen and Lobo, 2013; Ehlers and Gibbard, 2004; Hanebuth et al., 2002; Reijenstein et al., 2011). Such rapid inundating event due to sea-level rise and consequent trapping of OFGVs occurred between 17 and 7 ka BP and culminated during the Holocene

(e.g., Lambeck et al., 2014; Smith et al., 2011). Thus, our main hypothesis is that offshore fresh groundwater volumes are formed by recharge during sea-level low stands and subsequently trapped by deposited low permeable sediments.

The above explained global effects of rapid sea-level rise leading to trapping of OFGVs suggests that such reserves are non-renewable on much shorter human-usage time scales (Post et. al, 2013 and Stone et al., 2019). However, a recent study by Michael et al. (2016) showed that large fresh groundwater fluxes (submarine groundwater discharge) can occur under certain conditions (linked to geological heterogeneity) and thus replenish the OFGVs. We do not attempt to determine the source of potentially found OFGVs in our study. Also, their vicinity to and intercalation with non-fresh shelf groundwater volumes of marine nature means that OFGVs are likely to gradually shrink due to natural salinization processes (namely advection and hydrodynamic dispersion). Therefore, pumping these offshore fresh water reserves shouldn't be considered as 'mining' in the negative sense and could on the contrary even lead to reducing the current negative effects of onshore groundwater pumping (Kooi and Groen, 2001). However, the study by Yu and Michael, 2019 found that offshore pumping could potentially impact the onshore land subsidence rates and submarine groundwater discharge depending on geological complexity. Hence, a need exists for better understanding of coastal geological heterogeneity when assessing OFGVs for potential exploitation, and to secure that such is not harmfully impacting hydrogeological conditions in the adjacent onshore.

The most recent OFGV discovery and quantification in the northeast U.S. Atlantic continental shelf has a magnitude comparable to the largest onshore aquifers (Gustafson et al., 2019). Other regions where OFGV was recently documented and studied are Malta, South Island of New Zealand (Micallef et al., 2018) and the Perth Basin in Australia (Morgan et al., 2018). Since a certain degree of salinization in such water bodies is to be expected, e.g., due to hydrodynamic dispersion, desalinization treatment would be necessary to make the extracted water from this source safe for human consumption (Gustafson et al., 2019). Tapping into the OFGV may not yet be needed in northeast U.S., but it might play a significant role in regions already experiencing fresh water shortages and relying increasingly on desalinization. The latter brings about numerous environmental threats, the most urgent being generation of brine by-product that requires considerable economical and technical resources to be dealt with (Jones et al., 2019). These can be largely reduced by using fresh or slightly brackish water (i.e., OFGV) as feedwater to desalination plants and thus cutting down the brine output and energy costs (Ghaffour et al., 2013). Moreover, OFGV could supply low-cost water in areas with offshore oil production activities (Yu and Michael, 2019). This adds to the urgency of better understanding and quantifying the OFGV occurrence before these can be successfully mined for human consumption.

Recent analytical and SEAWAT (Langevin et al., 2008) modelling studies underline the importance of heterogenic geological conditions (mainly presence and extension of aquitards) on potential OFGV occurrence (Engelen et al., 2018; Knight et al., 2018; Morgan et al., 2018; Solórzano-Rivas and Werner, 2018), turning away from earlier simulations embedding homogeneous geological conditions (Ketabchi et al., 2016; Michael et al., 2013;

Ranjan et al., 2009; Werner et al., 2013) and moving towards more complex heterogeneous subsurface representation (e.g. Michael et al., 2016; Thomas et al., 2019; Zamrsky et al., 2018).

The main objective of this study is an estimation of the geologically heterogeneous structure of regional coastal unconsolidated groundwater systems (CUGSs) in order to arrive at an estimate of the OFGVs in these systems. Performing this estimation leads to schematizations in which we experimentally vary additional uncertain properties. These are limited to the ratio between thicknesses of permeable and low permeable layers (aquifers resp. aquitards), cross-sectional geometry of aquitards and within that aquitard discontinuity and degree of consolidation. When using the schematizations to simulate trapping of OFGVs and assess their potential sizes, we assume that the distribution of low permeable layers has had the largest influence on OFGVs. This is the outcome of sediment delivery to and dispersal over the shelf while changing according to sea-level oscillations between repeated low and high stands (OFGVs being recharged during low stands, trapped and stored during high stands).

A major constraint to the hydrogeological heterogeneity estimations is a lack of direct observational information suitable for use at the global scale. Another issue is, besides the practical problem of uneven coverage, the non-uniformity and proprietary restrictions on what data is there (geological and hydrological; seismic swaths; cores and wells). A further fundamental problem is that data acquired in the few sectors of shelves for which data is reasonably disclosed (references above), cannot be simply assumed to also be representative for the shelves rest of the world. In practice, this means that attempts to estimate shelf architectural heterogeneity and their OFGV contents, have to rely on synthetic hydrogeological representations that are built on the global data (bathymetry, mapping the size of shelves) and geological insights (age of shelves, relations with the continents that fed them, understanding of sea-level cyclicity and sediment routing to the deep sea) that are available, and the geological-history shared versus the geographically diverse aspects herein. Such provides a baseline synthetic geohydrological representation of the shelf subsurface of use in independent OFGV modelling (this study), also functioning as a primer that alternative approaches starting from direct data (i.e., non-synthetic shelf geomodelling) can compare to.

Based on such insights and rationale, we populate and re-aggregate a global shelf map with relevant geological information, use it to draw synthetic geological sections with explicitly simulated architectural heterogeneity. Subsequently, we use these as input for variable-density groundwater flow and coupled salt transport models. In such way, it is possible to estimate the volumes of fresh groundwater located both the inland and offshore domains and asses the influence of varying geological conditions on these volumes. We demonstrate the workflow to quantify OFGVs for seven selected coastal regions. In SEAWAT (Langevin et al., 2008) model simulations, we consider a full glacial-interglacial cycle in order to correctly capture OFGV temporal dynamics under changing sea-levels and also test our hypothesis that such volumes can be preserved over a time scale of tens of thousands of years. We also include a future prediction of OFGV shrinking due to salinization but do not take into account any sea-level rise predictions.

The decision to limit the aim to CUGSs only stems from high pressure on current and future fresh water availability in these areas compared to sedimentary rock groundwater systems (see also Zamrsky et al., 2018). For similar reasons, we excluded CUGS in Arctic and Antarctic regions and focus on shelf regions of the tropics and temperate latitudes (including those with shelf sediment delivery affected by glaciations during low stands). Including sedimentary rock groundwater systems (including karstic recharge systems) would require the implementation of very different geological complexity concepts which are beyond the scope of this paper.

3.2 Methods

3.2.1 General approach

In this study, we first focus on geological heterogeneity estimation of the unconsolidated continental shelf systems. The information gathered is then fed into a synthetic heterogenic parameterization algorithm to create multiple random geological approximations of these systems. Then, as the third and final step SEAWAT (Langevin et al., 2008) modelling procedures are designed to investigate the potential presence of OFGV in a set of chosen coastal regions. To achieve that, the globe is divided into regions connecting a continental shelf to a river basin that supplies its sediments. These regions are typified based on their geological character (sediment supply, sediment type, subsidence rate) using global datasets. Next, a methodology is devised to systematically generate average representative profiles (ARPs) of coastal regions that aggregate various regional characteristics (e.g., topography, geological input, groundwater recharge estimation, etc.). Thus, the ARP approach serves as a tool to estimate the mean groundwater concentration profile in each individual coastal region. This estimation is carried out by running for each ARP a large set of SEAWAT (Langevin et al., 2008) models simulating variable-density groundwater flow and coupled salt transport to quantify the probable range of fresh water occurrence in both coastal (inland) and continental shelf (offshore) domains, given the local geological uncertainty. Expecting that large model runtimes might be a potential bottleneck due to high spatial resolutions over very long simulation times (>150ka); we investigate whether a reduced number of geological realizations per ARP will provide sufficiently accurate results compared to a larger random set. This approach is tested on a selected set of COSCAT regions and corresponding ARPs and later compared to past studies dealing with OFGV assessments.

3.2.2 CUGSs regionalization using COSCAT river basin and continental shelf divisions

The COSCAT (Coastal Segmentation and related CATchments, Meybeck et al., 2006) and MARCAT (MARCATS: MARgins and CATchments Segmentation, Laruelle et al., 2013) divisions carve the land of the globe into large river basin-based regions (COSCATs) acting as sediment sources connected to the corresponding sediment depositional areas (sinks) located along the continental shelf (MARCATs). Coupling between these two datasets is

carried out to match the continental shelf domain segments to the corresponding COSCAT region. This division into COSCAT regional areas is the cornerstone of our study. It provides the spatial dimensions of the shelf terrains as major sink areas, and allows to connect these areas to the continental source catchment areas for which size, elevation and climatology is specified within our study. Various state-of-the art global datasets are collected to characterize the geological conditions of these regional areas (see Table 3-1). These datasets are then combined through a set of equations to determine continental shelf architecture (interlayering aquifer and aquitard layers). A detailed description is provided in Text B-1.

The resulting estimated continental shelf architectures are quantified by parameterizing the geological heterogeneity conditions per COSCAT region and its corresponding continental shelf domain segment (see Section 3.2.3). Table 3-1 lists the full suite of datasets used to generate and populate the coastal profile SEAWAT models. Extracting individual datasets along the cross-section perpendicular to the coast and running through individual coastal points located along the global coastline is performed in the same fashion as in Zamrsky et al. (2018). The distance between each of the individual coastal profiles is 5km while the cross-section points along each profile are 0.5km apart. This is a far greater resolution than the number of COSCAT regions that can stretch over hundreds or even thousands of kilometers of coastline. This scale difference, however, serves to include a realistic amount of variation in continental shelf architecture.

Not included in the geological parameterization are polar shelf regions (e.g., around Antarctica), partly due to missing input datasets, and partly due to low population density and the presence of permafrost. However, subpolar shelf regions affected by major glaciation (e.g., around North America and Scandinavia) are included. Finally, regions without any CUGS are omitted from the SEAWAT modelling step.

Table 3-1 Global datasets collected and used as input. [1] used for estimating the global geological heterogeneity, [2] used as input for SEAWAT models, implemented using SEAWAT (Langevin et al., 2008).

Dataset name	***Description***	***Resolution***	***Reference***
GEBCO 2014[1,2]	Global topography and bathymetry	30"	(Weatherall et al., 2015)
ATE[2]	Unconsolidated groundwater system thickness estimation (unconsolidated sediments only)	Vector	(Zamrsky et al., 2018)
P[2], *ET*[2]	Long term average annual precipitation and evapotranspiration	30"	(NTSG, 2019)
GLHYMPS[2]	Bottom aquifer hydraulic conductivity	30"	(Gleeson et al., 2014)
GLHYMPS 2.0 (GUM)[2]	Upper aquifer hydraulic conductivity	30"	(Huscroft et al., 2018)
Soilgrids[2]	Soil layer thickness	30"	(Hengl et al., 2014)
Soil hydraulic properties[2]	Global soil hydraulic conductivity	30"	(Montzka et al., 2017)
COSCAT[1,2]	Segmentation of the shelf and basins	Vector	(Meybeck et al., 2006)
MARCAT[1]	Segmentation of the shelf and basins, typology	Vector	(Laruelle et al., 2013)
WTD[2]	Water table depth (relative to sea-level)	30"	(Fan et al., 2017)
Ocean floor age[1]	Age of oceanic bottom	2'	(Muller et al., 2008)
Delta dispersion[1]	Dispersion system classification	Vector	(Walsh and Nittrouer, 2009)
Delta location	Location of 40 largest deltas worldwide	Vector	(Tessler et al., 2015)
LGM[1]	Last glacial maximum global extent	Vector	(Ehlers and Gibbard, 2004)
Tectonic plate boundaries[1]	Indicates passive/active margins	Vector	(Coffin et al., n.d.)
GLIM[1]	Global lithology classification	Vector	(Hartmann and Moosdorf, 2012)
Seafloor sediment type	Seafloor lithology classification	6'	(Dutkiewicz et al., 2015)

3.2.3 Global geological heterogeneity parameterization

This section provides only a general summary of the methodology to derive parameters quantifying geological heterogeneity of the continental shelf architecture (see detailed explanation in Text B-1). To do that, a number of global datasets were used as inputs into various conceptual schematizations gathered from literature translated into equations (Table 3-1). Among the main natural forces taken into account are the past sea-level oscillations that heavily influenced the sedimentation conditions over the past one million years (last 10 glacial-interglacial cycles). Sediment layers deposited during this time period constitute the bulk of CUGS worldwide. It is also necessary to mention that our focus is only limited to passive tectonic plate margins. These are generally older and more extensive than active tectonic plate margins and thus dominating the global continental shelf domain.

Continental shelf architecture is mainly characterized by assessing the accommodation and sedimentation properties for each COSCAT region including factors influencing that ratio. The sedimentation/accommodation ratio *Y* (-) is derived as follows (Eq. 3-1):

$$Y = \frac{Sedimentation}{Accommodation} = \frac{q_s * M * D}{R} \tag{3-1}$$

Where $q_s\,[m\,/\,yr * 10^6]$ is the sediment flux (supply) into the continental shelf domain, M [–] is the sand/mud composition ratio, D [–] is the sediment dispersion modifier and $R\,[m\,/\,yr * 10^6]$ represents the long-term net subsidence (thermal term + compaction term).

The outcome for each of these individual factors and their influence on continental shelf architecture is shown in Figure 3-1. Sediment supply (q_s) magnitude mainly affects the thickness of individual sediment layers and is estimated based on (Syvitski et al., 2003). The sediment type forming these layers is defined by the M (sand/mud composition) ratio, based on inner continental shelf sample collection (e.g., Hayes, 1966) with modifications for the composition during glacial times (e.g., Nam et al., 1995). The factor influences the presence, thickness and composition of aquitard layers within the CUGS (next sections). The sediment dispersion modifier D determines the fraction of sediment that is deposited on the continental shelf compared to the continental slope. Lastly, the long-term net continental shelf subsidence factor R plays a crucial role in assessing the continental shelf architecture. The thermal subsidence term is dependent on oceanic crustal age (Karner and Watts, 1982). The compaction term (e.g., Reynolds et al., 1991) is calculated making use of the q_s and D parameters. A more detailed description of the global geological heterogeneity parameterization is provided in Text B-1.

External control	Outcome	Shelf characteristics
M: Sand/Mud composition ratio	High M ratio	Relatively abundant sand, meaning lesser number of or missing aquitards
	Low M ratio	Relatively abundant mud, well developed, thicker aquitards
q_s: Sediment supply	High sediment supply	Thick sequences: progradation in addition to shelf aggradation
	Low sediment supply	Thin sequences: little progradation, mainly aggradation
R : Subsidence	High subsidence	Steep shelf slope, narrow shelf, tilted sequences
	Low subsidence	Gentle shelf slope, wide shelf, near horizontal sequences
D : Dispersion	PAD/MDD/SDC/EAD	Sedimentation on shelf (100%)
	CC	Most sediment by-passed via sub-marine canyon, 10% sediments trapped on shelf

Figure 3-1 Hydrogeological summary variables for COSCAT/MARCAT shelf regions. The sediment dispersion modifier D is 1 for all but one of Walsh & Nitrouer (2009)'s shelf categories (EAD: Estuarine Accumulation Dominated; PAD: Proximal Accumulation Dominated; SDC: Subaqueous delta clinoforms; MDD: Marine dispersal dominated). It is set to 0.1 for those shelved captured by major submarine canyon systems.

Both the integrate *Y* parameter and its constituent variables *R*, *D*, *M* and q_s are used as input parameters for the geological heterogeneity algorithm for the ARPs. Two additional geological parameters are used in that algorithm. First, we define a parameter to characterize preservational discontinuities in the shelf architecture as produced by alternating deposition and erosion over multiple glacial-interglacial cycles. To determine this parameter, we used the information available from surficial lithology descriptions describing the discontinuities of sediment layers deposited during the Holocene era. To overcome insufficient knowledge on older sediment layers and their discontinuities we simply reproduce the same parameter value stochastically over these layers. The parameter is called aquitard patchiness factor, defined to capture the vertical and horizontal continuity of low permeable aquitard layers in the geological heterogeneity algorithm. Areas with high Y values (leading to coastal erosion) also have a high aquitard patchiness value. Second, to define the sediment type of the upper sediment layer in the offshore domain, we use the offshore lithology classification which is based on the dataset

generated by Dutkiewicz et al. (2015), see Table 3-1 Multiple lithological classes are merged into two large groups (permeable and non-permeable).

3.2.4 Average Representative Profiles (ARP) concept

As mentioned above, constructing ARPs is used as a concept to depict a mean profile for a selected set of seven COSCAT regions considered in this study. The averaging process involves parameters determining coastal prism dimensions such as the mean topographic and bathymetric profiles together with the inland and offshore extent of the ARP (Weatherall et al., 2015), and the mean aquifer (groundwater system) thickness estimation (ATE) at the coastline (Zamrsky et al., 2018) for each selected COSCAT region. Since COSCAT regions spread over areas with similar climatic conditions, the averaged difference between long term net annual precipitation and evapotranspiration (NTSG, 2019) is taken as the groundwater recharge estimate. Lastly, the regional geological characteristics described in Section 3.2.3 are derived for individual COSCAT regions and therefore can directly be used as input for estimating the average thickness of the CUGSs.

3.2.4.1 Coastal profiles and types

The individual coastal profiles perpendicular to the coastline are evenly spaced along the coastline where unconsolidated sediments are found. Parameter values derived from the datasets listed in Table 3-1 are extracted for each individual coastal profile by a Python toolbox. Subsequently, these profiles are aggregated into the ARP per COSCAT region as described above in Section 3.2.4. Figure 3-2 shows a schematized COSCAT region with individual coastal profiles positioned perpendicular to the coastline.

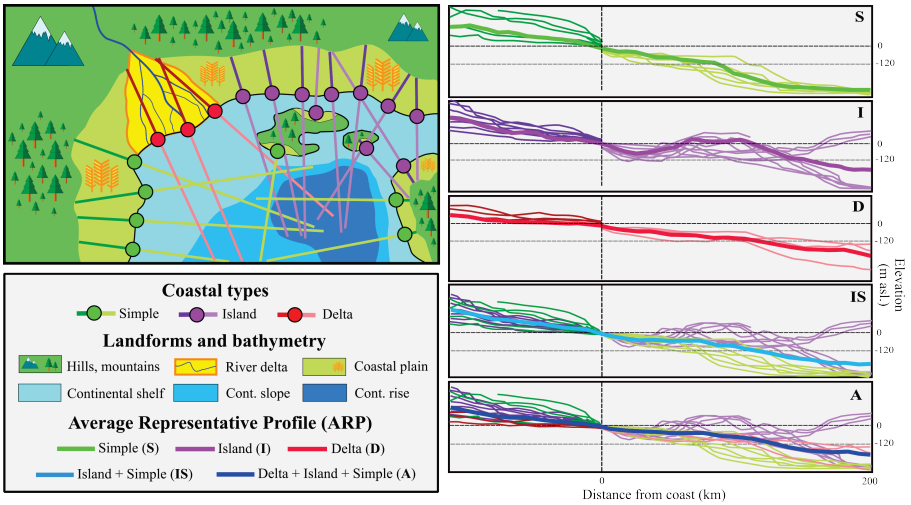

Figure 3-2 Average Representative Profile (ARP) and coastal type schematization. The bathymetry classes are based on elevation and slope of the ocean floor. Pinet (2003) defines the three main bathymetry classes based on depth below sea level and topographical slope. Continental shelf is the shallow and relatively flat part of the ocean floor with its depth below sea level not exceeding 120m below sea level (assumed to be the lowest sea level throughout a glacial cycle, see Figure 3-6). At the edge of the continental shelf there is an abrupt change in slope which marks the beginning of the continental slope. At the end of continental slope is the continental rise that is defined by lower slope and large depths (generally deeper than 3000m below sea level).

The inland areas are classified based on the GLIM lithological classification (Hartmann and Moosdorf, 2012) and elevation (Weatherall et al., 2015). These databases split the hinterland into higher elevated and mostly rocky hilly or mountainous areas and the low-lying coastal plain consisting of unconsolidated sediments. The border between these two classes also corresponds to the landward boundary position in the 2D SEAWAT models. Since deltaic areas are assumed to have generally thicker unconsolidated groundwater systems (Zamrsky et al., 2018), a special attention is paid to the largest deltaic systems worldwide (Tessler et al., 2015) creating a separate inland class on its own. The offshore domain is divided into three classes based on two criteria: a. the ocean floor depth below sea-level and b. the bathymetry slope. These criteria are used to determine the position of the continental shelf edge (CSE) and foot of continental slope (FOS) points (Figure 3-3) using the algorithm presented by Wu et al. (2017).

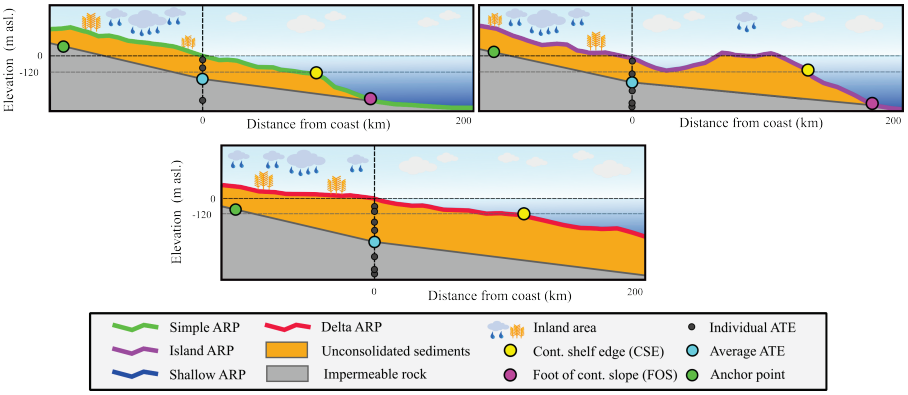

Figure 3-3 Defining the subsurface extent of Average Representative Profiles (ARP)s: the foot of continental slope (FOS), the continental shelf edge (CSE) is based on Wu et al. (2017) and the average aquifer thickness estimation (ATE) is established from Zamrsky et al. (2018).

Figure 3-2 also shows a coastal type classification that is defined by topographic and bathymetric criteria. When the coastal profiles have a clearly distinguished inland and offshore domain they are classified as "Simple (S)" profiles. However, in quite a few cases, there can be a clearly detectable island (or barrier island) area present in the coastal profile and the profile is then classified as "Island (I)". Coastal profiles that fall within the areas marked as large deltas by Tessler et al. (2015) fall into the "Delta (D)" ARP class. Combining the profiles belonging to each of these coastal types leads to the formation of the ARPs per COASCAT region for each of the three coastal types. It is possible that combining coastal types can lead to an ARP that captures the characteristics of these coastal types. This can happen when the "Island (I)" ARP -after combining all the profiles-has no island in the offshore domain anymore and can therefore be merged with "Simple (S)" coastal type ARP, classifying it as an "Island + Simple (IS)" ARP, see Figure 3-2. Additionally, if the "delta" ARP shows similar topographical shape and coastal aquifer thickness, all three coastal types are merged, classifying it as a "Delta + Island + Simple (A)" ARP.

3.2.4.2 Creating synthetic heterogenic parameterization of coastal unconsolidated groundwater systems (CUGS)

After determining the model domains upper topographic and bathymetric limits, the next step is to define the depth of the impermeable bottom boundary. Using the average aquifer thickness estimation (ATE) value at the coastline and the thickness at the anchor point location (Zamrsky et al., 2018) a simple straight line is drawn between these two points, as shown in Figure 3-3. In the offshore domain the bottom boundary is determined as a straight line between the average ATE point and the foot of continental slope. However, in cases where the foot of continental slope point is not found (e.g., the continental shelf domain stretches further offshore than 200km), the bottom boundary is

set to follow the average slope of the ARP's bathymetric profile, see Figure 3-3 ("Delta (D)" ARP).

To fill the domain between the upper and bottom cross-section boundaries, an algorithm is designed to create a synthetic heterogenic CUGS. This geological heterogeneity algorithm uses as input the datasets listed in Table 3-1 and the geological parameters described in Section 3.2.3. It is assumed that during periods with high eustatic sea-level (high stands comparable to current sea-level) finer sediments are deposited both at the usually low-lying coastal plain and at the continental shelf. The properties of the top layer are determined using the SOILGRIDS and GUM datasets (Table 3-1) in the inland domain of the ARP, and the offshore lithology dataset to establish the properties of the top layer in the offshore domain. Lower permeability of this top layer leads to slower infiltration of saline water into the CUGS and thus preservation of OFGVs (Post et al., 2013).

The form and structure of the offshore domain of the CUGS is determined by the sediment flux and sand/mud composition ratio parameters as described in Section 2.3. In systems with high sediment fluxes the deposition of new sediment layers stretches further offshore and generally covers previously deposited layers. This leads to a forward protruding of continental shelf edge points as shown in Figure 3-5. Opposite to that, when the sediment flux is low there is not enough sediment volume to cover the whole extent of older sediment layers and therefore there are no protruding continental shelf edge points. The sand/mud composition ratio is used to establish the aquifer and aquitard layer fractions in the whole CUGS. The total sand and mud fractions are then split into the desired number of aquifer and aquitard layers respectively.

A so-called stacking factor is applied to determine the clay cell location within the aquitard. Varying it allows us to test the influence of aquitard leakiness in groundwater salinity simulations. A higher value of the stacking factor means higher probability of low permeable (e.g., clay) model cells towards the top of the aquitard that in turn leads to increased groundwater flow confinement. Lithologically, this resembles the fining upward sequence that is typically observed towards the top of low stand fluvial depositional systems (e.g., Bridge, 2009; Miall, 2014) and at the base of transgressive to high sea-level stand coastal deposits (e.g., Cattaneo and Steel, 2003). The overall proportion of clay cells in the aquitard is made to equal the parameter *M* as specified per COSCAT region in Section 3.2.3; the remainder is fine sediment based on the GLHYMPS data set (Table 3-1 and below). Presumably, the aquitard layers are formed and buried over the half glacial-interglacial cycle from low stand to high stand, such as lastly between 20 and 7ka BP. To what degree the aquitard is preserved spatially, however, is determined after deposition and the architectural outcome of that is captured by applying the aforementioned aquitard patchiness factor (Section 3.2.3). Doing so builds conduits between aquifers, short circuiting the aquitards. These conduits are created randomly in the aquitard layers by removing an amount of low permeable cells corresponding to the aquitard patchiness factor and thus simulating the coastal erosion process. In such a way, we are able to create links between permeable aquifer layers and increase their connectivity which presumably has a large influence on groundwater flow patterns in CUGSs. The geological heterogeneity algorithm outcomes thus mimic the hydrogeological properties of the

modelled domain. The process of creating this synthetic heterogenic CUGS is further illustrated in Figure 3-5.

3.2.5 SEAWAT modelling

The computer code SEAWAT (Langevin et al., 2008) is used to simulate variable-density groundwater flow and coupled salt transport for the corresponding coastal type ARPs found in each selected COSCAT region. It is highly probable that in some parts of the world large OFGVs were formed during low sea-levels tens of thousands of years ago, when shelf floors were exposed during the Last Glacial Maximum (26.5 to 19 ka BP), and/or when riverine discharge increased during the termination of the Last Glacial (19 to 8 ka BP; also considering long-periodic variations in monsoonal strength) – both facilitating increased fresh water recharge. For such reasons (see also: Post et al., 2013), the timescale considered in this study stretches beyond one full glacial-interglacial cycle to determine not only the current situation but also the temporal dynamics of these regional groundwater systems. The average OFGV (and its standard deviation) is estimated for the selected set of COSCAT regions and its corresponding coastal type ARPs under varying geological conditions. This set consists of seven COSCAT regions (Figure 3-4), some of them with multiple coastal type ARPs (amounting to nine in total), where offshore fresh groundwater presence was documented by Post et al. (2013). This also serves as an additional validation procedure to gauge the fit of our modelling results. Two different modelling concepts are developed leading to a total number of 1116 SEAWAT model simulation runs (124 per ARP). In the SEAWAT models, the offshore extent is limited to 200km, to keep model runtimes reasonable. All these simulations are performed on the Dutch HPC (high performance computing) cluster Cartesius facilitated by the SURFsara services.

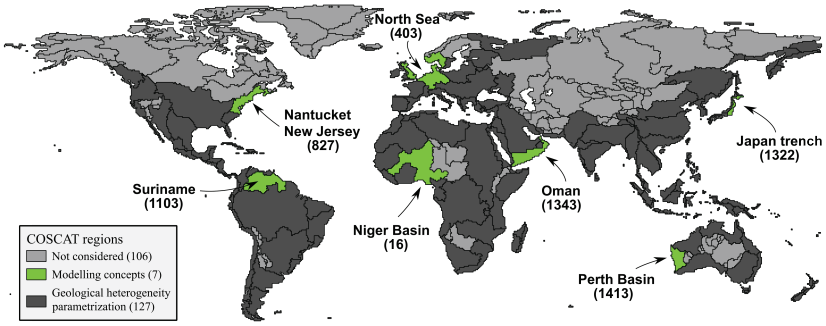

Figure 3-4 COSCAT regions selected for comparison of the two modelling concepts and the geological heterogeneity parameterization study. Northern arctic and inland COSCAT regions are not considered for this study. COSCAT region names (in brackets) correspond to areas with proven or highly possible presence of offshore fresh groundwater reserves (Post et al., 2013).

3.2.5.1 Hydrogeological properties

The geological heterogeneity algorithm described in Section 2.4.2 specifies the location of sediment layers deposited during past high and low sea-level stands. Hengl et al. (2014) provides a global thickness estimation dataset of the sediment layer (unconsolidated) presumably deposited during the last low sea-level stand. In our study it is used to define the thickness of the upper-most unconsolidated sediment layer in the model domain. The original GLHYMPS (Gleeson et al., 2014) and GUM (Huscroft et al. 2018) datasets define the overall hydraulic conductivity of the unconsolidated sediments. GLHYMPS shows values on average approximately one order of magnitude lower than that of the upper unconsolidated sediment layer (GUM). Since aquitard layers are usually deposited during high sea-level stands and have generally low permeability (i.e., low hydraulic conductivity values) they are assigned the GLHYMPS values. The opposite is the case for more permeable aquifer layers that are deposited during the low sea-levels and are therefore linked to the GUM datasets.

Unfortunately, the exact information about the number of preserved aquifer-aquitard layer combinations for each selected COSCAT and their thickness is missing and thus needs to be approximated. We use the sand/mud ratio (see Section 3.2.3) to determine the fractions of aquitard and aquifer sediment layers deposited over a single full glacial-interglacial cycle. Subsequently, the number of aquifer-aquitard layer combinations is randomly assigned (see Figure 3-5). In a similar fashion, thickness of each aquifer-aquitard layer is also randomly determined until the whole total CUGS thickness is filled up. The upper most sediment layer thickness is determined based on Hengl et al. (2014) and hydraulic conductivity properties derived from the GUM dataset (Huscroft et al., 2018). This results in creating an approximate geological profile for the selected set of COSCAT regions and the corresponding ARPs. The exact aquitard position within the CUGS is also unknown and is therefore parameterized to start at a random distance (positive or negative) from the current coastline. In such way, it is possible to examine the effects of the aquitard layer position on the estimated groundwater salinity profile.

The aquifer and aquitard layers are differentiated in the SEAWAT models via varying hydraulic conductivity values provided by the GUM and GLHYMPS datasets respectively (Table 3-1). These hydraulic conductivity values are extracted along each individual cross-section at equidistant points as in Zamrsky et al. (2018) and then combined into a single group (per sediment layer type) for each COSCAT region to draw realizations from. A lognormal distribution for both the GUM and GLHYMPS values is then created for each

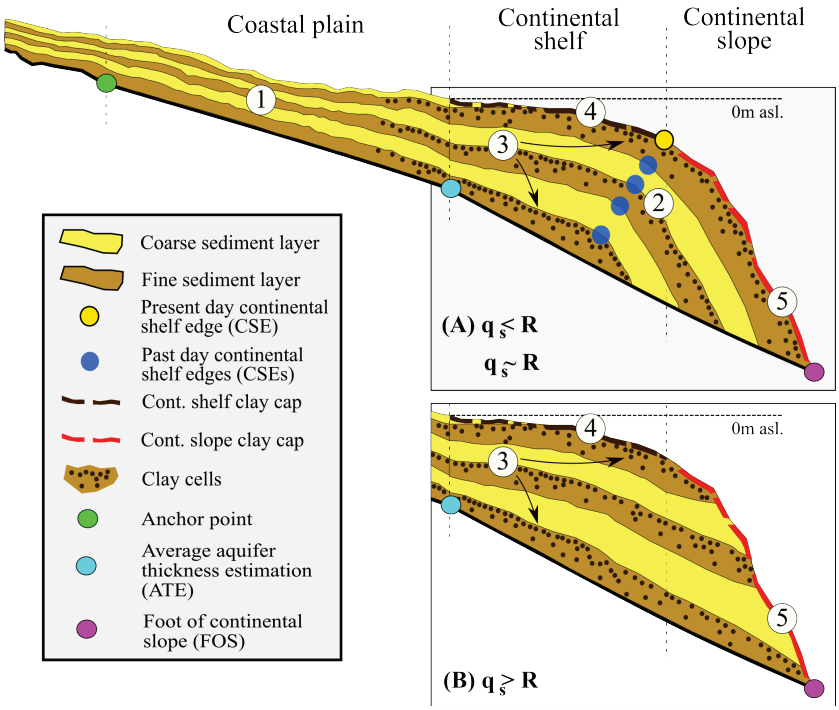

Figure 3-5 Conceptual schematization showing the process of translating the geological information and parameter values into a synthetic heterogenic CUGS profile. 1) The total number of high stand (coarser sediments/aquifers) and low stand (finer sediments/aquitards) layer pairs is determined on sediment sand/mud composition ratio R specified in Section 3.2.3.) The offshore layers shape is based on the sediment flux parameter value q_s; in this example the value is 'high' meaning that the sediment supply is so high that the shelf edge is being pushed further away from the coastline (A). In the opposite cases the individual sediment layers are stacked on top of each other without fully over topping the lower layers (B). 3) Assuming that during maximum high stand sea levels mostly very fine sediments are deposited (e.g., as during Holocene sea level transgression (Oude Essink et al., 2010)) both inland and offshore (due to low river gradient) individual clay layers (represented by model cells) are inserted into the larger fine sediment layers. A so-called stacking factor is applied to determine how close these model cells containing clay are placed relative to the top of the fine sediment layer. 4) A clay cap layer is potentially placed on top of the ocean floor depending on the main sediment type as provided by Dutkiewicz et al. (2015). 5) Same as in 4) but in the continental slope area.

group and COSCAT region. A chosen value from these lognormal distributions is then assigned to each model cell in the model domain depending on the sediment layer type (aquifer or aquitard) allocated to the model cell as explained in Section 2.4.2. To simulate

lower permeability of these aquitard layers clay cells are then synthetically inserted into aquitard layers. Hydraulic conductivity values for clay cells are selected randomly (using Python randomization tools) and vary between 0.01 m/d and 0.0001 m/d. This allows us to create a characteristic representation of regional hydrogeological conditions based on available state of the art global datasets.

3.2.5.2 Boundary conditions of the SEAWAT models

The bottom of the active model domain is assumed to be impermeable and is therefore set to a no-flow boundary. In the offshore domain the upper most model cells are assigned a general head boundary (GHB) with concentration of sea water and sea-level head elevation. The extent of the offshore domain changes with sea-level fluctuations and the GHB extent is adjusted accordingly. Sea water GHB cells are also assigned to all model cells in the last offshore model column (in vertical direction) in cases where the foot of continental slope is not found and the offshore model domain extent is limited to 200km. A water divide in the inland domain is determined using the ARPs topographical profile as described in Section 2.4.1. At this water divide, all the model cells are assigned a GHB with fresh water concentration and head elevation equal to the water table depth (relative to sea-level).

A simple top system is used to enable groundwater recharge through the model cells located on top of the inland model domain whose extent shifts according to the sea-level fluctuations (as the GHB extent explained above). The groundwater recharge rate is calculated as the difference of annual average precipitation and annual average evapotranspiration (Table 3-1) and is applied to the first active model cells of the inland areas of the model domain. Groundwater recharge is limited to a maximum rate taken as equal to the hydraulic conductivity of the cells the recharge is applied to.

3.2.5.3 Modelling stress periods and sea-level fluctuations

Grant et al. (2012) approximated the global eustatic sea-level variations over the last glacial-interglacial cycle. This time span covers more than one full glacial-interglacial cycle that usually spans over around 125ka based on the time elapsed between two maximum sea-level high stands. Our main hypothesis is that OFGVs are stored during the sea-level low stands covering the largest time span of the full glacial-interglacial cycle, see Figure 3-6. Paleo fresh groundwater recharge from precipitation spanning across the area corresponding to current continental shelf led to deposition of these OFGVs (Post et al., 2013). Therefore, the last maximum sea-level high stand (125ka BP) is considered as starting sea-level position for the numerical groundwater flow models. Figure 3-6 shows the temporal division within the modelling approach of SEAWAT: the so-called stress periods (SPs), being time intervals during which the inputs for the model remain constant. Stress periods (SPs) are used to simulate fluctuating sea-level values and stretching over fixed time periods. Since sea-level drop represents a much larger part of the glacial-interglacial period and rate of sea-level change is also much slower than that corresponding to sea-level rise, the sea-level drop SPs are longer than sea-level rise SPs

(5ka and 2ka respectively). In this way, it is ensured that the sea-level fluctuation effect on groundwater flow and saline concentration dynamics are captured with enough detail.

The groundwater flow models are initially set to run for time duration of maximum one full glacial-interglacial cycle (125ka) with the sea-level boundary set to 0m bsl. (called the "saline" initial condition), see Figure 3-6 (SP0). This approach is adopted to estimate starting groundwater salinity condition before simulating the full glacial-interglacial cycle with fluctuating sea-level (SP1 to SP31). It also serves as a benchmark that is later compared to groundwater salinity of the individual SEAWAT models at absolute sea-level low and high stands (SP 21_DSP and SP 31_DSP, respectively). In such a way we can assess the so-called system inertia of a groundwater salinity profile per selected COSCAT region. The system inertia per SP is defined here as the rate of OFGV change (% of total volume) in time during SP 21_DSP and SP 31_DSP. This allows us to gain insight into the assumed non-renewability of the OFGV. The SP 21_DSP stress period is 20ka long and represents a scenario with sea-level kept at the absolute low stand (-120m BSL). Groundwater salinity evolution during this stress period is used to evaluate the maximum OFGV (if achieved within the SPs duration) present in the model domain. On top, it demonstrates whether the SEAWAT model of that specific ARP has achieved equilibrium of the groundwater salinity (see Section 2.5.5). In a similar fashion, the system inertia while maintaining constant sea-level high stand (SP 31_DSP) is used to assess the change in estimated OFGVs in future 20ka from the current condition (end of SP31) (we do not include sea-level rise scenarios into our analysis).

In certain ARPs we observe that the bathymetry elevation is higher than the lowest sea-level considered during the sea-level fluctuation simulation (-120m BSL). A different approach needs to be implemented for such areas with shallow ocean floor (i.e., COSCAT 403_A) since they were flooded by sea water only recently (some tens of thousands ka BP). In such cases the whole domain is set to fresh water (0.5 g TDS/L) initial salinity concentration, in contrast with the regular ARP where the initial groundwater salinity is saline groundwater. Only one stress period with a constant sea-level (0 m bsl.) is simulated given that the sea-level rise curve is very steep in the simulated time period. To assess the current OFGV in such a case, the lowest elevation of the ocean floor in the model domain is compared to the sea-level curve showed in Figure 3-6. The time elapsed between the corresponding stress period and sea-level value and present-day is then the time step at which the current OFGV is estimated. From that moment on, with the constant sea-level value (0m BSL), the SEAWAT model simulation is extended for another 20ka to assess the future evolution of the salinity concentration profile. This stress period corresponds to the SP 31_DSP explained above.

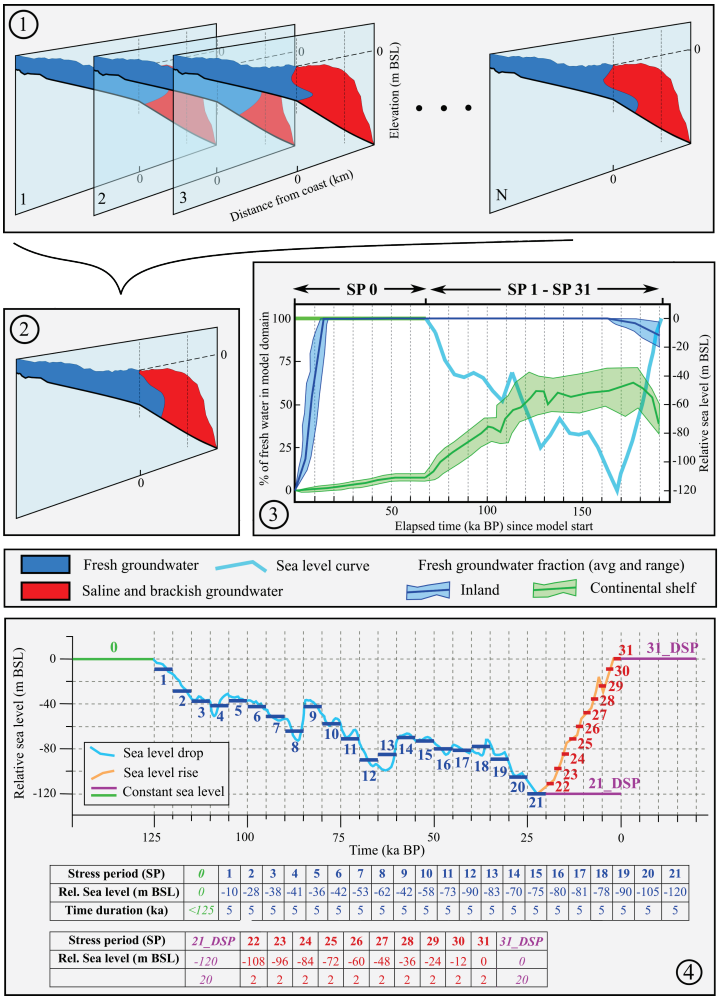

Stress period (SP)	0	1	2	3	4	5	6	7	8	9	10	11	12	13	14	15	16	17	18	19	20	21
Rel. Sea level (m BSL)	0	-10	-28	-38	-41	-36	-42	-53	-62	-42	-58	-73	-90	-83	-70	-75	-80	-81	-78	-90	-105	-120
Time duration (ka)	<125	5	5	5	5	5	5	5	5	5	5	5	5	5	5	5	5	5	5	5	5	5

Stress period (SP)	21_DSP	22	23	24	25	26	27	28	29	30	31	31_DSP
Rel. Sea level (m BSL)	-120	-108	-96	-84	-72	-60	-48	-36	-24	-12	0	0
	20	2	2	2	2	2	2	2	2	2		20

4

Figure 3-6 Combining all SEAWAT models per COSCAT region into an average presentation: 1) a number of N generated SEAWAT models (with different synthetic heterogenic CUGS and other model input parameters, see Table 2), each with a different groundwater salinity distribution. The fresh groundwater fractions (FGFs) are measure in both the inland (first 10 km inland from the present coastline) and the continental shelf (stretch from present coastline to continental shelf edge) areas; 2). all model outputs at all time steps are then averaged into an aggregated average profile; 3). graph showing the average fresh groundwater fraction and the range of fresh groundwater fraction across all individual SEAWAT models (overall minimum and maximum value) through time with varying sea levels that are shown in 4) Stress periods (SP) with corresponding sea levels (m BSL) relative to current situation and their time duration in thousands of years. In the graph, the sea levels as a function of the past 125 ka (light blue and orange lines) are derived from Grant et al. (2012). The upper table shows stress periods with generally decreasing sea level trend (blue horizontal segments in the graph) while the lower table corresponds to a time period of comparatively fast sea level rise during the past 20 ka (red horizontal segments in the graph). So-called Dynamic Stress Periods (DSP) are also implemented to study the groundwater systems dynamics in the selected COSCAT regions. Green line is implemented in the SEAWAT models to simulate the initial salinity profile (saline initial condition only) and is set to last no more than 125ka (equal to one full glacial cycle); 21_DSP (20-0ka BP) is set up to investigate the system inertia at the absolute sea level low stand, while in 31_DSP (0-20ka) we investigate the system inertia and in the future 20ka with sea level kept at current level (0m BSL).

3.2.5.4 Model input parameters

As described in Sections 3.2.5.1 and 3.2.5.2, multiple parameter types and values such as groundwater recharge rates and geologic composition are COSCAT region specific. However, some model settings are kept constant throughout this study and applied to all SEAWAT models. The finite difference solver is chosen for simulating salt transport, while using standard values for porosity, hydrodynamic dispersion parameters, based on other regional SEAWAT modelling studies (Ketabchi et al., 2014; Mahmoodzadeh and Karamouz, 2019; Morgan et al., 2018). The chosen grid resolution of 100m wide and 10m thick model cells is in accord with other previously published similar scale SEAWAT models (Cobaner et al., 2012; Huang and Chiu, 2018; Michael et al., 2016). A summary of the parameter values applied to all SEAWAT models is presented in Table B-1.

3.2.5.5 Convergence criteria

Two different types of convergence criteria are distinguished in this study. First, numerical convergence criterions for head and water budget (SEAWAT parameters "hclose" and "rclose", see Table B-1) are defined to terminate a SEAWAT model simulation in case these convergence criterions are met. Note that since the total number of SEAWAT models is rather high (1116), some ARPs span over a large area (more than 200km) and a complex geological system is implemented, it can happen that some SEAWAT models do not meet this criterion within the defined time span of one full glacial-interglacial cycle (125ka) and individual stress periods. One of the reasons why this numerical convergence is not achieved is potential head or concentration value oscillation in an individual model cell.

The second convergence criterion type is set up for this study to evaluate the change in groundwater salinity in the model domain over a stress period of 1000 years; as to assess the system inertia we need to know when the groundwater salinity distribution has reached its dynamic equilibrium. The stress period is further divided into 10 time periods of 100 years delimiting the time points at which a groundwater salinity (and groundwater head) profiles are extracted. Next, the difference between two consecutive time steps is computed, both in absolute volumes of fresh water (model cells with fresh groundwater concentration count) and in the maximum absolute change in concentration (and head elevation) across the whole model domain of the ARP. The model is marked as converged if the maximum absolute change in both groundwater salinity and head is lower than 0.05 g TDS/L and 0.05m respectively. In cases when this condition is not satisfied, assuming mainly due to numerical oscillations in head or salinity, the secondary convergence criterion is examined since the changes in the groundwater salinity distribution over the whole model domain can be negligible. If the change in fresh groundwater volume is lower than 300m^3 per stretched meter, taking into account porosity (0.3) and total volume of one model cell (1000m^3) over the 1000-year long stress period, the secondary convergence criterion is said to be reached. If either of these two criterions is reached the current stress period simulation is terminated and the next one is started. Combining these two criterions allows us to potentially save computation times when at least on is reached. Also, it assures the certainty of model simulation results by measuring the changes throughout the model simulation in groundwater concentration and heads.

3.2.5.6 Comparison of two modelling concepts to estimate OFGVs under geological uncertainty

Two concepts of modelling and estimating OGVs under geological uncertainty are tested and compared to examine if it is possible to estimate OFGVs using only extreme geological heterogeneity parameter values (Parameter Extremes, PE) compared to results of completely randomized Monte Carlo approach (MC). The underlying reason for comparison is to save computation time considering that the large number of model cells, the long integration times and the high total number of SEAWAT model simulations all leading to high model runtimes. The geological parameters whose value are varied across SEAWAT model simulations of both concepts are the aquifer-aquitard layer combinations, clay layer stacking factor, clay layer start and offshore clay cap thickness (exact values provided in Table B-2). In the first concept only the PE combinations are used as input to the geological heterogeneity algorithm (see Sections 2.4.2 and 2.5.1) leading to a total 24 SEAWAT model simulations. The second modelling concept randomly selects a value within each parameter's boundary values and creates a randomized MC parameterization set of 100 SEAWAT model simulations.

The total offshore fresh groundwater volume V_{total} (km^3) is calculated as:

$$V_{total} = SB * D_{shelf} * L_{coast} * \frac{FGF_{mean}}{100} * p \quad (3\text{-}2)$$

where SB represents the continental shelf edge distance from the coastline (km), D_{shelf} is the average sediment thickness in the continental shelf domain (km), L_{coast} is the length of the given coastal (ARP) type along the COSCATs coastline (km), FGF_{mean} is the mean estimated fresh groundwater fraction (FGF) for the COSCAT region (%) and p is the effective porosity (-). The FGF_{mean} value is determined by averaging the fraction of fresh groundwater cells in the shelf domain as simulated by all individual SEAWAT models for each selected COSCAT region. The FGF is thus calculated as the total number of model cells with fresh groundwater concentration over the total amount of model cells in the shelf zone. Dividing the total estimated volume V_{total} by the coastal length L_{coast} allows for calculating the offshore fresh groundwater volume per kilometer of coastline as $V_{stretch} = V_{total} / L_{coast}$.

The two concepts are tested on the average estimated OFGV in the inland and offshore domains. The averaging process leading to analysis schematization of the final modelling result is shown in Figure 3-6, and displays the total average and range of the FGFs through time with varying sea-levels. This comparison is performed for the selected set of seven COSCAT regions (resulting in nine ARPs) where offshore fresh groundwater presence was proven by Post et al. (2013), see Figure 3-4. This also serves as an additional validation procedure to gauge the fit of our modelling results.

3.3 Results

3.3.1 Characteristics of regional CUGS

3.3.1.1 Global geological heterogeneity parameterization

The overall results for each individual geological heterogeneity parameter simulated as part of the global geological heterogeneity parametrization are shown in Figure 3-7. Quantitative estimations for seven selected sample COSCAT regions (total of nine ARPs) are provided in Table 3-2. A closer look at Figure 3-7 reveals that a large majority of global continental shelves is either aggrading (represented by a medium aquitard patchiness value) or forced regressive (high aquitard patchiness value). As explained in Section 2.3, this has to do with the sedimentation/accommodation ratio (Y). Cases where accommodation is larger than sediment supply occur mainly in the arctic shelves or in areas with no large rivers. Conversely, continental shelves in regions with high sediment supply via a large river and low subduction rate tend to have a high sedimentation/accommodation ratio value.

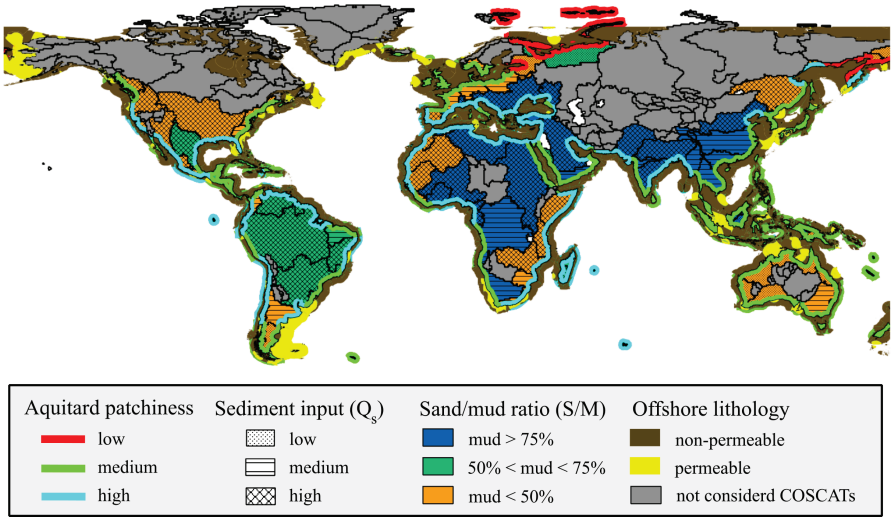

Figure 3-7 Geological heterogeneity parameterization results for COSCAT regions with CUGS present.

Table 3-2 Global geological heterogeneity parameter estimation for the seven selected sample COSCAT regions (Figure 3-4). Descriptions of the coastal types is schematized in Figure 3-2.

COSCAT name (ID)	***Coastal type***	***Sand [%]***	***Y [%]***	***Qs [-]***	***Avg. model domain thickness [m]***			***Avg. % fresh shelf***
					Inland	**Shelf**	**Offshore total**	
Niger Basin (0016)	S	30.0	31.0	high	120.0	350	310	27.5
	I	30.0	31.0	high	90.0	240	320	65.2
Suriname (1103)	A	47.0	27.3	high	330.0	570	580	26.4
Perth Basin (1413)	IS	54.0	1.1	small	100.0	200	350	69.9
Oman (1343)	IS	34.0	10.4	medium	120.0	300	170	40.5
Japan Trench (1322)	D	39.0	9.2	medium	250.0	420	350	84.3
	IS	39.0	9.2	medium	160.0	210	230	84.9
North Sea (0403)	A	57.5	24.3	medium	140.0	260	260	34.4
Nantucket, NJ (0827)	IS	83.8	6.5	small	300.0	600	670	59.7

Regions with high sediment supply into the continental shelf can be characterized by a large hinterland area with high relief and/or high temperatures. These attributes increase the chances of progradation, aggradation and thick strata deposition over the coastal plain and continental shelf domains. Such conditions can be found in e.g., the Mississippi River delta, Amazon River delta, Yellow River delta, the North Sea, the Black Sea to just name a few. Similarly, to the sedimentation/accommodation ratio, the opposite conditions (small hinterland area, low relief and/or low temperatures) lead to small sediment supply rates which in turn cause low chances of progradation, aggradation and thick strata deposition (e.g., most of Australia).

The sand/mud composition ratio provides an insight into the potential presence of thick and numerous aquitards interlaying the aquifers. Most temperate and arid areas show high sand/mud composition ratio values while tropical regions or regions at active tectonic margin tend to have low sand/mud composition ratio values, as can be observed in Figure 3-7. In the offshore domain, most continental shelves and slopes are covered by non-permeable sediments and only a scattered set of areas worldwide is overlaid by permeable sandy sediments; this is assumed to increase the possibility for OFGV occurrence.

3.3.1.2 Synthetic heterogenic coastal unsaturated groundwater systems (CUGSs)

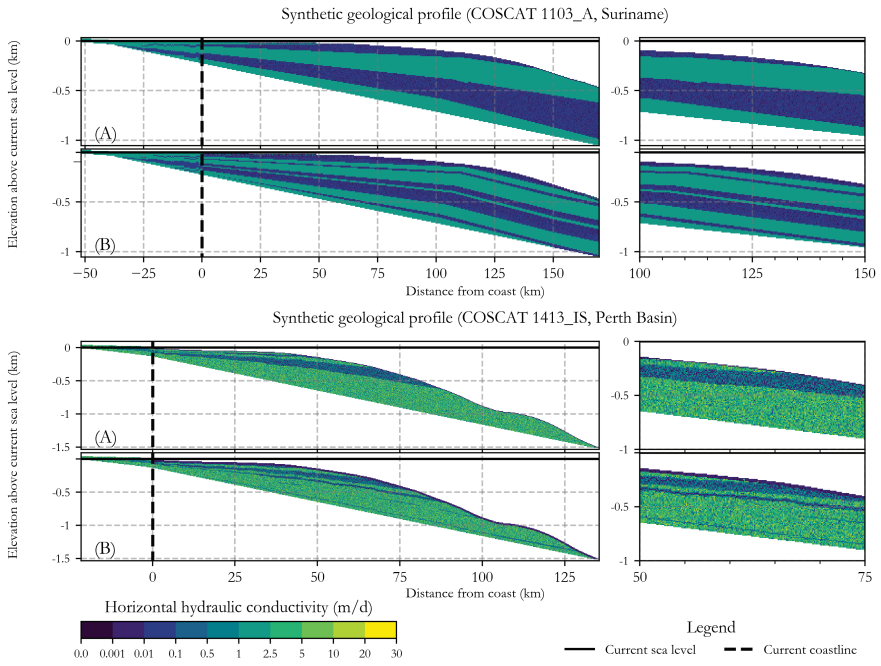

Figure 3-8 Examples of synthetic heterogenic coastal unconsolidated groundwater systems (CUGS) created using the geological heterogeneity algorithm described in paragraph 2.4.2. Randomly generated system with (A) two low and high stand layer combinations and (B) five such layers is presented for each of the two COSCAT regions considered in this example.

Figure 3-8 shows a set of synthetic heterogenic CUGSs created using the geological parameters described above. Sediment layer progradation is observed in COSCAT region 1103_A (Suriname, high sediment flux) and is recognizable by preservation of past continental shelf edges and change of the sediment layer slope in the offshore domain (Groen et al., 2000; Kooi and Groen, 2003). On the contrary, in areas with low sediment supply such as COSCAT 1413_IS (Perth Basin), the progradation effect is absent and individual sediment layers have constant slope over the whole offshore domain.

The hydraulic conductivity values are based on the GLHYMPS (Gleeson et al., 2014) and GUM (Huscroft et al., 2018) values randomly selected for each model cell based on their lognormal distribution in each selected COSCAT region. Therefore, in certain COSCAT regions the hydraulic conductivity pattern can appear grainy if the standard deviation of the lognormal distribution is high (e.g., like COSCAT 1413_IS).

3.3.2 Comparison of two modelling concepts to estimate OFGVs under geological uncertainty

In this Section we analyze the effects of the two modelling concepts on the simulated averaged groundwater salinity profiles and resulting fresh groundwater fractions (FGFs) and OFGVs. This analysis is performed over various stretches of the SEAWAT model domain (inland, continental shelf and whole offshore domains) and by investigating the change in groundwater salinity over time (e.g., through an analysis of the system inertia).

3.3.2.1 Fresh groundwater fractions (FGFs) in coastal zones

The inland domain is entirely composed of fresh groundwater (drinking water, <0.5 g TDS/L) in most models within the selected set of seven COSCAT regions, coastal (ARP) types and modelling concepts. The difference between the outcomes of the two modelling concepts in the inland domain is thus negligible. However, larger differences in mean estimated FGFs between the modelling concepts can be found in the continental shelf domains. The difference exceeds 10% in only one third of the cases while maximum difference is 20.5% (COSCAT 403, North Sea region). A similar trend is observed for estimates regarding the FGFs in the whole offshore domain (only one region has difference larger than 10%). Even in cases with larger differences in mean estimated values, the standard deviations are relatively large and mostly overlap each other suggesting a reasonably good fit (e.g., COSCAT region 403_A in Figure 3-9, exact values in Table B-3). The estimated FGFs for the selected COSCAT regions and their respective ARPs are given in Table B-3.

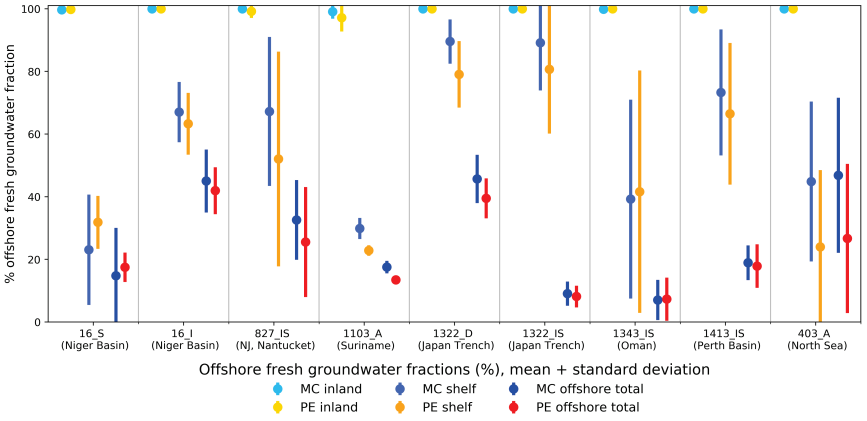

Figure 3-9 Estimated mean and standard deviation present-day offshore FGFs for both modelling concepts and the seven selected COSCAT regions and their respective coastal types considered.

Overall, the averaged estimated FGFs for continental shelf domains suggest that in most regions there is a high probability of substantial fresh offshore reserves ranging from the lowest value of 22.8% (COSCAT 1103, Suriname) to the highest of almost 90% (COSCAT 1322, Japan Trench). The low FGF estimated for COSCAT 1103 region can be explained by a lengthy continental shelf domain that is largely filled with saline water, see Figure 3-10. The estimated average groundwater salinity distributions show no large differences between the two modelling concepts outcomes except wider brackish zones suggested by the MC model outcome. This is probably due to a larger number of model realizations using MC leading to higher variability across individual groundwater salinity profiles.

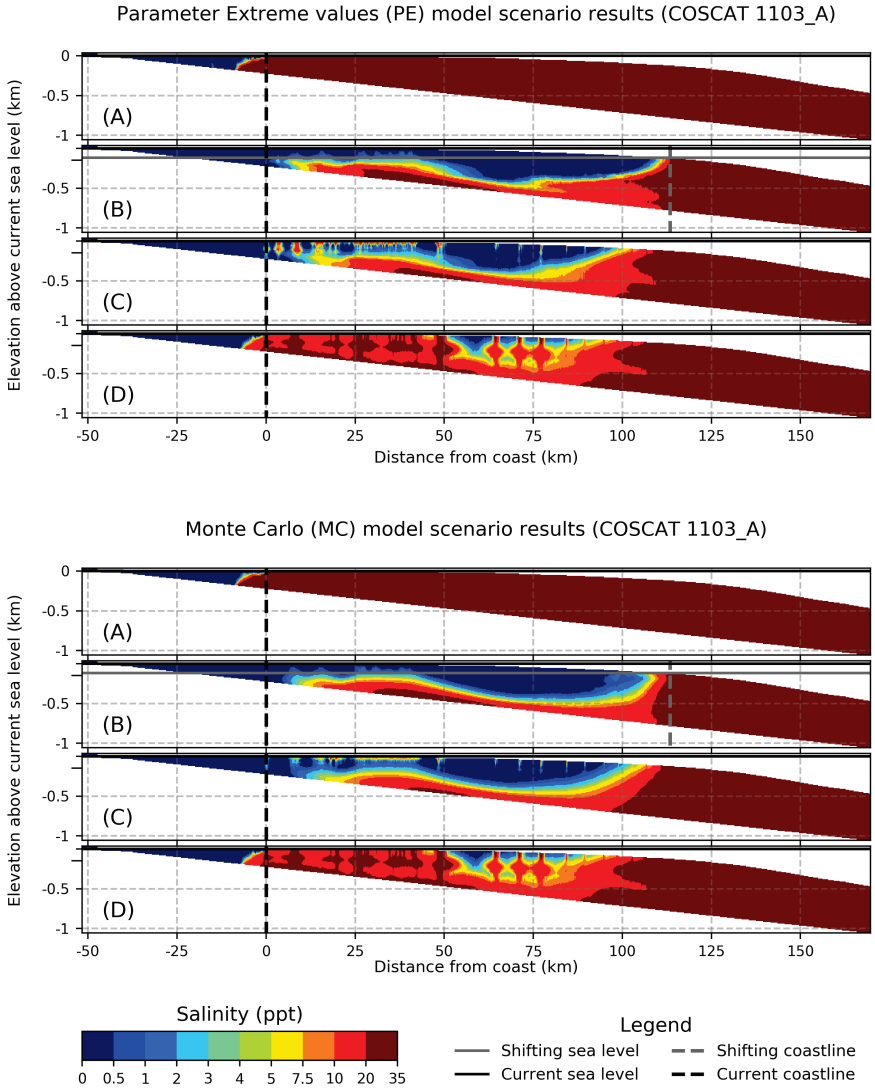

Figure 3-10 Averaged groundwater salinity profiles for both modelling concepts at four timeframes for COSCAT 1103_A region (Suriname). The estimated groundwater salinity in the 2D profiles is represented: (A) at the end of SP 0, groundwater salinity before fluctuating sea level SPs; (B) at the lowest sea level occurring at the end of the sea level drop represented by SP 21; (C) after the relatively fast sea level rise back to the current sea level at the end of SP 31; and finally (D) estimation of future conditions in 20 ka from present at the end of SP 31_DSP. The results of the other eight SEAWAT models is provided in Figure B-1.

3.3.2.2 Regional hydrogeological system inertia

Assessing the rate of change in the estimated groundwater salinity profiles provides an important insight into the behavior of regional CUGSs and OFGVs stored therein over time. In such way we can better evaluate the non-renewability of the OFGVs. Figure 3-11 shows the evolution of mean (and standard deviation) FGF in the future 20ka assuming constant sea-level equal to the current situation (also other stresses remain the same). The predicted FGF trends of both modelling concepts are almost identical for all seven selected COSCAT regions showing a varying degree of gradual decline. The estimated mean FGF in the continental shelf domain eventually drops below 25% in all but one COSCAT regions (1322_IS), reaching almost zero values in five out of nine cases.

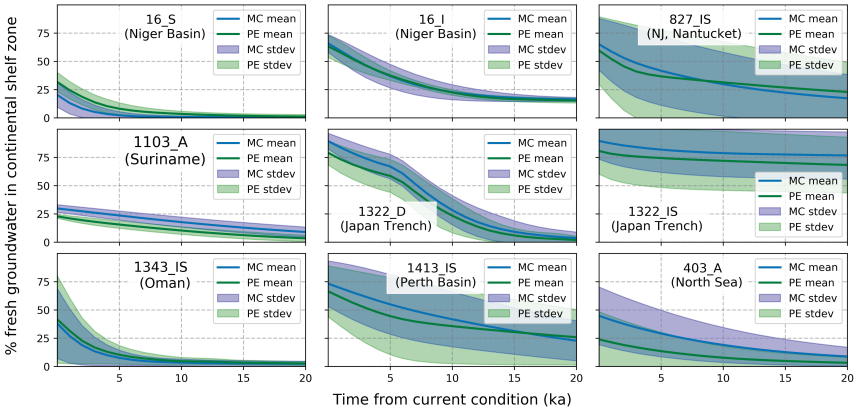

Figure 3-11 Estimated FGFs in the continental shelf domain for selected COSCAT regions (and respective coastal types) and both modelling concepts during the SP31_DSP time period. The current condition represents the estimated fractions at present time (here year = 0).

3.3.2.3 Model runtime difference between PE and MC

The average SEAWAT model runtime per one SEAWAT model simulation for all selected COSCAT regions is almost identical for both PE and MC model concepts (46 and 40 hours respectively). COSCAT region 827_IS has the highest average model runtimes for the two modelling concepts with 133 hours (PE) and 86 hours (MC). Two COSCAT regions show the lowest average model runtimes (both 16 hours) for the MC modelling concept (403_A and 1413_IS) and very close average runtime values for the PE modelling concept (12 and 10 hours respectively). Logically, the larger number of simulations in the MC modelling concept (100) to PE (24) leads to proportionally larger total model runtimes for all seven selected COSCAT regions. The total simulation time for all PE and MC models is 10031 and 35763 hours respectively. Final SEAWAT model runtimes (average and total) for all the selected COSCAT regions and ARPs are shown in Table B-4.

3.3.3 Influence of geological settings on offshore fresh groundwater fraction estimation

Out of the four geological parameters varied across the SEAWAT model simulations and both modelling concepts the thickness of the offshore clay cap layer has the most influence on estimate FGFs. SEAWAT model simulations with thicker offshore clay capping layers show above average (positive values on Y axis) estimated FGF values, see Figure 3-12. The second most influential parameter is the number of aquifer and aquitard layers present in the synthetic heterogenic CUGS. SEAWAT model simulations with lower count of these layer combinations display on average somewhat above average estimated FGFs. However, the trend is not explicitly apparent (Figure 3-12), since some of the simulations with lower number of aquifer and aquitard layers also show lower than average estimated FGFs. Variations of the other two geological parameters do not show any discernible influence on the estimated FGFs.

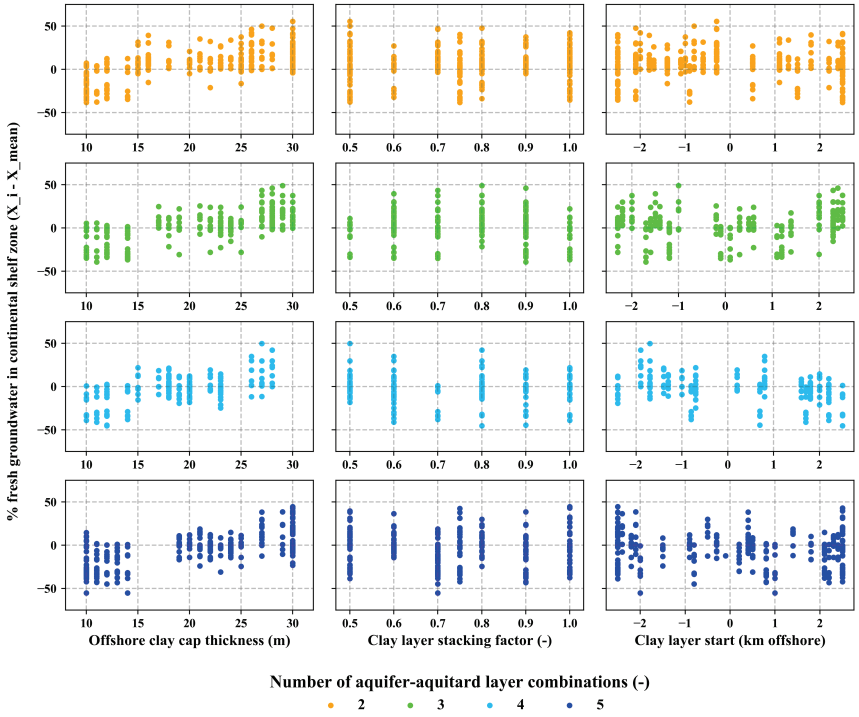

Figure 3-12 Influence of geological parameters on estimated FGFs (compared to mean value for each selected COSCAT region). Positive values correspond to SEAWAT models that estimate larger FGFs than average.

3.3.4 The estimation of offshore fresh groundwater volumes (OFGVs)

High estimated FGF values do not necessarily mean large OFGV as these depend largely on the physical dimensions of the COSCAT region and its corresponding ARP. Table 3-3 provides the values of the calculated fresh (and brackish) offshore groundwater volume for the selected COSCAT regions and shows that some areas can contain several tens of thousands cubic kilometers of fresh groundwater in the continental shelf domain (i.e., East coast USA: New Jersey and Nantucket subregions). The fraction and corresponding volume of brackish water was calculated in the same manner as FGF and OFGV values but with different span of salinity concentration (0.5 to 10 g TDS/l).

Table 3-3 Estimated offshore fresh (and brackish in brackets behind the OFGV value) groundwater volumes for the seven selected sample COSCAT regions (and respective coastal types); p = effective porosity (-). Comparison with OFGV values (and site-specific effective porosity values) given by (Post et al., 2013) for corresponding two COSCAT regions.

COSCAT name (ID)	Coastal type	Shelf edge distance (km)	Average thickness shelf (km)	Length of coast (km)	Avg. % fresh shelf (brackish)	p	OFGV (brackish), this paper		OFGV Post et al. (2013)
							(km^3)	(km^3/km)	(km^3/km)
Niger Basin (0016)	S	24.5	350	1750	27.5 (19.8)	0.3	1236.7 (889.1)	0.7 (0.5)	-
	I	43.6	240	1200	65.2 (8.9)	0.3	2455.2 (335.6)	2.0 (0.3)	-
Suriname (1103)	A	112.8	570	2850	26.4 (37.4)	0.3	14485.4 (20559.9)	5.1 (7.2)	6.3 (with p=0.3)
Perth Basin (1413)	IS	39.5	300	1500	69.9 (13.0)	0.3	3726.9 (694.3)	2.5 (0.5)	-
Oman (1343)	IS	10.0	200	1000	40.5 (9.1)	0.3	242.7 (54.4)	0.2 (0.1)	-
Japan Trench (1322)	D	28.0	420	2100	84.3 (12.6)	0.3	6246.4 (930.5)	3.0 (0.4)	-
	IS	13.1	210	1050	84.5 (7.6)	0.3	732.2 (66.2)	0.7 (0.1)	-
North Sea (0403)	A	187.6	260	1300	34.4 (17.0)	0.3	6548.5 (3235.8)	5.0 (2.5)	-
Nantucket, NJ (0827)	IS	104.1	600	3000	59.7 (5.2)	0.3	33534.5 (2900.6)	7.5 (1.0)	4.8 (with p=0.2)

3.4 Discussion

In our study, we adapt and combine a geological heterogeneity algorithm with a collection of global datasets showing that it is possible to successfully estimate first-order quantifications of the global geological heterogeneity of regional CUGSs. This involves derivation of various geological parameters and their subsequent application in generating synthetic profiles (ARPs) allowing heterogenic CUGS simulations. The ARPs then serve as hydrogeological schematizations in SEAWAT models which compute variable-density groundwater flow with coupled salt transport. Further implications and hypotheses are discussed in more detail in the sections below.

3.4.1 Estimating global CUGS geological heterogeneity

The three derived and quantified geological parameters (aquitard patchiness, sand/mud composition ratio, sediment supply (Figure 3-7) provide a satisfactory geological classification of CUGS worldwide. This parameterization is a first step to quantify geological heterogeneity of CUGS and can be directly used as input to large-scale hydrogeological (e.g., SEAWAT) models. However, despite the auspicious outcome of our study, feeding relatively simple conceptual models dealing with continental shelf architecture by available global datasets requires simplifications and assumptions since some information is still not available on such a large-scale.

Major simplifications are made in establishing the relative sea-level change rate which can have an impact on estimated accommodation factor (see Eq. 3-1) by assuming a constant average absolute sea level globally (Pirazzoli, 1997). By implementing a sea-level fluctuation over multiple glacial-interglacial cycles and taking into account regional variations in sea levels it would be possible to indicate shelves where either amplified (far from ice sheets) or subdued (near to ice sheets) sea-level low stands occur leading to i.e., arguably more accurate dispersion modifier estimation. Furthermore, improving the accuracy of the thermal subsidence and compaction values could improve the geological estimation outcome in shelves positioned on lithosphere older than 70 Ma and in relatively thin sediment successions (compaction). Expanding the spatial and temporal knowledge on sediment accumulation on continental shelves beyond the areas investigated by Walsh and Nittrouer (2009) would lead to an improved accuracy of the dispersion modifier assessment. This would help to account for situations where not all sediments discharged from the continents accumulate on the shelf. Additional improvements can be achieved by accounting for changes in climate and drainage area size over the time period instead of assuming constant conditions as in the current state of the geological model.

3.4.2 SEAWAT modelling of OFGVs

Combining the estimated geological heterogeneity parameterization results with the developed modelling concepts describing the geological structure of coastal areas formed by unconsolidated sediments. This allows us to build synthetic hydrogeological CUGSs represented as interlaid aquifer-aquitard layer combinations. Nevertheless, there are still

several parameters that are to be estimated to improve the accuracy of simulating regional scale CUGS in the coastal zones. This would have required a large data collection effort of geological boreholes and hydrogeological profiles that is beyond the scope of this study. Performing this data collection could extend the use of the hereby presented approach to build more detailed local scale hydrogeological models, as in the current state, the average representative profile (ARP) methodology is fit only for regional scale applications.

Our SEAWAT modelling approach consisted of setting up two modelling concepts to deal with geological uncertainty to investigate the temporal variation in groundwater salinity profiles and potential presence of OFGVs in seven selected COSCAT regions. The idea to achieve comparable estimation results with lower numerical proved successful. This result gains further significance when we take into account that we only selected seven COSCAT regions (= nine ARPs) out of 127 for our geological heterogeneity parametrization study. Approximately 508,000 computation hours would be necessary if one would extend the MC modelling concept to the rest of the COSCAT regions (see Geological Heterogenic Parameterization COSCAT regions in Figure 3-4). This is a significant difference compared to 140 208 computation hours with the PE modelling concept that results in similar simulated OFGVs.

Our SEAWAT model simulations for the seven selected COSCAT regions (apart from Figure 3-10, see Figures B-1 to B-8 for eight other salinity profiles) show that there are potentially large offshore fresh groundwater volumes stored in continental shelves worldwide as suggested by Post et al. (2013). Accounting for different coastal types shows that the presence and magnitude of these OFGVs can vary within a single COSCAT region. The non-renewability and potential short-term presence (from a geological point of view) of these OFGVs is demonstrated by extending the SEAWAT models beyond the present timeline (by 20ka), see Section 3.2.2. In our approach, we assessed the diminishing trend of OFGV by maintaining the current sea-level (0m asl) over a period of 20ka showing a rapid decline (from a geological point of view) in FGFs in the continental shelf domain in most selected COSCAT regions (Figure 3-11).

Considering a time scale stretching over more than one full glacial-interglacial cycle (> 125ka) allows us to simulate the effect of sea-level change on the estimated groundwater salinity profile. Leaving out overwash events has negligible impact on the simulated OFGVs because the temporal impacts of these events on the groundwater salinity are likely limited to decades (Yu et al., 2016) which is beyond the temporal resolution of our SEAWAT modelling approach. However, these events can have a relatively large influence on the inland domain of the local groundwater salinity profiles (Michael et al., 2016; Yang et al., 2018) and should be considered when building local models with higher temporal resolution. The influence of rivers on groundwater recharge in the inland part of the model domain was also omitted in our study. This potentially leads to higher groundwater fluxes in the seaward direction and over-estimation of OFGVs. However, we believe that this issue is compensated by limiting the recharge rates to hydraulic conductivity values of the upper most model cells. Furthermore, implementing rivers into cross-sectional 2D groundwater flow models is highly uncertain and untested and realizing that is well

beyond the scope of this study. Additionally, given the large climate changes that occurred during the last glacial-interglacial period (e.g. Fleitmann et al., 2003), including a more detailed paleo precipitation (and thus groundwater recharge) estimations could increase the accuracy (and reliability) of our OFGVs estimations.

While analyzing the influence of geological settings on OFGVs we found that only one geological parameter (out of four) has discernible effects on the simulated groundwater salinity distribution. The presence and thickness of offshore clay cap layer in the continental shelf and/or continental slope domains shows the largest influence on the groundwater salinity distribution. Groundwater systems with thicker offshore clay cap layers show larger FGFs in the continental shelf domain, suggesting fresh groundwater deposition during sea-level low stand period and subsequent shielding this off from mixing with infiltrated sea water through the offshore clay cap layer deposited shortly afterwards. This implies that large non-renewable OFGVs can be trapped under such (very) low permeable clay capping layers deposited on the ocean floor during a sea-level low stand period. The number of preserved aquifer-aquitard layer combinations, deposited during low and high stands respectively, also influences the simulated groundwater salinity in the 2D profiles. Arguably, groundwater systems with a higher number of such sequences tend to have thinner or discontinuous aquitards that allow for easier vertical saltwater intrusion with rising sea-levels as shown by (Kooi et al., 2000; Kooi and Groen, 2003, 2001; Post et al., 2013).

The OFGVs expressed as per stretch kilometer of coastline are compared with values reported by Post et al. (2013) in two sample COSCAT regions. In the Suriname continental shelf domain our OFGV estimate amounts to 5.1 km^3/km (compared to 6.3 km^3/km reported by Post et al. (2013)) and 7.5 km^3/km (compared to 4.8 km^3/km reported by Post et al. (2013)) in the New Jersey and Nantucket continental shelf domain. The total volumes of potentially usable groundwater (e.g., also for desalination purposes) further increase if we take into account the potential use of brackish water, see Table 3-3. In the case of New Jersey and Nantucket continental shelf domain, our modelled OFGV is overestimated by roughly 30% compared to the reported value by Post et al (2013). This could be due to constant porosity value applied in our SEAWAT models (0.3), which in this case is one third higher than the porosity reported by Post et al. (2013) amounting to 0.2. However, changing porosity values could also lead to a different estimated salinity distribution and assuming a linear change in OFGV while varying the porosity parameter is an oversimplification. This discrepancy further stresses the importance of additional geological inputs to improve the performance of the methodology presented in this study. This discrepancy further stresses the importance of additional geological inputs to improve the performance of the methodology presented in this study. Even though in our study we purely focus on OFGVs occurrence, similar conceptual models could be applied to investigate the effects of other stress factors on fresh groundwater resources in coastal zones (e.g., increased human extraction rates, climate change effects including future sea-level rise and groundwater recharges and possible mitigation strategies like aquifer storage and recovery). This can help regional water management bodies to investigate the

possibility of tapping the OFGV to be then used as a potential supplementary supply of fresh water or as feedwater to desalination plants.

3.5 Summary and conclusions

The need for a better understanding and definition of heterogeneous coastal hydrogeology at the global scale is addressed in this study by combining various conceptual geological models with state-of-the-art freely available global datasets. The combination of these is used as input into the global geological heterogeneity algorithm. Even though only three geological parameters are explicitly quantified (another four need to be randomized) we show that adequate information is provided to create synthetic heterogenic CUGSs.

These synthetic heterogenic CUGSs are used as input to SEAWAT models (using the SEAWAT code), simulating variable-density groundwater flow and coupled salt transport. The SEAWAT models estimate fresh groundwater fractions (FGFs) and offshore fresh groundwater volumes (OFGVs) over the past glacial-interglacial cycle and extending to the near future. Thus, we are able to estimate the magnitude and future decrease of OFGVs in seven selected COSCAT regions. Comparing the estimated OFGVs with literature values for the selected COSCAT regions shows a potential for expanding the hereby presented methodology to the rest of coastal COSCAT regions worldwide (being 127 in number). By extending our approach to the global coastline, thus we would gain valuable insights into current and near future OFGV occurrence and magnitude in CUGSs. The analysis of the influence of geological settings on OFGVs shows that the presence and thickness of an offshore low permeable (e.g., clay) layer overtopping the more permeable offshore aquifers has the highest positive influence on simulated OFGV. Therefore, the focus of the geological data collection shouldn't be limited to the inland areas but should also include as many offshore locations as possible.

Four geological parameters could not be quantified within the scope of this study. To overcome this, two different modelling concepts were designed to randomize the values of these geological parameters for seven selected COSCAT regions (= nine ARPs). The first modelling concept only takes into account the extreme values of the geological heterogeneity parameter values (PE) resulting in 24 SEAWAT models in total. The second modelling concept is based on a randomized Monte Carlo (MC) randomization of the geological heterogeneity parameter values and amounts to 100 SEAWAT models. The average groundwater salinity profiles calculated by these two modelling concepts showed to yield very similar results. This means that using the PE-method to estimate averaged regional OFGVs results in a 75% reduction in total SEAWAT model runtimes, while maintaining the same degree of confidence in the model outcome as when conducting a full Monte Carlo simulation. This is an important implication for future global and large regional modelling studies dealing with missing geological information on such large scales. Collecting local coastal geological data (e.g., borehole datasets) and implementing these into the conceptual geological model would be a logical next step in clearing the

path to a better understanding and quantification of global hydrogeological heterogeneity, leading to improved water management strategies and decision making. The hereby presented new dataset and methods can be applied on a regional scale (tens to hundreds of kilometers) to investigate the effects of geological heterogeneity in coastal unconsolidated systems on offshore fresh groundwater volumes presence and to quantify their magnitude.

Acknowledgements

This research was partially funded by the Netherlands Organization for Scientific Research (NWO) and the Ministry of Infrastructure and Water Management under TTW Perspectives program Water Nexus (project no. 14298). *We thank anonymous reviewers for their thorough reading and comments that have considerably improved the quality of this paper.* The modelling study was carried out on the Dutch national e-infrastructure (HPC Cartesius) with the support of SURF Cooperative.

4 Offshore fresh groundwater in coastal unconsolidated sediment systems as a potential fresh water source in the 21st century

Abstract

Coastal areas worldwide are often densely populated and host regional agricultural and industrial hubs. Strict water quality requirements for agricultural, industrial and domestic use are often not satisfied by surface waters in coastal areas and consequently lead to over-exploitation of local fresh groundwater resources. Additional pressure by both climate change and population growth further intensifies the upcoming water stress and raises the urgency to search for new fresh water sources. In recent years, offshore fresh groundwater reserves have been identified as such a potential water source. Here, we quantify, for the first time, the global volume of offshore fresh groundwater in unconsolidated coastal aquifers and show that it is a viable option as additional fresh water source in coastal areas. Our results confirm previously reported widespread presence of offshore fresh groundwater along the global coastline. Furthermore, we find that these reserves are likely non-renewable as they were deposited during glacial periods when sea-levels were substantially lower compared to current sea-level. We estimate the total offshore fresh groundwater volume in unconsolidated coastal aquifers to be approximately 1.06 ± 0.2 million km³, which is roughly three times more than estimated previously and about 10% of all terrestrial fresh groundwater. With extensive active and inactive offshore oil pumping present in areas of large offshore fresh groundwater reserves, they could be considered for temporary fresh groundwater exploration as part of a transition to sustainable water use in coastal areas on the long run.

4.1 Introduction

During recent decades, coastal communities settled along the global coastline have been subject to rising fresh water stress caused by both natural (Faneca Ŝanchez et al., 2012; Oude Essink et al., 2010; Rasmussen et al., 2013; Yang et al., 2018; Yu et al., 2016) hazards and anthropogenic (Giosan et al., 2014; Minderhoud et al., 2017; Syvitski et al., 2009; Tessler et al., 2015; Van Camp et al., 2014; Yamanaka et al., 2011) threats. It might appear that the onshore and offshore zones of the global coast are clearly defined and stable as sea level stayed relatively constant (Lambeck et al., 2014b) throughout human recorded history. However, this coastal boundary is in reality rather dynamic when considering a larger geologic time scale. Before around 20,000 years ago, during the Last Glacial Maximum, global mean sea-level was more than 120 m lower than current sea-level. As a result, extensive continental shelf areas, nowadays submerged under shallow seas, were exposed to terrestrial conditions for tens of thousands of years and hosted an environment full of rivers and fresh water lakes (Head and Gibbard, 2005). Under such circumstances, vast fresh groundwater volumes developed through precipitation (i.e., meteoric water), via increased fresh groundwater inflow from inland due to greater groundwater gradient and through extensive surface water systems covering the current continental shelf areas.

Following the first global overview of offshore fresh groundwater (OFG) (Post et al., 2013), which is based on numerous case studies since 1979 (Hathaway et al., 1979), several regional scale studies (Gustafson et al., 2019; Levi et al., 2018; Morgan et al., 2018; Thomas et al., 2019) have been conducted in recent years. It has been documented that OFG can be found tens or even hundreds of kilometers offshore while reaching depths of up to several kilometers. One of the most thoroughly studied and documented OFG occurrences is in the continental shelf off the New Jersey coast(Gustafson et al., 2019; Meisler et al., 1984; Thomas et al., 2019). An extensive data acquisition of both geological and geophysical data was combined with numerical groundwater flow modelling (Gustafson et al., 2019; Thomas et al., 2019) to quantify the OFG volume stored in the porous unconsolidated sediments deposited at the continental shelf. OFG can also be stored in fractured karstic rocks as has been documented in e.g. Western and South-eastern Australia (Morgan et al., 2018; Varma and Michael, 2011). The abovementioned studies show that OFG is often preserved under low permeable geological layers that limit vertical seawater infiltration. Furthermore, OFG can be a result of higher hydraulic gradients driving fresh groundwater flow from inland areas into the continental shelf due to low permeable layers preventing near shore discharge (Paldor et al., 2020). These complex heterogeneous geological systems are found in both unconsolidated and karstic systems, stressing the need for a variety of geological information sources to successfully reconstruct regional offshore groundwater conditions.

Here, we combine global thickness estimates (Zamrsky et al., 2018) and geological heterogeneity assessments (Zamrsky et al., 2020) of unconsolidated sediment systems with variable-density groundwater flow and coupled salt transport modelling to estimate OFG volumes of the global coast (Chapter 4.2 and Figure C-1). Our study is solely focused

on unconsolidated sediment systems, due to the lack of globally available data and the high variation in local characteristics of karstic systems (Chen et al., 2017) (e.g. their complex conduit networks). Thus, when referring to global OFG volumes we refer to those in unconsolidated coastal aquifers only. In estimating OFG volumes, we divided the global coastline into 116 regions linking inland sediment sources with coastal and offshore sediment sinks (Laruelle et al., 2013; Meybeck et al., 2006) to capture global geological differences. For each region, we analyze 24 likely geological scenarios to capture unknown variation in regional geological heterogeneity (Chapter 4.2 and Figure C-2). In these geological scenarios, which are informed by regional sediment influx and size upstream from the coast and by preservation potential of coastal sediments, we vary the thickness and number of low permeable (aquitards) and highly permeable (aquifers) sediment layers and their shape in the offshore domain (Zamrsky et al., 2020). These regional geological scenarios, alongside other hydrogeological parameters (elevation, groundwater recharge estimation), are used for quantifying regional OFG volumes and their uncertainty by means of cross-sectional 2D variable-density groundwater flow and coupled salt transport models (called "groundwater models" hereafter; Figure C-3). The temporal resolution of our numerical models covers the sea-level fluctuation over one full glacial-interglacial cycle (Grant et al., 2012) (approx. 125,000 years). This allows us to simulate past fresh water infiltration into the aquifers and aquitards that make up the present-day continental shelves during sea-level low stands, and the subsequent salinization of fresh groundwater resources, or their preservation under less permeable clay deposits, during fast rising sea levels in the past 20,000 years (Lambeck et al., 2014b). Averaging the modelled groundwater salinity concentration results for all 24 geological scenarios for each of the 116 coastal regions then yields an estimate of an OFG volume per coastal region and its uncertainty. Herein, we measure salinity as total dissolved solids (g/l TDS) with fresh groundwater threshold defined as 1 g/l TDS which is the upper limit considered acceptable to consumers, as defined by World Health Organization (World Health Organization, 2017).

4.2 Methodology

4.2.1 Regional representative coastal groundwater flow models

The global analysis approach in our study consists of dividing the global coast into regions with similar geological characteristics. This is based on the assumption that coastal zones act as sinks for sediments transported downstream by rivers. These unconsolidated sediments are deposited both onshore, forming so called coastal plains, and offshore, on top of the continental shelves. Splitting up the global coast is based on the COSCAT (Meybeck et al., 2006) and MARCAT (Laruelle et al., 2013) datasets that define the sediment sources and sinks respectively. Combining these two datasets allows us to define regions with similar geological characteristics and to implement the geological heterogeneity quantification and geological scenario algorithm to create regional groundwater representations in each individual region. We refer to previous research

(Zamrsky et al., 2020) for an elaborate description of this approach and provide a summary below.

Equidistant cross-sectional profiles perpendicular to the coastline are constructed in areas formed by unconsolidated sediments in each coastal region (COSCAT) (Figure C-1A). These regions are outlined by using the Global Lithological Map (Hartmann and Moosdorf, 2012) (GLiM) dataset describing surficial lithology on global scale. Various attribute values are extracted along each profile (i.e. topography (Weatherall et al., 2015), bathymetry (Weatherall et al., 2015), long term average actual evapotranspiration and precipitation (NTSG, 2019), hydraulic conductivity (Gleeson et al., 2014; Huscroft et al., 2018), soil type (Montzka et al., 2017) and thickness (Hengl et al., 2014), water table depth (Fan, 2013)). Two coastal types are defined to take into account variations in topography and aquifer-aquitard system thickness. A "delta" coastal type represents major deltaic systems (Tessler et al., 2015) which likely have a wider (and thicker) coastal plain and continental shelf than the other profiles in the same region due to higher sediment input transported by rivers. Coastal types that are located in non-deltaic regions are named "coastal stretch" and represent the vast majority of coastal profiles considered in this study.

An average representative profile (ARP) is built for each coastal type / COSCAT region combination which delineates its average geometrical conditions (topography and sediment depth) (Figure C-1B). To this end, all topography and bathymetry profiles are combined first to create the upper ARPs boundary. Next, after defining the current coastline position, an average thickness of the unconsolidated groundwater system is calculated and set as depth of the ARP at the coastline. In the following step, the continental shelf edge is identified as well as the foot of continental slope using a bathymetry slope algorithm (Wu et al., 2017), which requires elevation as main input. When the foot of continental slope is successfully estimated, the bottom boundary of the offshore domain is defined as a line between the unconsolidated groundwater system depth at coastline and the foot of continental slope. If continental slope is not found (e.g., in case of shallow bathymetry stretching far offshore), the offshore extent of the ARP is limited to 200 km and the bottom boundary is set to follow the average bathymetry slope of the offshore domain.

4.2.2 Geological heterogeneity of unconsolidated groundwater systems

The geological heterogeneity of unconsolidated groundwater systems is used as input into the groundwater models is based on a method developed in Zamrsky et al. (2020); the text below provides a brief summary of this method**.** Once the outer boundaries of an ARP profile are defined, we proceed with the hydrogeological settings conceptualization (Figure C-1B). Regional-scale geological heterogeneity quantification and simulation algorithms (Zamrsky et al., 2020) are used to create a set of 24 geological scenarios for each ARP (coastal type / COSCAT region combination). The geological heterogeneity quantification (Zamrsky et al., 2020) provides an estimate of a so-called sand/mud composition ratio (R), sediment flux rate (Qs) and aquitard patchiness (Ap). These factors

define the shape and inner architecture of individual aquifer and aquitard layers. The total subsurface fraction occupied by aquifer material (sand) and aquitard layers (clay) is directly determined by the R ratio. These fractions are used to divide the total ARP thickness into total aquifer and aquitard thicknesses. The offshore shape of these aquifer-aquitard layers depends on the Qs factor. Individual sediment layers (both aquifer and aquitards) overtop each other completely in regions with medium to high Qs, leading to a shape with distinct past continental shelf edges (Figure C-1B). Figure C-2 shows examples of the medium to high sediment flux geologies. In the case with low Qs factor values, there is not enough sediment flux to accommodate the total overtopping of older sediment layers. This leads to a horizontally layered inner architecture in the offshore subsurface domain (Zamrsky et al., 2020). The Ap factor represents erosion forces that (both oceanic and fluvial) that remove part of clay sediments deposited during higher sea-level stands. Applying this factor removes a specified fraction of clay model cells which are randomly selected, in such way we can simulate creation of local conduits in otherwise homogenous low permeable layers. The last fixed geological heterogeneity parameter is the presence or absence of low permeable clay capping layers laying on top of the ocean floor (both for the continental shelf and slope areas), which is derived from a global ocean floor lithology dataset (Dutkiewicz et al., 2015).

Due to missing information about their regional values, the remaining factors that determine geological heterogeneity need to be varied over plausible ranges. The number of aquifer-aquitard combinations is determined based on literature review (Zamrsky et al., 2020) and in this study we use the most common lower and upper values of number of aquifer-aquitard combinations (2 and 5 respectively). The number of aquifer-aquitard combinations is then combined with the ARP-specific aquifer and aquitard thicknesses (see the abovementioned paragraph) to randomly generate the thickness of individual aquifer and aquitard layers. Parts of the aquitard layers, corresponding to the mud composition ratio, are then filled with low permeable model cells with clay hydraulic conductivity properties (values varying between 0.01 and 0.0001 m/d). The number of clay model cells corresponds to the mud fraction of the R factor and each individual aquitard layer is then filled with the respective number of clay model cells. We use a so-called stacking factor to guide the vertical position of these clay model cells within the aquitard layers. Higher stacking factor values lead to higher probability that these cells will be located in the upper part of the aquitard layers, mimicking a stronger fining upward sequence, and therefore resulting in less permeable aquitards. The clay model cells are inserted at a maximum distance from the current coastline (-2.5 or 2.5 km) to take into account the potential effect of lower leakiness of the aquitard layer directly in the coastline zone. Once all the clay model cells have been assigned, we apply the Ap factor to simulate erosion forces and in such way remove parts of the clay model cells, thus increasing the leakiness of the aquitard layers. Implementing this procedure simulates fine sediment deposition during past sea-level high stands when river gradients were lowest leading to finest sediment grain size. Low permeable clay model cells are also implemented to offshore clay capping layers (Figure C-1B). The regional values of the thickness of these capping layers are also unavailable on global scale and therefore set to

either 10 m or 30 m, which provides enough thickness variation to simulate different clay cap layer leakiness levels.

4.2.3 Variable-density groundwater flow and coupled salt transport modeling

A set of variable-density groundwater flow and coupled salt transport models (referred to as "groundwater models" hereafter) is built for each ARP (coastal type/COSCAT region combination) (Figure C-3) in order to estimate groundwater salinity profiles. The hydrogeological schematization of each profile is following the fixed geological conceptualization resulting from the sand/mud composition ratio (R), sediment flux rate (Qs). Hydraulic conductivities of the aquitards and aquifers for each ARP are obtained from the GLHYMPS (Gleeson et al., 2014) and GUM (Huscroft et al., 2018) datasets respectively. The uncertainty of the remaining heterogeneity parameters, e.g., number of aquifers/aquitards (2 or 5), hydraulic conductivity clay model cells (between 0.01 and 0.0001), the stacking factor (0.5, 0.75, 1.0) and the clay cap thickness (10 or 30 m), are taken into account by using scenarios using combinations of alternative values for each parameter. As a result, a total of 24 geological scenarios per ARP is generated. For each of these individual geological scenarios one groundwater model simulation is carried out. This number of 24 groundwater models is shown to yield almost identical mean estimated groundwater salinity profiles (Zamrsky et al., 2020) (mean of all 24 scenarios) as a more extensive set of 100 groundwater models (viz. hundred randomized geological scenarios) while reducing simulation time roughly four times.

The groundwater models are set up with the SEAWAT (Langevin et al., 2008) computer code, designed for variable-density groundwater flow and coupled salt transport modelling. All groundwater models are set up with a regular grid with layer thickness of 10 m, column width of 100 m and the "confined" SEAWAT layer type. The extent of the groundwater models can vary from several tens to more than two hundred kilometers. Longitudinal and transverse dispersivity values (1 m and 0.1 m respectively) and the molecular diffusion coefficient (0.0000864 m^2/d) are chosen (Engelen et al., 2019; Oude Essink et al., 2010; Zech et al., 2019, 2015). To reduce the number of computational runs, the effective porosity (0.3) is also kept constant for all groundwater models, since these are less spatially variable then other parameters (Zech et al., 2019, 2015) and since no local or regional information is available on global scale. We varied porosity (to 0.2 and 0.4) in one ARP groundwater model to examine the effects of varying porosity values on salinity distribution. The results are shown in Figure C-4. The SEAWAT finite difference solver is used to simulate the variable-density flow and salt transport; the time step is determined by stability criteria (Zheng and Wang, 1998).

A full glacial-interglacial cycle (approx. 125 ka) and sea-level fluctuations that occurred within that cycle (Grant et al., 2012) are considered in our study to examine the potential preservation of offshore fresh groundwater volumes deposited during the past sea-level low stands (Post et al., 2013). An extra stress period (max. 125 ka long) is implemented prior to the sea-level fluctuations with current sea-level that starts with all cells at seawater

concentration (35 g/l TDS) to estimate a steady-state salinity distribution under long-term constant recharge conditions. The underlying assumption of this approach is that the groundwater salinity profile estimated this way provides a relatively saline initial condition for the groundwater model simulation of the glacial-interglacial period, and thus curbs the potential over-estimation of offshore fresh groundwater volumes if the initial salinity distribution was acquired using a lower sea-level or shorter stress period duration. A total of 21 stress periods (each 5 ka long) are used to simulate the sea-level decline (approx. from 125 ka BP until 20ka BP; Figure C-1D). The sea-level during each individual stress period is kept constant and is approximated as average sea-level at the sea-level fluctuations corresponding time interval (Grant et al., 2012). The same applies for the 10 stress periods representing the sea-level rise (each 2 ka long), simulating the time period 20 ka BP to present. The 24 groundwater salinity profiles at the end of the last stress period are taken as 24 alternative equally plausible estimates of the current groundwater salinity profile for each ARP.

Implementing sea-level fluctuations into the groundwater models is realized through a horizontally shifting top system. The landward boundary is determined based on the topographical profile and set at the closest groundwater flow divide to the current coastline. All model cells located at the landward (vertical) boundary are assigned a general head boundary (third type or Robin boundary condition) with fresh water concentration (1 g/l TDS) and head elevation equal to the present water table elevation (Fan, 2013). Model cells with elevation above sea level during a given stress period receive a fresh groundwater recharge while a general head boundary with seawater concentration and head elevation equal to sea-level at that stress period is assigned to cells located below sea-level. The groundwater recharge rates are estimated based on differences between regional averaged long term precipitation and actual evapotranspiration (NTSG, 2019). These values, extracted along each profile belonging to an ARP, are aggregated into an ensemble used to create a lognormal distribution of groundwater recharge rates. A random chain of values is then generated prior to the groundwater model simulation (for the whole span of the cross-sectional model domain) and applied to the cells above the fluctuating sea-level. A surface level drainage system is used for each groundwater model to tackle potentially high groundwater recharge values and drain/discharge the excess recharge. The drain conductance is based on the soil horizontal hydraulic conductivity (Montzka et al., 2017). The drainage system also acts as a proxy for the surface water system with main drainage direction towards the sea, which is difficult to implement in a 2D cross-sectional groundwater model.

4.2.4 Offshore fresh groundwater (OFG) volume estimation

The groundwater salinity profiles of each simulation are aggregated for all ARPs 24 groundwater models based on the associated 24 geological scenarios, see Figure C-1C. The mean groundwater salinity concentration value is then calculated for each groundwater model cell resulting in a mean groundwater salinity profile throughout the whole simulation duration. Thus, it is possible to examine the dynamic nature of the OFG volumes during the last glacial-interglacial sea-level fluctuations. A threshold of 1 g/l TDS is chosen

as a boundary between fresh and brackish water which is in line with previous studies (Post et al., 2013). The OFG volumes estimated for all ARP groundwater models for the same COSCAT region are aggregated to calculate the total OFG volumes for the COSCAT region, see equation 4-1.

$$V_{total} = L_{off} * D_{shelf} * L_{coast} * \frac{FGF_{mean}}{100} * p \quad (4\text{-}1)$$

Where L_{off} stands for modelled offshore distance from the coastline (km), D_{shelf} represents the average unconsolidated sediment thickness at the coastline (km), (L_{coast} is the coastal length (km) of each coastal type withing the COSCAT region and is then matched with the corresponding ARP's mean fresh groundwater fraction (FGF_{mean}) to translate the cross-sectional estimates into a 3D volume (km^3), with p a constant porosity of 0.3 (-). The final OFG volumes per COSCAT region presented in this study are the sum of all ARPs located within the COSCAT region. The shallow OFG volume is estimated as all fresh groundwater located offshore and above 300 m asl (Figure C-9), chosen arbitrarily as a depth when economically viable groundwater pumping is feasible. Equation (4-1) is repeated by using FGF_{min} and FGF_{max} from the 24 groundwater models of each ARP to obtain uncertainty ranges per COSCAT region as well as for the global total OFG volume. The uncertainty of the latter is inflated because it assumes that geological uncertainties between COSCAT regions are fully correlated.

Brackish water is deemed better suited for desalination purposes (for the osmosis reaction) than actual fresh water. That is why, additionally, the volumes of brackish offshore groundwater were also estimated using Eq. 4-1 above with OFG fraction representing volume of groundwater with concentrations lower than 10 TDS g/l. The OFG is then subtracted from the calculated brackish offshore groundwater so only groundwater with concentrations between 1 and 10 TDS g/l is taken into account as brackish. These brackish offshore groundwater volumes are shown in Figure C-10.

We also estimated OFG replenishment time scales by fresh groundwater inflow from the landwards direction through submarine groundwater discharge (SGD) (Burnett et al., 2006; Moosdorf and Oehler, 2017; Taniguchi et al., 2002; Zhou et al., 2019). This SGD flux is calculated by summing up the lateral flux in cells with fresh water concentration at the coastline location. Since our SEAWAT models are 2D representations of the coastal groundwater flow conditions, the resulting SGD flux values are multiplied by the coastal length and the average unconsolidated sediment thickness at the coastline for each COSCAT region to estimate actual SGD flux (km^3/yr). The replenishment time for a given COSCAT region is then calculated as OFG volume divided by the SGD flux. This yields the estimated time it would take to fill the estimated OFG volume under current SGD conditions. The results are shown in Figure C-11 suggesting that most OFG is a non-renewable resource taking up to hundreds of thousands of years to be replenished.

4.2.5 Regional water demand and onshore groundwater extractions

We used the global hydrological model PCR-GLOBWB (Sutanudjaja et al., 2018) to estimate regional water demand and groundwater extractions. To calculate the regional coastal water demand and groundwater extractions, we created a buffer reaching 200 km inland for each COSCAT region. The resulting buffer zones were then overlaid over the 5 arcmin PCR-GLOBWB raster output files. In such way, we were able to extract the four components of the total sectoral water demand, namely domestic, livestock, industrial and irrigation water demands. To account for climate variation and dry/wet years we averaged over 30 year time-spans to create three water demand time slices, 2020 (2005 to 2035), 2050 (2035 to 2065) and 2075 (2060 to 2090). The future domestic, industry and livestock water demand estimations are based on the SSP2 scenario. To take into account the effects of climate change on the irrigation water demand, we forced PCR-GLOBWB with the outputs of five global climate models from the RCP 6.0 climate change scenario of CMIP5, selected and bias-corrected under the ISIMIP program (Hempel et al., 2013). The resulting future irrigation water demand is then calculated as median value of all the resulting global climate model runs. Future regional water demands together with estimated OFG volumes are shown in Figure C-6.

4.3 Results

Summing up all regional OFG volume estimates we approximate the global OFG volume to be 1.06 ± 0.2 10^6 km^3 (≤ 1 g/l TDS). However, since our groundwater models have a constant porosity value (0.3), we assess the porosity value effect on estimated OFG volume by carrying out a groundwater modelling study with varying porosity value (0.1, 0.2, 0.4) in a randomly selected region. We can confirm that our groundwater models with the lowest porosity (0.1) show less than half OFG fractions than the case with porosity of 0.3 (Figure C-4). This suggests that the estimated uncertainty about the global OFG volume may be slightly underestimated due to constant porosity considered. With that in mind, our estimated global OFG volume amounts to about 10% of total fresh groundwater worldwide (estimated to be 10.5 10^6 km^3) and roughly 3% of total global fresh water (Shiklomanov, 1993). The OFG volumes are most likely non-renewable as they were deposited during glacial periods when sea-levels were substantially lower compared to current sea-level. Indeed, when we calculate renewal times by the ratio of OFG volume and submarine fresh groundwater discharge from the groundwater models (Figure C-11), we see that renewal rates exceed 1000 years for most of the coastal regions, rendering the OGV volumes effectively non-renewable.

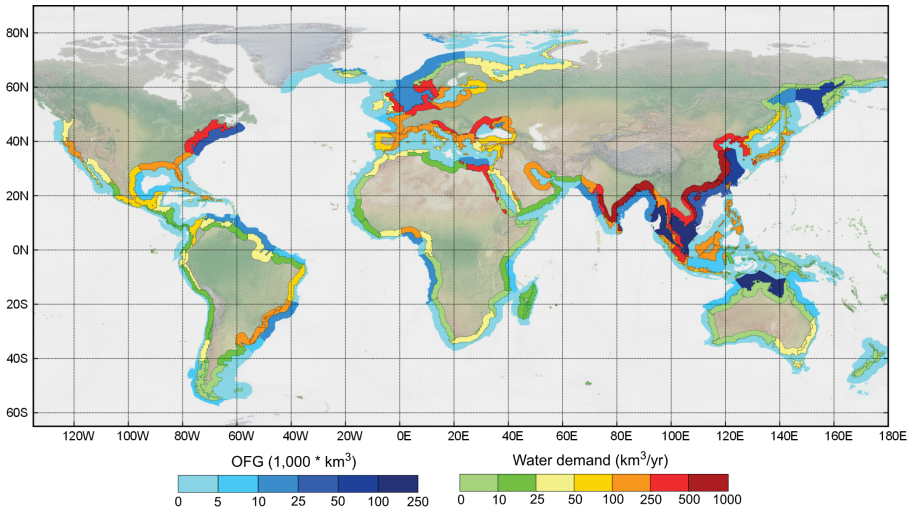

Figure 4-1 Estimated regional OFG volumes (in 1,000 km3) plotted with regional coastal current water demand (km3/yr) based on the global hydrological and water resources model PCR-GLOBWB (Sutanudjaja et al., 2018). Note that gross water demand is plotted, which includes losses and return flows. South-east and East Asia stands out as regions where OFG could provide an additional source of fresh water and therefore has most potential for OFG exploration.

The estimated OFG volumes vary considerably between the world's coastal regions (Figure 4-1). Regions such as North-east USA, North Australia and South-east Asia accommodate substantial OFG volumes. However, due to unknown heterogeneity in geology and other hydrological factors (e.g., groundwater recharge, influence of rivers), the uncertainties in OGV volumes can be considerable for certain regions, e.g., the coasts around Arabian Peninsula, the Gulf Coast and the North Sea basin (Figure C-5). To put these OFG volume estimations into perspective, we compared them with extracted present day total water demand per year from simulations with a global hydrology and water resources model (Sutanudjaja et al., 2018) for a 200 km inland buffer in each coastal region. South and South-east Asia stand out as regions with high current water demand and large OFG volumes, which calls for further investigations into more accurate quantification and potential exploration of these volumes. Water demand is projected to increase steadily during 21st century due to population growth and climate change (Prudhomme et al., 2014; Wada and Bierkens, 2014), and OFG could prove a vital additional fresh water source in regions such as West Africa and East South America as well (Figure C-6).

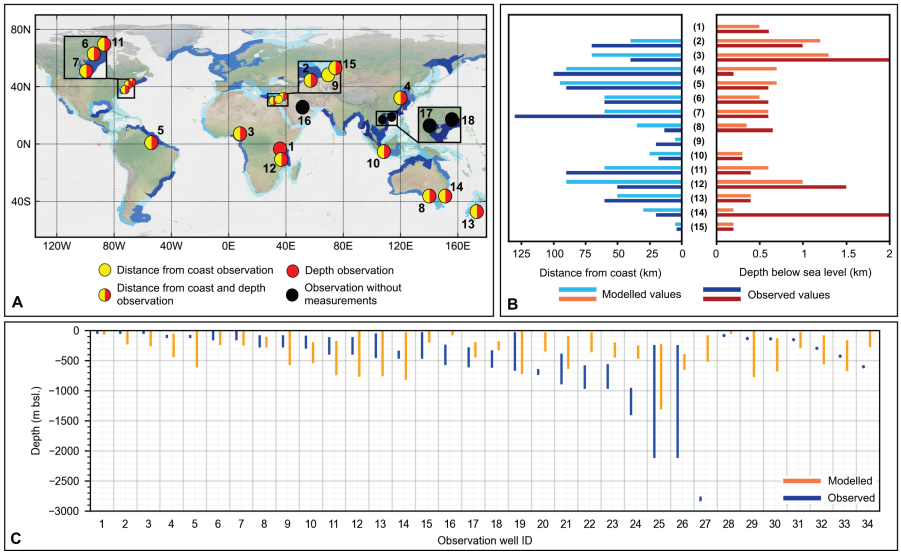

Figure 4-2 (A) OFG occurrence in unconsolidated sediments based on regional scale literature studies, see Table C-1 for more information. (B) Due to lack of OFG volume estimates in these regional studies, we selected two criteria (distance from coast (km) and depth below sea level (km)) to assess the accuracy of our estimates. (C) Additional validation comparing estimated OFG with observation wells (Micallef, 2020), only locations in unconsolidated sediments were selected and therefore the limited number of observation wells shown (see Table C-2). Only top OFG elevation is provided for some observation wells; in those cases, only a point is plotted (e.g., observation well 26).

We compared our OFG estimates with several regional scale studies (Amir et al., 2013; Bakari et al., 2012; Bertoni et al., 2020; Engelen et al., 2019; Geldern et al., 2013; Groen et al., 2000; Gustafson et al., 2019; Haroon et al., 2018; Jiao et al., 2015; Knight et al., 2019; Larsen et al., 2017; Oteri, 1988; Paleologos et al., 2018; Pauw et al., 2014; Person et al., 2012, 2003; Thomas et al., 2019; Varma and Michael, 2011; Zhang et al., 2011) and a set of offshore observation wells (Micallef, 2020) limited to areas with unconsolidated sediments, see Figure 4-2. Unfortunately, the majority of these regional scale studies do not provide volume estimates. Therefore, OFG's distance from coastline and depth below sea-level were chosen as proxies. Several studies only provide one of the two proxies, while few only show OFG observations without measurements (see Figure 4-2A). Fifteen regional studies covering all continents are taken into account, most of which contain both depth and distance from coast information. Our estimates match observed values reasonably well (Figure 4-2B), with only few areas showing large discrepancies. This mostly concerns estimated thickness of OFG where our study shows thinner OFG bodies offshore as compared to literature sources. The offshore observation well dataset (Micallef, 2020) gives a point measurement at a certain offshore distance and also the observed top and bottom OFG elevation. The OFG extent is then extracted from the corresponding groundwater model of the same region at the same offshore distance as each observation

well (Figure 4-2C). While in the same order of magnitude, some mismatch can be observed between observed and modelled OFG extent at some locations.

4.4 Discussion and conclusion

Our global OFG volume estimate is in line with a previous global OFG assessment (Post et al., 2013), which considers a more generous fresh water threshold (< 10 g/l TDS) and estimated global OFG volume along passive continental margins to be 0.3 10^6 km^3. However, this value may vary up to factor of two (Post et al., 2013) due to uncertainty about porosity values ranging between 0.03 to 0.4, and explains our higher estimate which is based on a constant porosity of 0.3. Our results are further confirmed by the most recent OFG study (Micallef et al., 2021), that also estimated the global OFG volume (<15 g/l TDS), but also including karstic aquifers systems, to be in the order of 10^6 km^3. This suggests that our study possibly overestimates the OFG volume along the global coastline but nevertheless provides an estimate in the same order of magnitude as previous global studies (based mostly on qualitative analyses). This can be partly explained by simplifications made during our groundwater modelling study (24 geological scenarios per coastal region) and subsequent OFG volume calculation for each coastal region, where we assume a single cross-sectional groundwater salinity distribution over lengthy coastline stretches. Comparing regional cross-sectional OFG schematizations with our groundwater model results shows a relatively good match in terms of OFG extent and depth (Figure 4-2B), but we can also observe some discrepancies presumably due to the large-scale nature of our analysis. As expected, this scale discrepancy is more pronounced when comparing top and bottom of OGV estimates with local observation wells (Figure 4-2C). Furthermore, since in our study we only consider unconsolidated sediment systems, older unconsolidated sediment aquifers overlayed by hard rock formations (e.g., sandstone, limestone) are not accounted for in our approach. This can lead to completely missing OFG reserves in the deeper formations by our groundwater models as is the case for the Gippsland basin in South Australia (Varma and Michael, 2011) (Figure 4-2C, observation well 2). Despite this, a satisfactory match is observed in shallower depths (up to 500m) which suggests that our approach can be used to estimate regional OFG volumes.

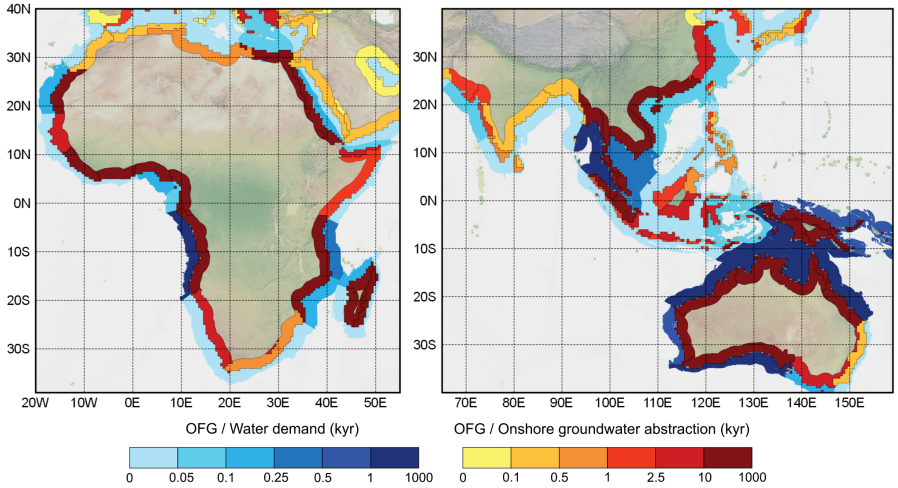

Figure 4-3 Ratio of estimated OFG volumes for Africa, South-east Asia and Australia with current regional water demand and onshore groundwater extraction obtained from the global hydrology and water resources model PCR-GLOBWB (Sutanudjaja et al., 2018). showing the time scale (order of magnitude in kyr) to which OFG could contribute to the fresh water demand. A global map is provided in the Figure C-7 Ratio of estimated OFG volumes with current regional water demand and onshore groundwater extraction. Estimates obtained from the global hydrology and water resources model PCR-GLOBWB (Sutanudjaja et al., 2018) showing the time scale (orders of magnitude in kyr) to which OFG could contribute to the fresh water demand per coastal region..

Comparing the estimated OFG volume with current regional water demand highlights areas where OFG exploration could provide an additional fresh water source over long periods of time (up to millennia). South-east Asia, West Africa and most of Australia show the highest potential for OFG exploration (Figure 4-3; Figures C-7 and C-8), especially since offshore areas in these regions already accommodate offshore pumping infrastructure (Figure 4-4). Exploring OFG as potential fresh water source could be especially interesting in densely populated and intensely farmed deltaic areas (Table C-3). The Niger, Grijalva, Rio Grande, Yangtze, Irrawaddy and Indus deltas are the most promising regions since they have both high OFG volumes and substantial water demand rates. OFG volumes found in these regions could provide multiple centuries (even up to 2 millennia) worth of fresh groundwater under current and under future water demand rates. The calculation of these time estimates does not take into account the salinization of OFG volumes caused by potential pumping, so these time estimates are probably lower in reality and should be further studied. In other regions, such as the Nile, Mekong and Chao Phraya deltas, the water demand rates are too high compared to estimated OFG volumes to make OFG exploration over long times a viable option, although it may still be useful as a temporary provision as part of a transition to more sustainable water use. Furthermore, several deltaic regions (e.g., Orinoco, Fly, Burdekin, Congo and Tana deltas) have large estimated OFG volumes but are sparsely populated with low water demand rates that make OFG exploration unnecessary.

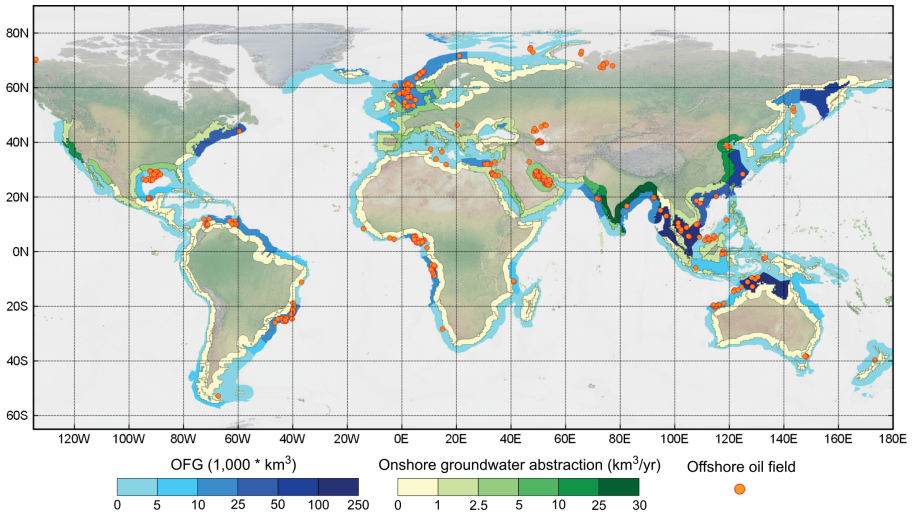

Figure 4-4 Estimated OFG volumes plotted with onshore groundwater extraction for coastal regions worldwide (km3/year based on PCR-GLOBWB (Sutanudjaja et al., 2018)) and location of large offshore oil fields (both active and inactive) (Horn, 2020).

Extracting OFG as an additional source of fresh water for coastal communities is deemed to have potential impacts (Knight et al., 2018) on environmental and human conditions while its feasibility should be evaluated for each site (Haakon and Fridtjof, 2012). Presumably, OFG extraction is financially and technically demanding as offshore drilling costs are so far only estimated in relation to oil extraction, while a large fresh water offshore mining project is yet to be undertaken. Initial costs to build offshore drilling platforms are generally at least one order of magnitude higher than those of desalination infrastructure initial investments (Amado, 2013). However, an extensive network of inactive (or soon to be inactive) offshore wells is already in place (Horn, 2020) and could be used for fresh or brackish groundwater extraction (Figure 4-4), and to our knowledge such activities already take place to enhance offshore oil recovery (Person et al., 2017). We also evaluated total OFG volume at shallow depths (higher than 300 m below average sea-level; Figure C-9), considering that pumping from deeper formations might be much more expensive and potentially disturb onshore groundwater heads (Yu and Michael, 2019) (when onshore and offshore aquifer layers are interconnected). We estimate the total volume of shallow OFG to be approximately 30% of total OFG volume (~0.31 10^6 km^3), showing still substantial shallow OFG volumes in e.g., South and South-east Asia.

The replenishment calculated as ratio of OFG volume and submarine fresh groundwater discharge provides a good first order estimate of OFG renewability under natural conditions. However, the calculated replenishment rates do not provide information on extraction rates that would keep the OFG volumes sustainable for human usage and

shouldn't be used as for this purpose. Further studies and information will be necessary to determine the regional potential for OFG extraction and its sustainability. Even if not used directly as water for agricultural or domestic purposes, offshore water resources, even when brackish, could serve as feedwater into desalination plants, providing another alternative water source of high quality in coastal areas. Desalination technology brings about numerous environmental threats, of which the generation of brine water as by-product is the most urgent one, and requires considerable economical and technical resources that are currently only available in high income developed countries (Jones et al., 2019). The current cost of desalination amounts to 0.5 to 1.2 USD/m³ using the globally most common remote osmosis technique (Jones et al., 2019). Additional costs are required for building the necessary infrastructure are estimated to be between 1.2 to 2.2 million USD per medium to large sized desalination plant (Shemer and Semiat, 2017) and energy demands in the range of 2.5 to 4.0 kWh/m³. Energy costs can be significantly reduced by improving the feedwater quality from seawater to brackish concentrations (by 0.5 up to 2.5 kWh/m³) while also reducing the brine discharge (Ghaffour et al., 2013) providing another argument for considering future offshore fresh or brackish exploration, particularly if infrastructure is already partly present. Estimated volumes of offshore brackish groundwater are presented in Figure C-10 showing promising potential for desalination feedwater purposes.

To conclude, our analysis shows that there are potentially large OFG volumes of up to 10% of total fresh terrestrial groundwater deposited in unconsolidated sediment systems in many regions worldwide. Exploring these offshore resources could provide additional fresh water sources for agricultural, industrial or domestic use, possibly via desalinization. The financial costs could be curbed by investigating the possibility of using (closed) offshore oil pumping infrastructure and wells. Such conditions can be found in South-east and East Asia, West Africa and several regions in South America. OFG could prove to be a vital water stress mitigating factor in regions facing near future increases in water demand due to population growth and climate change throughout the 21st century. Further research should investigate the effects of offshore pumping on groundwater levels inland as those could be interlinked. The OFG extraction can potentially lead to onshore groundwater level drops (Yu and Michael, 2019) which could have negative impact environmental conditions and societal fresh water needs. Moreover, searching for new hydrogeological data sources, implementing these in local to regional scale hydrogeological modelling studies would help to better understand the extent and behavior of these offshore fresh (and brackish) groundwater reserves.

Acknowledgements

This study's calculations were performed on the Dutch national supercomputer Cartesius with the support of SURF. This research was funded by the Netherlands Organization for Scientific Research (NWO) under the STW project 'Water Nexus: Resource Analysis and Regional Water Management' (no. 14298).

Data availability

We provide final groundwater salinity estimations for each COSCAT region (as 2D profiles) and shapefiles containing offshore fresh (and brackish) groundwater volumes together with inland water demand and groundwater extraction rates via the Zenodo repository (DOI - 10.5281/zenodo.3937204). Any additional data are available upon request.

5 Global impact of sea-level rise on coastal fresh groundwater resources

Abstract

In many densely populated and industrialized coastal areas around the world, groundwater is the main fresh water source. Growing fresh water demand caused by population growth and economic development is projected to increase the water stress in these coastal areas, potentially leading to groundwater overexploitation, salinization and land subsidence. This situation is likely to be aggravated by climate change and the associated projected sea-level rise of 0.4-0.7m by the end of 21st century, and reaching up to 3.7m by year 2300. Here, we assess the impact of sea-level rise on fresh groundwater resources in coastal areas worldwide. We use a large set of 2D groundwater numerical models to estimate the past, present and future groundwater salinity in 1200 coastal regions along the global coastline, resulting in estimates of future decline in inland fresh groundwater volume under three sea-level rise scenarios following RCP 2.6, 4.5 and 8.5. Our results show large differences in projected inland fresh groundwater decline between RCP scenarios. Roughly 60 million people could lose more than 5% of their fresh groundwater resources by 2100 according to RCP 8.5 scenario compared to only 8 million people based on RCP 2.6 scenario. This trend is observed also further into the future, with the negative impacts worsening close to exponentially for RCP 8.5. We conclude that sea-level rise will have severe consequences for coastal populations that heavily depend on local fresh groundwater, stressing the need for climate mitigation and adaptation for coastal communities.

5.1 Introduction

Low elevated coastal zones (LECZ) represent coastal areas with elevation ranging from 1m up to 20m above current sea level. At the beginning of 21st century the LESZ were inhabited by 638 million people worldwide (Merkens et al., 2016). Following different Shared Socioeconomic Pathways (SSP), this number is estimated to increase to more than 1 billion people by 2050 under all SSP scenarios considered, and slightly decrease (to 830–907 million) or increase (to 1.184 billion) depending on SSP scenario by 2100 (Merkens et al., 2016). Looking further landward, (Small and Nicholls, 2003) estimated that around 1.2 billion people lived within 100km from the coastline at the beginning of 21st century indicating that the population density in the LECZ is multiple factors larger than in the higher elevated coastal areas. These coastal zones are often important commercial, agricultural and industrial hubs and as such are large fresh water consumers, frequently using groundwater as the main fresh water source (Carrard et al., 2020). Such increased demand and pressure on fresh groundwater resources leads to overexploitation and can result in saltwater intrusion (Custodio, 2002). Additionally, changing boundary conditions due to indirect anthropogenic impacts pose another threat to the fresh groundwater resources in the LESZ. One such threat is climate change-induced sea-level rise which is estimated by the latest IPCC report (H.-O. Pörtner et al., 2019) to reach anywhere between 0.4m to 0.7m by 2100 and 0.8m to 3.7m by 2300 (comparing RCP scenarios 2.6 and 8.5). While these ranges of future sea-level rise urge humanity to limit further global warming and associated sea-level rise, it is important to understand the scale of sea-level rise impacts on fresh groundwater resources in the LESZ worldwide. It is projected that the immediate impacts will transpire as increased surface permanent submergence or short-term flooding while in long-term the groundwater quality would be compromised by seawater intrusion (Nicholls and Cazenave, 2010). Given fast population and economic growth projected to happen coming years and decades, LESZ areas in continents such as Africa and Asia are considered to be the most threatened (Nicholls and Cazenave, 2010).

This combination of direct and indirect anthropogenic pressures on groundwater resources in coastal areas is called coastal groundwater squeeze (Michael et al., 2017) and can already be observed in numerous regions around the world. Coastal flooding leading to erosion and actual disappearance of small islands around the world can already be observed (Ketabchi et al., 2014; Nicholls and Cazenave, 2010; Terry and Chui, 2012) and will lead to migration related to climate change (Warner et al., 2010). This threat is also looming over the Ganges-Brahmaputra-Meghna Delta which is already facing seawater intrusion effects on agricultural production and increased coastal flooding caused by sea-level rise and exacerbated by mangrove forest removal (Faneca Sànchez et al., 2015; Khan et al., 2014; Michael and Voss, 2009), potentially leading to large-scale climate change-induced migration. The effects of sea-level rise can be further intensified by land subsidence which has been observed in many deltaic areas around the world (Herrera-García et al., 2021; Nicholls et al., 2021; Syvitski et al., 2009), e.g. the Nile (Mabrouk et al., 2018), Ganges-Brahmaputra-Meghna (Becker et al., 2020) and Mekong Deltas (Minderhoud et al., 2017). Land subsidence is caused by combination of overexploitation of coastal groundwater bodies, lower sediment deposition due to upstream dam construction and new

infrastructure and construction leading to increased terrain compaction. This need for fresh water to support human development is likely to continue given the projected population growth trends (Merkens et al., 2016) which calls for adaptation in water management strategies and policy development.

In this study we focus on the effects of sea-level rise on coastal groundwater resources and present the first global, spatially explicit quantitative analysis of sea-level rise impact on coastal groundwater salinity. To this end we divide the global coast into 1200 coastal sub-regions of limited length with representative coastal profiles perpendicular to each coastal stretch. For reasons explained hereafter, we solely focus on regions with unconsolidated sediment formations. For each SRM, a two-dimensional variable-density groundwater flow and salt transport model (groundwater models hereafter) is built to simulate future groundwater salinization due to sea-level rise projections following RCP scenarios 2.6, 4.5 and 8.0 (H.-O. Pörtner et al., 2019). A paleo-reconstruction is conducted for each SRM by simulating the historical sea-level rise since the Last Glacial Maximum starting at 30000 years BP, starting with a sea-level of -120m below current sea-level and continuing with a sharp sea-level rise in the past 20000 years. For each SRM we use three global DEM datasets (Kulp and Strauss, 2019; Weatherall et al., 2015; Yamazaki et al., 2017) to study their impact on estimated levels of groundwater salinization due to sea-level rise. By including sub-regional hydrogeological uncertainty through the analysis of multiple realizations including three different DEMs, eight different geological scenarios and three RCP scenarios, our investigation/research is based on 86,400 individual model runs. It is worth mentioning that Ferguson and Gleeson (Ferguson and Gleeson, 2012) previously investigated the sensitivity of the interface between fresh and saline groundwater in the coastal zone to sea-level rise. However, these results were not spatially explicit, based on simplified assumptions about groundwater salinity changes, coastal geology and groundwater dynamics, and used very moderate sea-level change scenarios from the 4th IPCC assessment report.

A recently conducted global analysis of sea-level rise influence on coastal groundwater systems (Michael et al., 2013) identified two types of coastal environments based on their hydrological limiting factors. So-called recharge limited areas have higher topography that allows the groundwater table to rise in response to sea-level rise and thus curb the ensuing groundwater salinization. On the other hand, topography limited areas do not have such leeway (due to a limited unsaturated zone) and thus have higher salinization rates compared to recharge limited areas. Even though such findings do neither provide local or regional quantifications nor directly help water management authorities, this classification helps to better understand the factors determining salinization risks in coastal areas. Thus, topography, as explained above (Michael et al., 2013), is one of the main drivers influencing local and regional groundwater salinity patterns. This is especially true in low-lying coastal environments, where digital elevation model (DEM) input dataset errors can have immense impact on the quality of groundwater models and sea-level rise analysis (Minderhoud et al., 2019). Another important driver is local geological setting, particularly the type of rock formation in which groundwater is found and its heterogeneity (Zamrsky et al., 2018). Limiting ourselves to high-permeability hydrogeological systems that are

most sensitive to salinity incursions due to sea-level rise, we can distinguish two main types: karstic and porous rocks formations accommodating groundwater in complex fracture and fissure systems (Gingerich and Voss, 2005; Perriquet et al., 2014); and unconsolidated sedimentary formations composed of varying sized grained particles (Amir et al., 2013; Engelen et al., 2019). Building groundwater models representing karstic systems is only possible on small scale due to the highly variable and location dependent fracture systems. Unconsolidated sedimentary formations are a result of deposition and erosion processes governed by landward (rivers) and seaward forces. It is therefore possible to estimate and quantify geological heterogeneity characteristics in such formations on a global scale by combining available global datasets with empirical knowledge (Zamrsky et al., 2020). Thus, our results pertain to the LECZ with unconsolidated coastal sedimentary groundwater systems only, which constitute 25% of the global coast (Zamrsky et al., 2018).

5.2 Methodology

Our global scale analysis is based on subdividing the global coastline into so-called sub-regional coastal stretches and building sub-regional representative models (SRMs) of variable-density groundwater flow and salt transport perpendicular to the coastline. This allows us to both implement local characteristics and increase the computational efficiency of groundwater models (see Section 5.2.1). Sea-level rise effects on local groundwater salinization are studied in more than 1200 SRMs spanning over all continents. Their coastal extent (distance covered along the coastline) ranges from few tens to several hundred kilometers. The SEAWAT code (Langevin et al., 2008), see Section 5.2.2, is used to build 2D cross-sectional groundwater models perpendicular to the coastline is set up for each SRM (see Section 5.2.3). The collected global datasets help us to define individual SRMs while taking into account local characteristics, illustrate the local hydrogeological conditions (see Section 5.2.4) and define boundary conditions (see Section 5.2.5).

Rapid changing sea levels in the past 20000 years (see Section 5.2.6) and associated climate variations had a significant impact on groundwater dynamics in coastal areas (Post et al., 2013). To properly pick up these dynamics, our groundwater models follow past rapid sea-level rise and climate evolution. The latter is implemented via estimated paleo groundwater recharge rates (see Section 5.2.7) which are calculated based on past potential evapotranspiration rates (calculated via temperature records), precipitation, land use and soil clay content. We also perform a sensitivity study to assess to what extent groundwater model results are affected by model resolution (see Section 5.2.8) and the choice of the used digital elevation model (see Section 5.2.9).

5.2.1 Defining spatial extent of SRMs along the global coastline

In our study we focus solely on coastal hydrogeological systems formed by unconsolidated sediments carried by rivers from higher elevated inland areas (sources) into these coastal

lowlands (sinks). This sediment deposition has been continuously happening for millions of years and lead to a creation of coastal groundwater systems of varying thickness and geological complexity (heterogeneity). Sediment types and quantities deposited in the coastal areas depend on multiple regional factors, e.g., inland lithology, average temperature and elevation gradient. Our first task is therefore to divide the global coastal zone into regions whose uplands share similar geological characteristics.

To achieve this we use the so-called COSCAT regions that link the inland sources (Meybeck et al., 2006), i.e. river basins, with the coastal sinks (Laruelle et al., 2013), i.e. coastal plains and continental shelves. These COSCAT regions share the upland hydrogeological factors listed above, which provides an opportunity to use them to classify the coast into coastal stretches with similar upland hydrogeology resulting in a related similar coastal hydrogeology (Zamrsky et al., 2020). The average coastal hydrogeological system thickness (Zamrsky et al., 2018) is based on an approach that combines topographical profiles based on the GEBCO digital elevation model (Weatherall et al., 2015) and lithological information (Hartmann and Moosdorf, 2012).

Presumably, elevation in coastal areas is one of the most (if not the most) important factors influencing the inland groundwater salinization severity in the coastal zone. Coastal COSCAT regions can stretch over thousands of kilometers of coastline and using such large areas to derive an average representative elevation profile can potentially lead to over-simplifications. It is therefore desirable to further split the coastal COSCAT regions into smaller sub-regions.

This procedure is based on establishing 2D cross-sectional profiles perpendicular to the coastline (as in (Zamrsky et al., 2020, 2018). These coastal profiles are assigned three different coastal types based on their topographical (Weatherall et al., 2015) characteristics and potential location within a large deltaic area (Tessler et al., 2015), see Figure 5-1. Coastal profiles with clearly determined onshore and offshore parts are assigned a coastal type Simple (S). If there are multiple stretches with above sea-level elevations present in a coastal profile then it is labeled as the coastal type Island (I). The Delta (D) coastal type is designated for coastal profiles that lie within a large deltaic region regardless of the topographical characteristics.

A set of rules is defined to create sub-regions in every coastal COSCAT region. First, a sub-region has to contain at least five coastal profiles to be considered part of our study. This limit is imposed to limit the total computation time and also to narrow down the focus on larger coastal areas. The second rule specifies the maximum gap (two missing coastal profiles allowed) between individual coastal profiles in order to be considered part of the same sub-region. The third and last rule defines the maximum number (two) of coastal profiles of different coastal type allowed within a cluster of other coastal type profiles. Implementing such rule allows us to create larger sub-regions that share similar characteristics instead of generating multiple, yet almost identical, sub-regions. Figure 5-2 shows an example of different sub-regional representative models (SRMs) differentiated in a coastal COSCAT region.

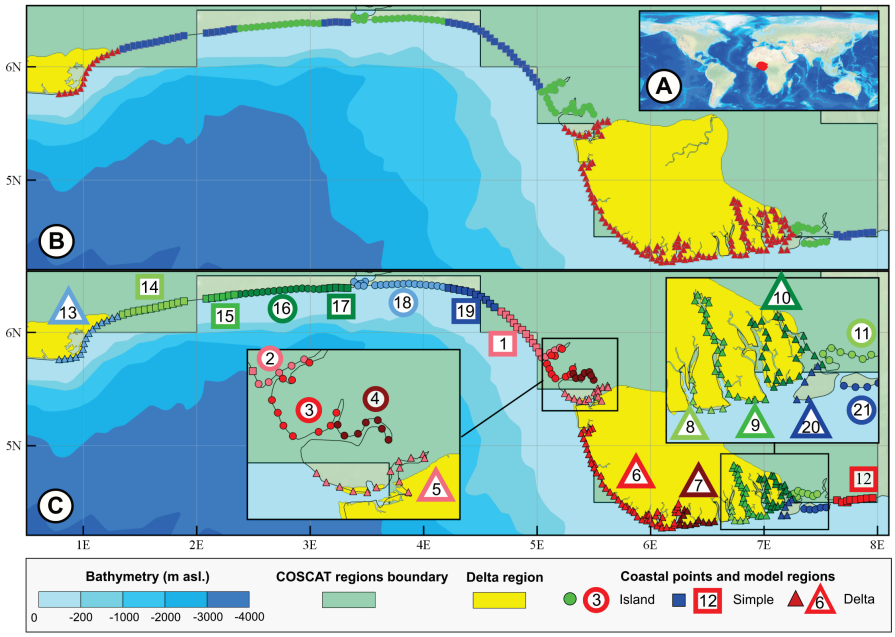

Figure 5-1 Example of a coastal COSCAT region and subdivision into smaller sub-regions. (A) The coastal COSCAT region is located in equatorial Africa, around the Niger river delta. (B) It covers two large deltaic regions - Niger river delta in the east and Volta river delta in the west. Three different coastal profile types are distinguished- Simple (S), Island (I) and Delta (D) – based on their topographical profile characteristics or location within a deltaic area. (C) Individual coastal profiles are clustered together based on their proximity and coastal type resulting in this case into 21 sub-regions. A sub-regional representative model (SRM) will then be built for each of these sub-regions. This procedure is implemented for all selected coastal COSCAT regions.

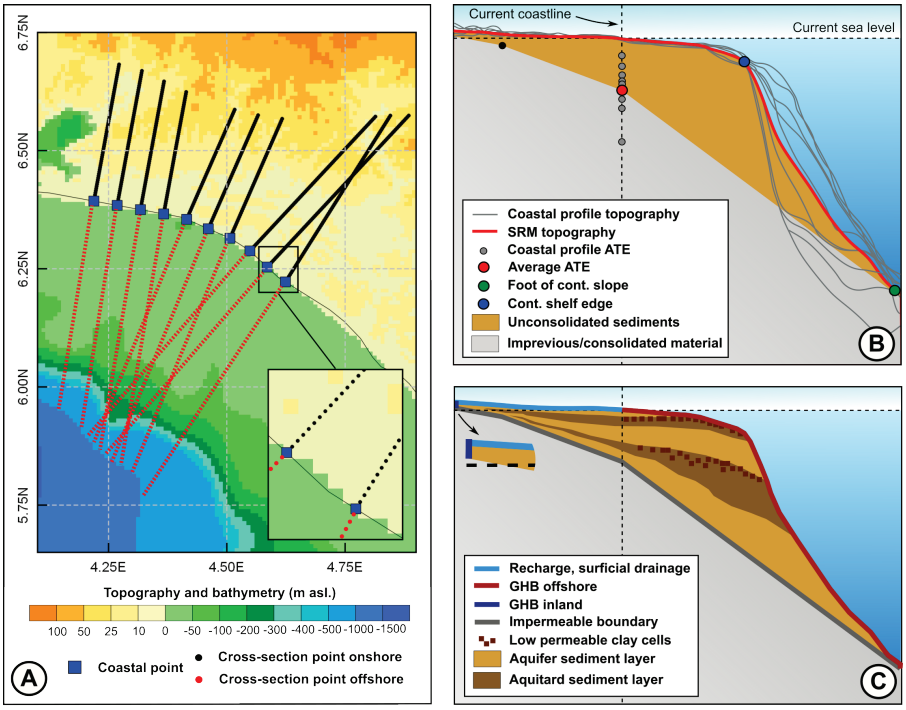

Figure 5-2 Building an SRM out of individual coastal profiles. (A) Coastal profiles in SRM number 19 (see Figure 5-1) with schematized individual cross-section points where the values from various datasets are extracted. In this case the GEBCO digital elevation model (Weatherall et al., 2015) is shown, providing both inland topography and offshore bathymetry. The extent of each coastal profile in this figure spans from topographical divide inland until the offshore limit, forming the physical boundaries. (B) Combining all individual topographical coastal profiles leads to establishing and averaged SRM topography. Individual aquifer thickness estimations (ATE, based on Zamrsky et al., 2018) are also combined and an average ATE is defined for the SRM. This allows us to define the bottom boundary of the SRM. (C) In the next step we define the input and boundaries of the SEAWAT models. A recharge and surficial drainage systems are applied to the top of the inland domain while general head boundaries (GHB) simulate the influx of fresh (inland side) and saline (offshore) groundwater into the model domain. Hydrogeological characteristics of the inner model domain are based on methodology developed in a previous study that fills in the domain with alternating aquifers and aquitards (Zamrsky et al., 2020). A more detailed description of this process is provided in Section 5.2.4.

5.2.2 Variable density groundwater flow coupled with salt transport modeling

The main objective of this study is to assess the effects of sea-level rise on fresh groundwater resources in coastal areas formed by unconsolidated sediments worldwide. This means evaluating the scale and rate of presumably increasing salinization with rising sea-levels. To do so we used the SEAWAT computer code (Langevin et al., 2008) to model variable-density groundwater flow and coupled salt transport, in 2D cross-sectional profiles. The models are called SEAWAT models throughout the following text. A SEAWAT

model is set up for each SRM (see Figure 5-2), this setup is based on previous research into offshore fresh groundwater volumes around the world which also used large-scale 2D cross-sectional SEAWAT models to estimate groundwater salinization over large geological time scales (Zamrsky et al., 2020, 2018).

5.2.3 SEAWAT models for SRMs

Each SRM contains multiple coastal profiles based on coastal type and proximity. Once these SRMs are defined, the next step is to extract all necessary information to build 2D cross-sectional SEAWAT models. This extraction along the coastal profiles is based on the methodology established in (Zamrsky et al., 2018) and consists of reading values from various datasets for equidistant cross-section points spaced along each individual coastal profile. An example of creating an SRM from individual coastal profiles is given in Figure 5-2.

First, to define the SRM's extend, we extract topography and bathymetry values from the GEBCO dataset (Weatherall et al., 2015) for each coastal profile within the given SRM. With its 30 arcmin resolution (approximately 1km * 1km at equator), the GEBCO dataset is assumed to be fit for regional scale applications, and used in this study to define the SRM's mean topographical profile. Moreover, the GEBCO dataset is the only global digital elevation model (DEM) that combines both onshore topography and offshore bathymetry into a single grid corrected to one vertical datum. This is important for a consistent definition of onshore and offshore domains in each coastal profile.

However, since the main focus of this study is on sea-level rise impacts on onshore fresh groundwater resources, it is desirable to also include other DEM datasets with higher resolution, given that sea-level rise is estimated to be in order of decimeters or few meters by 2300 (H.-O. Pörtner et al., 2019). In our study we chose to use the Multi-Error-Removed Improved-Terrain DEM (MERIT DEM) (Yamazaki et al., 2017) and CoastalDEM (Kulp and Strauss, 2019) datasets, both based on SRTM (Rodriguez et al., 2006) data but corrected for vertical errors (vegetation in MERIT DEM, vegetation and urban areas in CoastalDEM). Both MERIT DEM and CoastalDEM are corrected to mean sea-level (MSL). Figure 5-3 illustrates a comparison of these three DEM datasets in an urban and a non-urban area. Even though major landscape features are captured by all the DEM datasets it is easy to spot the differences in elevation between the MERIT DEM dataset (lower values) and other two DEM datasets in non-urban areas. Similarly, in an urban area, the CoastalDEM dataset shows much lower elevations than the other two datasets. These differences in

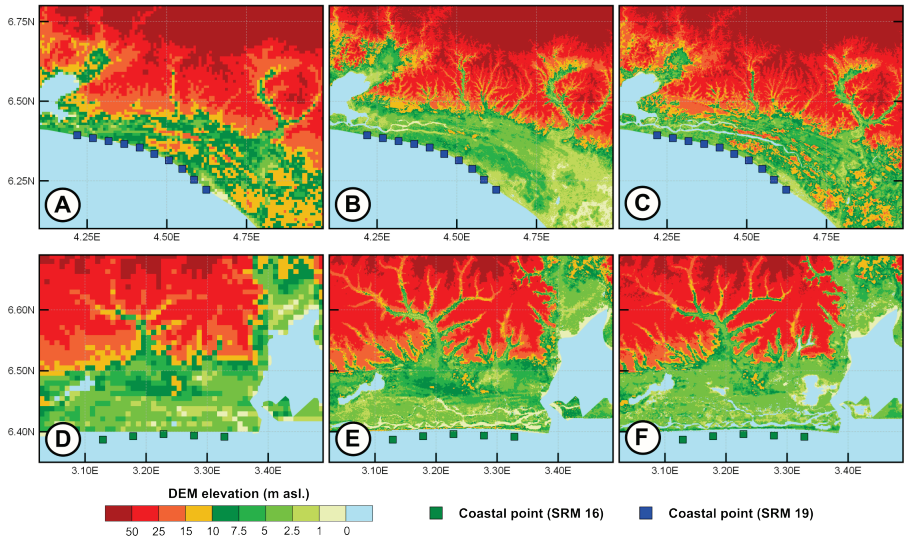

*Figure 5-3 Comparison of three different DEM datasets used to implement the upper topographical boundary in the SEAWAT models. Two areas with different characteristics are considered to show differences in elevation given by these DEMs, a non-urban area (A-C) and an urban area (D-F). (A, D) The coarsest DEM dataset with resolution of roughly 1km*1km at equator is the GEBCO (Weatherall et al., 2015). (B, E) The MERIT DEM (Yamazaki et al., 2017) dataset with 90m*90m resolution at equator and focused on the vegetation correction factor. (C, F) CoastalDEM (Kulp and Strauss, 2019) dataset that also includes urban areas correction factor and has the highest resolution of all DEM datasets considered (30m*30m).*

elevation have potentially a large effect on sea-level rise impacts on fresh groundwater resources in low-lying coastal areas.

5.2.4 Hydrogeology

The hydrogeological schematizations used as input to the SEAWAT models are based on a collection of global geological datasets and a randomization of unknown parameters. This approach is necessary due to lack of globally available lithological borehole data that could otherwise be used to create more accurate local hydrogeological representations. To create different hydrogeological schematizations, we use the geological heterogeneity estimation and simulation approach derived in (Zamrsky et al., 2020). The basis in this approach is to fill the model domain with random combinations of permeable aquifers and low-permeable aquitards with varying thickness, see Figure 5-2C.

Several global geological datasets are used as direct input into this approach and help us constrain geological parameters. Amongst these are global thickness estimation of coastal unconsolidated sediment systems (Zamrsky et al., 2018), global horizontal hydraulic conductivity estimations datasets GLHYMPS (Gleeson et al., 2014) and GLHYMPS 2.0 (Huscroft et al., 2018) applied to aquitards and aquifers , presence of low permeable clay capping layer in continental shelf and slope domains (Dutkiewicz et al., 2015) and soil

thickness and type SOILGRIDS datasets (Hengl et al., 2014). A previous study (Zamrsky et al., 2020) provides further information about the shape of individual aquifers and aquitards offshore and their respective volume fractions of the total estimated unconsolidated sediment volume. Other parameters have to be estimated, such as thickness of continental shelf and slope clay capping layer (10m and 30m) and the number of aquifer and aquitard combinations in the model domain (2 and 5). The clay content of the aquifers is related to the sand/mud ration of the upstream sediment supply. Assuming that small size sediment particles such as clay are deposited during periods with higher sea-levels, low permeable clay cells are randomly but preferentially assigned to the upper parts of each aquitard. Also, dependent on the upstream sediment supply and the subsidence rate that determine preservation potential, an erosion factor is determined and applied which results in removing a certain amount of these clay cells in random locations (Zamrsky et al., 2020). The clay stacking factor (between 0.5-1) determines where clay cells are likely to be positioned within an aquitard in vertical direction. Higher clay stacking factor values mean that a clay cell is more probably going to be placed in the upper part of an aquitard. In such cases, the aquitard will act as flow barrier compared to situations where clay cells are randomly distributed throughout the aquitard and potentially leaving space for permeable groundwater flow conduits.

5.2.5 SEAWAT model boundaries

Once the spatial dimensions of a SRM are defined (see Figure 5-2), we assign hydrological boundaries to the SEAWAT model domain. The bottom boundary is assumed to be impervious since our approach only takes into account unconsolidated sediment groundwater systems. This is probably an oversimplification in some cases since there might be consolidated sedimentary aquifers underneath which would mean a possible groundwater flow connection. However, simulating groundwater flow in such consolidated systems would require a large amount of local geological data (that are not available on a global scale), long simulation times and a different modelling approach all together.

A general head boundary (GHB) is assigned at the landward extremity of SEAWAT model to simulate groundwater flow from the landward direction. These cells are assigned a head elevation equal to the topographical elevation in given SEAWAT model column and a fresh water concentration (= 0 g TDS/l). The landward boundary location corresponds to a groundwater flow divide that is estimated based on the DEM elevation input. If the groundwater flow divide is not located within the first 50km inland a general head boundary is placed 50km landward from the coastline. The rest of the inland domain (where cell elevations are above sea-level) receives fresh groundwater recharge and is also assigned a drainage system to simulate overland flow. The drain elevation is equal to surface level and is implemented to avoid overestimating the forcing of fresh water into the model and thus artificially increase groundwater heads in the model domain. The upper most active cells in each offshore column (depending on fluctuating sea-level) are assigned GHB condition with head elevation equal to sea-level and a seawater

concentration (= 35 g TDS/l). The same applies to the last active column of the model domain, if submerged below sea-level.

The Last Glacial Maximum (LGM) sea-level conditions are chosen to be the starting paleo conditions for the SEAWAT models. This time period occurred approximately 20000 years BP (before present) and the average global sea-level is estimated to be -130m compared to current sea-level (Lambeck et al., 2014a). Initial salinity concentration (g TDS/l) and groundwater heads (m bsl.) profiles for an SRM is derived based on LGM conditions estimated for a corresponding COSCAT region (see Chapter 4), see Figure 5-4.

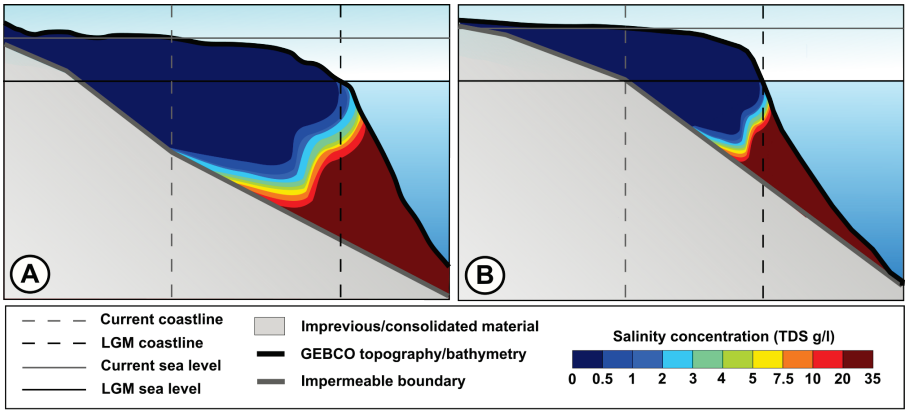

Figure 5-4 Interpolating initial salinity at time step 20ka BP (g TDS/l) concentration profile from an averaged COSCAT representative profile SEAWAT model into the SRM boundaries. Despite the two model domains having different dimensions the concentration profile's shape is maintained.

5.2.6 Paleo sea-level conditions

The LGM period was followed by rapid sea-level rise over the next 20000 years until sea-levels stabilized to current conditions. To simulate this process we divide this whole time period into separate stress periods each with different sea-level approximated from the sea-level rise estimations (Lambeck et al., 2014a), see Figure 5-5. An extra stress period (SP0, 10 ka long, from 30000 - 20000 years BP) is implemented at LGM conditions to allow the SEAWAT model to adapt the interpolated salinity conditions to the SRMs boundary conditions. The temporal resolution of following stress periods (SP1 – SP18) is 1ka until sea-level stabilized at current condition around 2000 years BP. From then onwards the stress periods are 100 years long (SP19 – SP43), to take into account varying groundwater recharge, as is explained below. To finish the SEAWAT model simulations, we implement five stress periods with estimated global mean sea-level (GMSL) rise conditions (H.-O. Pörtner et al., 2019) based on three different Representative Concentration Pathway (RCP) scenarios (2.6, 4.5, 8.5 taking the GSML 50th percentile values). The reason we decided to use the GMSL dataset instead of the regional sea-level rise predictions is its

temporal span that provides estimations until 2300 compared to 2100 for the regional estimations

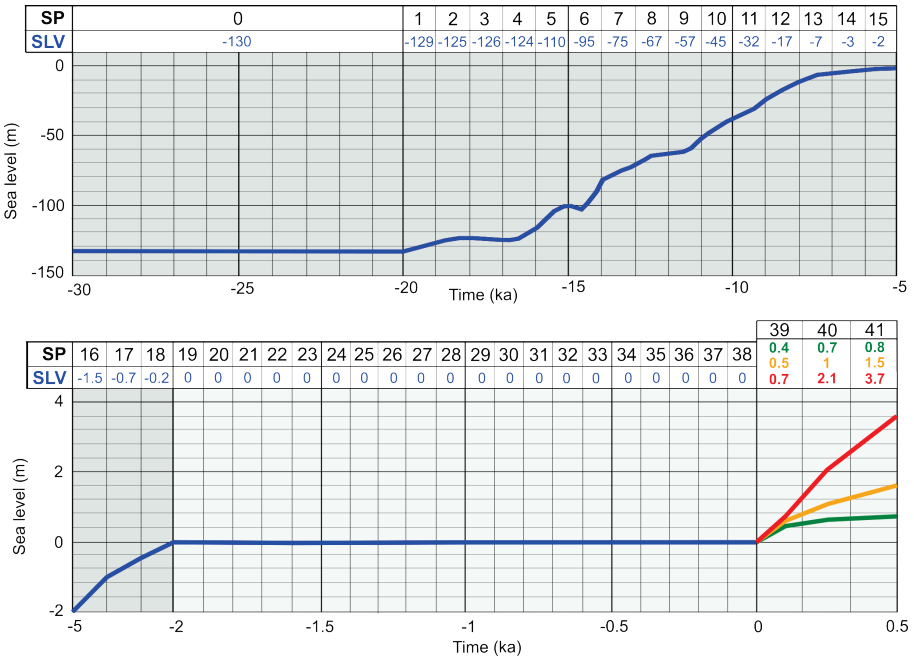

Figure 5-5 SEAWAT model total simulation period split into individual stress periods (SP) and their respective sea levels (SLV), values from 20ka BP are approximated (Lambeck et al., 2014), sea level is kept constant during the time period between 30ka and 20ka BP. Future sea level rise is simulated using the global mean sea level (GMSL) predictions for coming centuries based on three different climate scenarios (H.-O. Pörtner et al., 2019), RCP 2.6 (green), 4.5 (orange) and 8.5 (red).

5.2.7 Paleo groundwater recharge estimation

More detailed groundwater recharge information and input is essential to improve the quality of our SEAWAT models which we use for the entire paleo reconstruction. Estimating past changes in groundwater recharge in colder and warmer (drier and wetter) time periods in the past 20000 years can play an important role in estimated current coastal groundwater conditions. Global estimates of groundwater recharge are available as output of several global hydrological models, e.g., PCR-GLOBWB (de Graaf et al., 2015) and WaterGAP (Döll, 2009). Unfortunately, these estimates only span across the second half of 20th century and beyond. These models cannot be used to estimate groundwater recharge at paleo timescales due to high computational demands and quality of input data required. However, a global model (Mohan et al., 2018) was recently used to estimate global groundwater recharge rates using a multiple linear regression approach and several global meteorological, land use and soil characteristics datasets as input. The best

performing multiple linear regression model (Mohan et al., 2018) uses precipitation P (mm/yr), potential evapotranspiration PET (mm/yr), land use (LU) and clay content (CC) as input into a square root transformation of groundwater recharge, see Eq 5-1. We emulate this approach by collecting historical datasets, feed them into the multiple linear regression model and in such way estimate paleo groundwater recharge rates (up to 30000 years BP) on global scale.

$$GWR = (6.3781 + 0.0086 * P - 0.0044 * PET + 1.0335 * LU - 0.0606 * CC)^2 \quad (5\text{-}1)$$

The first obstacle in our approach is a missing paleo PET global dataset. To solve this issue, we decided to estimate PET values using annual average temperature T (K) values as proposed by (Gardner, 2009), see Eq. 5-2 which is as follows:

$$PET = 1.2 * 10^{10} * e^{(-\frac{4620}{T})} \quad (5\text{-}2)$$

We first estimate current PET values using this approach and compare those to the global PET dataset (years 1981 to 2014), provided by CRU climatological datasets (Harris et al., 2014), and used as input (Mohan et al., 2018). The WorldClim 2.0 provides the current global annual average P and T datasets between years 1970 and 2000 (Fick and Hijmans, 2017). These annual datasets are further averaged over this whole time period (1970-2000) to create a single global mean dataset for each variable. A dataset containing 713 locations with direct PET measurements distributed worldwide are also provided (Mohan et al., 2018) and used to validate our approach. Once we are able to estimate the current PET using Eq. 5-1, we can proceed to calculate paleo PET values feeding past global average annual temperature estimations into the following equation:

$$PET_{past} = PET_{current} * [\frac{e^{\left(-\frac{4620}{T_{past}}\right)}}{e^{\left(-\frac{4620}{T_{current}}\right)}}] \quad (5\text{-}3)$$

We were able to find global T and P datasets for only two other time periods, the LGM (approx. 22ka BP) and mid-Holocene (approx. 6ka BP), both produced by the WorldClim 1.4 database (Hijmans et al., 2005). The mean annual temperature is then inserted into Eq. 5-3 together with the calculated current PET and mean annual current temperature to calculate PET at LGM and mid-Holocene time periods. Another historical climate dataset is provided by the Last Millenia Reanalysis study (Tardif et al., 2019) estimating the annual anomaly (P and T) compared to long term average temperature and precipitation over the

Common Era (past two millennia). We average these anomalies for every century in the Common Era (corresponding to SP19-SP38 in Figure 5-5) and in such way derive corresponding P and T datasets.

The P and T (and therefore PET) global estimations in between the time steps described above (LGM, mid-Holocene, beginning of Common Era) are established using simple linear interpolation. Constant P and T values are applied to the whole SP0, assuming stable conditions during LGM. Gradual warming and wetting of the climate between LGM and mid-Holocene between SP0 and SP14 are then simulated via the mentioned linear interpolation. The same applies to values for SP15 through SP18 where we apply linear interpolation between mid-Holocene and start of Common Era values. We do not apply any changes in future groundwater recharge based on climate model projections as we solely want to focus on sea-level rise effects on groundwater conditions. Estimated global groundwater recharge rates for several time steps showing variations between different time (and climate) periods are presented in Figures D-1 to D-6.

Land use (LU) is another key input into Eq. 5-1 and several global datasets providing information on current LU distribution are available. Since in our study we are also interested in the past conditions we decided to use the HYDE 3.2 dataset (Goldewijk et al., 2017) which provides LU data for time period between 12ka BP until present. To account for lower sea-levels and therefore more extended coastline we interpolated land use values for the LGM conditions using the LU distribution at 12ka BP. During this process, the most common LU value in a buffer around a given non-value cell is assigned as LU type in that given cell. The global groundwater recharge model (Mohan et al., 2018) considers five different land use categories, namely "cropland", "pasture", "forest", "urban" and "barren" compared to twenty one in the HYDE 3.2 dataset (Goldewijk et al., 2017). Therefore, we reclassified land use types from the latter study to fit the five land use types applied by (Mohan et al., 2018). The five classes have different coefficient values that are fed into Eq. 5-1, "cropland" being the highest (5) followed by "pasture" (4), "forest" (3), "urban" (2) and "barren" (1).

The last necessary input variable into Eq. 5-1 is clay content in the top soil layer. Since no historical datasets were found we decided to apply a constant clay content value for all estimations. For this purpose we used the SOILGRIDS dataset (Hengl et al., 2014) that cover the current global land mass. A mean clay content value in given SRM is applied in areas that are currently submerged but were previously above sea-level.

5.2.8 Grid convergence analysis

Before setting up and running all SEAWAT models for each SRM considered in this study, we conducted a sensitivity analysis to determine mainly the influence of 2D grid dimensions on simulated groundwater salinity profiles. Three coastal areas were considered (see Figure 5-6). First, we set up a base scenario with 100m column width and 10m layer thickness. Next, a set of groundwater models with varying grids were built and the results compared against the base scenario groundwater model. Four different model cell column widths (500m, 250m, 50m, 25m) and model layer thicknesses (50m, 25m, 5m,

2.5m) were taken into account leading to fourteen grid sizes (we only implemented groundwater models with column width to layer thickness ratio higher than 10). We analyzed the difference in total volume of fresh water in the groundwater model domain and total runtimes (in hours). The results in Figure D-8 show that the chosen column width (100 m) and layer thickness (10 m) in our simulation yield similar fresh groundwater volumes as found with finer grid sizes at a fraction of the run time.

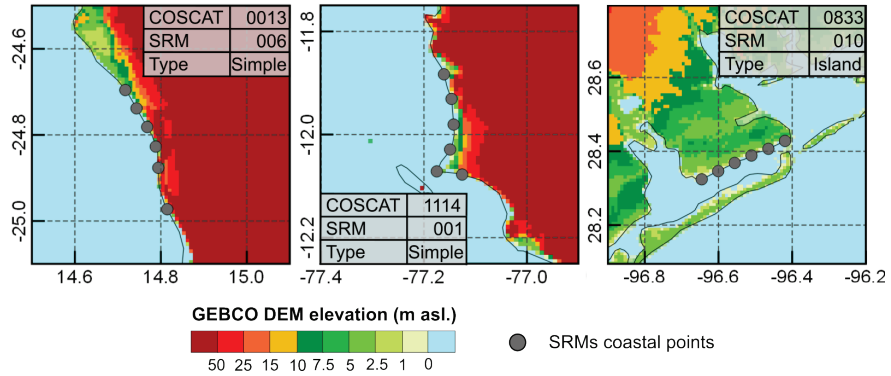

Figure 5-6 Location of SRMs chosen for sensitivity analysis. The SRMs are selected so the ensemble covers all continents and has a large degree of variation in latitudes affecting the climate conditions and coastal types.

5.2.9 Sensitivity of projected fresh groundwater decline to DEM dataset used

We investigated the effects of varying DEM input on estimated IFGV decline in all affected SRMs over time for each RCP scenario (see Figure D-32). Out of all three DEMs, groundwater models using the Coastal DEM (Kulp and Strauss, 2019) as topography input show the largest fraction of SRMs with a IFGV decline over 5% as well as SRMs with higher declines. MERIT DEM (Yamazaki et al., 2017) based groundwater models show the lowest impact on fresh groundwater availability (expressed as decline in IFGV) in the SRMs out of all three DEM inputs. This leaves GEBCO DEM (Weatherall et al., 2015) based groundwater models and their decline in IFGV estimates as intermediate between the other two DEM. Interestingly, the total amount of SRMs with IFGV decline over 5% seem to even out for all three DEMs in RCP 8.5 scenario. However, the severity in decline in IFGV follows the same trend as described above, with largest proportion of areas with decline in IFGV over 25% for Coastal DEM based groundwater models, followed by GEBCO and MERIT DEM. It is important to note that the same trend is observed for all three RCP scenarios and that the differences in fractions of SRMs showing decline in IFGV are in order of several percent, not larger.

5.3 Results

5.3.1 Sea-level rise effects on future fresh groundwater volumes

We quantify the sea-level rise effects on future fresh groundwater volumes by first estimating the current inland fresh groundwater volume (IFGV) from paleo-groundwater modeling and then comparing future IFGV projections among three RCP scenarios (H.-O. Pörtner et al., 2019). Additionally, to study the potential effects of inertia we extend our groundwater model simulation time for 200 extra years after year 2300 where sea-level rise predictions end. As such, we study the relative rate of change of IFGV in the future (expressed as decline in IFGV in year 2100 compared to situation in year 2000) rather than absolute IFGV change. This allows us to better identify and compare the threatened areas around the globe. The IFGV is calculated as the total volume of fresh groundwater in model cells that contain fresh groundwater and located in the area spanning 10km from the current coastline position in the landward direction. Fresh water salinity concentration is defined as lower than and equal to 0.5 g/l TDS.

Figure 5-7 provides global maps (one for each RCP) of the estimated impacts of sea-level change on coastal fresh groundwater volumes. Differences between RCPs are quite large; the estimated IFGV decline being severe for RCP 8.5 for several regions (e.g., East coast USA, Caribbean, Northern Java) that potentially lose more than 25% of their IFGV compared to the year 2000. Contrarily, future sea-level rise according to the RCP 2.6 scenario shows only a very minor decline in IFGV by the end of the 21st century with the vast majority of SRMs only experiencing a IFGV decline lower than 5% compared to situation at the start of the century. End of 21st century estimates following RCP 4.5 show intermediate results with most SRMs experiencing a decline in IFGV lower than 5%, while several local hotspots (e.g., West coast Africa, Mekong Delta and the Netherlands) are visible where the decline in IFGV is larger than 25%.

Our global projections shows that a steady decline in IFGV worldwide will continue well after the year 2100 (Figures D-20 to D-31). The differences between the outcomes for the three RCP scenarios become more pronounced over time. Based on the RCP 2.6 scenario, sea-level rise is projected to level off after year 2200 with only 0.3m rise during the 22nd century and 0.1m during the 23rd century (see Figure 5-5). These limited rates of sea-level rise show little impact on the worldwide decline in IFGV (Figures D-20 to D-23) as estimated by our groundwater models as compared to the estimated situation in year 2100 shown in Figure 5-1A. By the end of the time period considered in our analysis in year 2300 (see Figure D-23), the decline in IFGV worldwide under RCP 2.6 scenario is almost identical to the decline in IFGV projected to happen by 2100 under RCP 4.5 scenario (see Figure 5-7B). Projected sea-level rise under RCP 4.5 follows an almost linear trend of 0.5m per century until year 2300 (Figure 5-5). This will translate into a steady decline in IFGV until year 2300 (Figures D-24 to D-27), at which IGVF decline to matches that projected in 2100 under RCP 8.5 (Figure 5-7C). However, the majority of SRMs representing the global coastline would still experience only a minor decline in IFGV (< 5%) in the coming centuries. As anticipated, the largest decline in IFGV over the coming centuries is projected if sea-level rises following the RCP 8.5 scenario, with a sea-level that is 3.7m higher than current level in 2300 and the

rates of sea-level rise increasing over the subsequent centuries: 0.7m during 21st, 1.4m during 22nd and 1.6m during 23rd century, see Figure 5-5). Such high rates of sea-level rise create large hydraulic gradient changes and seawater overtopping in coastal areas which leads to substantial declines in IFGV over the coming centuries (Figures D-28 to D-31). The projected situation at the end of 21st century, where several regions are already badly affected but majority of SRMs still shows low decline in IFGV, steadily worsens through the 22nd century and by the end of 23rd century clearly identify additional regions that show declines in IFGV higher than 25% compared to IFGV in year 2000. Among these regions are for example the coast of West Africa, North-east Indian coast and the coastal areas in the Red Sea. These are densely populated and currently relatively impoverished areas and therefore probably not economically ready to deal with the consequences of decreased fresh groundwater supplies. The situation at the end of our simulation period in year 2500 is comparable to the situation in year 2300, with a slight increase in affected areas and IFGV decline (Figure D-32).

The salinization of coastal aquifers resulting from sea-level rise can also be is observed by considering the landward shift of saline groundwater, see Figure 5-8. For the RCP 8.5 scenario, already by the year 2100 several coastal areas could experience groundwater salinities higher than the salinity level half of ocean water (17.5 g/l TDS) further than 10km inland than the situation in year 2000. Especially areas in eastern USA, northern Europe and western Africa could experience significant aquifer salinization extents. Similar to the trend of decline in IFGV, the estimated shift in landward groundwater salinity extent is significantly lower for the RCP 2.6 scenario and between RCP 8.5 and 2.6 scenarios widens into the future.

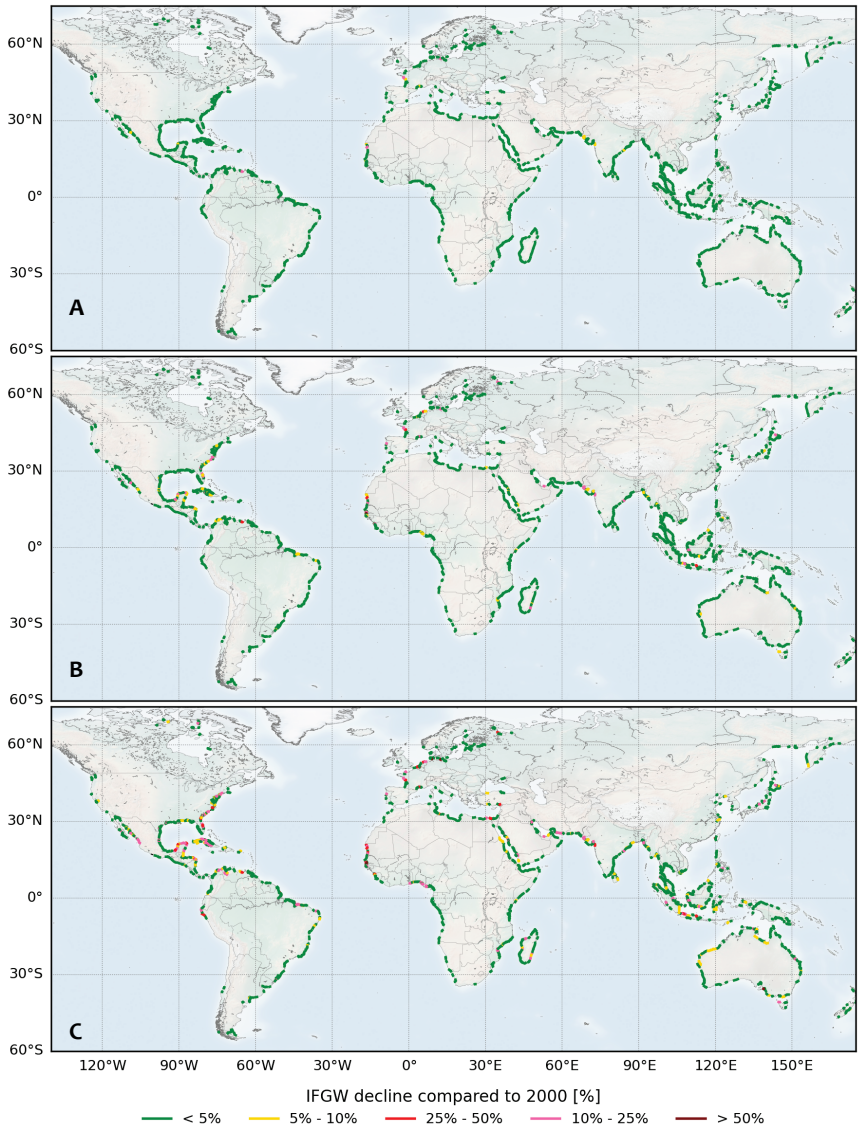

Figure 5-7 Difference in inland fresh groundwater volume (IFGV) in year 2100 expressed as percentage IFGV compared to situation in year 2000. Results are averaged over the three different DEM inputs used in our modelling study for each RCP scenario – (A) RCP 2.5, (B) RCP 4.5 and (C) RCP 8.5.

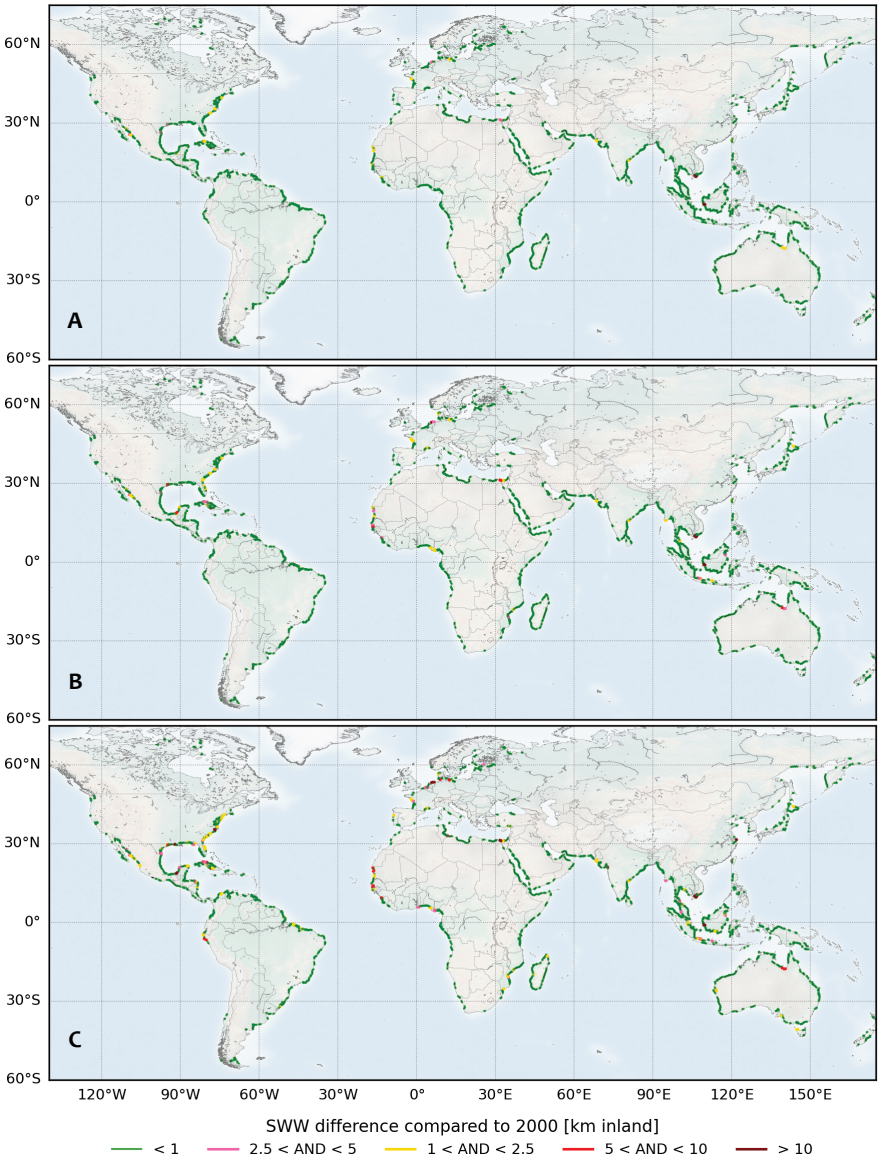

Figure 5-8 Increased inland salinization extent estimated in year 2100 expressed as inland shift (km) of saline water (17.5 g/l TDS considered as boundary – half of ocean water salinity) compared to situation in year 2000. Results are averaged over the three different DEM inputs used in our modelling study for each RCP scenario – (A) RCP 2.5, (B) RCP 4.5 and (C) RCP 8.5.

5.3.2 The impact of sea-level rises per RCP scenario for a given SRM is highly elevation dependent

Areas with elevated coastal elevation profile (Figures S14-19) show almost no changes in IFGV for all RCP scenarios. This is due to the larger fresh water influx from the inland hydrological boundary which can match the rising sea-level pressure changes. Moreover, the groundwater recharge in this study is considered equal to the current situation for the future 500 years, which further limits the potential for seawater intrusion due to sea-level rise. Such areas correspond to the earlier defined recharge-limited coastal areas and the rather negligeable impact of sea-level rise matches the findings of a previous study (Michael et al., 2013). On the other hand, as expected, our groundwater model simulations show that coastal areas with low topography (i.e., topography-limited) experience a much more severe seawater intrusion due to sea-level rise than recharge-limited areas. Naturally, large-scale overtopping (several kilometers up to tens of kilometers) by seawater due to sea-level rise does not occur in topography-limited areas with elevation higher than projected sea-level rise rates. In such cases the seawater intrusion tends to be limited to a first few kilometers at the coastline (Figures S20-22). This can be explained partly by low elevation of the first few hundred meters leading to small-scale overtopping but mostly by decrease in hydraulic gradient which leads to a landward shift of fresh-saline groundwater interface. If changes in the hydraulic gradient are only minor this shift can only be limited to few hundred meters depending on the RCP scenario.

The effects of sea-level rise on fresh groundwater volumes are the most visible in topography-limited coastal areas with very low elevation profile (i.e., lower than projected sea-level rise) stretching over a large portion of the inland coastal zone. The sea-level rise magnitude clearly impacts the magnitude of these effects where RCP 2.6 seem to have negligible effects (Figure D-17), RCP 4.5 effects are clearly visible by year 2300 (Figure D-18) and RCP 8.5 clearly impacts the fresh groundwater volumes already during the 21st century (Figure D-19). A large variation in severity of sea-level rise impacts can be observed between scenarios, especially scenario RCP 2.6 and the scenarios RCP 4.5 and RCP 8.5. The hydraulic gradient in these topography-limited coastal areas is already quite low under current conditions and therefore very sensitive to any variation due to sea-level rise. In combination with seawater overtopping of the inland areas this leads to a seawater intrusion spanning over several kilometers (Figure D-18 and Figure D-19). Variation in projected seawater intrusion severity is also observed amongst groundwater models with a different DEM input under the same RCP scenario (Figures S24-25). A few decimeters or meters change in elevation can already have significant impacts on estimated seawater intrusion in topography-limited coastal areas with very low elevation profile. This is in line with previous research conducted in low-lying areas (Minderhoud et al., 2019), and stresses the need to include the uncertainty in elevations when projecting sea-level rise effects on groundwater salinity in coastal zones.

5.3.3 Global sea-level rise impacts on IFGV decline in the coming centuries

The overall evolution of sea-level rise impacts on IFGV decline in the coming centuries is presented in Figure 5-9. As already mentioned above, a clear distinction can be made between the severity of seawater intrusion (leading to IFGV decline) estimated for each RCP scenario considered in this study. If the future sea-level rise follows the RCP 2.6 scenario, less than 10% of the SRMs would experience a decline in IFGV by the year 2500 and for more than half of the affected areas the decline would be limited to 5%-10%. Under the RCP 2.6 scenario, human societies inhabiting the coastal areas would likely have enough time and resources to design adaptation measures to tackle the impacts of sea-level rise on fresh groundwater volumes. Figure 5-9 shows that global adaptation efforts would be much larger under the RCP 4.5 and RCP 8.5 scenarios. For RCP 4.5 approximately 10% of the SRMs are projected to lose more than 5% of their IFGV for RCP 4.5 by the end of 21st century and around 5% of the SRMs a IFGV decline larger than 10%. Under RCP 8.5 the fraction of SRMs losing more than 5% of the IFGV around 2100 is about 20% and more than 10% of the SRMs show a decline of more than 5%, with a non-negligible fraction of SRMs larger than 25% reaching up to 50%. We note that these numbers are averaged over the results for three individual DEMS (Kulp and Strauss, 2019; Weatherall et al., 2015; Yamazaki et al., 2017). We have analyzed the impact of DEM input on IFGV decline for given scenarios (Section 5.2.9 and Figure D-32) and found results between DEMs to be limited to a few percent.

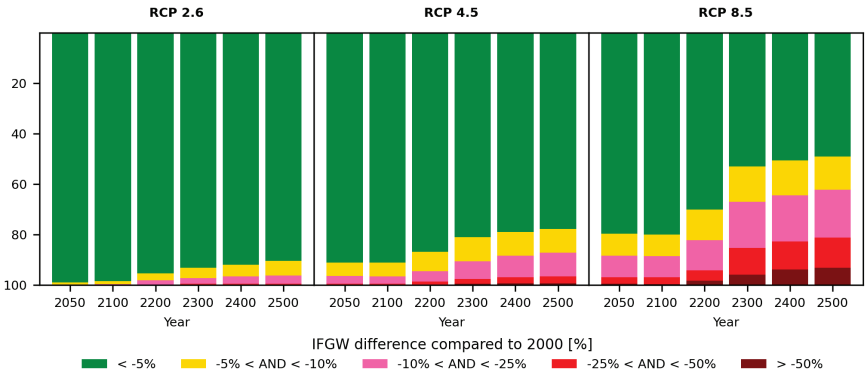

Figure 5-9 Proportional schematization of affected SRM areas per RCP scenario quantified by decline in IFGV compared to situation in year 2000.

Based on global gridded population count for year 2020 (CIESIN, 2017) around 224 million people currently live in close proximity to the current coastline (closer than 10km) in the SRMs considered in this study, see Table 5-1.By the end of the 21st century, almost 60 million people could be directly affected by limited access to fresh groundwater (decline

in IFGV between 5% and 50%) based on the RCP 8.5 scenario sea-level rise projections. Approximately one sixth of the 60 million people is estimated to live in severely impacted areas with decline in IFGV larger than 25%. In contrast, less than 8 million people would experience decline in IFGV ranging between 5% and 10% if sea-level rise follows the RCP 2.6 scenario projections. The differences between RCP2.6 and RCP8.5 increase further when projecting further into the future with 16 million and 120 million people affected by 2300 respectively. The number of people living in severely affected areas by 2300 (decline in IFGV larger than 25%) is estimated to be only 0.1 million for RCP 2.6 scenario but more than 45 million (one third of total population affected) for RCP 8.5 scenario.

The economic costs are expressed as total GDP for year 2015 in constant international 2011 USD (Kummu et al., 2018) generated in the affected coastal regions (closer than 10km to current coastline). Overall, the total yearly GDP produced in these areas is around 4625 billion USD per year, see Table 5-1. Our estimates show that under RCP 2.6 in year 2100, a GDP of around 41 billion USD per year will be affected in coastal areas with a IFGV decline of 5% or larger. None of these coastal areas will experience a decline in IFGV above 25%. By 2300, under the same scenario, the affected GDP in areas with an IGFGV decline larger than 5% rises to 214 billion USD per year. However, only 3.3 billion USD in yearly GDP would be located in severely impacted coastal areas where decline in IFGV would surpass 25%. Economic losses are far higher under more severe future sea-level rise projected by the RCP 8.5 scenario. The total yearly GDP affected in coastal areas experiencing a decline in IFGV larger than 5% would reach 1123 billion USD by year 2100, out of which 75 billion USD is located in coastal areas with decline in IFGV above 25%. By 2300, total yearly GDP affected in coastal areas with an IFGV decline larger than 5% than doubles compared to 2100, reaching 2352 billion USD per year, of which 1016 billion USD is located in coastal areas with more than 25% decline in IFGV.

Table 5-1 Total number of people living in the SRMs (up to 10km from current coastline) and the total yearly GDP produced in these areas summarized for each RCP scenario and time step. The population numbers are from year 2020 (CIESIN, 2017) and the GDP is in USD and is taken from global analysis for year 2015 (Kummu et al., 2018).

RCP	Time	Total number of people affected (millions) by % decline in IFGV compared to year 200					Total GDP affected (billion international USD) by % decline in IFGV compared to year 200				
		< 5%	5% - 10%	10% - 25%	25% - 50%	> 50%	< 5%	5% - 10%	10% - 25%	25% - 50%	> 50%
2.6	2050	215.6	7.0	0.0	0.0	0.0	4596.2	27.0	1.6	0.0	0.0
	2100	214.6	7.8	0.1	0.0	0.0	4583.0	39.1	2.1	0.0	0.0
	2200	209.5	6.3	7.9	0.0	0.0	4439.0	159.5	40.5	0.0	0.0
	2300	207.5	5.5	10.7	0.1	0.0	4427.7	146.5	63.8	3.3	0.0
	2400	204.2	7.2	12.9	0.1	0.0	4379.8	84.2	177.9	3.3	0.0
	2500	190.0	21.0	7.2	6.5	0.0	4114.5	346.2	172.6	23.3	0.0
4.5	2050	191.3	22.0	11.3	0.1	0.0	4152.4	427.4	70.2	3.3	0.0
	2100	191.2	22.8	10.5	0.1	0.0	4149.9	432.9	67.6	3.3	0.0
	2200	182.0	27.9	8.9	7.9	0.0	4007.7	428.4	285.9	39.9	0.0
	2300	171.1	27.6	19.7	1.9	6.6	3689.2	513.8	515.8	24.1	20.4
	2400	169.9	25.5	21.0	4.0	6.8	3668.7	467.9	552.3	55.4	21.5
	2500	166.6	24.5	25.5	4.1	6.8	3623.7	470.6	593.3	58.0	21.5
8.5	2050	168.0	27.3	21.2	10.4	0.1	3641.5	487.2	559.2	76.2	0.3
	2100	167.4	22.0	27.1	10.3	0.1	3640.5	455.4	592.3	75.3	0.3
	2200	138.0	34.7	36.1	11.3	7.6	3304.5	568.1	653.8	196.5	42.8
	2300	107.6	21.0	53.9	28.4	17.4	2473.8	332.5	1003.1	757.1	258.9
	2400	95.8	30.0	48.3	34.5	20.9	2340.3	433.4	958.4	729.7	387.1
	2500	95.2	28.3	49.0	34.9	22.1	2323.2	409.1	959.5	746.3	408.4

5.4 Discussion

The objective of this study is to analyze the impacts of sea-level rise on fresh groundwater resources in regions with unconsolidated sedimentary systems along the global coastline. In our analysis we opted to determine these impacts by calculating the decline in inland fresh groundwater volume (IFGV) rather than providing quantitative IFGV estimates. We stress that this is a global study using global datasets and parametrizations that, albeit specific for the coastal regions identified, may deviate from local salinity measurements or local groundwater models with higher complexity, local input data input and grid resolution. Thus, expressing the future trend in IFCV decline in percentage change compared to the estimated situation in year 2000 ensures that we can identify the potentially most threatened regions by sea-level rise (and its impact on fresh groundwater volume) despite the lack in local data and information. Our results show that the future state of fresh groundwater resources in coastal zones considered in this study varies dramatically between different RCP scenarios. The worst-case scenario RCP 8.5 would lead to around 20% of all SRMs experiencing reduced IFGV volumes by 2100, rising to almost 50% by year 2300. In comparison, the fraction affected SRMs under RCP 2.6 would be only around 1% by 2100 and 7% by year 2300. Coastal areas with low topography will be the most threatened, as concluded by previous global study of sea-level rise impacts on coastal groundwater salinization (Michael et al., 2013). These coastal areas with low topographical gradients also have low hydraulic gradients and are shown to be more prone to increased salinization as result of sea-level rise (Ferguson and Gleeson, 2012). In areas with higher hydraulic gradient, defined as 1m groundwater vertical head difference per 1000m profile length (Ferguson and Gleeson, 2012), sea-level is deemed to have only very limited impacts on IFGV. In our study we observe the same trend with relatively low IFGV decrease on global scale by the end of 21st century. However, if sea-level rise continues and even accelerates over the next centuries (RCP 8.5) the negative impacts will be much more severe and will affect even areas with higher hydraulic gradients.

For simplicity, we used a fixed but spatial varying groundwater recharge (Figure D-6) for all RCP sea-level scenarios. The groundwater recharge used is on the high side (globally 20 963 km³/yr) when compared to other global studies, with values ranging from 12 666 to 17 000 km³/yr (Mohan et al., 2018). On the other hand, the estimated average yearly groundwater recharge rate (142,8 mm/yr) is only slightly different from the recent global study (Mohan et al., 2018) showing the average value to be 134 mm/yr. This suggests that there are possible areas where groundwater recharge rates are somewhat overestimated. The used paleo groundwater recharge reflects the climate changes that occurred since the Last Glacial Maximum (Lone et al., 2018), showing a wetter period followed by a dry and arid period between 6000 years BP and 3000 years BP, as well as regional studies dealing with paleo groundwater recharge (Mabrouk et al., 2019; Trabelsi et al., 2020). Due to our attention to the effect of sea-level rise while limiting the number of climate runs, we did not consider future changes in groundwater recharge. However, as changes in future groundwater recharge may be considerable between different regions (Wu et al., 2020), it will be of interest to include it in future impact studies.

The chosen grid size for our groundwater models (100m column width and 10m layer thickness) provides almost identical estimates to finer grid size-based groundwater models while performing at much smaller runtimes (Section 5.2.8; Figure D-7). This grid size also fits in the range of previous large-scale studies on coastal fresh groundwater salinization (Engelen et al., 2018; Feseker, 2007; Michael et al., 2016, 2013; Pham et al., 2019; Thomas et al., 2019; Været et al., 2012; Van Camp et al., 2014; Vandenbohede and Lebbe, 2006; Xiao et al., 2018). The time resolution of our groundwater models consists of 42 stress periods (see Figure 5-5) spanning from 30000 years BP to 500 years into the future. Including these long integration times, combined with changing paleo groundwater recharge rates, are necessary to correctly simulate the current salinity patterns, including past climate change and sea levels and particularly the early Holocene rapid-sea-level rise (Cohen et al., 2010; Delsman et al., 2014; Engelen et al., 2019; Gossel et al., 2010; Larsen et al., 2017; Meisler et al., 1984; Meyer et al., 2019).

Recent literature review dealing with sea-level rise effects on seawater intrusion in coastal aquifers concluded that it is crucial to move away from hypothetical or highly simplified coastal aquifer representations towards more complex hydrogeological representations (Ketabchi et al., 2016). In our study we navigate around missing local geological data (e.g., boreholes) by implementing a semi-randomized generation of hydrogeological schematizations (reflecting sub-regional coastal geological settings. This approach is based on several key global geological datasets (Gleeson et al., 2014; Hartmann and Moosdorf, 2012; Huscroft et al., 2018; Montzka et al., 2017) and an estimation of regional geological heterogeneity conditions (Zamrsky et al., 2020, 2018); further details are provided in Section 5.2.1. In accordance with aforementioned review (Ketabchi et al., 2016), our groundwater modelling approach also includes past sea-level rise (over multiple stress periods) and topographic slopes based on three different global DEM datasets. Although this approach brings our large-scale analysis closer to actual regional conditions, there is still a gap to close to arrive at accurate sub-regional to local estimates. This gap could be closed by including local geological data (once available on global scale) into our hydrogeological simulations, but also other local drivers such as pumping wells and river systems. These drivers were not included in our current groundwater models due to both lack of information on global scale (e.g., pumping station locations and pumping rates) and because they require three-dimensional simulations that are as yet too expensive to apply globally. It can be assumed that especially groundwater pumping over long periods of time (i.e., decades) could have a large negative impact on the estimated fresh groundwater volume in coastal zones (Ferguson and Gleeson, 2012; Pauw et al., 2015; Van Camp et al., 2014). Therefore, future studies should involve three-dimensional groundwater models and include groundwater pumping effects to provide more accurate current and future groundwater salinization estimates.

DEM datasets (and their vertical accuracy) play a crucial role when estimating groundwater flow and salinization patterns, as previously shown in a study in the Mekong Delta (Minderhoud et al., 2019). Therefore, we evaluate the impact of three different global DEM datasets on coastal groundwater salinization caused by sea-level rise. We observe limited yet significant differences between the groundwater model outcomes for

the three DEM datasets. The recently developed Coastal DEM dataset (Kulp and Strauss, 2019) is focused on low lying areas and enhances the vertical correction of original SRTM input (Rodriguez et al., 2006) in urban areas (defined as an area with more than 100.000 inhabitants and "urban" land use type). Groundwater models using the Coastal DEM as input show higher number of SRMs in urban areas affected, compared to groundwater models using the other two DEMs (Figure D-32). These differences confirm that DEM datasets play an important role in coastal groundwater modelling and sea-level rise impacts analyses.

Rising sea-levels will also lead to increase coastal flooding hazards (Muis et al., 2016; Vousdoukas et al., 2016; Wahl, 2017) which we do not take into account. However, we can compare our projection of total number of people living in the coastal areas that will be affected by IFGV decline to similar projections in global coastal flooding analyses (Kirezci et al., 2020; Kulp and Strauss, 2019). These studies project that between 176 - 287 million people (Kirezci et al., 2020) to 630 million people (Kulp and Strauss, 2019) will be living in areas affected by coastal flooding by year 2100 under RCP 8.5. Our projections suggest that approximately 225 million people that live in close proximity to current coastline (up to 10km) will be threatened by a decline in IFGV (albeit lower than 5%) due to sea-level rise by 2100, with 60 million experiencing a decline larger than 5%, which is similar in magnitude as estimated for coastal flooding. The decrease in IFGV will negatively impact the fresh water availability in affected areas and could lead to fresh water shortages for domestic, industrial and agricultural use. Increased groundwater salinity and flooding by rising sea-levels can also lead to soil salinization further increasing the stress on agricultural production in affected areas (Daliakopoulos et al., 2016; Herbert et al., 2015; Pitman and Läuchli, 2002; Qadir et al., 2014). The economic losses by coastal floods could potentially be devastating for human communities living in coastal areas; it is estimated that coastal flooding could expose assets totaling between 8813 and 14178 billion USD in GDP by the end of the 21st century (Kirezci et al., 2020). In comparison, we estimate that about 4625 billion USD in GDP worth of assets would be threatened by IFGV decline in year 2100. This alone is an alarming number and if we take into account the combined effects of both sea-level rise and coastal flooding, the costs (human, environmental and economic) for coastal areas in the coming century could be immense. Avoiding the path of the RCP 8.5 scenario should be prioritized as a global challenge for humanity in this century, along with adaptation and mitigation plans for limiting the impacts of sea-level rise (and associated effects) on fresh groundwater volumes and thus also securing fresh water availability in coastal areas worldwide.

6 Synthesis

6.1 Introduction

The main objective of this research is ***to assess the current and future state of groundwater resources in coastal areas hosting unconsolidated sediment systems around the world***. The steps undertaken to achieve this goal are discussed in more detail in Chapters 2 to 5. Answers to research questions posed in the Introduction (Chapter 1.3) are discussed in the sections below, followed by recommendations for further research.

6.2 Research questions

How to estimate regional coastal unconsolidated sediment aquifer thickness based on available global topographical and geological datasets? (Chapter 2)

Aquifer thickness is an important input in groundwater models, even more so in coastal areas where it influences the saltwater intrusion extent inland. Several global datasets provide an estimate sediment thickness on global scale but unfortunately only for the soil layer (Montzka et al., 2017; Pelletier et al., 2016) or do not differentiate between the unconsolidated and consolidated sediments (De Graaf et al., 2015). The underlaying assumption in our approach is that unconsolidated sediment aquifers and aquitards overtop older consolidated bedrock formations that outcrop further inland. First, a topographical profile along individual cross-sections perpendicular to the coastline is extracted from a global digital elevation model (Weatherall et al., 2015). Next, the unconsolidated sediment thickness is estimated by approximating the slope of the bedrock and extending it in the seaward direction. Final thickness estimation is then gathered as a difference between the DEM elevation and estimated depth to bedrock at the coastline.

The estimated unconsolidated sediment thickness values are in the same order of magnitude as collected literature sources and geological boreholes. However, occasional large differences between the estimated thickness values and borehole data suggests that this approach is not suited to estimate local scale variations in thickness. On the other hand, validation with literature sources and borehole data shows an improved performance in areas with unconsolidated sediment thickness varying between 100m and 300m. The results show largely underestimated thickness values in deeper systems, found for example in deltaic areas. This is probably caused by limited extent of the coastal cross-sections (200km) compared to the extent of some deltaic areas which leads to inaccurate bedrock slope estimates. In general, the global estimation of unconsolidated sediment thickness provides a suitable first-order estimate and complements the already existing global datasets.

In addition to the thickness estimation, the influence of varying aquifer thickness is tested using numerical variable-density groundwater flow models. Substantial differences in estimated groundwater salinity profiles are observed for simulations with extreme values (minimum and maximum considered thickness). Testing several geological scenarios shows that geological heterogeneity has a larger impact on estimated groundwater salinity than small variations in aquifer thickness, which is in line with other recent studies (Ketabchi et al., 2016; Werner et al., 2013) and comparison with local to regional scale studies (Trapp Jr. et al., 1997; Yechieli et al., 2010). Based on this observation, the focus of the thesis is directed to estimating the geological heterogeneity in coastal profiles.

How to quantify geological heterogeneity in unconsolidated sediment systems in coastal areas worldwide and what is its influence on offshore fresh groundwater presence? (Chapter 3)

Estimating and quantifying geological heterogeneity in unconsolidated sediment aquifer-aquitard systems worldwide is a necessary step before building large-scale variable-density groundwater flow numerical models. A geological heterogeneity methodology using available global datasets is designed to provide a first-order quantification of global geological heterogeneity in unconsolidated sedimentary aquifer-aquitard systems. Limitations in globally available data and information requires simplifications and assumptions and leads to defining several proxy geological heterogeneity parameters allowing for regional stratigraphical profiles estimation based on number, position and thickness of individual aquifers and aquitards. However, we show that these geological heterogeneity parameters can be used to ensemble synthetic representative geological profiles by randomizing several input parameters. These parameters include the number of aquifers and aquitards, the thickness of individual aquifers and aquitards, presence (or absence) of offshore low permeable capping layer (clay), and a parameter simulating clay deposition in upper parts of aquitards during higher sea-level stands.

These randomly generated synthetic representative geological profiles aim at reproducing the nature of regional geological heterogeneity and as such are used as input for variable-density groundwater models set up for seven coastal regions. By testing numerous randomized synthetic representative geological profiles, it is shown that there are potentially large offshore fresh groundwater volumes in several regions, which is in agreement with a previous global study (Post et al., 2013). The non-renewability of the offshore fresh groundwater demonstrated by other studies (Morgan et al., 2018; Thomas et al., 2019) is confirmed by our groundwater models and shows that it has been deposited by fresh groundwater recharge (precipitation) during past sea-level low stands. Our groundwater models show that the preservation of this deposited fresh groundwater during the rapid sea-level rise in the past 20 000 years is dependent on the presence of a low permeable (clay) capping layer in the continental shelf domain. Similarly, coastal unconsolidated sediment systems with higher number of aquifer-aquitard sequences are

more prone to have thinner and discontinuous aquitards which leads to easier vertical saltwater intrusion (Kooi et al., 2000; Kooi and Groen, 2001).

Comparing the estimated offshore fresh groundwater volumes to observed values (Post et al., 2013) in two sample regions shows the potential viability of our approach on regional scale. However, assuming constant porosity values can lead to overestimations and should be taken into account if such information is available. While more detailed local geological information is not yet available, the presented stochastic synthetic representative geological profile methodology and geological heterogeneity quantification can provide a good first order estimate of offshore fresh groundwater presence in coastal regions around the world.

Can offshore fresh groundwater be a viable source of fresh water in coastal areas with high water stress? (Chapter 4)

Presence of offshore fresh groundwater (OFG) is examined by building a large set of groundwater models and applying the geological heterogeneity parameters to build ensembles of random synthetic representative geological representations to regions with unconsolidated sediment systems along the global coastline. The global OFG volume in unconsolidated sediment systems is estimated to be 1.06 ± 0.2 million km³ which is approximately three times higher than estimated by previous global study that was based on purely literature review (Post et al., 2013). The most recent study that focuses on global OFG occurrence (Micallef et al., 2021) estimates the total volume to be also approximately 1 million km³ but state that majority is stored in siliciclastic aquifers, suggesting that our global estimations may overestimate the total OFG volume. This can be explained by a relatively high constant porosity value (0.3) considered in our groundwater models which leads to overestimating the OFG volume. This hypothesis is tested by building groundwater models with low porosity (0.1); the results show half the OFG volume estimates as compared to groundwater models with higher porosity value (0.3).

Comparison with observed occurrence of OFG is challenging due to the regional scale of the groundwater model analysis where a single region could cover thousands of kilometers of coastline. However, comparing our OFG volume estimations with proven OFG occurrences (Micallef, 2020) shows relatively good fit (see Figure 6-1) where most locations correspond to regions with higher estimated OFG volumes. Additionally, the extent (depth and offshore extent) of estimated OFG by our groundwater models is compared to a set of collected regional studies. A good match between our estimations and literature sources can be observed in all but several locations. Nevertheless, further validation with local and regional observations as well as larger level of detail in groundwater model input and scale should be considered to obtain more accurate OFG volume estimations.

Several regions with high fresh water demand where OFG could act as an additional fresh water source are identified. Offshore pumping infrastructure is already present in some of

these regions which demonstrate it is feasible and could lower the costs of OFG exploitation. This potential of offshore fresh groundwater resources to alleviate water stress should be especially studied in several densely populated deltaic regions with estimated high OFG volumes (e.g., Niger, Grijalva, Rio Grande, Yangtze, Irrawaddy and Indus deltas). Potential environmental impacts (Haakon and Fridtjof, 2012; Knight et al., 2018) and high investment costs into extraction infrastructure (Amado, 2013) should be considered in any further exploration of OFG as viable source of fresh water in a specific region. The quality of extracted OFG might not directly correspond to drinking water standards but could be used as input into desalination plants. Due to currently high costs of desalination infrastructure (Jones et al., 2019), using offshore fresh to brackish groundwater resources for desalination purposes might be possible in highly developed countries.

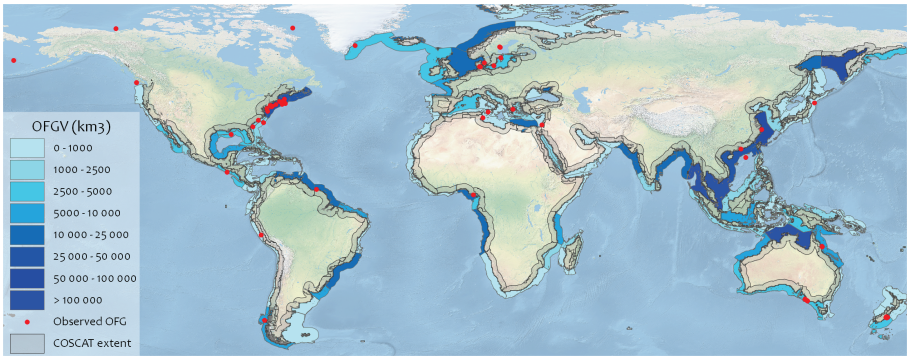

Figure 6-1 Estimated occurrence and offshore fresh groundwater volume (OFGV) in unconsolidated sediment systems along the global coastline. The red dots represent locations where offshore freshened groundwater (OFG) was observed, observations limited to unconsolidated sediments only (Micallef, 2020).

What are the threats of different sea-level rise scenarios on future coastal fresh groundwater resources? (Chapter 5)

Latest climate research (H.-O. Pörtner et al., 2019) states that global warming and climate change will cause rising sea levels in 21st century and beyond, where the severity of sea-level rise highly depends on the CO2 emission (RCP) scenario considered. Potentially devastating impacts on the coastal fresh groundwater resources are assessed by combing the geological heterogeneity (see Chapter 3 and 4) with regional scale groundwater modelling technique (see Chapter 5) resulting in a large set of groundwater models. Coastal regions considered in Chapter 4 are further split into smaller coastal stretches to account for smaller scale elevation variations which play an important role in the severity of sea-level rise impacts on coastal fresh groundwater resources (Michael et al., 2013; Yu

et al., 2016). The effects of three RCP scenarios are studied, ranging from RCP 2.6 scenario, predicting limited sea-level rise over the coming centuries, to RCP 8.5 scenario estimating sea-level rise of more than 3.5m by year 2300. Furthermore, because vertical errors in elevation can have large impacts on estimated groundwater head and salinity profiles (Minderhoud et al., 2019) we study the outcome of applying three different global digital elevation models (DEMs) as input into the groundwater models.

The impact of sea-level rise on future inland fresh groundwater volume (IFGV) is measured by comparing estimated IFGV for the year 2000 with future estimations (up to the year 2500). The proposed regional scale approach is better suited to estimate future relative decline in IFGV, rather than quantifying the absolute values of IFGV itself since our groundwater models represent rather large coastline stretches (up to few hundred kilometers). In accordance with a previous global study of sea-level rise effects on coastal groundwater (Michael et al., 2013), decline in IFGV is smaller in higher elevated coastal areas than in low lying coastal areas. This is a result of both seawater inundation of the land in low lying areas and lowering of hydraulic gradients leading to lower fresh groundwater flow from inland.

Our findings show that by the end of the 21st century several coastal regions are likely to experience a large decline in IFGV if the sea-level rise follows the RCP 8.5 sea-level projections. On the other hand, under the RCP 2.6 scenario almost no coastal regions would experience a significant decline in IFGV. The difference is even larger when looking further into the future. By year 2300 approximately 50% of considered coastal regions in our study could experience significant decline in IFGV for the RCP 8.5 scenario compared to 7% for RCP 2.6. This would lead to an immense difference in number of people affected as well as economic losses in coastal areas worldwide, stressing the need to curb CO2 emissions in order to avoid the worst-case RCP 8.5 scenario. While the DEM datasets have lesser impact on predicted decline in IFGV than RCP scenarios, a significant difference in groundwater model outcome can still be observed. Vertical differences between the different DEM datasets are especially influential on estimated decline in INFGV in low lying urban areas with high population densities. Therefore, the quality of DEM input and its suitability for a specific region should be always taken into account in smaller scale studies.

6.3 Recommendations for further research

Despite the efforts and advances presented in this study, there are still several key aspects that should be addressed in the future to improve the quality of the estimates of large-scale groundwater salinity and salinization trends.

6.3.1 Global hydrogeological database

Arguably the most limiting factor encountered during this study was the lack of global hydrogeological information, both regarding geological boreholes and groundwater salinity measurements. Several recent studies focused on collecting global salinity data

both offshore (Micallef, 2020) and inland (Thorslund and van Vliet, 2020). These studies already provide valuable information for global studies but further development is necessary to improve the quality of large-scale groundwater models in coastal areas. Collecting such data from literature sources, private entities, academic and governmental bodies require an extensive effort and collaboration and should be approached in dedicated manner by preferably multiple institutions and researchers.

A global geological borehole dataset would improve the overall accuracy of groundwater models. In our case it could be used to constrain several randomized geological heterogeneity parameters that lay the foundation for creating the ensembles of synthetic geological profiles (see Chapter 3). Both collecting the borehole data and unifying the lithological classification of the many potential data sources would be a major challenge. Private companies often possess large amount of data that are unfortunately unavailable for academic purposes. Convincing these companies to share their data could lead to major scientific advancements in coming years. Australia is a leading example by forcing oil exploration companies to share their drilling data in unused and closed wells. Unfortunately, this seems to be the sole example around the world and it is only wishful thinking that private companies would willingly share their data with the public.

6.3.2 Building large-scale 3D models

Only 2D groundwater models are considered in this study which required several simplifications as well as excluding the influence of rivers and groundwater pumping which need a 3D groundwater model to be simulated. The developed 2D groundwater models should be seen as a basis for further more complex groundwater modelling studies that will involve 3D models. The vast computational requirements of 3D models often lead to compromises in their temporal and spatial extent. For example, computation time could be saved by using 2D groundwater models for paleo reconstruction and interpolating the 2D cross-sectional results into a 3D grid. Realistic initial salinity and groundwater head conditions could be acquired in such manner while saving computational resources. Recent developments in PCR-GLOBWB global hydrological model involving higher resolution and parallel computation (Verkaik et al., 2019) are a major step in global hydrological modelling. Implementing variable-density groundwater flow modelling into this global model could bring a first global 3D saltwater intrusion assessment. The computational demands would still be high despite parallelization and applying 2D models for initial condition estimation.

6.3.3 Investigate the potential of offshore fresh groundwater

Our study shows that there are potentially large reserves of offshore fresh groundwater trapped in relatively shallow depths in the continental shelves along the global coastline. This non-renewable source of fresh (or brackish) groundwater should be further studied as potential source of water for agricultural, domestic and industrial use, either directly or through desalination (Jones et al., 2019).

6.3.4 Mitigation and adaptation measures

Sea-level rise is the only future risk factor considered in our global groundwater modeling analysis. To secure fresh water resources in coastal areas for the coming decades, many more risks should be studied. If the interpolation from 2D to 3D groundwater head and salinity is developed, 3D groundwater models simulating conditions in past and future decades or centuries could be computationally achievable on larger scales. The effect of other risks such as groundwater extractions, land subsidence, storm surges, droughts and urbanization should also be studied while at the same time adaptation and mitigation strategies (e.g., managed aquifer recharge) should be considered to guarantee fresh water remain available to humans and nature in coastal areas around the world.

Appendices

A Appendix to Chapter 2

Table A-1 Borehole validation dataset sources.

Dataset Name	*Source*
CPRM	Geological survey of Brazil, c2016, published by Companhia de Pesquisa de Recursos Minerais [Accessed 2016, August], http://www.cprm.gov.br/
GeoVIC	Online geology portal of Victoria, Australia, c2016, published by the state of Victoria [Accessed 2016, October], http://er-info.dpi.vic.gov.au/sd_weave/anonymous.html
CGS	China Geological Survey, 2012. Groundwater serial maps of Asia: Hydrogeological map, Groundwater resources map, Geothermal map, Sinomaps Press.

Table A-2 Literature validation dataset sources.

Polygon ID	*Source*
1	Lagudu, S. et al., 2013. Use of Geophysical and Hydrochemical Tools to Investigate Seawater Intrusion in Coastal Alluvial Aquifer, Andhra Pradesh, India. In C. Wetzelhuetter, ed. Groundwater in the Coastal Zones of Asia-Pacific. Dordrecht: Springer Netherlands, pp. 49–65.
2	Singh, S.C., 2013. Geophysical Viewpoints for Groundwater Resource Development and Management in Coastal Tracts. In C. Wetzelhuetter, ed. Groundwater in the Coastal Zones of Asia-Pacific. Dordrecht: Springer Netherlands, pp. 67–87.
3	Duerrast, H. & Srattakal, J., 2013. Geophysical Investigations of Saltwater Intrusion into the Coastal Groundwater Aquifers of Songkhla City, Southern Thailand. In C. Wetzelhuetter, ed. Groundwater in the Coastal Zones of Asia-Pacific. Dordrecht: Springer Netherlands, pp. 155–175.
4	Sherif, M., Almulla, M. & Shetty, A., 2013. Seawater Intrusion Assessment and Mitigation in the Coastal Aquifer of Wadi Ham. In C. Wetzelhuetter, ed. Groundwater in the Coastal Zones of Asia-Pacific. Dordrecht: Springer Netherlands, pp. 271–294.
5	Leonhard, L., Burton, K. & Milligan, N., 2013. Gascoyne River, Western Australia; Alluvial Aquifer, Groundwater Management and Tools. In C. Wetzelhuetter, ed. Groundwater in the Coastal Zones of Asia-Pacific. Dordrecht: Springer Netherlands, pp. 359–378.
6	Wagner, F., Tran, V.B. & Renaud, F.G., 2012. Groundwater Resources in the Mekong Delta: Availability, Utilization and Risks. In F. G. Renaud & C. Kuenzer, eds. The Mekong Delta System: Interdisciplinary Analyses of a River Delta. Dordrecht: Springer Netherlands, pp. 201–220.
7	Benkabbour, B., Toto, E.A. & Fakir, Y., 2004. Using DC resistivity method to characterize the geometry and the salinity of the Plioquaternary consolidated coastal aquifer of the Mamora plain, Morocco. Environmental Geology, 45(4), pp.518–526. Available at: http://link.springer.com/10.1007/s00254-003-0906-y.

Polygon ID	*Source*
	Amharref, M. et al., 2007. Cartographie de la vulnérabilité à la pollution des eaux souterraines: Application à la plaine du Gharb (Maroc). Journal of Water Science, 20(2), pp.185–199.
8	Chen, J. et al., 2014. Clay minerals in the Pliocene - Quaternary sediments of the southern Yangtze coast, China: Sediment sources and palaeoclimate implications. Journal of Palaeogeography, 3(3), pp.297–308. Available at: http://dx.doi.org/10.3724/SP.J.1261.2014.00057.
9	Cobaner, M. et al., 2012. Three-dimensional simulation of seawater intrusion in coastal aquifers: A case study in the Goksu Deltaic Plain. Journal of Hydrology, 464-465, pp.262–280. Available at: http://dx.doi.org/10.1016/j.jhydrol.2012.07.022.
10	Carretero, S. et al., 2013. Impact of sea-level rise on saltwater intrusion length into the coastal aquifer, Partido de La Costa, Argentina. Continental Shelf Research, 61-62, pp.62–70. Available at: http://dx.doi.org/10.1016/j.csr.2013.04.029.
11	Rasmussen, P. et al., 2013. Assessing impacts of climate change, sea-level rise, and drainage canals on saltwater intrusion to coastal aquifer. Hydrology and Earth System Sciences, 17(1), pp.421–443. Available at: http://www.hydrol-earth-syst-sci.net/17/421/2013/.
12	Kalm, V. & Gorlach, A., 2014. Impact of bedrock surface topography on spatial distribution of Quaternary sediments and on the flow pattern of late Weichselian glaciers on the East European Craton (Russian Plain). Geomorphology, 207, pp.1–9. Available at: http://dx.doi.org/10.1016/j.geomorph.2013.10.022.
13	Chen, J. et al., 2014. Clay minerals in the Pliocene - Quaternary sediments of the southern Yangtze coast, China: Sediment sources and palaeoclimate implications. Journal of Palaeogeography, 3(3), pp.297–308. Available at: http://dx.doi.org/10.3724/SP.J.1261.2014.00057.
14	Sefelnasr, A. & Sherif, M., 2014. Impacts of Seawater Rise on Seawater Intrusion in the Nile Delta Aquifer, Egypt., 52(2), pp.264–276.
15	Singaraja, C. et al., 2015. A study on the status of saltwater intrusion in the coastal hard rock aquifer of South India. Environment, Development and Sustainability, 17(3), pp.443–475. Available at: http://dx.doi.org/10.1007/s10668-014-9554-5.
16	Khaki, M. et al., 2016. Integrated geoelectrical and hydrogeochemical investigation for mapping the aquifer at Langat Basin, Malaysia. Environmental Earth Sciences, 75(4), pp.1–14. Available at: "http://dx.doi.org/10.1007/s12665-015-5182-0.
17	Giresse, P. et al., 2000. Successions of sea-level changes during the Pleistocene in Mauritania and Senegal distinguished by sedimentary facies study and U / Th dating., 170. Sylla, M., Medou, J.O. & Samb, E.., 1997. Contribution of the instaneous well logging to the study of the indurations. Bulletin of the International Association of Engineering Geology, (55).
18	Nicholas, C.J. et al., 2006. Stratigraphy and sedimentology of the Upper Cretaceous to Paleogene Kilwa Group, southern coastal Tanzania. , 45, pp.431–466.
19	Yechieli, Y., Sivan, O. (2010), Using geochemical tools to study the distribution of saline groundwater in aquifers separated by aquitards: examples from Israel, paper presented at the 21th Salt Water Intrusion Meeting, Azores, Portugal

Polygon ID	*Source*
20	Dirks et al. (1988), Groundwater in Bekasi district, West Java, Indonesia, paper presented at the 10th Salt Water Intrusion Meeting, Gent, Belgium
21	McPherson, A. & Jones, A., 2005. Appendix D: Perth Basin geology review and site class assessment. Natural Hazard Risk in Perth, pp.313–344. Available at: https://www.icsm.gov.au/image_cache/GA6548.pdf.
22	Ransley, T.R., Radke, B.M., Feitz, A.J., Kellett, J.R., Owens, R., Bell, J., Stewart, G. and Carey, H. 2015. Hydrogeological Atlas of the Great Artesian Basin, Geoscience Australia, Canberra. http://dx.doi.org/10.11636/9781925124668
23	Yeates, A.N. et al., 1984. Regional geology of the onshore Canning Basin, Western Australia. The Canning Basin, Western Australia, pp.23–56.
24	Custodio, E. (1992), Preliminary outlook of saltwater intrusion conditions in the Donana National Park (southern Spain), paper presented at 12th Salt Water Intrusion Meeting, Barcelona, Spain Plata, J.L. and Rubio, F.M. (2004), Study of the salt water - fresh water interface in environments of low resistivity: Donana aquifer (Spain), paper presented at the 18th Salt Water Intrusion Meeting, Cartagena, Spain Custodio, E., V. Iribar, M. Manzano, A. Bayó and A. Galofré (1986), Evolution of sea water intrusion in the Llobregat Delta, Barcelona, Spain, paper presented at the 9th Salt Water Intrusion Meeting, Delft, The Netherlands
25	Falgas, E., Ledo, J., Teixido, T., Gabas, A., Ribera, F., Arango, C., Queralt, P., Plata, J.L., Rubio, F.M., Pena, J.A., Marti, A., Marcuello, A. (2004), Geophysical characterization of a mediterranean coastal aquifer: The Baixa Tordera fluvio-deltaic aquifer unit (Barcelona, NE Spain), paper presented at the 18th Salt Water Intrusion Meeting, Cartagena, Spain
26	Aunay, B., Duvail, C., Le Strat, P., Dorfliger, N., Lachassagne. P. and Pistre, S. (2004), Importance of a high resolution lithological and geometrical knowledge for Mediterranean coastal sedimentary aquifers management. Application to the Roussillon basin, South of France, paper presented at the 18th Salt Water Intrusion Meeting, Cartagena, Spain
27	Cau, P., Lecca, G., Muscas, L., Barrocu, G. and Uras, G. (2002), Seawater intrusion in the plain of Oristano (Sardinia, Italy), paper presented at the 17th Salt Water Intrusion Meeting, Delft, The Netherlands
28	Ardau, F., Balia, R., Barbieri, G., Barrocu, G., Gavaudo, E. and Ghiglieri, G. (2002), Recent development in hydrogeological and geophysical research in the Muravera coastal plain (SE Sardinia, Italy), paper presented at the 17th Salt Water Intrusion Meeting, Delft, The Netherlands
29	Ferrara, V. and Pennisi, A. (2004), Salt water intrusion and its influence on groundwater use in the Siracusa area (south-eastern Sicily), paper presented at the 13th Salt Water Intrusion Meeting, Cagliari, Italy
30	Bencini, A. & Pranzini, G. (1992), The salinization of groundwaters in the Grosseto Plain (Tuscany, Italy), paper presented at the 12th Salt Water Intrusion Meeting, Barcelona, Spain

Polygon ID	*Source*
31	Pranzini, G. (2002), Groundwater salinization in Versilia (Italy), paper presented at the 17th Salt Water Intrusion Meeting, Delft, The Netherlands
	Van Houtte, E., Lebbe, L., Zeuwts L. and Vanlerberghe, F. (2002), Concept for development of sustainable drinking-water production in the Flemish coastal plain based on integrated water management, paper presented at the 17th Salt Water Intrusion Meeting, Delft, The Netherlands
32	Lebbe, L.C. and K. Pede (1986), Salt-fresh water flow underneath old dunes and low polders influenced by pumpage and drainage in the Western Belgian coastal plain, paper presented at 9th Salt Water Intrusion Meeting, Delft, The Netherlands
	Lebbe, L. and K. Walraevens (1988), Hydrogeological SWIM-excursion to the western coastal plain of Belgium, paper presented at the 10th Salt Water Intrusion Meeting, Gent, Belgium
	Lotringen, I.G.J, van, and R. H. Boekelman (1986), Behaviour of circular fresh water lenses, paper presented at the 9th Salt Water Intrusion Meeting, Delft, The Netherlands
33	Meerten, J.J. van, and R.H. Boekelman (1986), Well-infiltration in fresh-water pockets in sandy ridges in Zeeland, paper presented at the 9th Salt Water Intrusion Meeting, Delft, The Netherlands
	Walraevens et al. (1988), Hydrogeological SWIM-excursion to the Black-Sluice Polder area in the Flemish Valley of Belgium, paper presented at the 10th Salt Water Intrusion Meeting, Gent, Belgium
	Delsman, J.R. et al., 2013. Palaeo-modeling of coastal salt water intrusion during the Holocene: an application to the Netherlands. Hydrology and Earth System Sciences Discussions, 10(11), pp.13707–13742. Available at: http://www.hydrol-earth-syst-sci-discuss.net/10/13707/2013/hessd-10-13707-2013.html.
	Oude Essink, G.H.P. (2002), Salinization of the Wieringermeerpolder, The Netherlands, paper presented at the 17th Salt Water Intrusion Meeting, Delft, The Netherlands
	Stuyfzand, P.J. (1992), Behaviour of major and trace consituents in fresh and salt intrusion waters, in the western Netherlands, paper presented at the 12th Salt Water Intrusion Meeting, Barcelona, Spain
34	Stuyfzand, P.J. (1988), Hydrochemical evidence of fresh- and salt-water intrusions in the coastal dunes aquifer system of the western Netherlands, paper presented at the 10th Salt Water Intrusion Meeting, Gent, Belgium
	Pomper, A.B. (1972), Evidence of the influence of man on the natural processes related with salinization of groundwater in the western part of West-Netherlands, paper presented at the 3rd Salt Water Intrusion Meeting, Copenhagen, Denmark
	Roebert, A.J. (1972), Salt water contamination of the wells along the Barnaart-Schuster Canal in the Amsterdam Dune Water Catchment Area, paper presented at the 3rd Salt Water Intrusion Meeting, Copenhagen, Denmark
	Roebert, A.J. (1972), Salt water contamination of the wells along the Barnaart-Schuster Canal in the Amsterdam Dune Water Catchment Area, paper presented at the 3rd Salt Water Intrusion Meeting, Copenhagen, Denmark

Polygon ID	*Source*
	Pomper, A.B. (1977), An estimation of chloride intrusion in the midwest Netherlands during the Pleistocene epoch, paper presented at the 5th Salt Water Intrusion Meeting, Medmenham, United Kingdom
	De Vries, J.J. (1981), The distribution of fresh and salt groundwater in the Dutch coastal area and the Quaternary-geological evolution, paper presented at the 7th Salt Water Intrusion Meeting, Uppsala, Sweden
35	Rogge, A. & V. Josopait (1992), Salinization caused by groundwater abstraction from an aquifer on the german North Sea coast, paper presented at the 12th Salt Water Intrusion Meeting, Barcelona, Spain
36	Fidelibus, M.D., Gimenez, E., Morell, I. & Tulipano, L. (1992), Salinization processes in the Castellon plain aquifer (Spain), paper presented at the 12th Salt Water Intrusion Meeting, Barcelona, Spain
37	Bayo. A., Loaso. C., Aragones, J.M. & Custodio, E. (1992), Marine intrusion and brackish water in coastal aquifers of Southern Catalonia and Castello (Spain): a brief survey of actual problems and circumstances, paper presented at the 12th Salt Water Intrusion Meeting, Barcelona, Spain
38	Fidelibus, M.D., Caporale, F. and Spilotro. G. (2004), Studies on different kinds of salinisation in the ground waters of the Ionian coastal plain of the Basilicata region, paper presented at the 18th Salt Water Intrusion Meeting, Cartagena, Spain
39	Planert, M. & Williams, J.S., 1995. Ground Water Atlas of the United States: Segment 1, California, Nevada - ed.,
40, 41	Olcott, P.G., 1995. Ground Water Atlas of the United States: Segment 12, Connecticut, Maine, Massachusetts, New Hampshire, New York, Rhode Island, Vermont - ed., Available at: http://pubs.er.usgs.gov/publication/ha730M.
42, 43, 44	Trapp Jr., H. & Horn, M.A., 1997. Ground Water Atlas of the United States: Segment 11, Delaware, Maryland, New Jersey, North Carolina, Pennsylvania, Virginia, West Virginia - ed.,
45	Ryder, P.D., 1996. Ground Water Atlas of the United States: Segment 4, Oklahoma, Texas - ed., Available at: http://pubs.er.usgs.gov/publication/ha730E.
46, 47, 48	Renken, R.A., 1998. Ground Water Atlas of the United States: Segment 5, Arkansas, Louisiana, Mississippi - ed.,
49, 50, 51	Whitehead, R.L., 1994. Ground Water Atlas of the United States: Segment 7, Idaho, Oregon, Washington - ed.,
52, 53, 54	Planert, M. & Williams, J.S., 1995. Ground Water Atlas of the United States: Segment 1, California, Nevada - ed.,
55, 56, 57, 58, 59	Miller, J.A., 1990. Ground Water Atlas of the United States: Segment 6, Alabama, Florida, Georgia, South Carolina - ed., Available at: http://pubs.er.usgs.gov/publication/ha730G.
60	Tuttle, M.L.W., Charpentier, R. & Brownfield, M.E., 1999. The Niger Delta Petroleum System: Niger Delta Province, Nigeria, Cameroon, and Equatorial Guinea, Africa. World Energy Project, (99-50-H), p.64.

Polygon ID	*Source*
61	Gennessaux, M., Burollet, P. & Winnock, E., 1998. Thickness of the Plio-Quaternary sediments (IBCM-PQ). Bollettino di Geofisica Teorica ed Applicata, 39(4), pp.243–284.
62	Al Farrah, N., Van Camp, M. & Walraevens, K., 2013. Deducing transmissivity from specific capacity in the heterogeneous upper aquifer system of Jifarah Plain, NW-Libya. Journal of African Earth Sciences, 85, pp.12–21. Available at: http://dx.doi.org/10.1016/j.jafrearsci.2013.04.004.
63	Van Camp, M. et al., 2014. Investigating seawater intrusion due to groundwater pumping with schematic model simulations: The example of the Dar es Salaam coastal aquifer in Tanzania. Journal of African Earth Sciences, 96, pp.71–78. Available at: http://dx.doi.org/10.1016/j.jafrearsci.2014.02.012.
64	Kumar, B. et al., 2011. Groundwater management in a coastal aquifer in Krishna River Delta, South India using isotopic approach. , 100(7).

Table A-3 Aquifer thickness information provided by the literature sources compared with the ATE values for each coastal area (spatial distribution shown in Figure A-1). For each are the location is also given. The values from literature are shown in columns below the "Measured values" header while our ATE values are below the "ATE values" header. The "Calc avg" column represents the calculated average value in cases where only min., max. or both were given by the literature. The "Calc avg" is calculated as either the arithmetic average between the min. and max. values or as min./max. value +/- half of min./max. "T" is a shortcut for thickness and therefore "T max" is the maximum, "T min" is the minimum and "T avg" is the average measured thickness based on literature.

	Measured values (m)				**ATE values (m)**			
ID	**T max**	**T min**	**T avg**	**Calc avg**	**Est avg**	**Est min**	**Est max**	**Location**
1	600			300	501.1	323.1	768.0	Godavari delta (IND)
2			130	130	174.8	76.2	386.9	Digha (IND)
3			80	80	76.2	35.7	173.9	Songkhla (THA)
4			100	100	84.6	36.0	124.1	Wadi Ham (UAE)
5			50	50	72.9	41.2	120.0	Carnavon (AUS)
6	600			300	272.2	51.0	897.8	Mekong (VNM)
7	100	20	70	70	116.9	30.6	244.3	Rabat (MAR)
8	500	300		400	281.0	41.7	648.4	South Jangtze coast, NE (CHN)
9	600			300	161.9	64.9	308.4	Goksu plain (TUR)
10	20			10	34.9	22.3	51.2	Mar de Ajo (ARG)
11			50	50	277.4	49.0	750.8	Falster island (DKN)
12			50	50	215.6	2.1	5143.4	Riga gulf (EST)
13			200	200	238.5	53.5	615.2	South Jangtze coast, SW (CHN)
14	900			450	484.8	33.5	1394.4	Nile delta (EGY)
15	45		25	25	210.1	83.8	333.9	Thamirabarani delta (IND)

	Measured values (m)				ATE values (m)			
ID	T max	T min	T avg	Calc avg	Est avg	Est min	Est max	Location
16	100			50	190.9	93.5	310.7	Kuala Lumpur (MYS)
17	150			75	79.9	2.2	371.3	Saloum delta (SEN)
18		1000			261.0	40.7	984.0	Kilwa group (TZA)
19	250		200	200	278.9	44.8	649.5	Coastal aquifer (ISR)
20	300		250	250	268.8	41.5	483.1	Bekasi (IDN)
21	420			210	110.9	9.4	331.7	Perth Basin (AUS)
22	1000	50	600	600	161.8	5.0	1091.9	Great artesian basin (AUS)
23	120			60	106.8	1.1	496.4	Canning Basin (AUS)
24	1000	150		575	166.0	53.4	399.6	Doñana National Park (ESP)
25	180	50		115	109.7	67.3	186.5	Barcelona (ESP)
26	200	80		140	119.0	39.8	163.9	Perpignan (FRA)
27	218	18	120	120	104.2	0.4	247.3	Oristano (ITA)
28	300			150	84.1	40.7	128.5	Muravera (ITA)
29	100			50	177.6	89.2	236.5	Siracusa (ITA)
30	200			100	150.8	81.1	201.2	Grosseto (ITA)
31		100		200	153.4	2.1	317.0	Versilia (ITA)
32	150	25	100	100	116.8	54.5	312.9	Coastal aquifer (BEL)
33	315	30	90	90	185.2	62.1	436.4	Northern dutch coast (NLD)
34	600	100	200	200	441.1	165.4	875.9	Zeeland (NLD)
35	175	125		150	66.3	16.6	261.9	Wilhelmshaven (GER)
36	200	80		140	125.7	58.4	180.0	Castellon de la Plana (ESP)
37			200	200	187.8	91.5	429.0	Ebro delta (ESP)
38			100	100	131.6	78.8	211.3	Scanzano (ITA)
39	300			150	123.7	13.5	331.6	Eureka aquifer, CA (USA)
40	300	30		165	165.8	28.3	520.4	Cape Cod (USA)
41	600	170		385	260.8	1.4	1245.4	Long Island (USA)
42	1200			600	285.0	33.7	815.5	North Atlantic coastal plain, NJ (USA)
43	2400			1200	295.9	21.8	2028.6	North Atlantic coastal plain, MA (USA)
44	3100			1550	444.8	6.4	4983.9	North Atlantic coastal plain, NC (USA)
45	2000	300		1150	266.5	24.5	2652.5	Coastal lowlands aq. system, TX (USA)
46	2400	1200		1800	83.9	72.9	94.8	Coastal lowlands aq. system SE, LA (USA)

	Measured values (m)				ATE values (m)			
ID	T max	T min	T avg	Calc avg	Est avg	Est min	Est max	Location
47	3600	1200		2400	367.7	120.6	1085.5	Coastal lowlands aq. system NW, LA (USA)
48	1000			500	204.7	22.2	815.7	Mississippi emayment aq. (USA)
49	1000			500	130.8	2.2	496.7	Puget-Williamette trough regional aq. system (USA)
50	35	15		25	97.4	16.2	388.0	Washington coast N (USA)
51	200	35		117.5	138.7	14.1	318.1	Washington coast S (USA)
52	300			150	75.7	3.7	182.3	Santa Clara valley (USA)
53	300			150	162.9	92.7	204.2	Salinas Valley (USA)
54	1200	30		615	286.6	130.3	492.4	Los Angeles - Orange county (USA)
55	1000	200		600	170.2	7.0	1762.3	FL - W and AL coast (USA)
56	1050	850		950	95.5	1.9	1172.4	FL - S (USA)
57	200	60		130	210.7	30.0	1293.4	SC - S (USA)
58	850	200		525	167.0	52.0	723.7	Georgia coast (USA)
59	850	700		775	189.5	6.1	2079.0	FL - N (USA)
60	2000			1000	171.7	1.3	805.5	Niger delta (NGA)
61	1200			600	415.4	46.3	929.4	Po delta (ITA)
62	180	30		105	247.3	4.7	490.5	Jifarah Plain (LBY)
63			150	150	295.2	88.0	1049.5	Dar es Salaam (TZA)
64	450	40		245	286.6	65.2	608.0	Kirishna river delta (IND)

Table A-4 Parameter values for the three cross-sections, the values are given for models with minimum and maximum estimated sediment thickness at the coastline. The total length of simulation for the test case in Virginia, USA is larger than for the other two test cases due to the complexity and size of the aquifer system. This was done to ensure that the steady-state (or near steady-state) is reached.

Parameter name	***Italy***		***Israel***		***Virginia, USA***	
Sediment thickness at coastline	50m	500m	100m	1400m	200m	1500m
Number of columns	1060	1588	385	494	547	578
Number of layers	53	411	43	110	44	106
Layer thickness (m)	3		10		10	
Column width (m)	25		100		500	
Top elevation (m asl.)	26		95		59	
Bottom elevation (m asl.)	-62	-1002	-335	-1005	-381	-1001
Length of simulation (years)	10000				100000	
Number of time steps	2500				10000	
Total active cells	13224	534879	3021	30332	9319	43630
Horizontal hydraulic conductivity aquifer (m/d)	10					
Vertical hydraulic conductivity aquifer (m/d)	1					
Horizontal hydraulic conductivity aquitard (m/d)	1.00E-04		1.00E-04		1.00E-04	
Vertical hydraulic conductivity aquitard (m/d)	1.00E-07		1.00E-07		1.00E-07	
Layer type	confined					
Total amount of GHB cells	887	1415	200	321	274	431
Recharge rate (m/d)	0.001		0.0005			
Head change criterion for convergence (m)	1.00E-04					
Residual criterion for convergence (m^3/d)	10					
Porosity	0.35					
Solver type	Finite Difference					
Longitudinal dispersivity	1					
Ratio horizontal transverse disp./ long. disp.	0.1					
Diffusion coefficient (m^2/d)	8.64E-05					

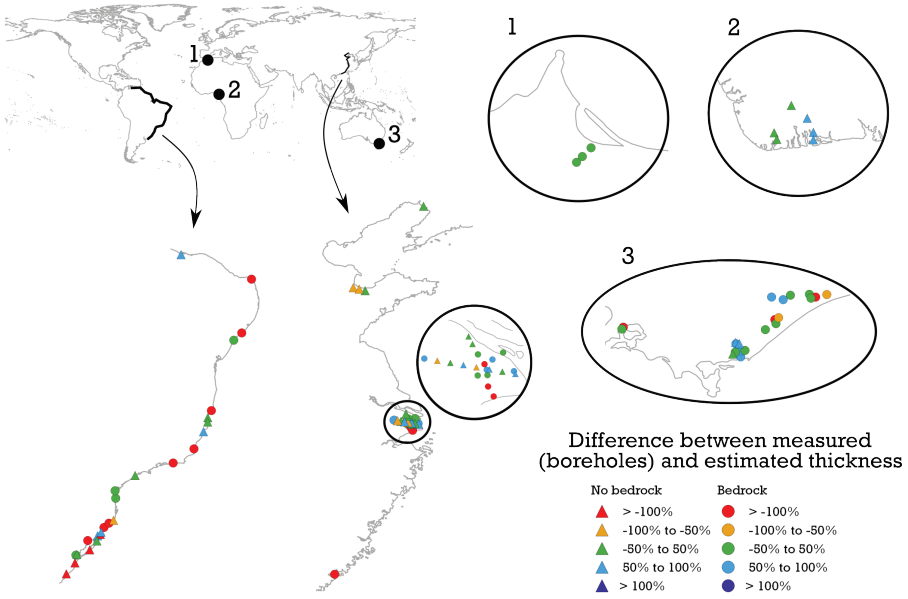

Figure A-1 Schematization of borehole validation using the difference between the measured sediment thickness and an average estimated thickness in a radius of 2.5km around the borehole location. The boreholes are divided into two groups depending on any bedrock formation indicated in the borehole report.

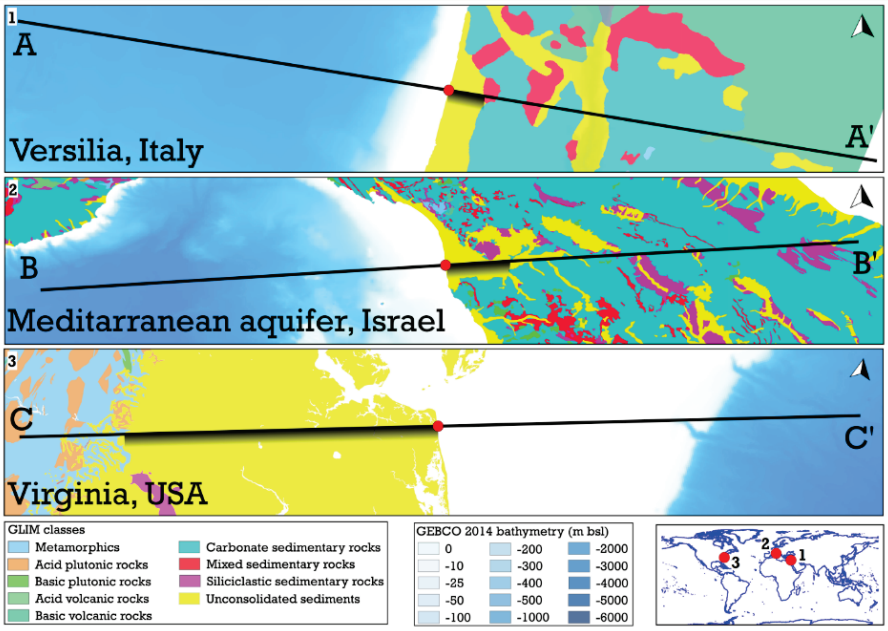

Figure A-2 Location of the cross-sections used as examples to illustrate the ATE method. The black shadow represents the extent of the coastal plain in each cross-section while the whole black line indicates the span of the cross-section (in total 400km).

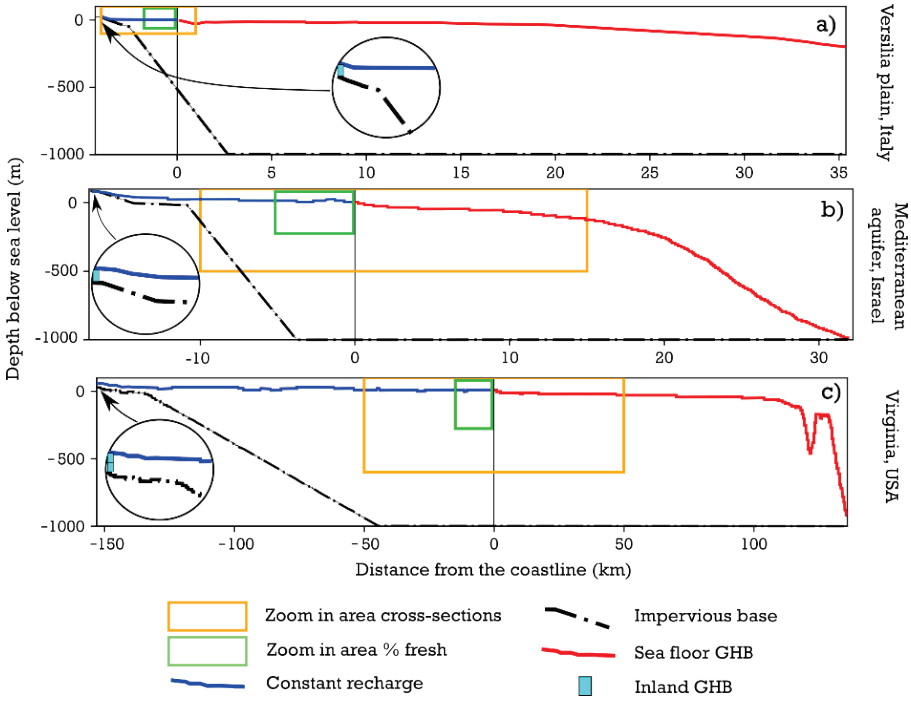

Figure A-3 Model concept schematization for all three test cases. a) Versilia plain, Italy, b) Mediterranean aquifer, Israel and c) Virginia, USA. The zoom in area cross-section corresponds to the areas shown in Figures A-4, A-5 and A-6 respectively.

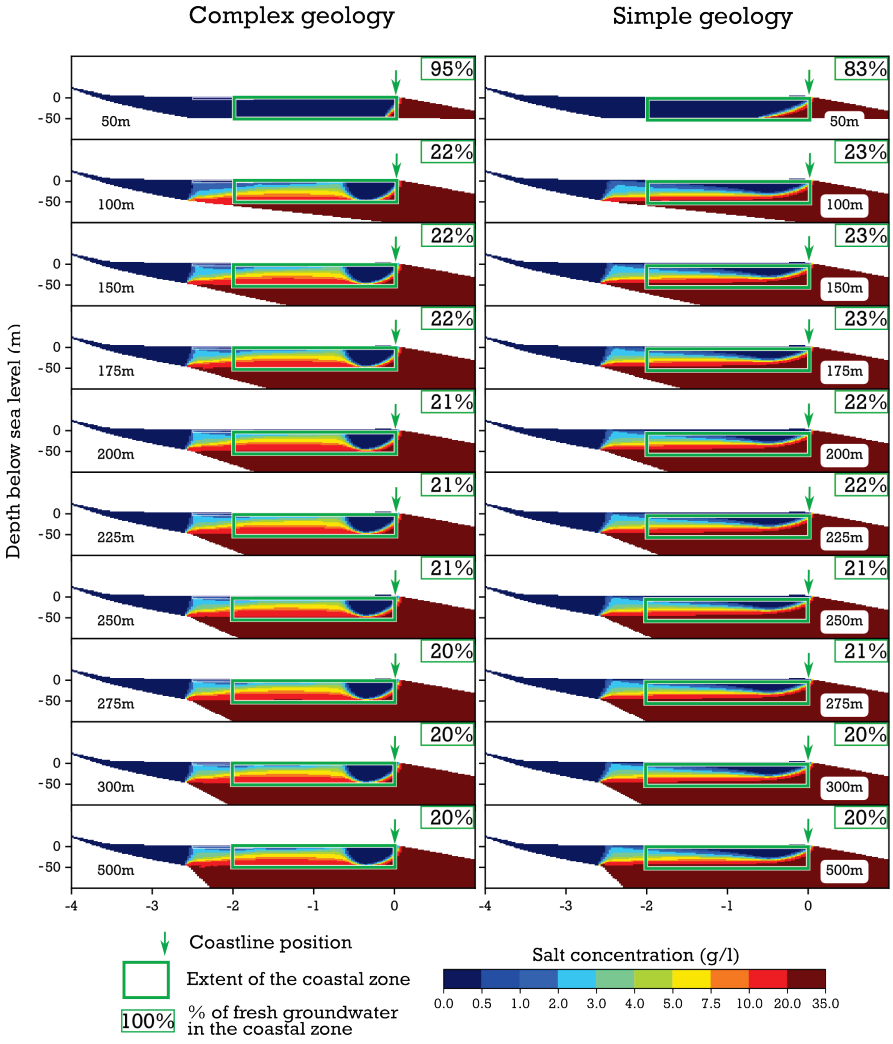

Figure A-4 Simulation results for the cross-section located in Versilia plain, Italy. Salt concentration profiles are given for various sediment thicknesses at the coastline and two different geological scenarios (homogeneous and heterogeneous based on information provided by literature).

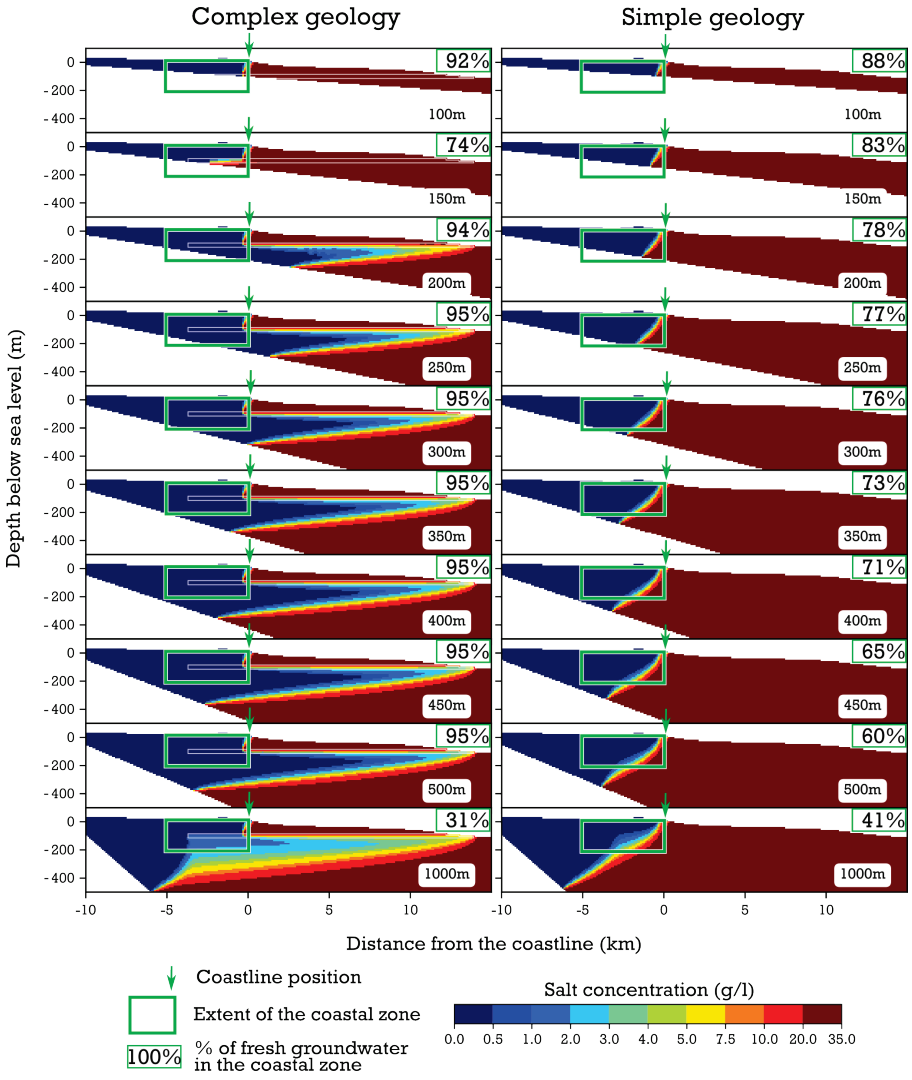

Figure A-5 Simulation results for the cross-section located in the Mediterranean coastal plain aquifer, Israel. Salt concentration profiles are given for various sediment thicknesses at the coastline and two different geological scenarios (homogeneous and heterogeneous based on information provided by literature).

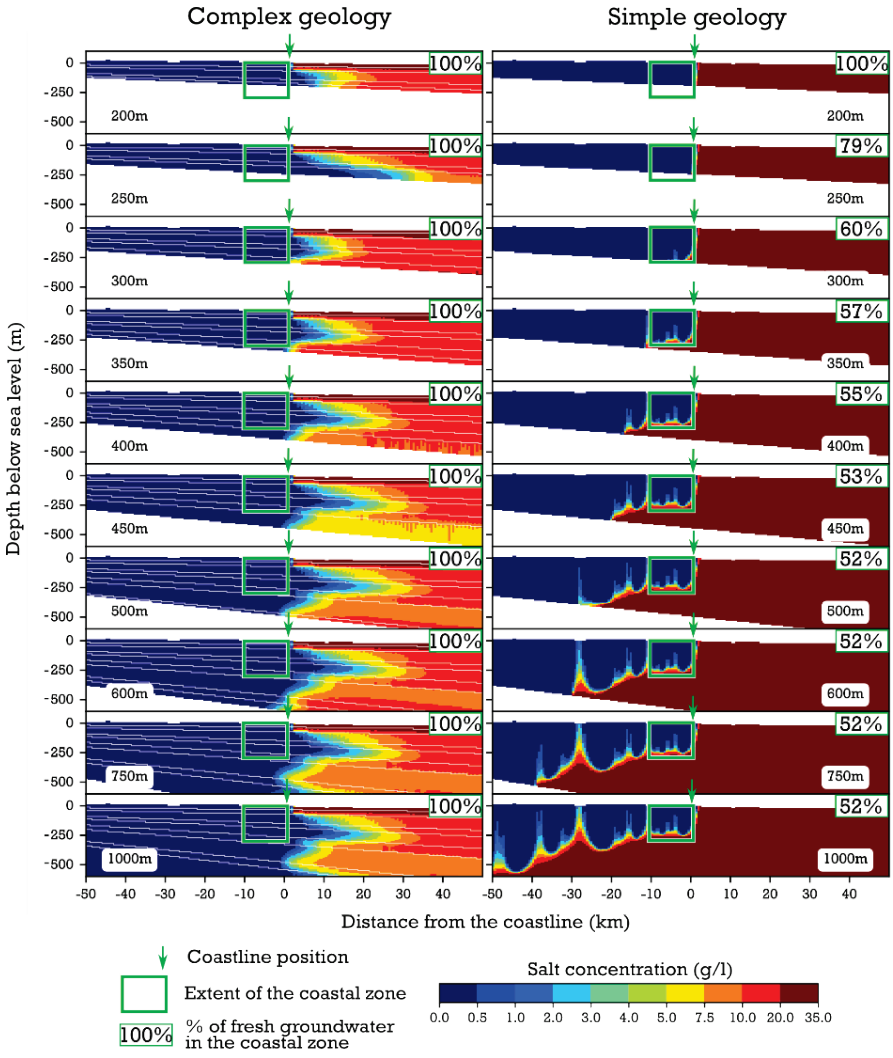

Figure A-6 Simulation results for the cross-section located in North Atlantic Coastal Plain, Virginia, USA. Salt concentration profiles are given for various sediment thicknesses at the coastline and two different geological scenarios (homogeneous and heterogeneous based on information provided by literature).

B Appendix to Chapter 3

Text B-1 The text below provides additional technical explanation and geological decision backgrounds to the Global geological heterogeneity parameterization covered by Section 3.2.3 of the main text.

Geological decision background

The set of equations in this supplementary text was developed to produce a first-order global continental shelf geological heterogeneity estimation. In setting up the equations, established general insights into the geological development of shelf along passive margins has been the starting point. Passive margin shelves are longer lived (many millions of years) and are larger than their active margin counterparts, meaning that they dominate the global shelf terrain. The increase in glacial low stand depths and glacial climate change severity by 1 Ma ago, is commonly echoed as a regionally traceable seismic reflector and a step change in lower shelf clinoform dimensions. This makes that for passive margin shelf regions (and also sectors of active margin shelfs supplied by good-sized rivers), one can test the aquitard count predictions, or apply data-assimilation techniques to the synthetic architecture and heterogeneity predictions of this paper (main text Section 3.2.2 – 3.2.4; this supplement).

As described in Section 3.2.3 of the main text, the parameterization aimed to capture average composition of shelf top-set architecture over the last one million years. Within that time frame, glacial-interglacial climatic cyclicity made sediment delivery fluctuate both in volumes and in composition. In parallel, global ice-volume and ocean sea-level oscillated with 100 ka dominant periodicity between low stands, some 120 meters below and high stands around present MSL (e.g., Waelbroeck et al. 2002), with half cycles towards high stands occurring faster (~20 ka) than half cycles towards low stand (~80 ka). Especially to the inner shelf and intermediate shelf, this caused repeated inundation and subaerial exposure of the shelf floor, stalling and accelerating sediment though pass to the deep sea, as well as lateral dispersal of shelf sediment (e.g., Cohen & Lobo, 2013).

The glacial-interglacial scale climatic oscillations affect sediment production on tropical latitudes differently than at higher latitudes where periglacial and temperate conditions alternated, because episodes of stronger and weaker monsoons alternate at higher frequency (precession dominated, 19-23 ka cycles) than ice-sheet inception and glacial termination (the aforementioned 100-ka cyclicity). A subset of MARCAT shelf regions, those in direct vicinity to major ice sheets (e.g., North Sea) and a few more connected to them by major meltwater rivers (e.g., Mississippi / northern Gulf) receives additional sediment supply, not just because from frost-affected catchments, sediment production is (temporally) larger – but also because the catchment source area is larger than the modern (interglacial) situation. MARCAT regions that were ice-sheet covered in glacial periods (Hudson Bay and the Baltic Sea: glacial erosional mega-landforms rather than plate-tectonic ocean-margin sedimentary shelfs), are treated as to only receive sediments during interglacial times. They are sediment starved in comparison to non-glaciated shelves of similar size, relief and climate zone; the sediments that were produced around are used to accommodate nearby ocean-margin.

Parameter and equation design

Architectural style of continental shelf subsurface composition is characterized by assessing the sedimentation/ accommodation ratio (Y) for each COSCAT/MARCAT region (Eq. 3-1 and Eq. B-1) and the main factors influencing that ratio. These main factors are sediment delivery (Q_s) (corrected for loss to deep sea), the so-called sediment dispersal modifier (D), sand/mud compositional ratio (factor M), and long-term net subsidence (the so-called shelf subsidence factor R). To start with, the sediment flux Q_s to each COSCAT/MARCAT region was estimated using the WHYMAP formulation (Syvitski et al. 2013):

$$Q_s = \alpha_3 * {A_{land}}^{\alpha_4} * R^{\alpha_5} * e^{k*T} \quad \text{(B-1)}$$

With	A_{land}	continental catchment area feeding the shelf segment [km²],
	R	maximum elevation in the catchment (relief factor) [],
	T	latitude-based long-term mean temperature [],
	α_3, α_4, α_5, k	regression coefficients cf. Syvitski et al. 2013: their Table 3

Next, further dataset-queries and algebraic estimations and conversions (Eq. B-2 to B-5) were executed to specify the factors defining the accumulation ratio Y (Eq. B-1). Herein, Eq. B-3 is a step of unit conversion (from Q_s in kg/s incoming, to q_s in m/Ma vertically accumulating). It uses a uniform bulk density of 2250 kg/m³ and porosity value of 30%, based on Reynolds et al. (1991). Equations 4a-h specify the 'sediment type' factor M as the long-term average sand/mud delivery ratio to the coastal zone. That calculation makes use of Holocene (interglacial) sand and mud proportions (by weight) as mapped across different shelves based on traditional sea-floor sampling (overview first compiled by Hayes 1967). For glaciation-affected shelves (those segments supplied by ice-marginal river systems; following the Pleistocene glaciation extents of Ehlers & Gibbard 2004), the interglacial sand/mud ratios are not representative for long term sediment supply. Eq. B-4e-h increase the proportion of sand and decrease that of mud to compensate for this (amount of increase based on Nam et al. 1995). The sediment dispersion modifier D (Eq. B-5ab) is 1 for all but one of Walsh & Nitrouer (2009)'s shelf categories (EAD: Estuarine Accumulation Dominated; PAD: Proximal Accumulation Dominated; SDC: Subaqueous delta clinoforms; MDD: Marine dispersal dominated). It is set to 0.1 for those shelved captured by major submarine canyon systems. The factors M and D are used as a modifier of Qs. The shelf subsidence factor R represents long-term provision of accommodation space owing to two components of subsidence (Eq. B-6): intrinsic tectonic subsidence owing to gradual cooling of oceanic crust underlying the typical passive-margin shelf (tailing out with increasing age; first term in Eq. B-5; based on Karner & Watch 1982) and a

sediment compaction component dependent on the sedimentation volume and the compositional weight (second term). The full set of factors can be seen as hydrogeological indicator variables, the meaning of which is summarized in Figure 3-1.

$$Y = \frac{Sedimentation}{Accommodation} = \frac{q*M*D}{R} \quad \text{(B-2)}$$

With $$q_s \left[\frac{m}{Myr}\right] = Q_s * 3600 * 8760 / 2250 / A_{shelf} / (1 - 0.3) \quad \text{(B-3)}$$

where:

Q_s = land-derived sediment delivered to the shelf [kg/s]

A_{shelf} = shelf segment area [m^2]

and M = sand/mud ratio [-] indicating the sediment type

$$M = p_{sand} * p_{mud} \quad \text{(B-4)}$$

$$p_{sand} = 0.5 * p_{sand,ig} + 0.5 * p_{sand,gl} \quad \text{(B-4a)}$$

$$p_{mud} = 0.5 * p_{mud,ig} + 0.5 * p_{mud,gl} \quad \text{(B-4b)}$$

with p for proportion and interglacial ('*ig*') and glacial ('*gl*') conditions attributed equal time

For *not* glacially influenced shelfs:

$$p_{sand} = p_{sand,ig} = p_{sand,gl} \quad \text{(B-4c)}$$

$$p_{mud} = p_{mud,ig} = p_{mud,gl} \quad \text{(B-4d)}$$

For glacially influenced shelfs:

$$p_{sand} = p_{sand,ig} * 1.25 \quad \text{(B-4e)}$$

$$p_{mud} = p_{mud,ig} / 1.25 \quad \text{(B-4f)}$$

i.e. $$p_{sand,gl} = 1.5\ p_{sand,ig} \quad \text{(B-4g)}$$

$$p_{mud,gl} = 0.6\ p_{mud.ig} \quad \text{(B-4h)}$$

and D = sediment dispersion modifier, for categories Walsh & Nitrouer (2009)

For shelf segments that are submarine-canyon captured:

D = 0.1 i.e., only 10% of sediment delivery stays on the shelf (B-5a)

For the other categories:

D = 1 i.e., 100% of sediment delivery is shelf-accommodated (B-5b)

and R = shelf subsidence factor [-]; is directly related to the long-term relative sea-level rise

$$R = thermal\ subsidence + compaction\ subsidence$$

$$R = \frac{320}{\sqrt{t}} + 0.5 * q_s * D * \left(\frac{p_{sand}}{100} * 0.2 + \frac{p_{mud}}{100} * 0.4\right) \quad \text{(B-6)}$$

with t = Age of ocean-crust below shelf [Ma].

The calculations weigh in and applied modifiers acknowledge that ocean sea-level oscillated some 130 meters during the last 10 glacial-interglacial cycles since the Early/Middle Pleistocene transition and less so in the Early Pleistocene before (e.g., Pillans et al., 1998), and that climatic conditions and sediment production fluctuated likewise (e.g., Nam et al., 1995; Syvitski et al., 2013). Sea-level oscillations have caused good parts of the coastal plain and shelf areas to be regressed and transgressed, and makes that preservation of aquitard strata within the shelf topset is spatially and vertically variable.

The full MSc thesis "The geology of coastal aquifer worldwide" written by Maria Karssenberg upon which the above summary is based can be provided on request. The references cited in this supplementary text are also cited in the main text (and its reference section).

Table B-1 Parameter values applied to the SEAWAT models of all Average Representative Profiles (ARPs).

Parameter type	***Value***
Model layer thickness (m)	10
Width of the model cell(m)	100
Time step length (years)	10
Layer type	confined
Head change criterion for convergence (m) (hclose)	1.00E-04
Residual criterion for convergence (m^3/d) (rclose)	10
Effective porosity (-)	0.35
Solver type	Finite Difference
Longitudinal dispersivity (m)	1
Ratio horizontal transverse disp./ long. disp. (-)	0.1
Diffusion coefficient (m^2/d)	8.64E-05

Table B-2 Geological heterogeneity parameter values for both modelling concepts (extreme parameter values combinations and randomized Monte Carlo parameterization), total number of numerical model simulations is highlighted in the brackets. [1]Randomized geological parameters, [2]Parameters quantified based on literature sources.

Geological parameter	***Parameter Extremes (24)***	***Monte Carlo (100)***
[1]Aquifer-aquitard layer combinations (-)	(2, 5)	rand(2, 5)
[1]Clay layer stacking factor (-)	(0.5, 0.75, 1.0)	rand(0.5, 1.0)
[1]Clay layer start (km offshore)	(-2.5, 2.5)	rand(-2.5, 2.5)
[1]Offshore clay cap thickness (m)	(10, 30)	rand(10, 30)
[2]Aquifer layer hydraulic conductivity (m/d)	(Gleeson et al., 2014)	
[2]Aquitard layer hydraulic conductivity (m/d)	(Huscroft et al., 2018)	
[2]Top sediment layer thickness (m)	(Hengl et al., 2014)	
[2]Offshore clay cap presence (shelf and slope)	(Dutkiewicz et al., 2015)	

Table B-3 Fresh groundwater fractions (volumes in km3 are shown in Table 3-3) comparison between the two modelling concepts (PE is extreme parameter values combinations and MC is randomized Monte Carlo), average fractions are extracted at the end of SP 31 (see Figure 3-6). The inland domain is defined as a stretch 10km long from the coastline in the inland direction, the continental shelf spans from the coastline to the continental shelf edge (see also Figures 3-3 and 3-5) and the offshore domain entails the whole part of the model domain that is submerged at present-day.

COSCAT name (ID)	**Coastal type (ARP)**	***avg. % fresh inland***			***avg. % fresh shelf***			***avg. % fresh offshore***		
		PE	**MC**	**abs. diff**	**PE**	**MC**	**abs. diff**	**PE**	**MC**	**abs. diff**
Niger Basin (0016)	S	99.8	99.7	0.1	31.8	23.1	8.7	17.5	14.8	2.7
	I	100.0	100.0	0.0	63.3	67.0	3.7	41.9	45.0	3.1
Suriname (1103)	A	97.1	99.1	2.0	22.8	29.9	7.0	13.4	17.6	4.1
Perth Basin (1413)	IS	100.0	100.0	0.0	66.5	73.3	6.8	17.9	18.9	1.1
Oman (1343)	IS	100.0	99.9	0.1	41.6	39.3	2.4	7.3	7.1	0.3
Japan Trench (1322)	D	100.0	100.0	0.0	79.1	89.6	10.5	39.5	45.7	6.2
	IS	100.0	100.0	0.0	80.7	88.3	7.6	8.2	9.1	0.9
North Sea (0403)	A	100.0	100.0	0.0	24.0	44.9	20.9	26.7	46.9	20.2
Nantucket, NJ (0827)	IS	99.2	100	0.8	52.1	67.2	15.2	25.6	32.6	7.0

Table B-4 SEAWAT model runtime comparison between the two modelling concepts. The Avg. runtime column displays the average runtime in hours (hrs) per one simulation for both modelling concepts. Total runtime is the sum of all simulations for the PE (24 simulations) and MC (100 simulations) modelling concepts.

COSCAT name (ID)	***Coastal type***	***Avg. runtime [hrs/simulation]***		***Total runtime [hrs]***	
		PE	**MC**	**PE**	**MC**
Niger Basin (0016)	S	41	38	995	3780
	I	68	71	1635	7135
Suriname (1103)	A	17	20	405	2047
Perth Basin (1413)	IS	10	16	233	1612
Oman (1343)	IS	19	22	459	2232
Japan Trench (1322)	D	45	36	1088	3563
	IS	72	52	1731	5218
North Sea (0403)	A	12	16	290	1616
Nantucket, NJ (0827)	IS	133	86	3195	8560
Mean		46	40	1115	3974
Sum		417	357	10031	35763

Table B-5 Global geological heterogeneity results for all considered COSCAT regions. The Qs, S/M and Y values are divided into three classes as follows: 1 – low, 2 –medium, 3 – high. The offshore sand and mud percentages are derived from the dataset by Dutkiewicz et al. (2015), see Section 3.2.3 in the main manuscript.

COSCAT ID	Sand %	Mud %	Qs [-]	S/M [-]	Y [-]	Sand % (shelf)	Mud % (shelf)	Sand % (slope)	Mud % (slope)
1	49.0	51.0	3	1	3	30.1	69.9	10.9	89.1
2	49.0	51.0	3	1	3	19.8	80.2	4.0	96.0
3	49.0	51.0	3	1	3	0.0	100.0	0.0	100.0
4	51.0	49.0	3	2	2	3.4	96.6	0.5	99.5
5	59.5	40.5	3	2	3	0.0	100.0	0.0	100.0
6	62.0	38.0	3	3	3	0.0	100.0	0.0	100.0
7	62.0	38.0	3	3	3	0.0	100.0	0.0	100.0
8	56.5	43.5	2	2	3	0.0	100.0	0.0	100.0
9	56.5	43.5	3	2	3	0.0	100.0	0.0	100.0
10	56.5	43.5	3	2	3	0.0	100.0	11.5	88.5
11	62.0	38.0	3	3	3	0.0	100.0	0.0	100.0
12	62.0	38.0	2	3	3	65.1	34.9	25.2	74.8
13	44.0	56.0	2	1	2	59.0	41.0	32.6	67.4
14	44.0	56.0	2	1	2	0.0	100.0	0.0	100.0
15	44.0	56.0	3	1	3	0.0	100.0	0.0	100.0
16	44.0	56.0	3	1	3	0.0	100.0	0.0	100.0
17	44.0	56.0	3	1	3	0.0	100.0	0.0	100.0
18	64.0	36.0	2	3	2	0.0	100.0	0.0	100.0
19	64.0	36.0	3	3	3	0.0	100.0	0.0	100.0
20	64.0	36.0	3	3	3	0.0	100.0	0.0	100.0
21	64.0	36.0	3	3	3	0.0	100.0	0.0	100.0
401	75.8	24.3	2	3	2	0.0	100.0	0.0	100.0
402	75.8	24.3	1	3	2	16.0	84.0	37.4	62.6
403	75.8	24.3	2	3	2	9.9	90.1	30.5	69.5
404	66.0	34.0	2	3	2	0.0	100.0	0.0	100.0
405	66.0	34.0	1	3	1	50.0	50.0	50.0	50.0
406	66.0	34.0	1	3	1	0.0	100.0	0.0	100.0
407	50.3	49.7	1	2	1	50.0	50.0	50.0	50.0
408	50.3	49.7	1	2	1	14.9	85.2	8.1	91.9
409	50.3	49.7	1	2	1	50.0	50.0	50.0	50.0
411	49.0	51.0	3	1	3	0.0	100.0	0.0	100.0
412	49.0	51.0	3	1	3	0.0	100.0	0.0	100.0
413	49.0	51.0	2	1	2	0.0	100.0	0.0	100.0
414	49.0	51.0	3	1	3	0.0	100.0	0.0	100.0
415	49.0	51.0	2	1	2	16.5	83.5	4.5	95.5
416	58.4	41.6	3	2	3	0.0	100.0	0.0	100.0

COSCAT ID	Sand %	Mud %	Qs [-]	S/M [-]	Y [-]	Sand % (shelf)	Mud % (shelf)	Sand % (slope)	Mud % (slope)
418	49.0	51.0	3	1	3	2.3	97.7	2.2	97.9
419	64.0	36.0	3	3	3	0.0	100.0	0.0	100.0
501	50.3	49.7	1	2	1	50.0	50.0	50.0	50.0
502	50.3	49.7	1	2	1	50.0	50.0	50.0	50.0
503	50.3	49.7	1	2	1	50.0	50.0	50.0	50.0
504	50.3	49.7	1	2	1	50.0	50.0	50.0	50.0
505	50.3	49.7	1	2	1	50.0	50.0	50.0	50.0
801	73.0	27.0	3	3	2	0.0	100.0	0.0	100.0
802	73.0	27.0	2	3	2	26.4	73.6	12.3	87.7
803	73.0	27.0	3	3	3	21.1	78.9	20.4	79.6
804	73.0	27.0	3	3	3	0.0	100.0	0.0	100.0
805	73.0	27.0	3	3	3	0.0	100.0	0.0	100.0
806	73.0	27.0	2	3	2	30.4	69.6	6.2	93.8
807	68.5	31.5	3	3	3	0.0	100.0	0.0	100.0
808	78.1	21.9	3	3	3	30.9	69.1	7.3	92.7
809	78.1	21.9	3	3	2	30.2	69.8	1.3	98.7
810	68.9	31.1	1	3	1	50.0	50.0	50.0	50.0
811	68.9	31.1	1	3	2	50.0	50.0	50.0	50.0
812	68.9	31.1	1	3	1	50.0	50.0	50.0	50.0
813	68.9	31.1	1	3	1	50.0	50.0	50.0	50.0
814	68.9	31.1	1	3	1	50.0	50.0	50.0	50.0
815	68.9	31.1	1	3	1	50.0	50.0	50.0	50.0
816	50.3	49.7	1	2	1	50.0	50.0	50.0	50.0
817	50.3	49.7	1	1	1	50.0	50.0	50.0	50.0
818	50.3	49.7	1	1	1	50.0	50.0	50.0	50.0
819	50.3	49.7	1	1	1	50.0	50.0	50.0	50.0
820	50.3	49.7	1	1	1	50.0	50.0	50.0	50.0
821	50.3	49.7	2	2	2	50.0	50.0	50.0	50.0
822	50.3	49.7	1	2	1	50.0	50.0	50.0	50.0
823	50.3	49.7	1	2	1	50.0	50.0	50.0	50.0
824	58.4	41.6	3	2	3	50.0	50.0	50.0	50.0
825	58.4	41.6	2	2	3	34.4	65.6	16.9	83.1
826	58.4	41.6	1	2	2	71.2	28.8	50.2	49.9
827	90.2	9.8	1	3	2	23.0	77.0	16.5	83.6
828	63.0	37.0	2	3	2	37.1	62.9	8.2	91.9
830	65.5	34.5	2	3	2	0.0	100.0	0.0	100.0
831	65.5	34.5	2	3	2	0.0	100.0	0.0	100.0
832	60.0	40.0	2	2	2	0.0	100.0	0.0	100.0
833	60.0	40.0	3	2	3	0.0	100.0	0.0	100.0
834	72.1	27.9	3	3	3	36.3	63.7	6.1	93.9

COSCAT ID	Sand %	Mud %	Qs [-]	S/M [-]	Y [-]	Sand % (shelf)	Mud % (shelf)	Sand % (slope)	Mud % (slope)
1101	65.5	34.5	2	3	2	0.0	100.0	6.9	93.1
1102	57.5	42.5	3	2	3	0.1	99.9	0.0	100.0
1103	57.5	42.5	3	2	3	0.0	100.0	0.0	100.0
1104	57.5	42.5	3	2	3	0.0	100.0	0.0	100.0
1105	57.5	42.5	2	2	2	0.0	100.0	0.0	100.0
1106	57.5	42.5	3	2	3	23.6	76.4	27.3	72.7
1107	57.5	42.5	1	2	2	1.3	98.7	0.0	100.0
1108	57.5	42.5	3	2	3	96.3	3.7	53.0	47.0
1109	68.0	32.0	2	3	3	100.0	0.0	100.0	0.0
1110	73.7	26.3	1	3	2	93.8	6.2	100.0	0.0
1111	73.7	26.3	2	3	2	44.7	55.4	33.0	67.0
1112	73.7	26.3	3	3	3	24.3	75.7	1.7	98.3
1113	55.0	45.0	3	2	3	11.6	88.4	14.3	85.7
1114	55.0	45.0	2	2	2	16.4	83.6	7.3	92.7
1115	55.0	45.0	3	2	3	0.0	100.0	0.0	100.0
1116	55.0	45.0	3	2	3	0.0	100.0	0.0	100.0
1301	49.0	51.0	3	1	3	0.0	100.0	0.0	100.0
1303	49.0	51.0	2	1	3	2.5	97.5	9.8	90.2
1307	50.3	49.7	3	2	3	50.0	50.0	50.0	50.0
1308	50.3	49.7	1	2	1	50.0	50.0	50.0	50.0
1309	50.3	49.7	1	2	1	50.0	50.0	50.0	50.0
1310	75.5	24.5	1	3	1	50.0	50.0	50.0	50.0
1311	75.5	24.5	1	3	1	50.0	50.0	50.0	50.0
1312	50.3	49.7	1	2	1	50.0	50.0	50.0	50.0
1313	75.5	24.5	1	3	1	50.0	50.0	50.0	50.0
1314	75.5	24.5	1	3	1	50.0	50.0	50.0	50.0
1315	75.5	24.5	1	3	1	6.6	93.4	18.7	81.3
1316	75.5	24.5	3	3	3	46.9	53.1	34.9	65.2
1317	75.5	24.5	1	3	1	4.6	95.4	9.4	90.6
1318	75.5	24.5	3	3	3	0.0	100.0	0.0	100.0
1319	66.0	34.0	1	2	2	3.6	96.4	1.8	98.2
1320	66.0	34.0	2	2	2	17.1	82.9	26.6	73.5
1321	56.5	43.5	2	2	2	19.6	80.4	5.6	94.4
1322	56.5	43.5	2	2	2	0.8	99.2	0.6	99.5
1323	42.5	57.5	1	1	2	26.2	73.8	5.8	94.2
1324	66.0	34.0	1	2	2	32.6	67.4	93.7	6.3
1325	43.5	56.5	3	1	3	32.6	67.4	93.7	6.3
1326	43.5	56.5	2	1	2	26.1	73.9	0.0	100.0
1327	43.5	56.5	2	1	2	0.0	100.0	0.0	100.0
1328	42.5	57.5	1	1	2	31.9	68.1	0.0	100.0

COSCAT ID	Sand %	Mud %	Qs [-]	S/M [-]	Y [-]	Sand % (shelf)	Mud % (shelf)	Sand % (slope)	Mud % (slope)
1329	36.5	63.5	2	1	2	33.1	66.9	2.4	97.6
1330	42.5	57.5	1	1	2	24.3	75.7	0.0	100.0
1331	42.5	57.5	2	1	2	1.4	98.6	5.6	94.5
1332	42.5	57.5	2	1	2	10.3	89.7	8.6	91.4
1333	42.5	57.5	3	1	3	0.0	100.0	8.1	91.9
1334	42.5	57.5	2	1	2	18.9	81.1	15.1	84.9
1335	33.5	66.5	2	1	2	9.0	91.0	23.7	76.3
1336	33.5	66.5	3	1	3	0.0	100.0	0.0	100.0
1337	33.5	66.5	3	1	3	0.0	100.0	0.0	100.0
1338	47.0	53.0	2	1	2	0.0	100.0	0.0	100.0
1339	47.0	53.0	2	1	2	0.0	100.0	0.0	100.0
1340	47.0	53.0	3	1	3	0.0	100.0	0.0	100.0
1341	59.5	40.5	3	2	3	0.0	100.0	0.0	100.0
1342	42.5	57.5	3	1	3	0.0	100.0	0.0	100.0
1344	51.0	49.0	3	2	2	3.5	96.5	0.0	100.0
1401	42.5	57.5	1	1	2	7.1	92.9	7.3	92.8
1402	42.5	57.5	2	1	2	15.6	84.4	2.9	97.1
1403	71.5	28.5	1	3	2	33.4	66.6	9.3	90.8
1405	75.0	25.0	2	3	2	16.0	84.0	3.6	96.5
1406	75.0	25.0	2	3	2	19.2	80.8	24.4	75.6
1407	84.2	15.8	2	3	2	21.9	78.2	19.8	80.2
1408	84.2	15.8	1	3	2	0.0	100.0	0.0	100.0
1409	75.0	25.0	2	3	2	2.2	97.8	0.0	100.0
1410	71.5	28.5	2	3	2	0.0	100.0	0.0	100.0
1411	71.5	28.5	2	3	2	21.3	78.7	5.0	95.0
1412	71.5	28.5	1	3	2	29.2	70.9	13.6	86.4
1413	71.5	28.5	1	3	2	9.1	90.9	9.1	90.9
1414	71.5	28.5	1	3	2	16.0	84.1	5.8	94.2
1415	71.5	28.5	1	3	2	61.9	38.1	33.5	66.5
1416	42.5	57.5	1	1	2	26.4	73.6	0.0	100.0
417	49.0	51.0	2	1	2	0.0	100.0	0.0	100.0
829	63.0	37.0	3	3	3	0.0	100.0	0.0	100.0
1501	50.0	50.0	1	1	1	50.0	50.0	50.0	50.0
1502	50.0	50.0	1	1	1	50.0	50.0	50.0	50.0
1503	50.0	50.0	1	1	1	50.0	50.0	50.0	50.0
1504	50.0	50.0	1	1	1	50.0	50.0	50.0	50.0
1505	50.0	50.0	1	1	1	50.0	50.0	50.0	50.0
1343	61.4	38.6	2	1	2	0.0	100.0	0.0	100.0

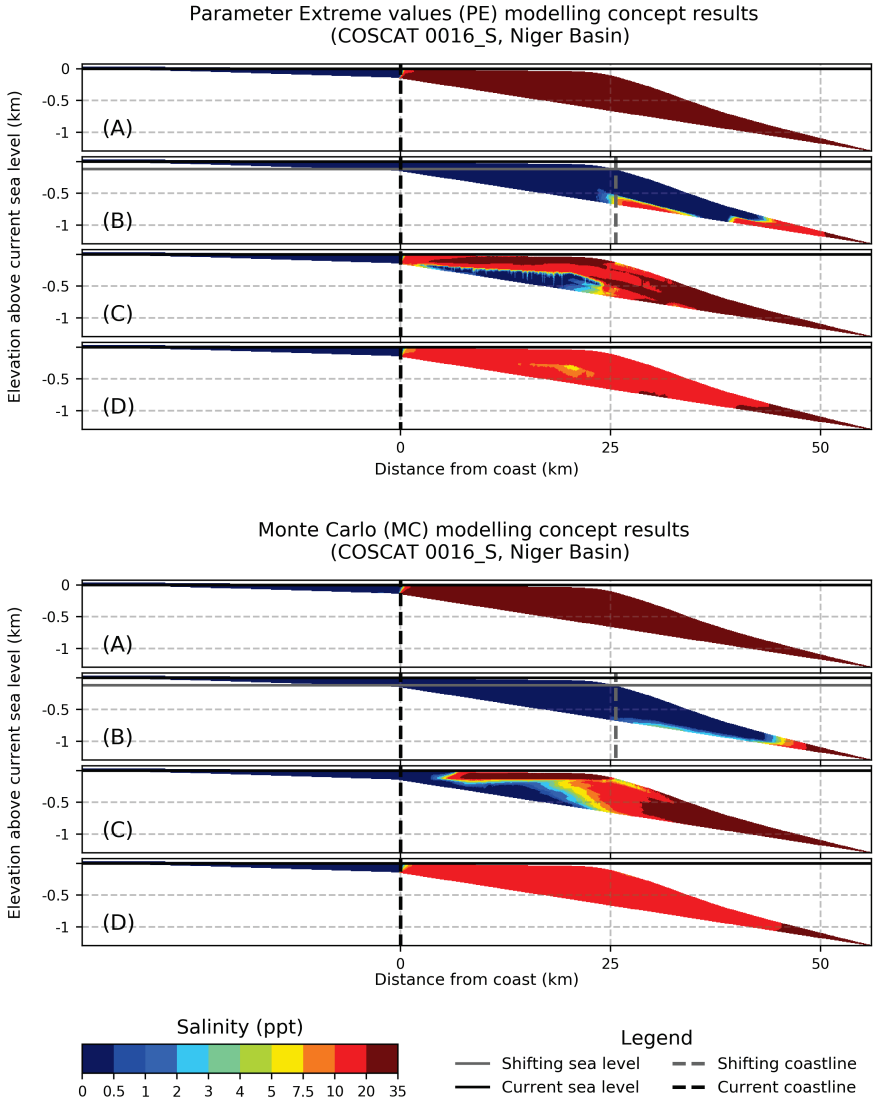

Figure B-1 Averaged salinity profiles for both modelling concepts at four timeframes for COSCAT 0016_S region (Niger Basin). The estimated salinity concentration in the 2D profiles is represented: (A) at the end of SP 0, salinity concentration before fluctuating sea level SPs; (B) at the lowest sea level occurring at the end of the sea level drop represented by SP 21; (C) after the relatively fast sea level rise back to the current sea level at the end of SP 31; and finally (D) estimation of future conditions in 20 ka from present at the end of SP 31_DSP.

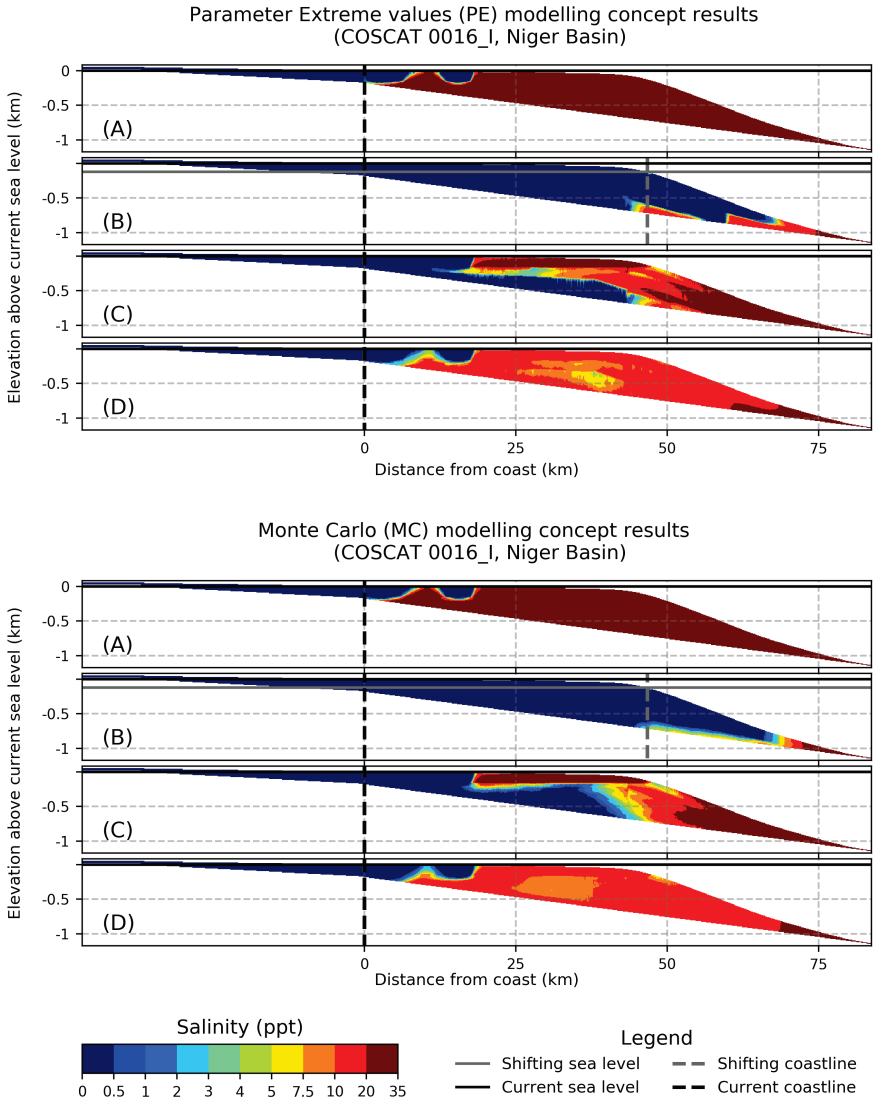

Figure B-2 Averaged salinity profiles for both modelling concepts at four timeframes for COSCAT 0016_I region (Niger Basin). The estimated salinity concentration in the 2D profiles is represented: (A) at the end of SP 0, salinity concentration before fluctuating sea level SPs; (B) at the lowest sea level occurring at the end of the sea level drop represented by SP 21; (C) after the relatively fast sea level rise back to the current sea level at the end of SP 31; and finally (D) estimation of future conditions in 20 ka from present at the end of SP 31_DSP.

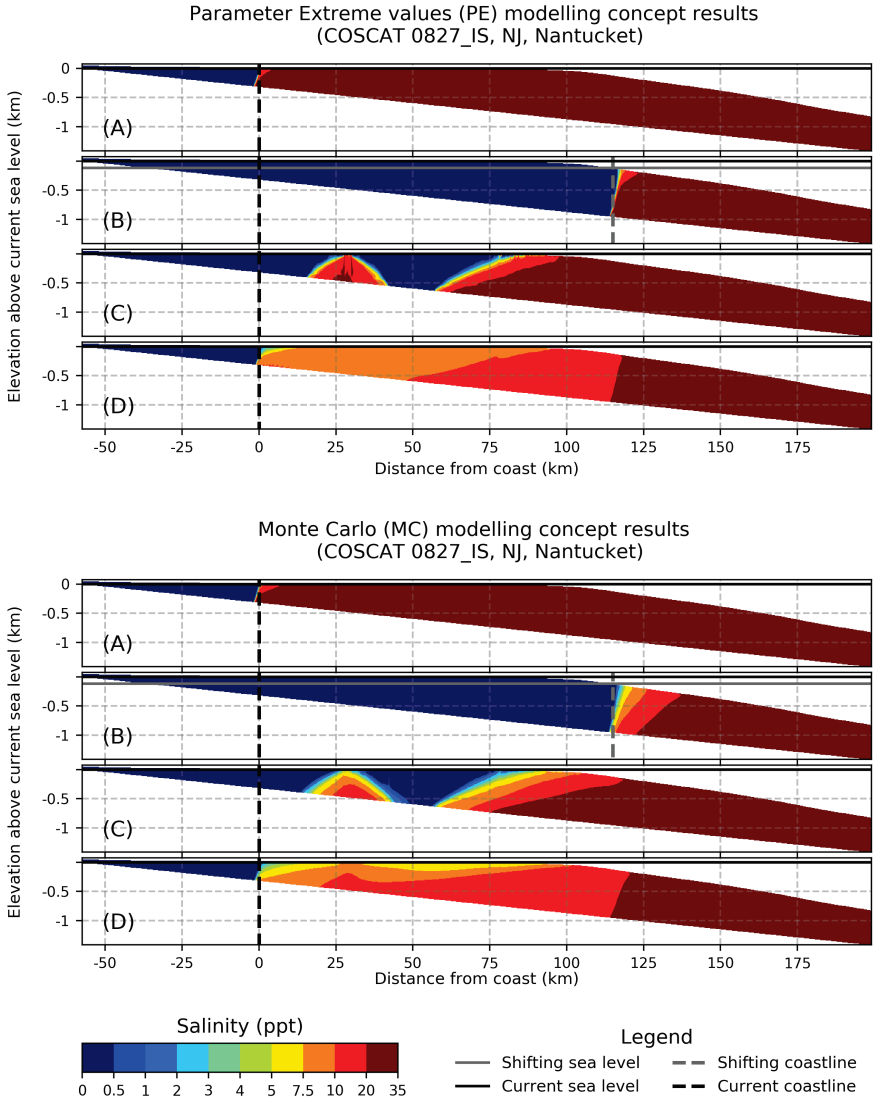

Figure B-3 Averaged salinity profiles for both modelling concepts at four timeframes for COSCAT 0827_IS region (NJ, Nantucket, east coast USA). The estimated salinity concentration in the 2D profiles is represented: (A) at the end of SP 0, salinity concentration before fluctuating sea level SPs; (B) at the lowest sea level occurring at the end of the sea level drop represented by SP 21; (C) after the relatively fast sea level rise back to the current sea level at the end of SP 31; and finally (D) estimation of future conditions in 20 ka from present at the end of SP 31_DSP.

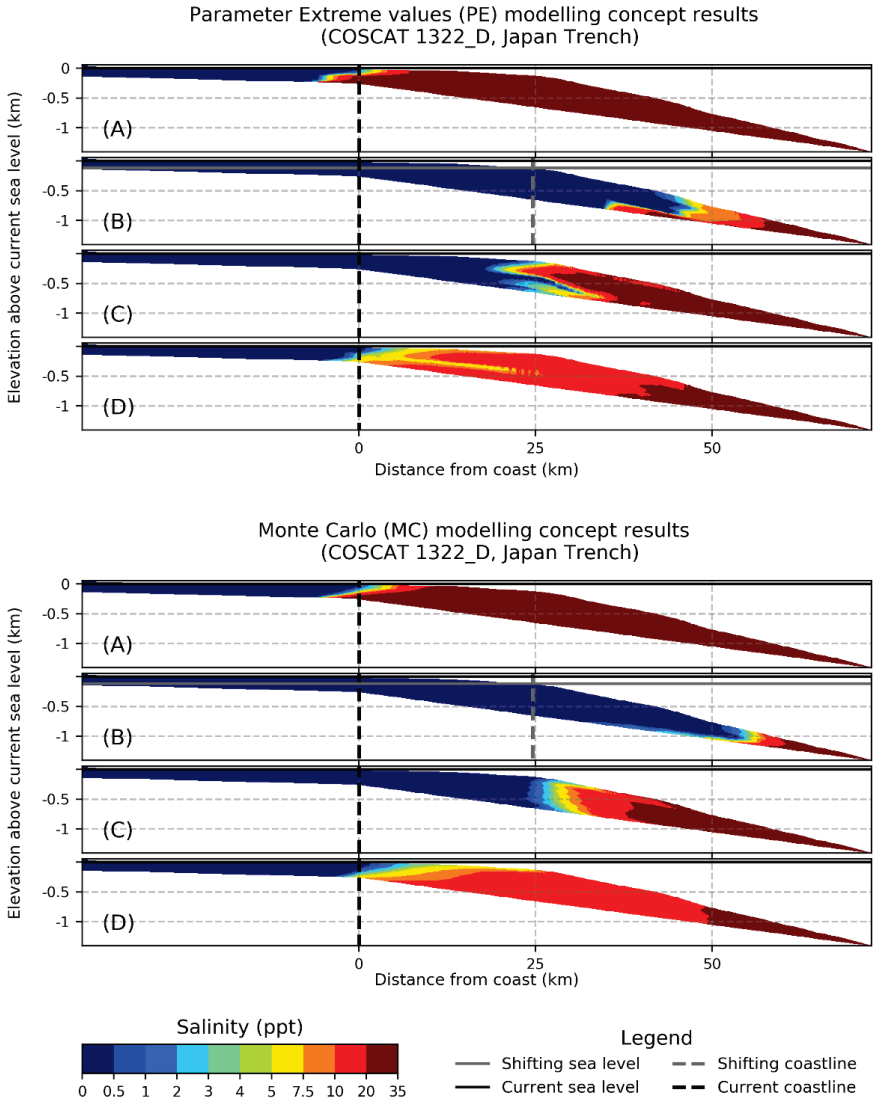

Figure B-4 Averaged salinity profiles for both modelling concepts at four timeframes for COSCAT 1322_D region (Japan Trench). The estimated salinity concentration in the 2D profiles is represented: (A) at the end of SP 0, salinity concentration before fluctuating sea level SPs; (B) at the lowest sea level occurring at the end of the sea level drop represented by SP 21; (C) after the relatively fast sea level rise back to the current sea level at the end of SP 31; and finally (D) estimation of future conditions in 20 ka from present at the end of SP 31_DSP.

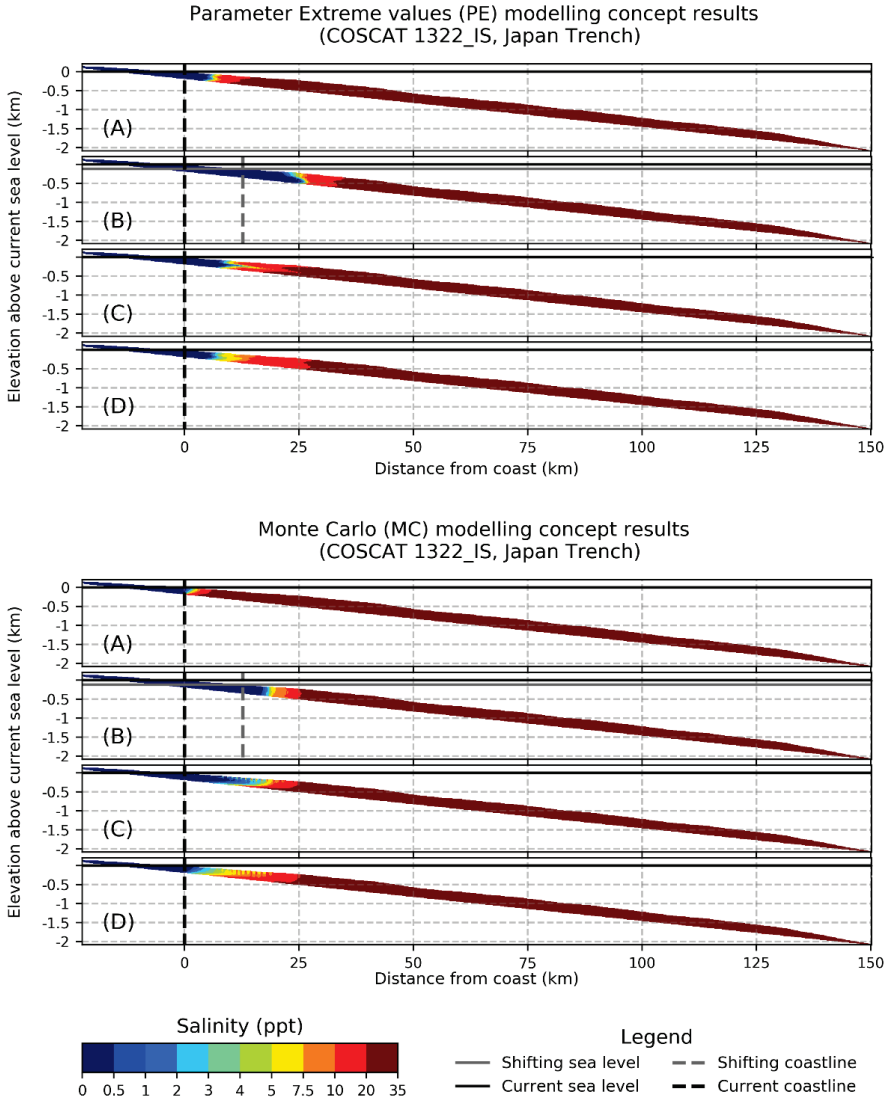

Figure B-5 Averaged salinity profiles for both modelling concepts at four timeframes for COSCAT 1322_IS region (Japan Trench). The estimated salinity concentration in the 2D profiles is represented: (A) at the end of SP 0, salinity concentration before fluctuating sea level SPs; (B) at the lowest sea level occurring at the end of the sea level drop represented by SP 21; (C) after the relatively fast sea level rise back to the current sea level at the end of SP 31; and finally (D) estimation of future conditions in 20 ka from present at the end of SP 31_DSP.

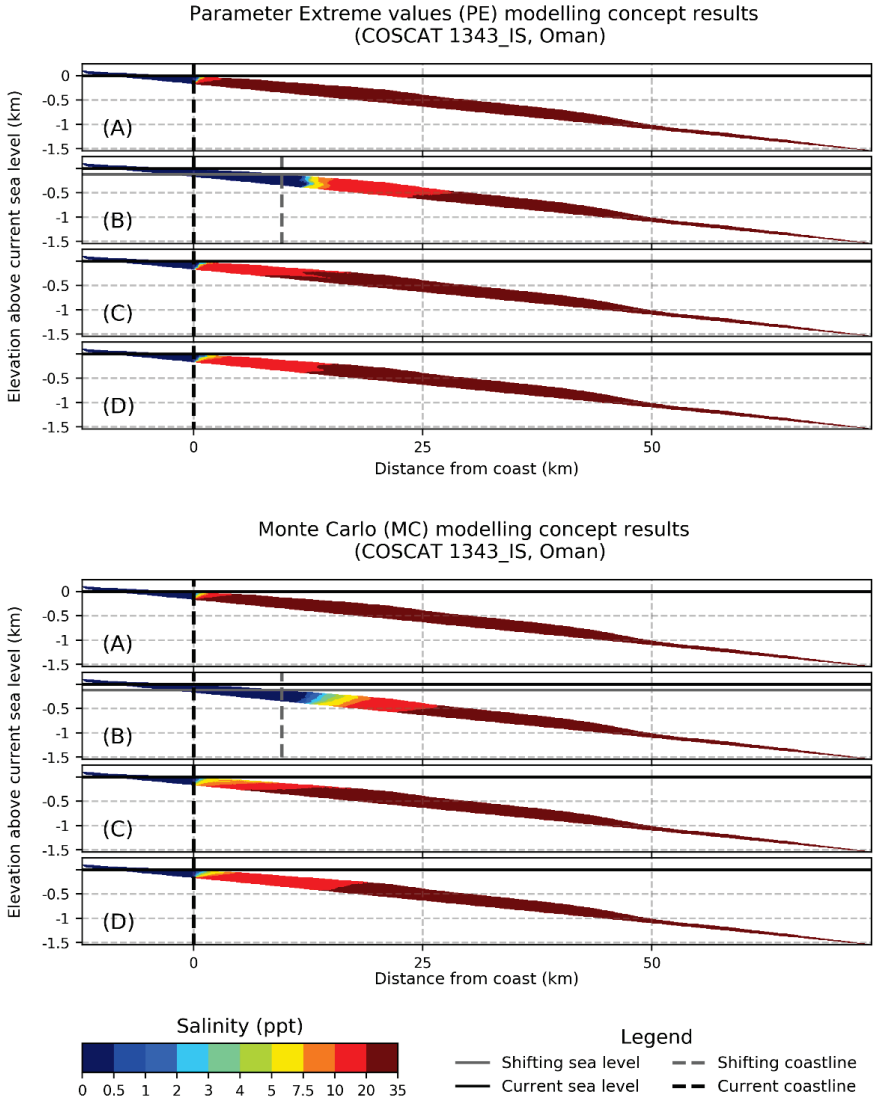

Figure B-6 Averaged salinity profiles for both modelling concepts at four timeframes for COSCAT 1343_IS region (Oman). The estimated salinity concentration in the 2D profiles is represented: (A) at the end of SP 0, salinity concentration before fluctuating sea level SPs; (B) at the lowest sea level occurring at the end of the sea level drop represented by SP 21; (C) after the relatively fast sea level rise back to the current sea level at the end of SP 31; and finally (D) estimation of future conditions in 20 ka from present at the end of SP 31_DSP.

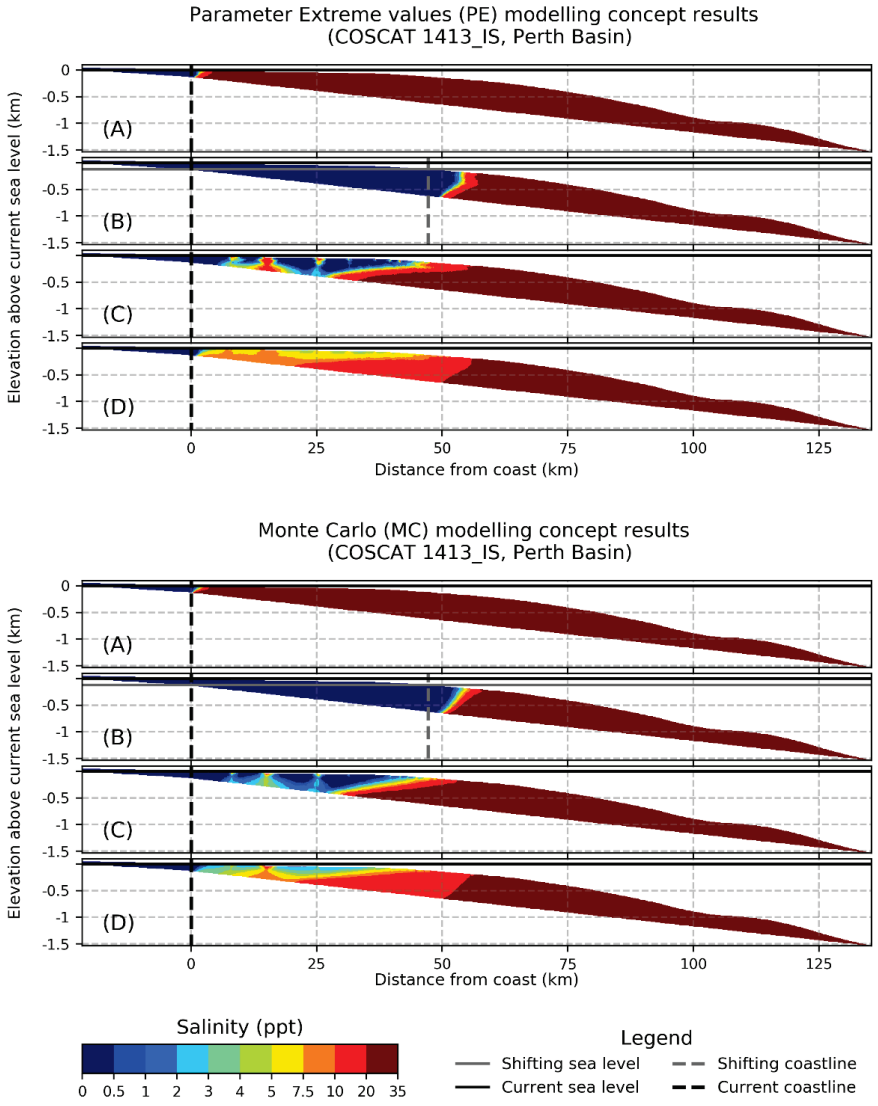

Figure B-7 Averaged salinity profiles for both modelling concepts at four timeframes for COSCAT 1413_IS region (Perth Basin). The estimated salinity concentration in the 2D profiles is represented: (A) at the end of SP 0, salinity concentration before fluctuating sea level SPs; (B) at the lowest sea level occurring at the end of the sea level drop represented by SP 21; (C) after the relatively fast sea level rise back to the current sea level at the end of SP 31; and finally (D) estimation of future conditions in 20 ka from present at the end of SP 31_DSP.

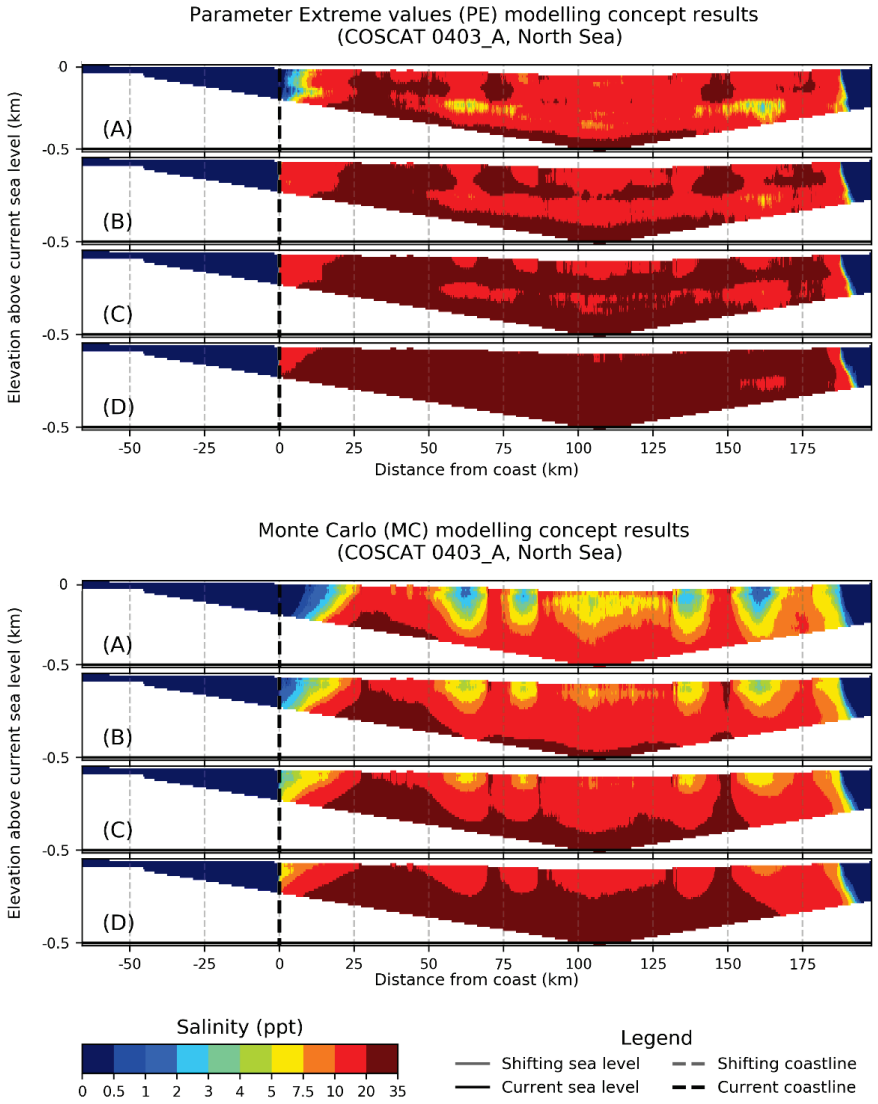

Figure B-8 Averaged salinity profiles for both modelling concepts at four timeframes for COSCAT 0403_A region (North Sea). The estimated salinity concentration in the 2D profiles is represented: (A) estimated current situation (B) 5ka from current situation; (C) 10ka from current situation; and finally (D) 20ka from current situation; and finally. Sea level is constant throughout the whole simulation and equal to 0m bsl (current sea level).

C Appendix to Chapter 4

Table C-1 ID number (and reference number) for each location shown in Figure 4-2 in the main article.

ID (reference)	***Location***	***COSCAT***	***Distance from coast (km)***		***Depth below sea-level (km)***	
			Observed	**Modelled**	**Observed**	**Modelled**
1 *(Bakari et al., 2012)*	Tanzania	7	-	-	0.61	0.5
2 *(Engelen et al., 2019)*	Nile delta	3	70	40	1	1.2
3 *(Oteri, 1988)*	Niger delta	16	40	70	2	1.3
4 *(Zhang et al., 2011)*	East China Sea	1326	100	90	0.2	0.7
5 *(Groen et al., 2000)*	Suriname	1103	90	95	0.6	0.7
6 *(Person et al., 2012, 2003)*	Nantucket	827	60	60	0.6	0.5
7 *(Geldern et al., 2013; Thomas et al., 2019)*	New Jersey	827	130	60	0.6	0.6
8 *(Knight et al., 2019)*	South Australia	1411	13.5	35	0.65	0.35
9 *(Amir et al., 2013)*	Israel	1301	20	5	-	-
10 *(Maathuis et al., 2000)*	Jakarta	1330	18	25	0.3	0.3
11 *(Gustafson et al., 2019)*	Martha's Vineyard	827	90	60	0.4	0.6
12 *(Bertoni et al., 2020)*	Tanzania	7	50	90	1.5	1
13 *(Bertoni et al., 2020)*	Canterbury Bight NZ	1407	60	50	0.4	0.4
14 *(Varma and Michael, 2011)*	Gippsland Basin, AU	1410	20	30	2.5	0.2
15 *(Haroon et al., 2018)*	Israel	1301	4	5	0.2	0.2
16 *(Paleologos et al., 2018)*	UAE	1342	-	-	-	-
17 (Larsen et al., 2017)	Red river delta	1327	-	-	-	-
18 *(Jiao et al., 2015)*	Hong Kong	1325	-	-	-	-

Table C-2 Selected observation offshore wells (Micallef, 2020) in regions with unconsolidated sediments providing observed (OBS) and estimated (EST) top and bottom depths of OFG. The ID offshore wells correspond to Figure 4-2C in the main article.

ID offshore well	Lat	Lon	Offshore distance	OBS OFG top depth (m bsl.)	OBS OFG bot depth (m bsl.)	Porosity (%)	EST OFG top depth (m bsl.)	EST OFG bot depth (m bsl.)
1	55.1357	9.8005	6.5	-25	-35		-51	-20
2	55.1357	9.8005	6.5	-25	-35		-27	-214
3	55.1357	9.8005	6.5	-25	-35		-20	-241
4	-11.952	-77.2616	20	-96	-106		-74	-428
5	-11.952	-77.2616	20	-96	-106		-31	-595
6	55.0048	10.1082	9	-23	-143		-38	-225
7	55.0048	10.1082	9	-23	-143		-20	-231
8	-44.7685	171.674	42	-99	-264	40-50	-122	-264
9	-44.7685	171.674	42	-99	-264	40-50	-31	-556
10	39.3656	-72.6946	130	-107	-280	25-45	-211	-524
11	-44.4893	171.8528	60	-130	-380		-193	-728
12	-44.4893	171.8528	60	-130	-380		-10	-747
13	39.5195	-73.4132	80	-70	-440		-20	-745
14	-44.9374	172.0227	83	-358	-448	40-50	-51	-798
15	39.6342	-73.6217	44	-53	-453	20 - 60	-10	-181
16	39.5657	-73.4972	56	-255	-555	20-60	-10	-60
17	-16.6465	146.2896	46	-299	-594	30-52	-211	-432
18	-38.0521	140.2711	40	-350	-600		-201	-312
19	6.2347	-55.1757	90	-50	-650		-40	-705
20	63.4714	-39.7818	42	-663	-718	35-45	-50	-333
21	-44.7555	172.3933	93	-407	-877	45-60	-111	-616
22	-38.2191	140.469	40	-600	-950		-50	-342
23	-16.624	146.3248	50	-581	-953	40-70	-221	-432
24	-16.423	146.2151	70	-972	-1385	35-62	-271	-452
25	4.0128	7.3349	40	-260	-2100		-241	-1294
26	4.0128	7.3349	40	-260	-2100		-410	-640
27	-45.896	-75.8528	60	-2781	-2821	37-48	-103	-500
28	38.4035	-74.8972	14	-80			-10	-40
29	37.2998	-74.6527	89	-130			-20	-755
30	41.1583	-68.6972	119	-135			-151	-665
31	31.9008	34.6282	3.5	-150			-41	-272
32	39.0617	-73.0983	112	-292			-101	-544
33	39.9928	-71.3348	124	-425			-181	-654
34	37.0323	13.1816	37	-600		50	-256	-10

Table C-3 Estimated OFG volumes, water demand (based on PCR-GLOBWB (Sutanudjaja et al., 2018) model output) and their comparison showing how many years OFG could sustain total regional water demand for 21 selected deltaic regions. PCR-GLOBWB (Sutanudjaja et al., 2018) model runs using SSP2 and RCP 6.0 scenarios, median value of five different global climate models, time period 2060 – 2090. The location of these deltaic regions is shown in Figure C-8.

Coastal region river delta name(s)	***OFG volume (km3)***	***Water demand (km3/yr)***			***OFG offshore / Water demand (yr)***		
		2020	**2050**	**2075**	**2020**	**2050**	**2075**
Moulouya	9 ± 5.2	0.53	0.65	0.75	16 ± 9.9	13 ± 8.1	11 ± 6.9
Nile	19927 ± 658.4	230.23	379.54	516.68	87 ± 2.9	53 ± 1.7	39 ± 1.3
Tana	35 ± 3.6	0.02	0.07	0.09	1478 ± 150.7	536 ± 54.7	371 ± 37.8
Congo	10013 ± 960.5	0.28	0.66	1.01	35283 ± 3384.6	15243 ± 1462.2	9907 ± 950.4
Niger	13538 ± 3960.7	13.17	33.96	49.15	1028 ± 300.8	399 ± 116.6	275 ± 80.6
Volta	267 ± 36.7	1.99	5.09	6.86	134 ± 18.5	52 ± 7.2	39 ± 5.3
Senegal	77 ± 65.1	2.43	3.12	3.78	31 ± 26.8	25 ± 20.9	20 ± 17.2
Sebou	16 ± 7.8	0.25	0.35	0.41	63 ± 30.8	45 ± 22.3	38 ± 18.8
Ebro, Rhone	3475 ± 1442.7	1.30	1.43	1.51	2674 ± 1110.1	2434 ± 1010.4	2307 ± 957.7
Grijalva	7920 ± 2820.9	5.27	7.48	9.11	1503 ± 535.5	1059 ± 377	870 ± 309.8
Rio Grande	7494 ± 311.2	13.74	17.80	21.49	546 ± 22.7	421 ± 17.5	349 ± 14.5
Magdalena	1325 ± 226.5	6.87	9.77	11.90	193 ± 33	136 ± 23.2	111 ± 19
Sao Francisco	340 ± 13.8	0.59	0.70	0.75	577 ± 23.4	482 ± 19.6	453 ± 18.4
Yangtze	47303 ± 0	147.58	160.88	155.03	321 ± 0	294 ± 0	305 ± 0
Mekong, Chao Phraya	40988 ± 29.1	235.26	275.22	282.95	174 ± 0.1	149 ± 0.1	145 ± 0.1
Mahakam	522 ± 103.8	1.67	2.42	2.64	313 ± 62.1	216 ± 42.9	198 ± 39.3
Irrawaddy	45642 ± 1788.4	33.03	34.28	34.75	1382 ± 54.1	1332 ± 52.2	1314 ± 51.5
Fly river, Burdekin	6391 ± 2528.6	0.29	0.35	0.40	21911 ± 8668.7	18386 ± 7274.2	16021 ± 6338.8
Brahmani, Mahanadi, Godavari, Krishna	9335 ± 2923.9	82.25	103.52	109.62	113 ± 35.6	90 ± 28.2	85 ± 26.7
Indus	9172 ± 4652	3.07	4.21	4.87	2985 ± 1513.9	2180 ± 1105.7	1883 ± 955
Orinoco	30470 ± 2133.2	0.29	0.43	0.52	106224 ± 7436.6	71657 ± 5016.6	58222 ± 4076

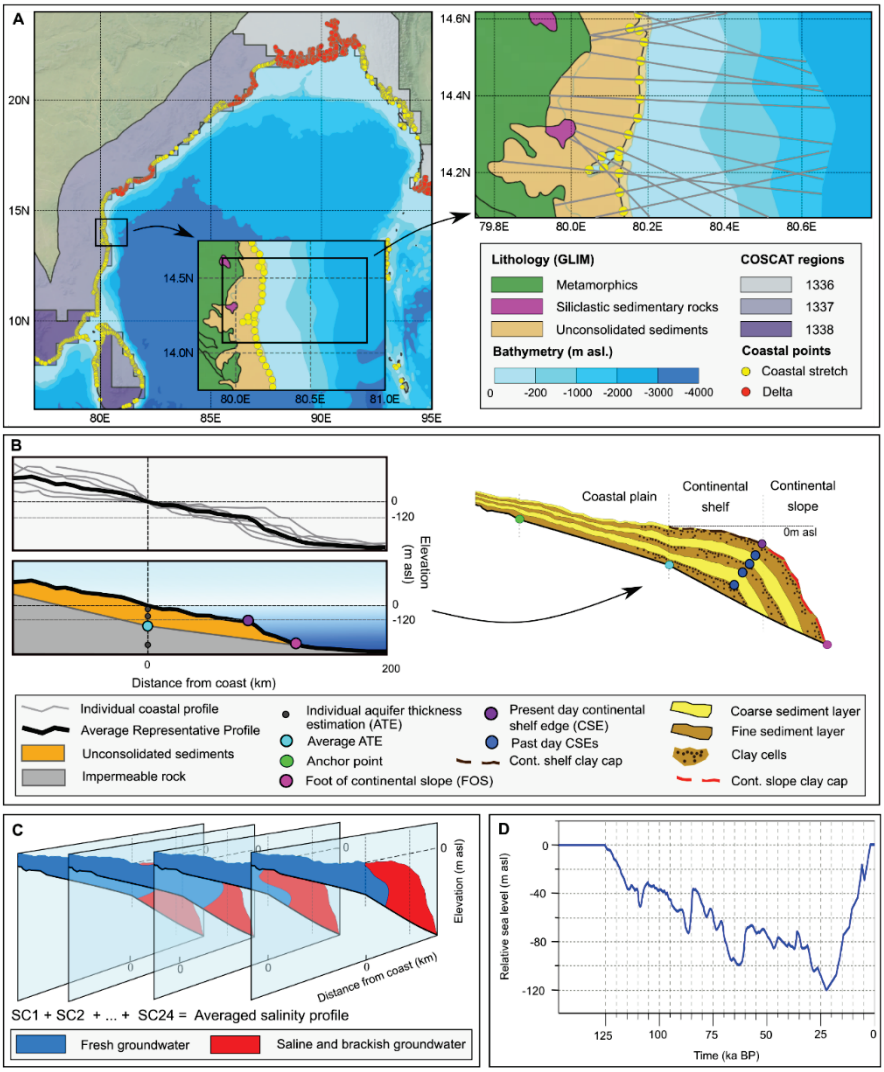

Figure C-1 Schematization summarizing the methodology applied to estimate OFG volumes in coastal regions worldwide. Detailed information is provided in (Zamrsky et al., 2020). (A) Example of coastal region boundaries and location of 2D profiles within the regions, "Delta" and "Coastal stretch" coastal types are differentiated in this coastal region. (B) Aggregating the individual 2D coastal profiles to create an average representative profile (ARP) which forms the outside boundary of the 2D coastal profile. In the next step the inner part of the profile is filled based on geological conditions and scenarios. (C) Groundwater models (using the computer code SEAWAT (Langevin et al., 2008)) for each geological scenario (SC1, SC2 etc.) are averaged into a single profile showing the mean groundwater salinity in the ARP. This final mean estimate is then used to calculate the current OFG volume in the coastal region. (D) Sea-level fluctuations over the last glacial-interglacial cycle are taken into account in our groundwater models.

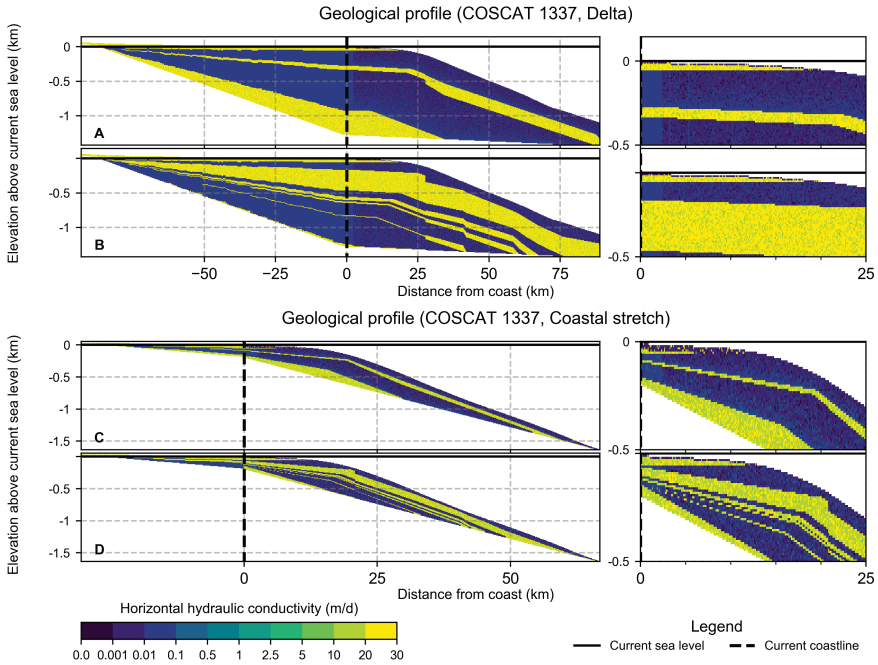

Figure C-2 Examples of geology profiles in COSCAT 1337, showing 2 out of the 24 geological scenarios corresponding to the "Delta" coastal type with the lowest (A) and highest (B) estimated OFG volume. Same applies to the "Coastal stretch" coastal type, highest (C) and lowest (D) respectively. The final groundwater salinity profiles are provided in Figure C-3.

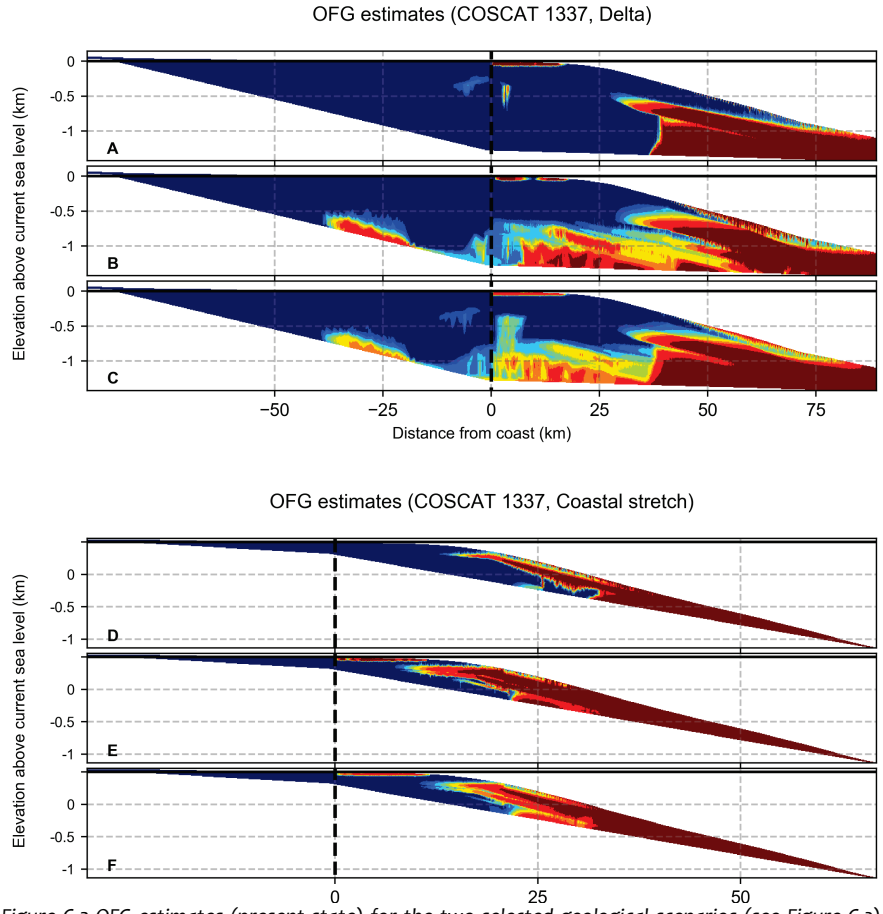

Figure C-3 OFG estimates (present state) for the two selected geological scenarios (see Figure C-2) in coastal region COSCAT 1337. Two coastal types are presented in this coastal region, Delta (A-C) and Coastal stretch (D-F). The upper most profiles (A and D) show estimates with highest OFG volume, the middle profiles (B and E) give the lowest OFG volume estimates, the bottom profiles (C and F) show the average OFG volume estimates over all 24 geological scenarios).

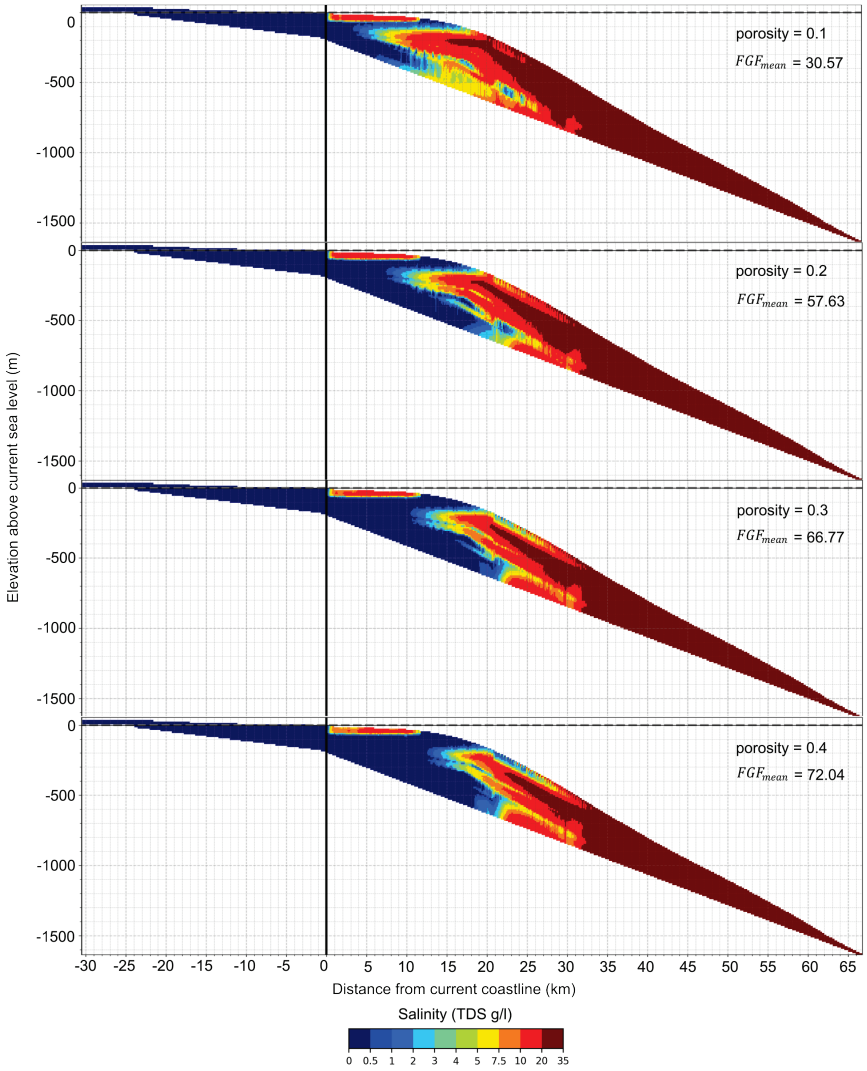

Figure C-4 Current salinity distributions estimated by groundwater models with varying porosity values in COSCAT region 1337 (Coastal stretch). The general salinity pattern stays largely constant (except for porosity value of 0.1) suggesting that variations in porosity do not substantially affect groundwater salinity distributions unless the porosity values are very low (0.1 and lower). FGF_{mean} represents mean fresh groundwater fraction (%).

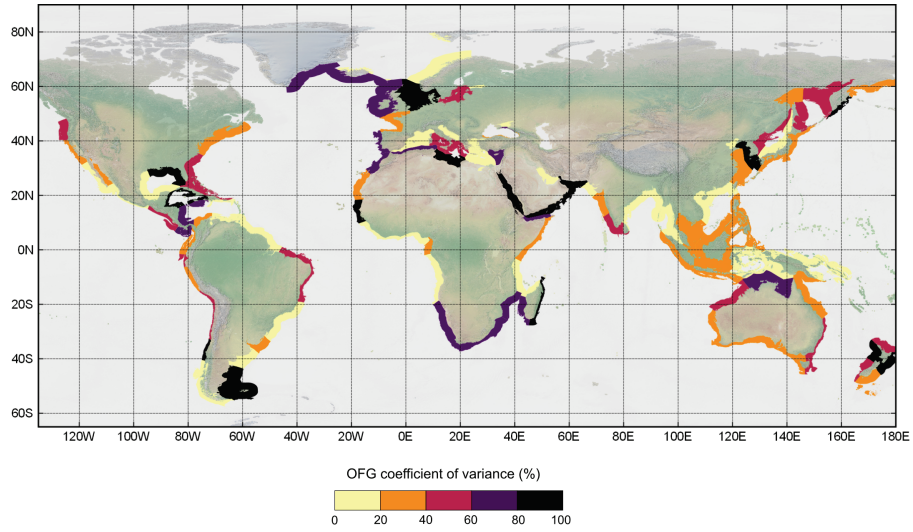

Figure C-5 Coefficient of variance of OFG estimates, calculated as $(OFG_{stdev}/OFG_{mean}) \times 100\%$.

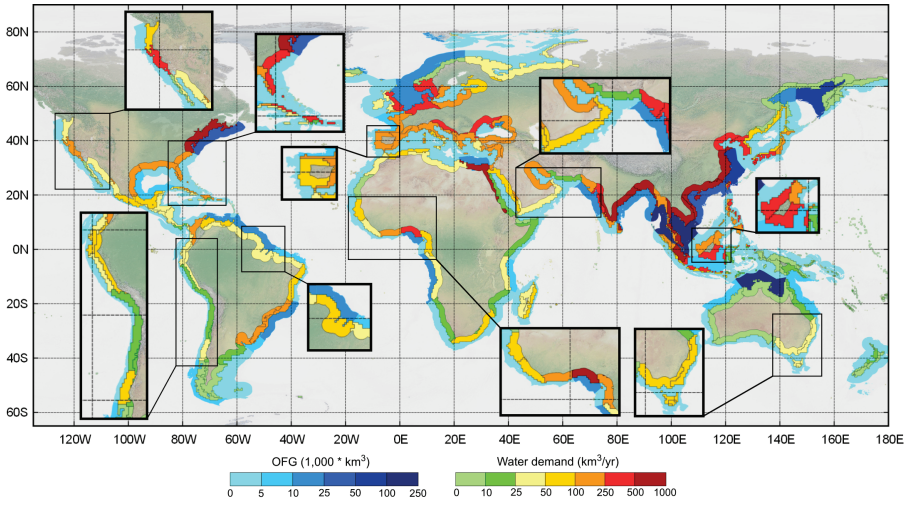

Figure C-6 Estimates of regional OFG volumes along the global coastline compared with future water demand for the year 2050 that are extracted from the PCR-GLOBWB (Sutanudjaja et al., 2018) global hydrological model. The zoom in regions show areas with increased water demand for the year 2075. The water demand is extracted from the PCR-GLOBWB (Sutanudjaja et al., 2018) model runs using SSP2 and RCP 6.0 scenarios, median value of five different global climate models, time periods 2035 - 2065 for year 2050 and 2060 - 2090 for year 2075.

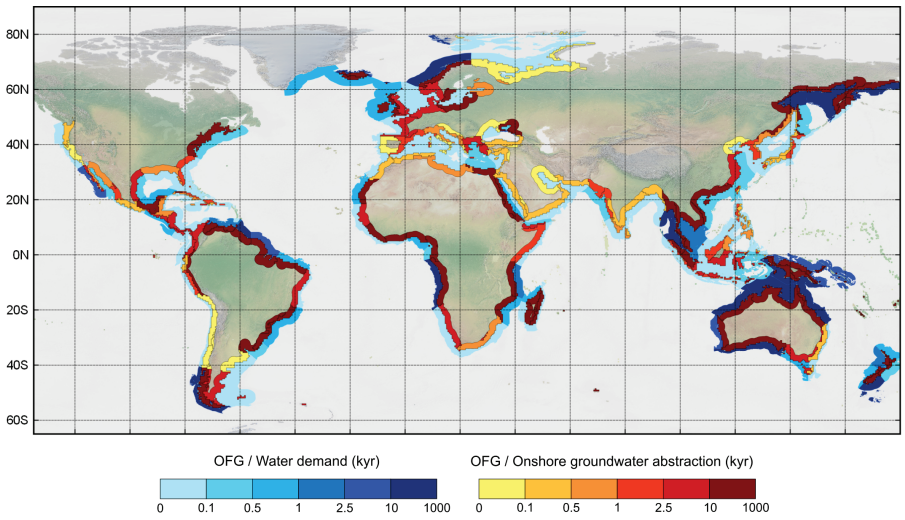

Figure C-7 Ratio of estimated OFG volumes with current regional water demand and onshore groundwater extraction. Estimates obtained from the global hydrology and water resources model PCR-GLOBWB (Sutanudjaja et al., 2018) showing the time scale (orders of magnitude in kyr) to which OFG could contribute to the fresh water demand per coastal region.

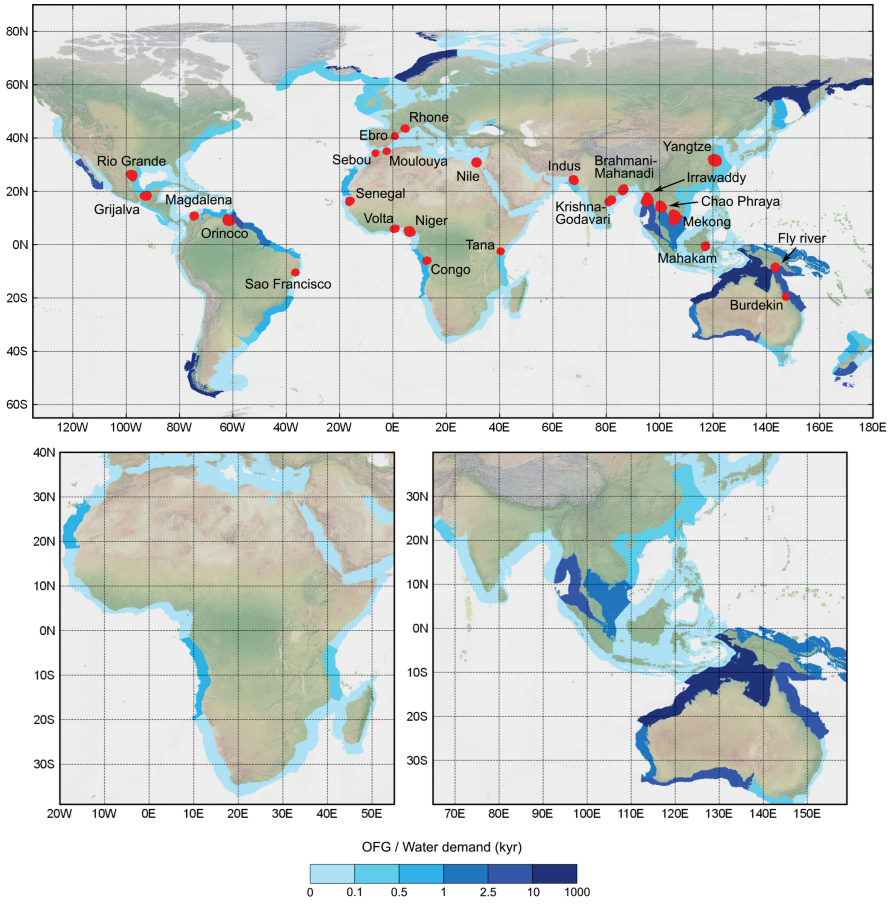

Figure C-8 Comparison of OFG volumes with estimated future regional water demand (year 2075) (no simulated increase in groundwater extractions). PCR-GLOBWB (Sutanudjaja et al., 2018) model runs using SSP2 and RCP 6.0 scenarios, median value of five different global climate models, time period 2060 – 2090. The upper part of the figure also shows delta (combined) locations for which we provide quantitative OFG volumes estimates in Table C-3.

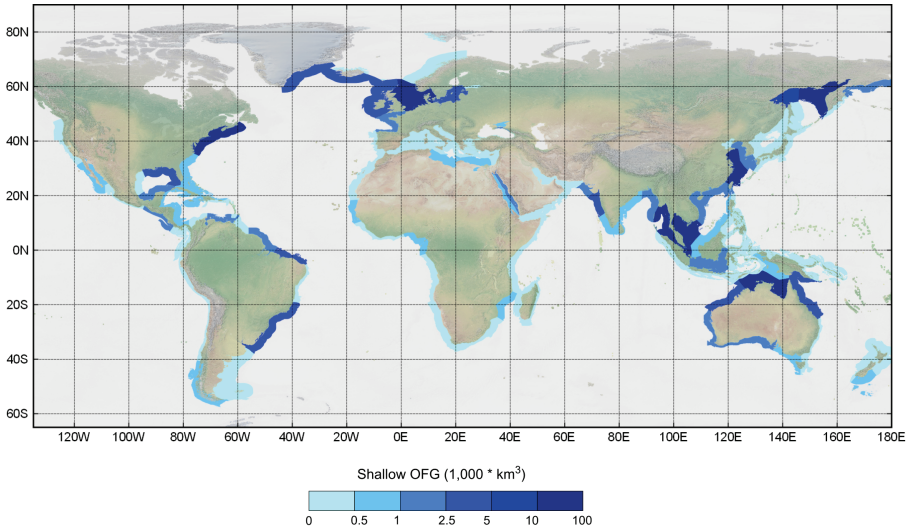

Figure C-9 Estimated volumes of OFG volumes shallower than 300 m below sea level.

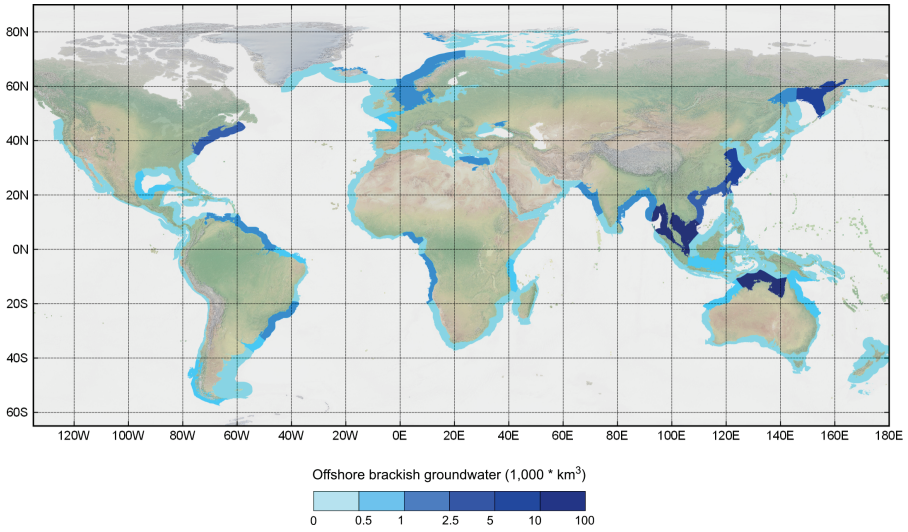

Figure C-10 Global volumes of offshore brackish groundwater (1 – 10 TDS g/l).

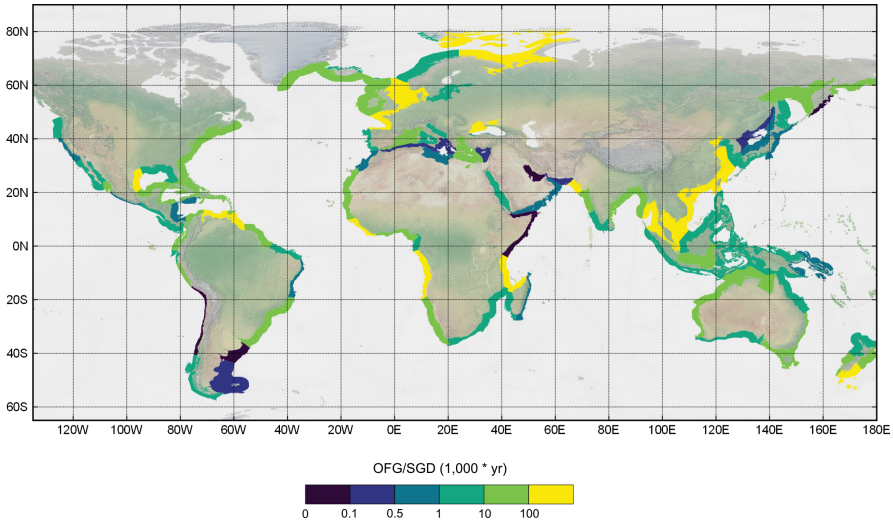

Figure C-11 Global map showing time scales (in thousands of years) on which regional OFG volume would get replenished by estimated current submarine groundwater discharge (SGD). Only few regions show renewable potential of OFG while the large majority is non-renewable with replenishment times with over 1,000 years.

D Appendix to Chapter 5

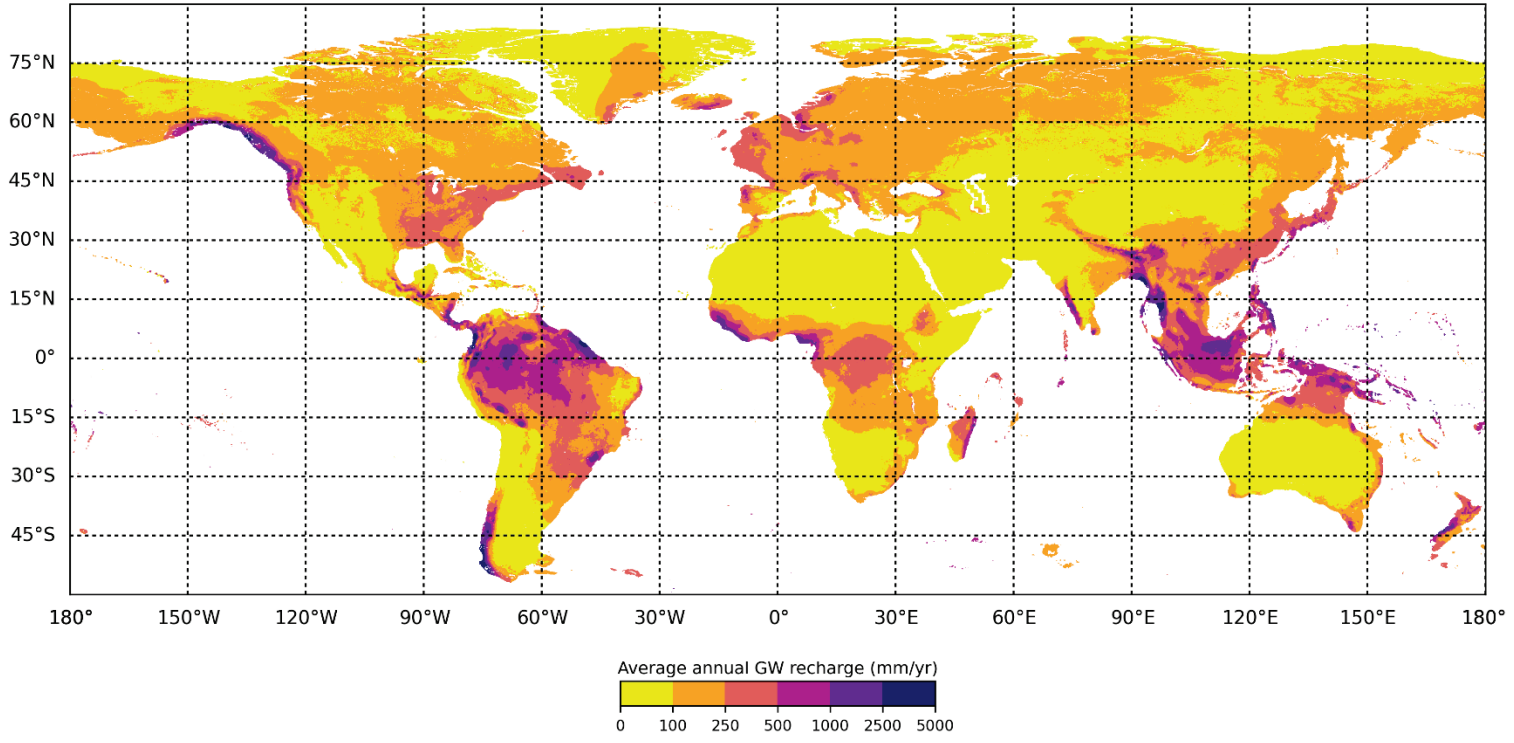

Figure D-1 Estimate groundwater recharge (mm/yr) 30,000 years before present (BP) until 21,000 years BP. Exposed areas due to lower sea level mean that some currently submerged continental shelves received fresh water recharge leading to deposition of paleo fresh groundwater.

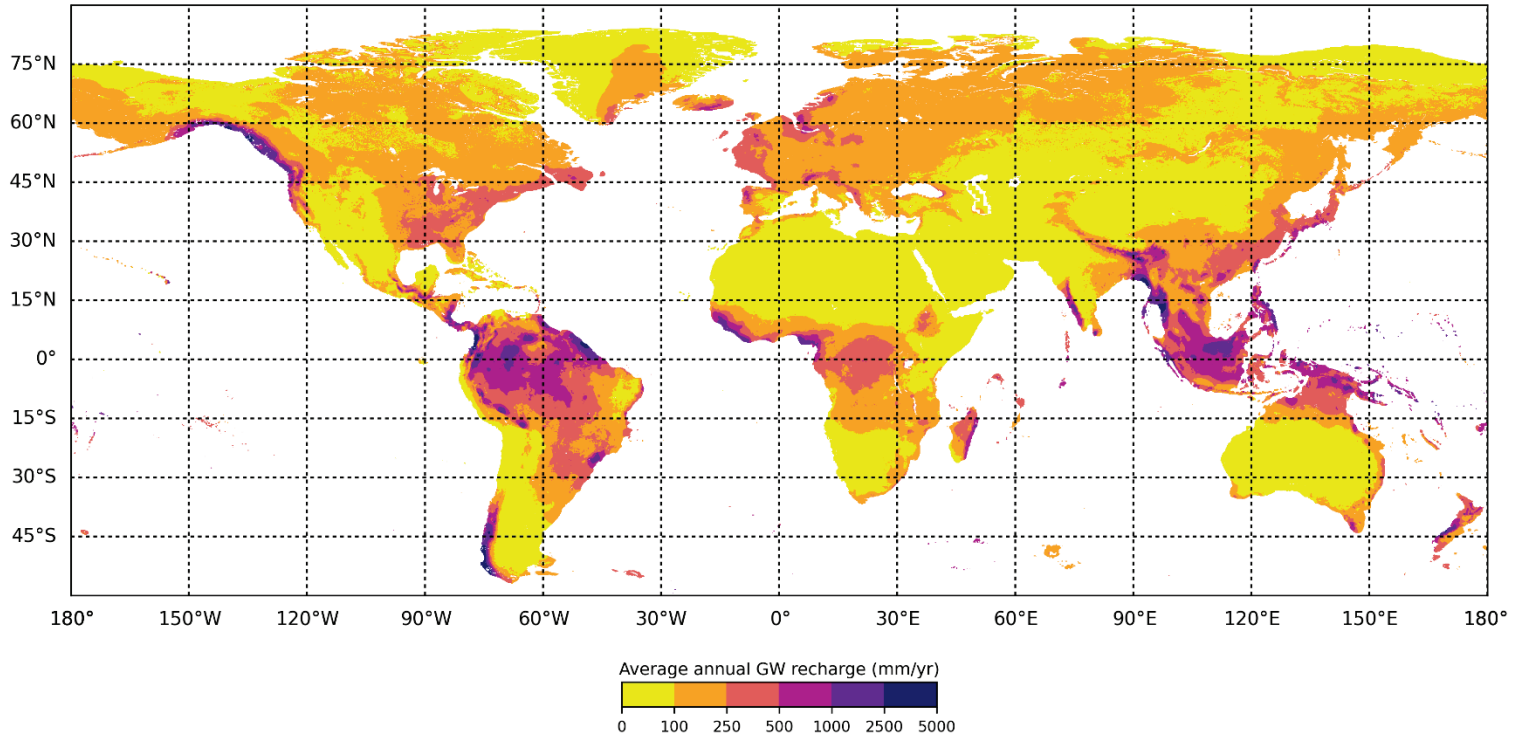

Figure D-2 Estimate groundwater recharge (mm/yr) 20,000 years (BP). Exposed areas due to lower sea level mean that some currently submerged continental shelves received fresh water recharge leading to deposition of paleo fresh groundwater.

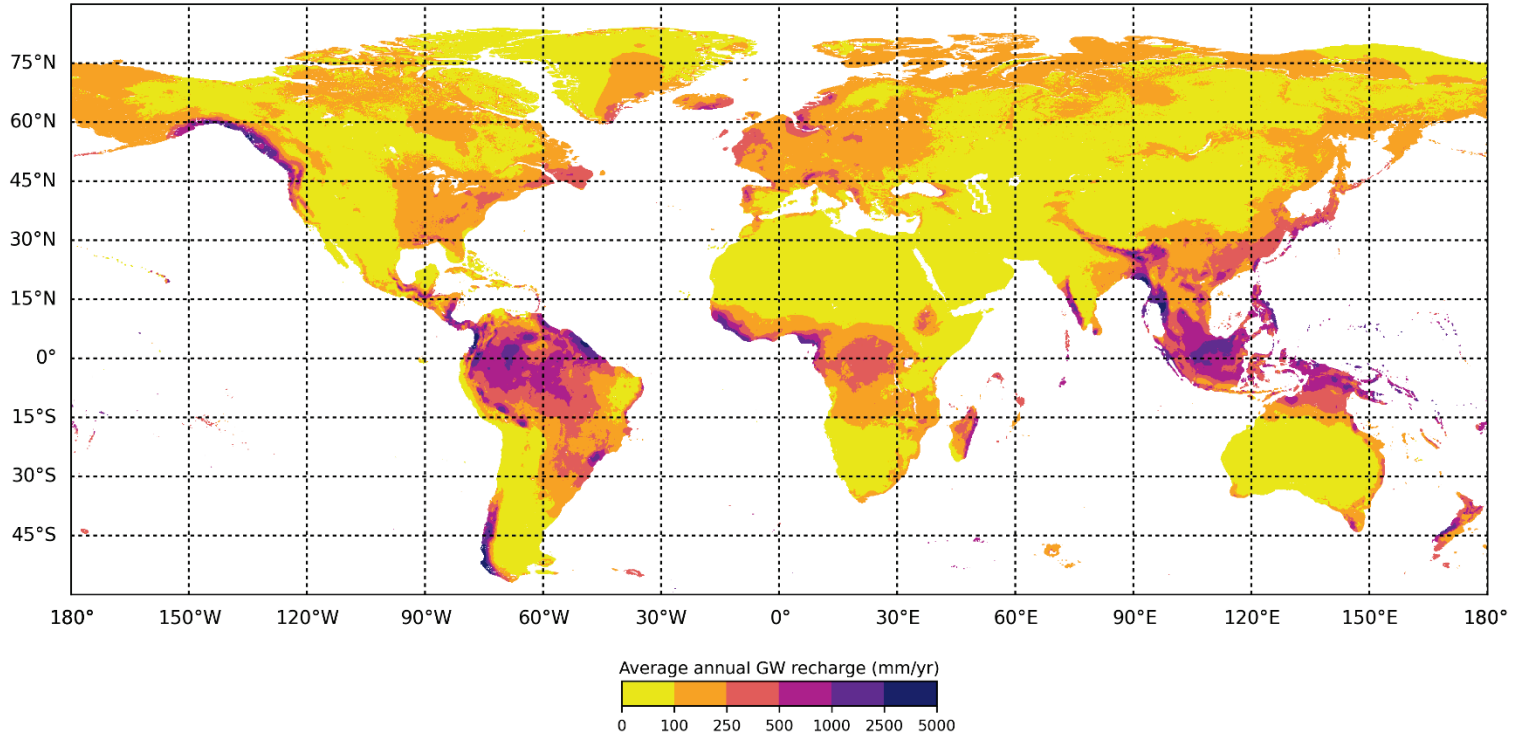

Figure D-3 Estimate groundwater recharge (mm/yr) 7,000 years (BP). Exposed areas due to lower sea level mean that some currently submerged continental shelves received fresh water recharge leading to deposition of paleo fresh groundwater. This is the last stress period where lower sea level is considered.

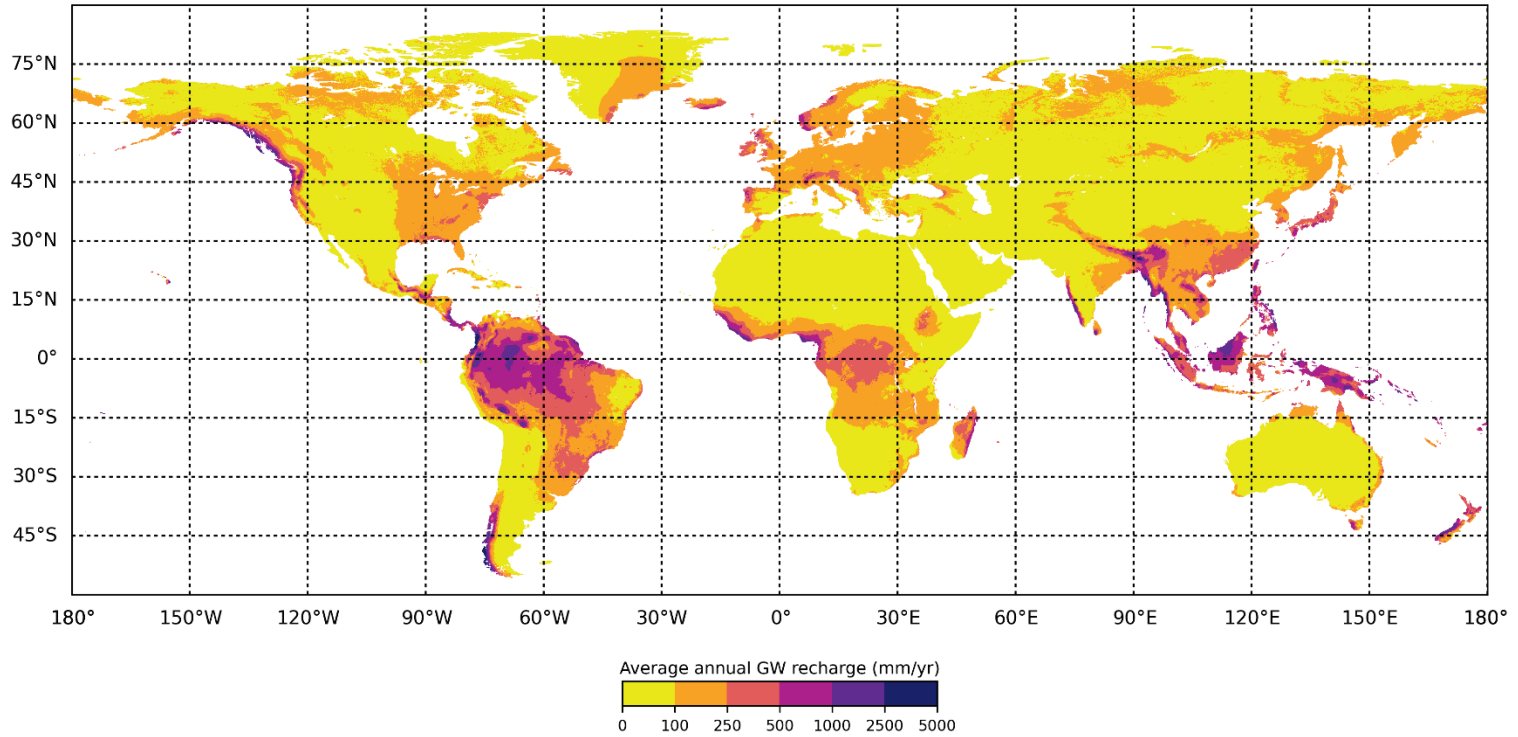

Figure D-4 Estimate groundwater recharge (mm/yr) 6,000 years (BP). At this time step the considered coastline (and sea level) is considered to match the current situation.

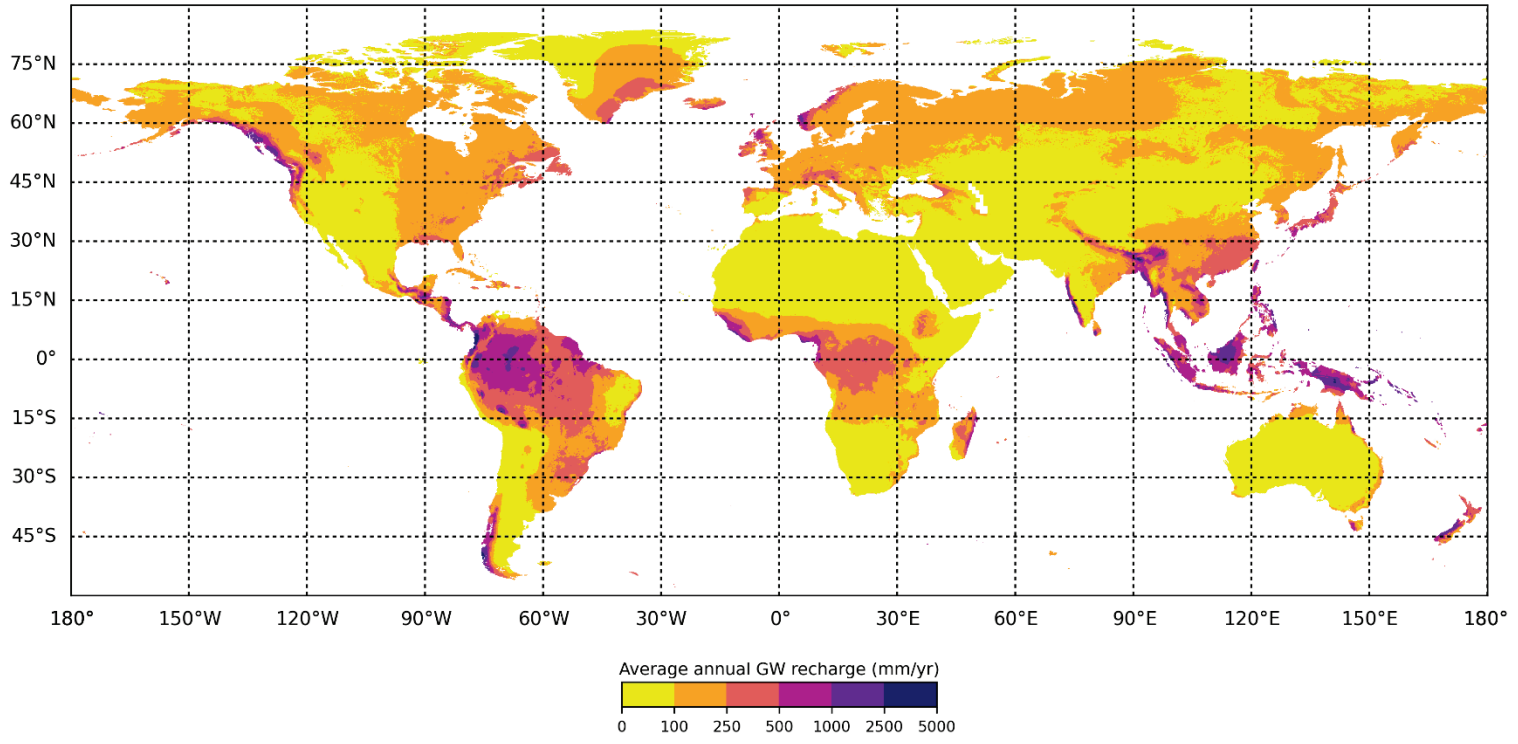

Figure D-5 Estimate groundwater recharge (mm/yr) 2,000 years (BP). After a dry climate period we can observe a wetter climate again leading to increased estimated groundwater recharge compared to Figure D-4.

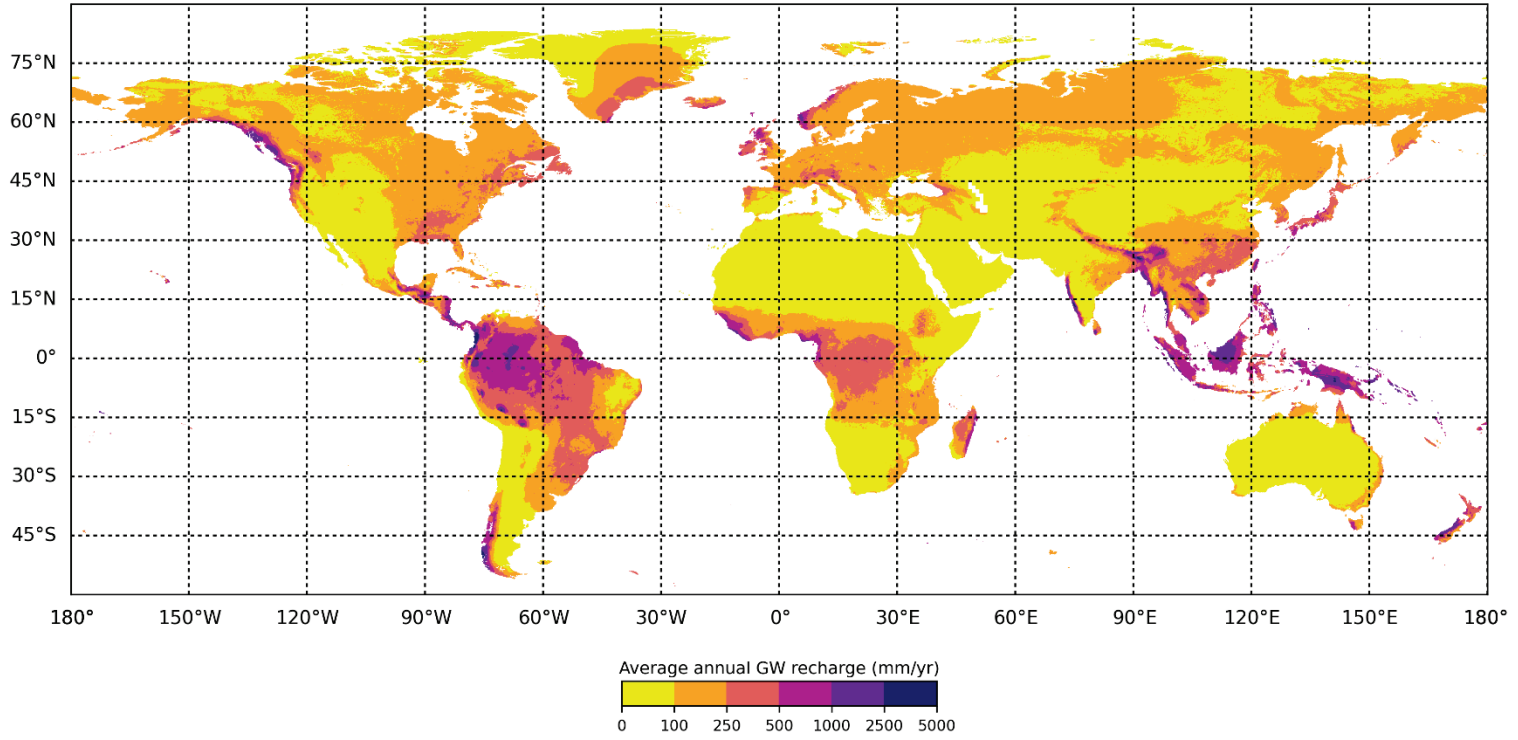

Figure D-6 Estimate current (year 2000) groundwater recharge (mm/yr).

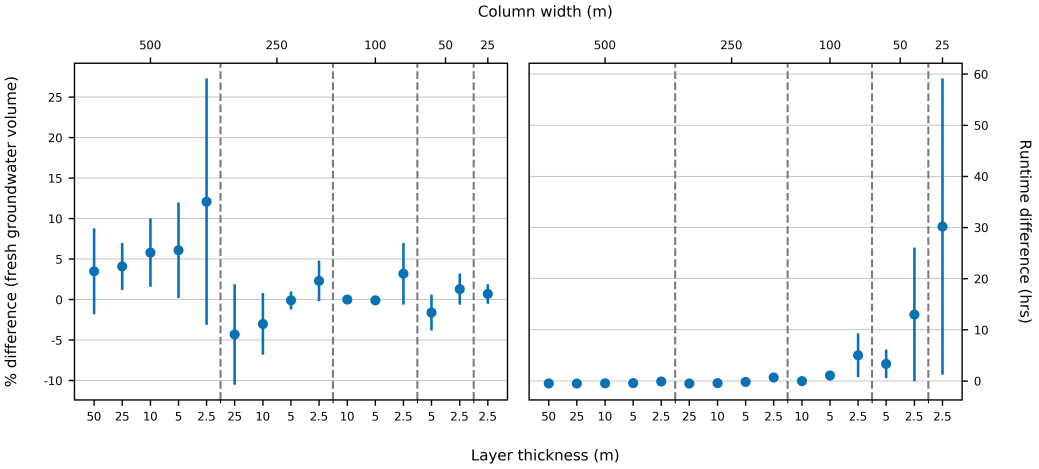

Figure D-7 Grid convergence analysis results, the left side graph shows the difference percentage in estimated groundwater volume (as compared to the default grid size groundwater model, 100m column width and 10m layer thickness). The difference in runtimes (as compared to the default grid size groundwater model) is shown in the graph on the right side of the figure.

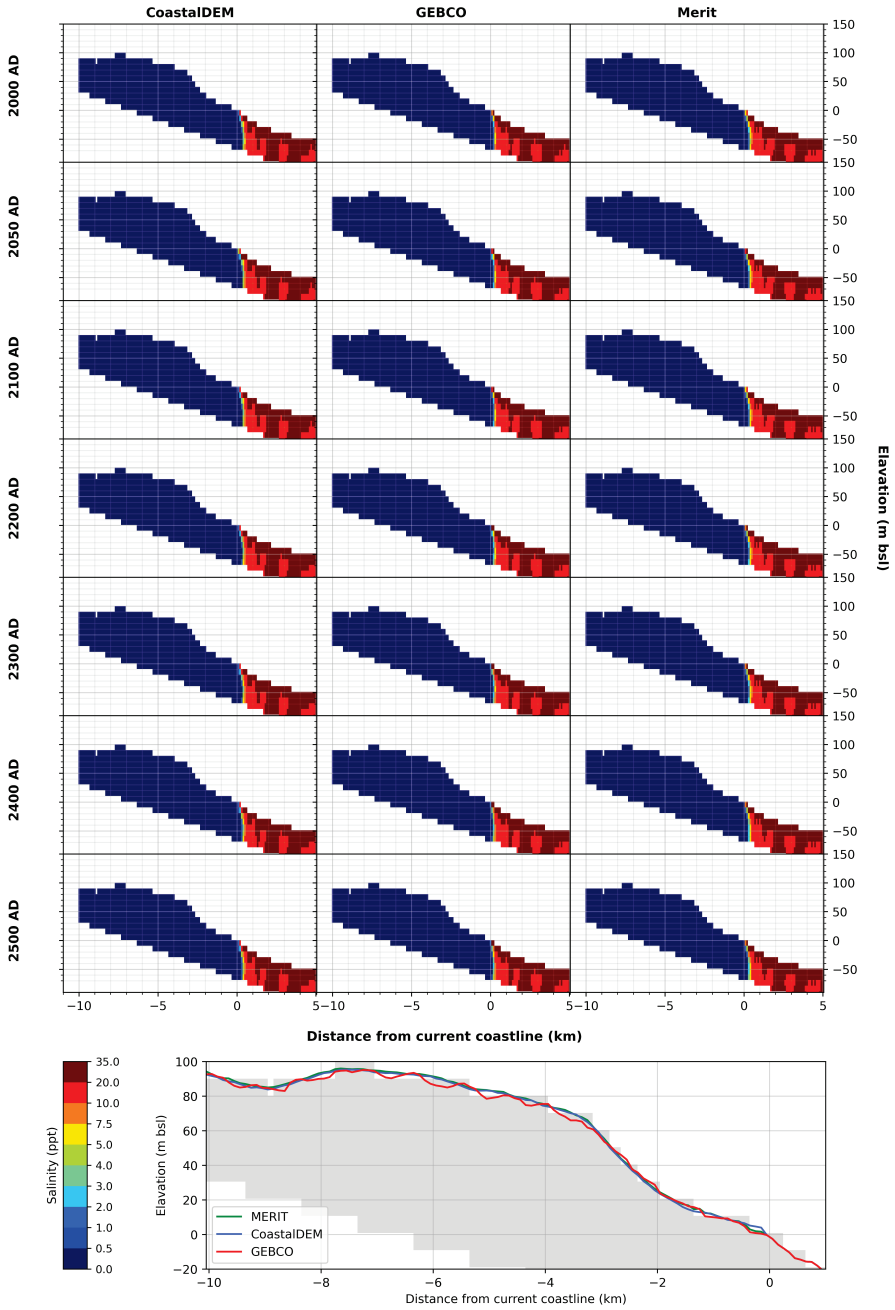

Figure D-8 Comparison of estimated groundwater salinity (SRM 0013_006) for the three DEM input datasets for the future 500 years under RCP 2.6 scenario. The bottom graph shows the variations in DEM elevation between the three DEM input datasets and active SEAWAT model grid (grey fill).

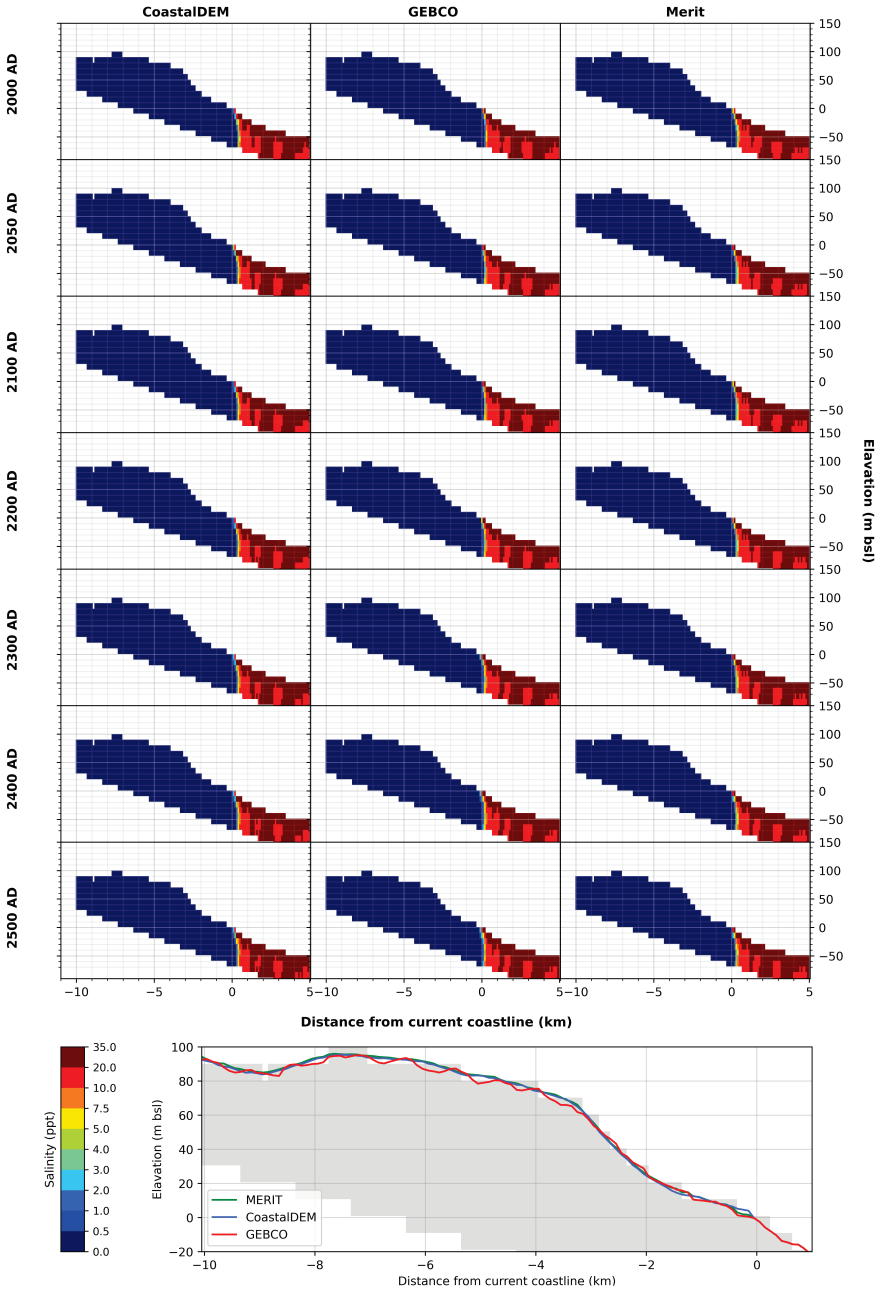

Figure D-9 Comparison of estimated groundwater salinity (SRM 0013_006) for the three DEM input datasets for the future 500 years under RCP 4.5 scenario. The bottom graph shows the variations in DEM elevation between the three DEM input datasets and active SEAWAT model grid (grey fill).

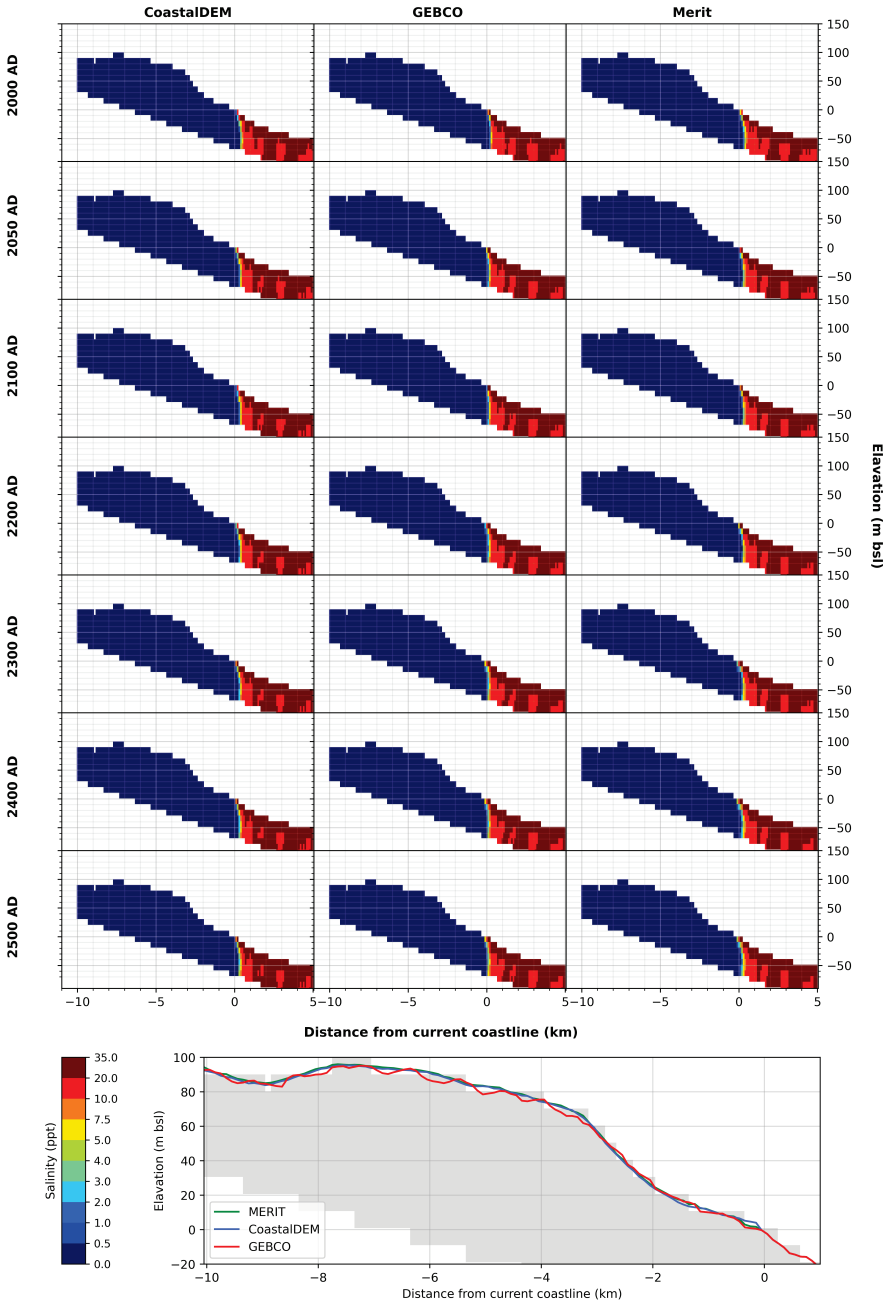

Figure D-10 Comparison of estimated groundwater salinity (SRM 0013_006) for the three DEM input datasets for the future 500 years under RCP 8.5 scenario. The bottom graph shows the variations in DEM elevation between the three DEM input datasets and active SEAWAT model grid (grey fill).

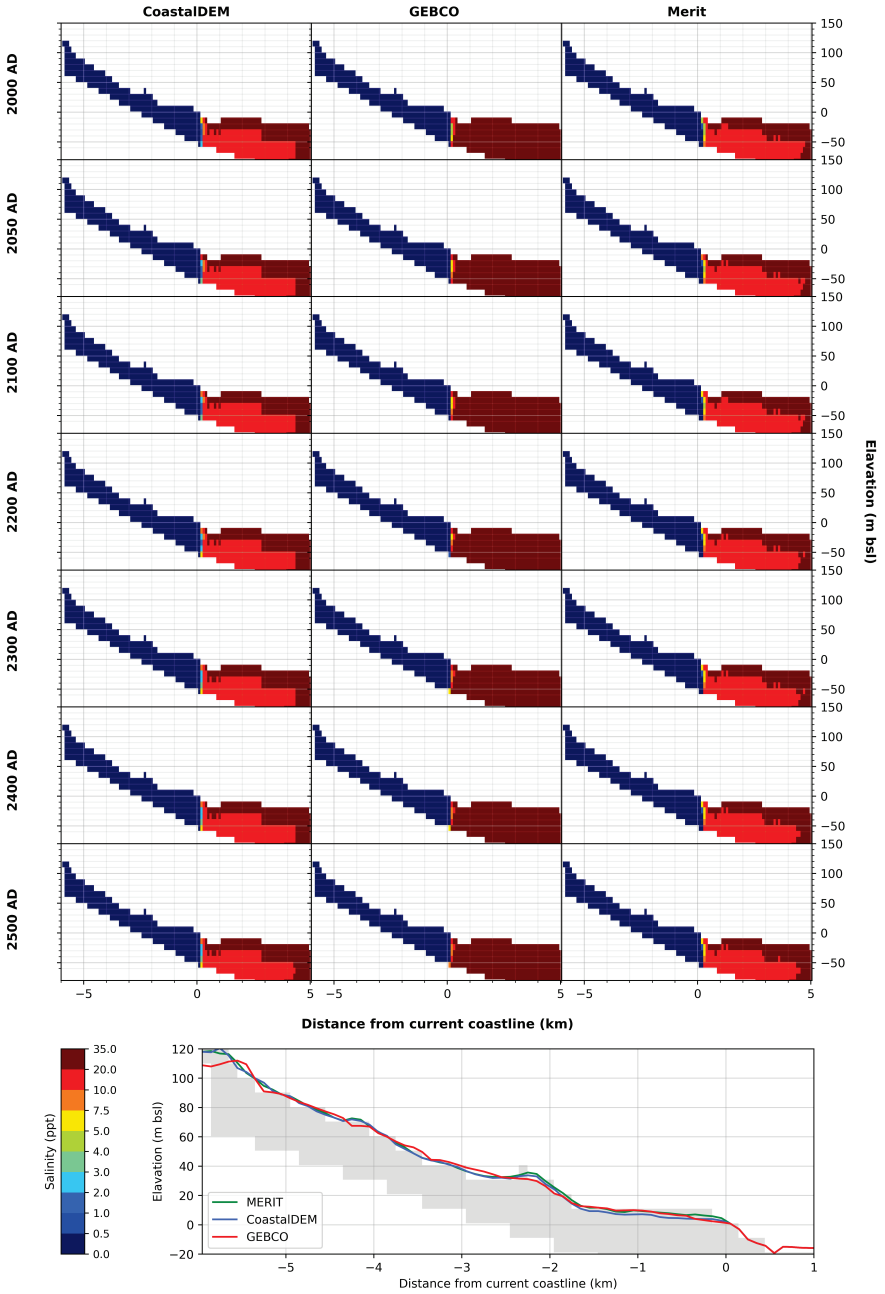

Figure D-11 Comparison of estimated groundwater salinity (SRM 1114_001) for the three DEM input datasets for the future 500 years under RCP 2.6 scenario. The bottom graph shows the variations in DEM elevation between the three DEM input datasets and active SEAWAT model grid (grey fill).

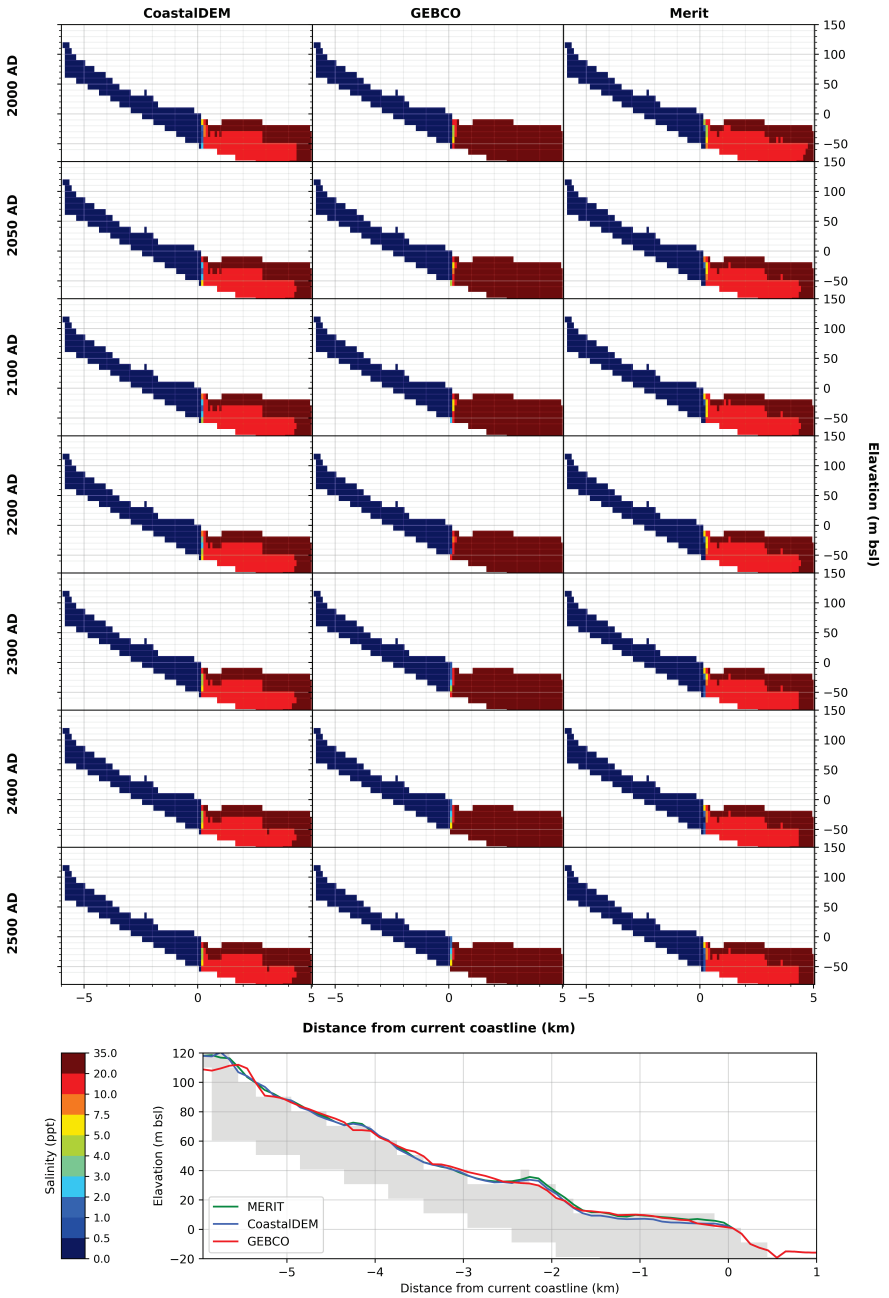

Figure D-12 Comparison of estimated groundwater salinity (SRM 1114_001) for the three DEM input datasets for the future 500 years under RCP 4.5 scenario. The bottom graph shows the variations in DEM elevation between the three DEM input datasets and active SEAWAT model grid (grey fill).

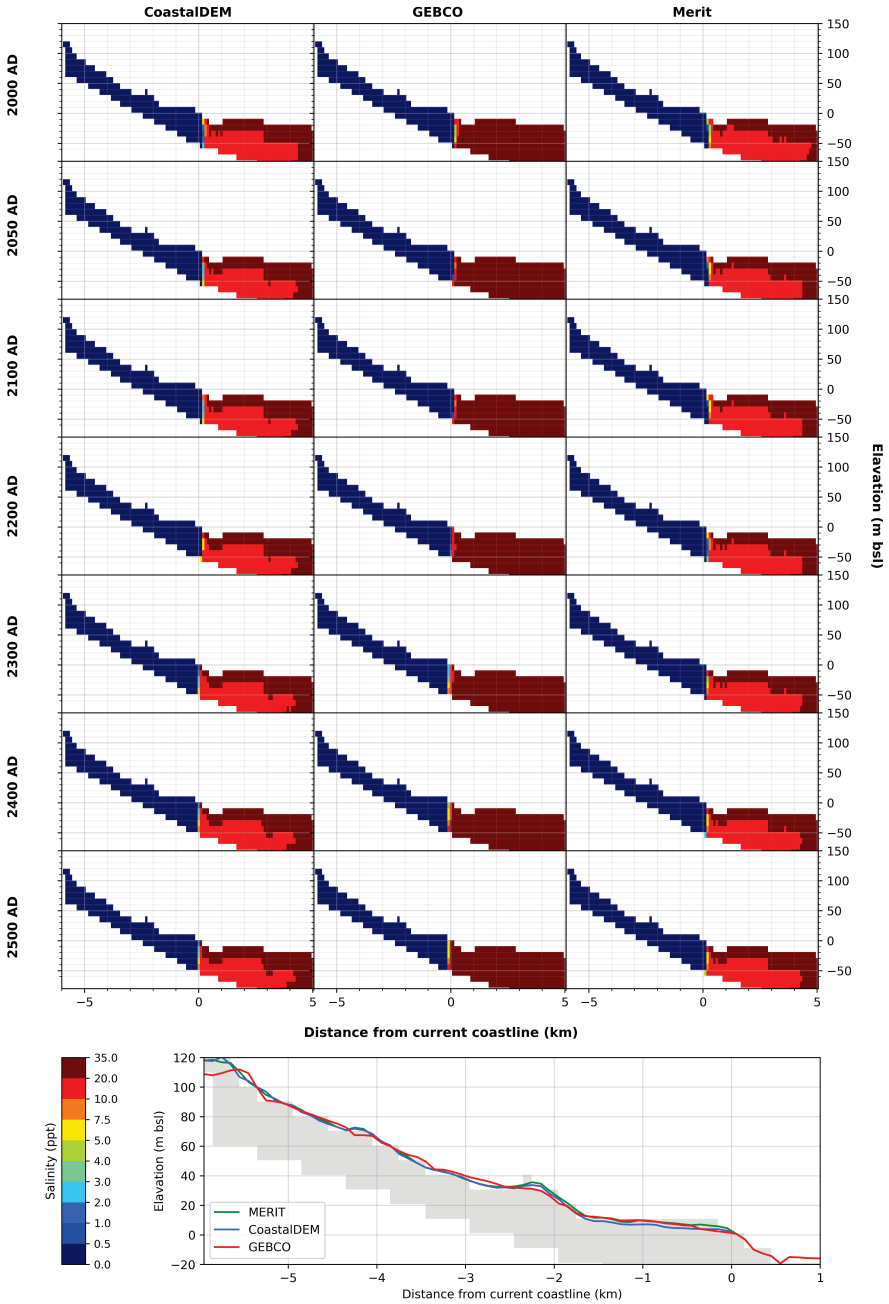

Figure D-13 Comparison of estimated groundwater salinity (SRM 1114_001) for the three DEM input datasets for the future 500 years under RCP 8.5 scenario. The bottom graph shows the variations in DEM elevation between the three DEM input datasets and active SEAWAT model grid (grey fill).

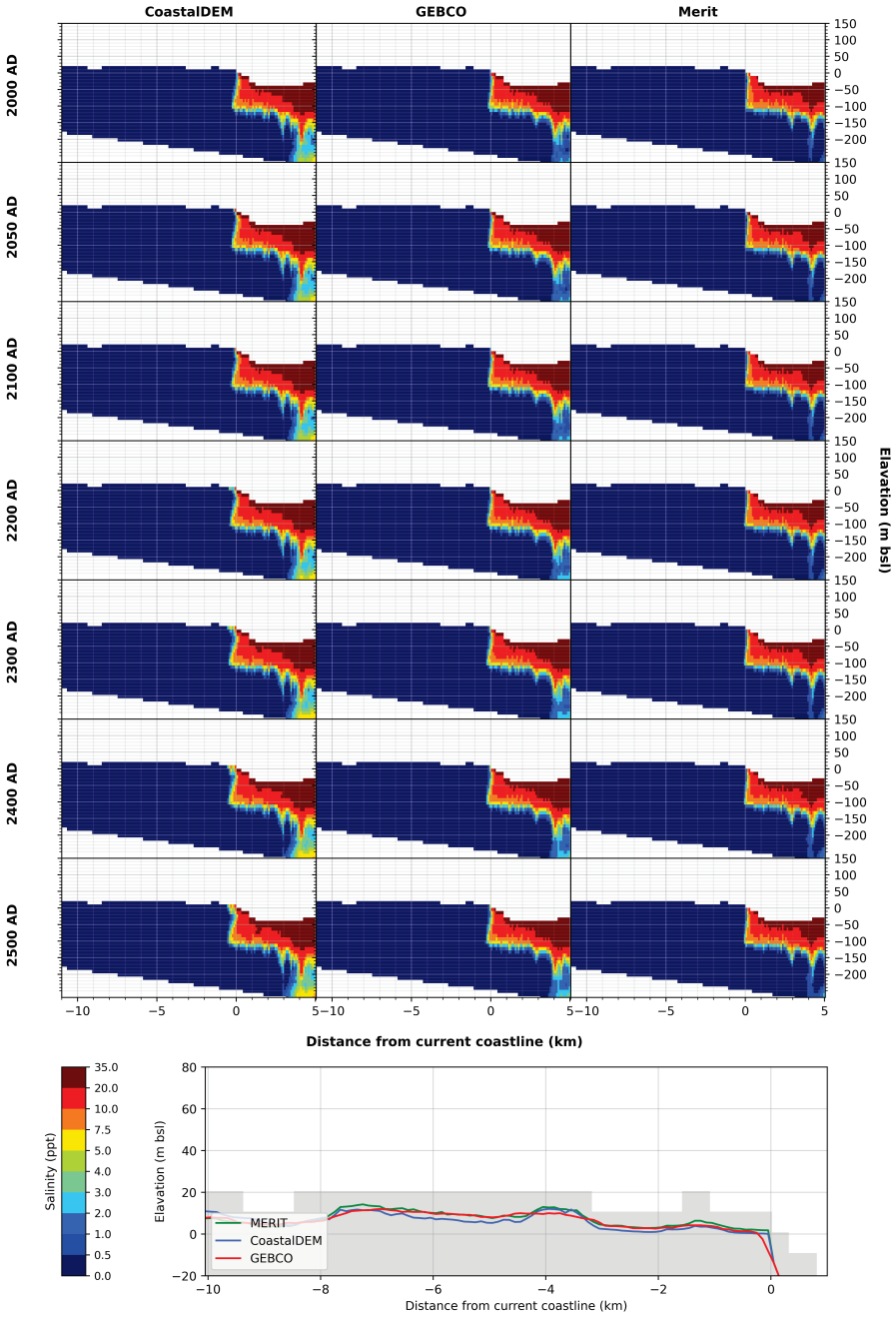

Figure D-14 Comparison of estimated groundwater salinity (SRM 0833_013) for the three DEM input datasets for the future 500 years under RCP 2.6 scenario. The bottom graph shows the variations in DEM elevation between the three DEM input datasets and active SEAWAT model grid (grey fill).

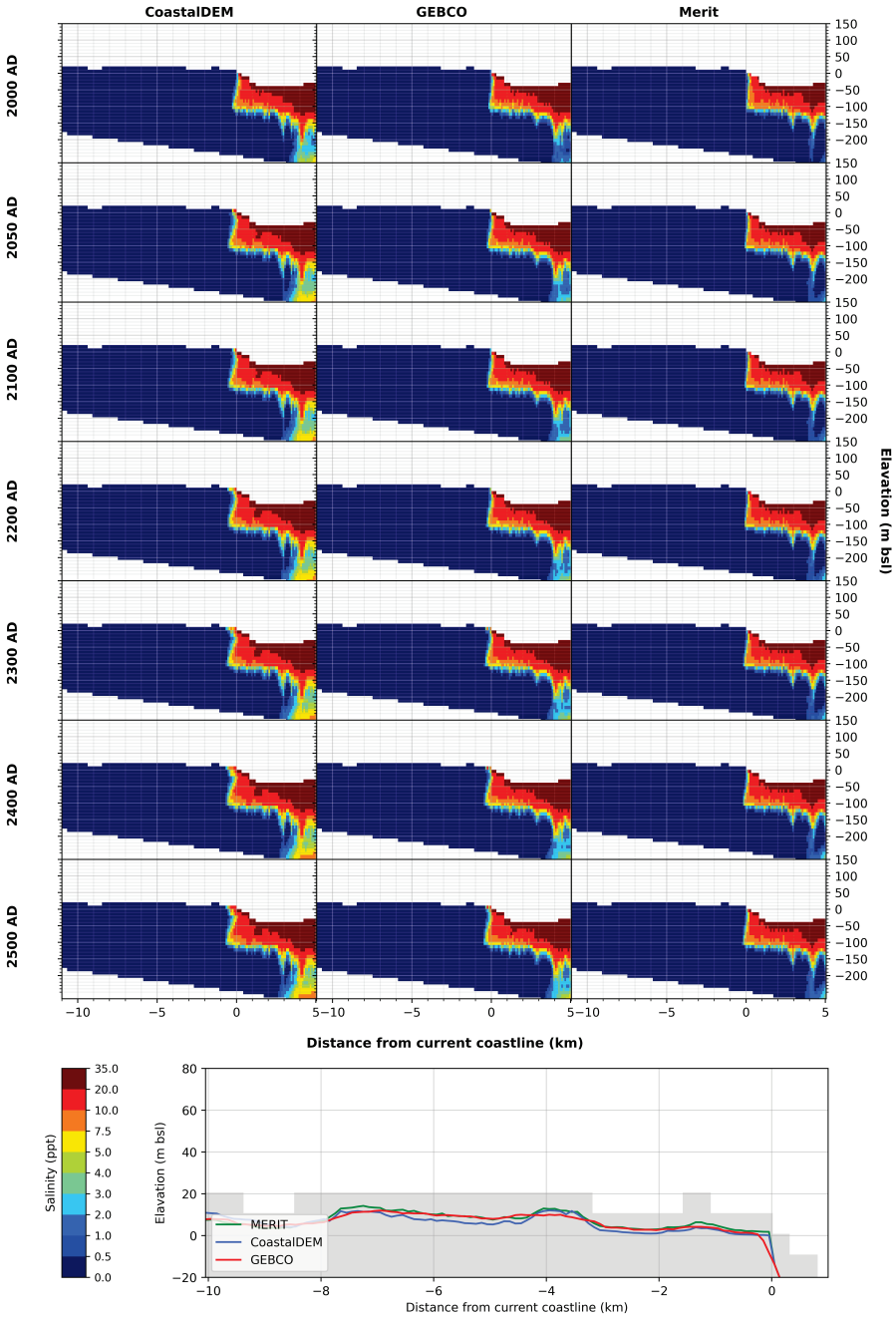

Figure D-15 Comparison of estimated groundwater salinity (SRM 0833_013) for the three DEM input datasets for the future 500 years under RCP 4.5 scenario. The bottom graph shows the variations in DEM elevation between the three DEM input datasets and active SEAWAT model grid (grey fill).

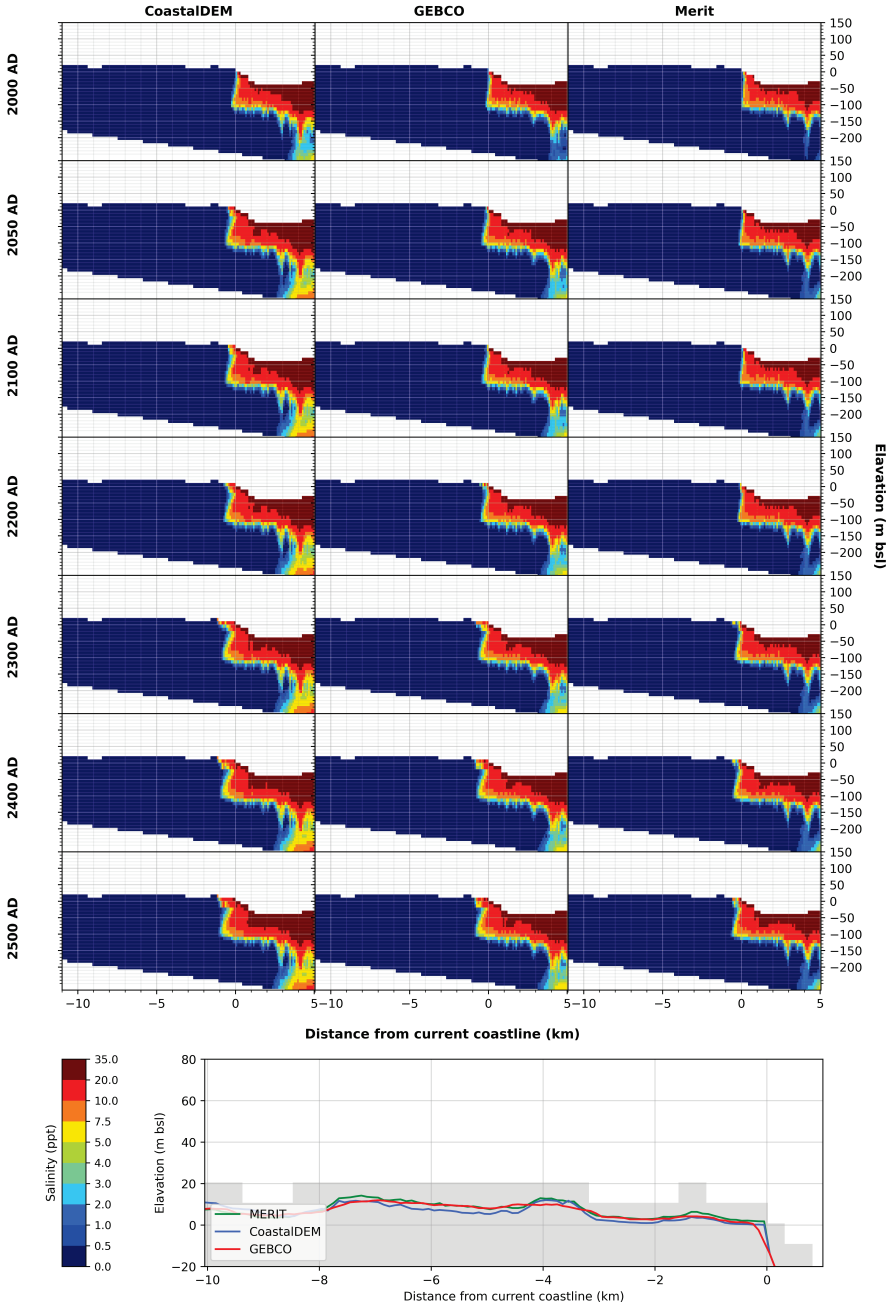

Figure D-16 Comparison of estimated groundwater salinity (SRM 0833_013) for the three DEM input datasets for the future 500 years under RCP 8.5 scenario. The bottom graph shows the variations in DEM elevation between the three DEM input datasets and active SEAWAT model grid (grey fill).

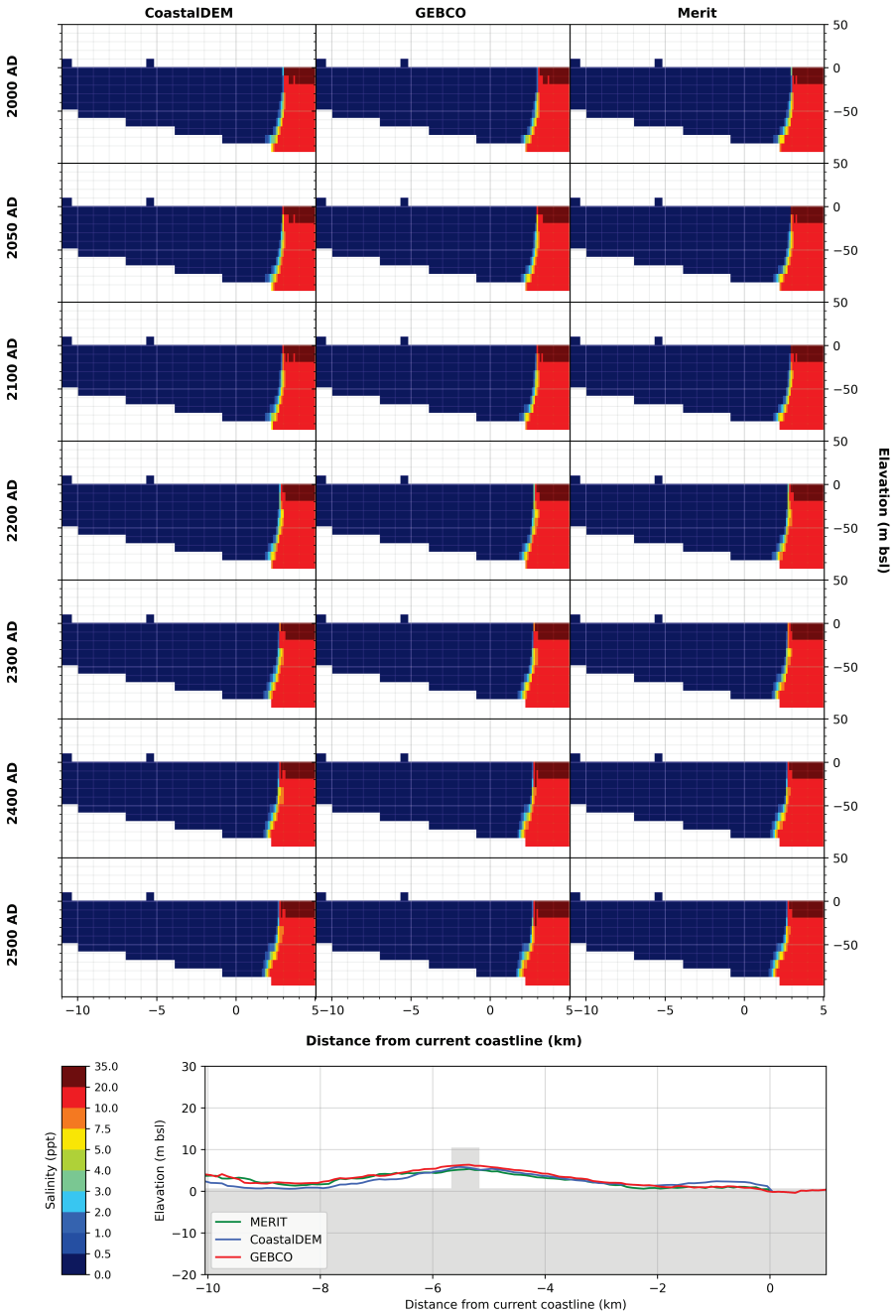

Figure D-17 Comparison of estimated groundwater salinity (SRM 1415_032) for the three DEM input datasets for the future 500 years under RCP 2.6 scenario. The bottom graph shows the variations in DEM elevation between the three DEM input datasets and active SEAWAT model grid (grey fill).

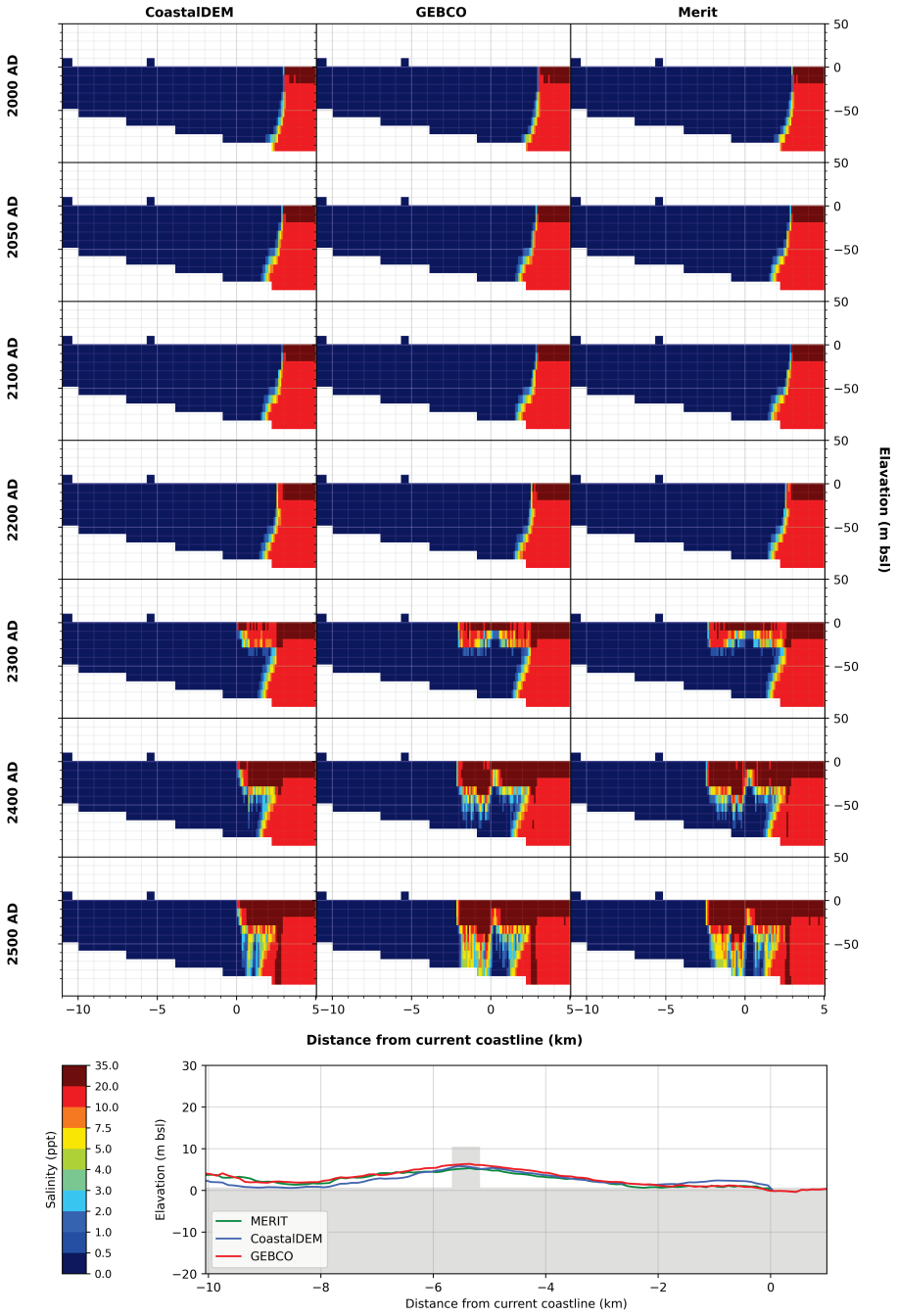

Figure D-18 Comparison of estimated groundwater salinity (SRM 1415_032) for the three DEM input datasets for the future 500 years under RCP 4.5 scenario. The bottom graph shows the variations in DEM elevation between the three DEM input datasets and active SEAWAT model grid (grey fill).

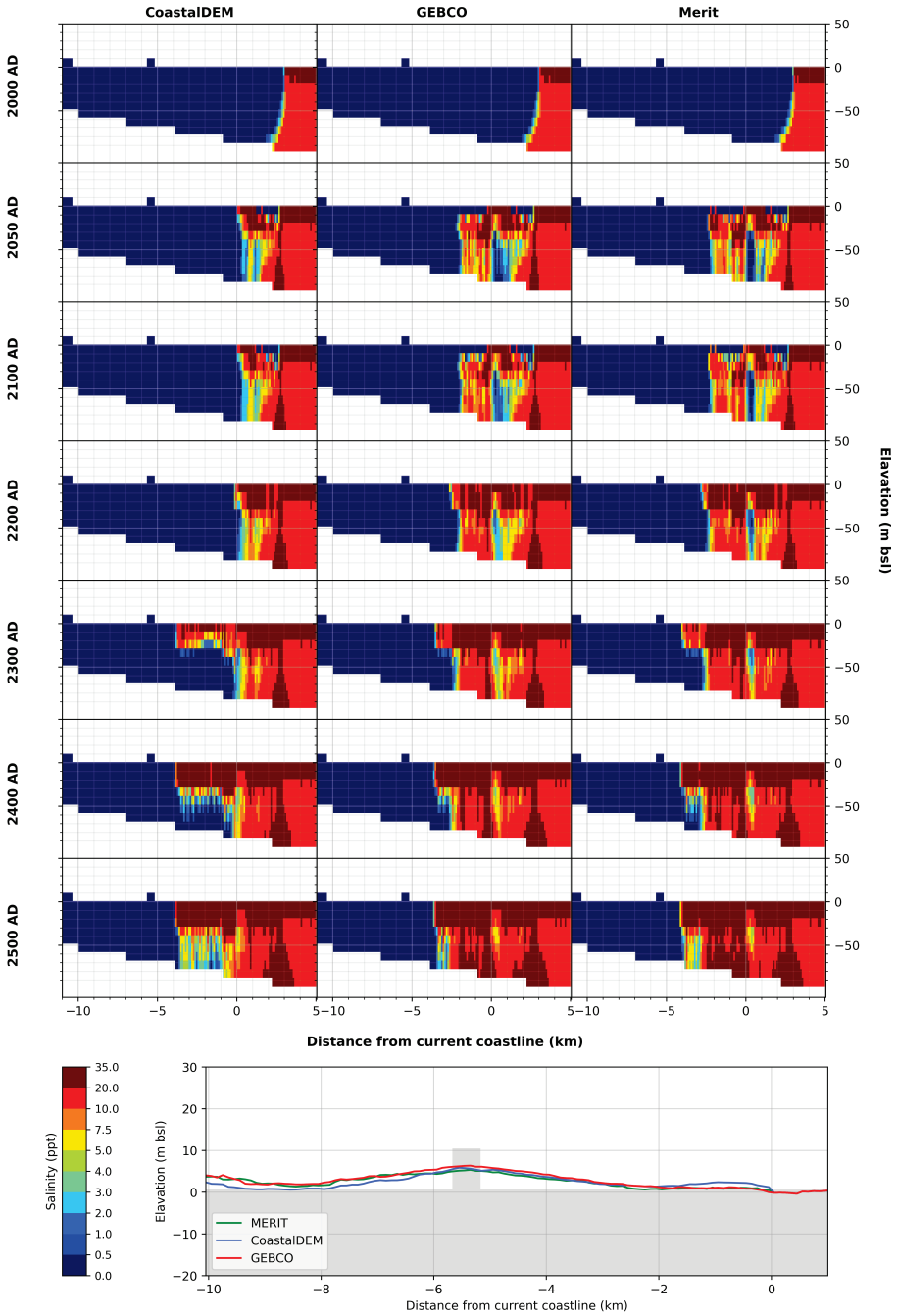

Figure D-19 Comparison of estimated groundwater salinity (SRM 1415_032) for the three DEM input datasets for the future 500 years under RCP 8.5 scenario. The bottom graph shows the variations in DEM elevation between the three DEM input datasets and active SEAWAT model grid (grey fill).

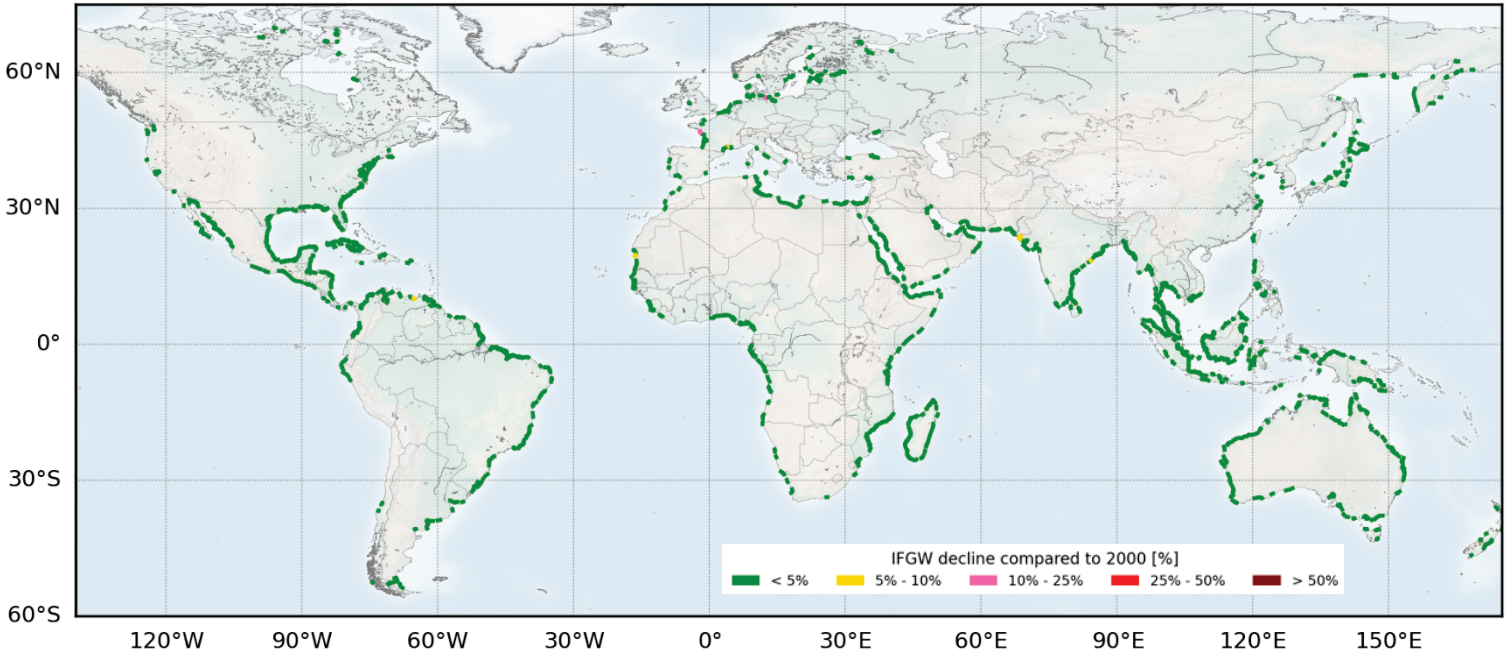

Figure D-20 Difference in inland fresh groundwater volume (IFGV) expressed as percentage IFGV in year 2050 and sea level rise for RCP 2.6 scenario compared to situation in year 2000. Results are averaged over the three different DEM inputs used in our modelling study.

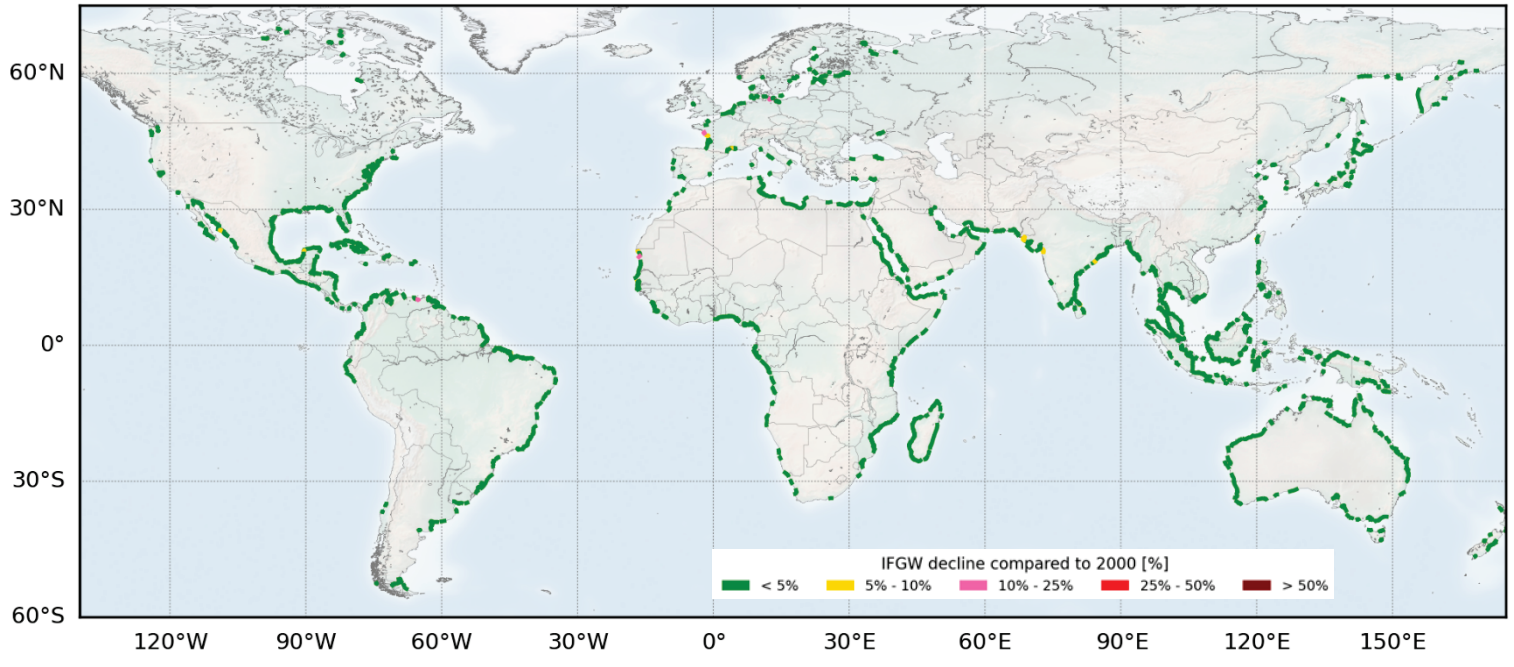

Figure D-21 Difference in inland fresh groundwater volume (IFGV) expressed as percentage IFGV in year 2100 and sea level rise for RCP 2.6 scenario compared to situation in year 2000. Results are averaged over the three different DEM inputs used in our modelling study.

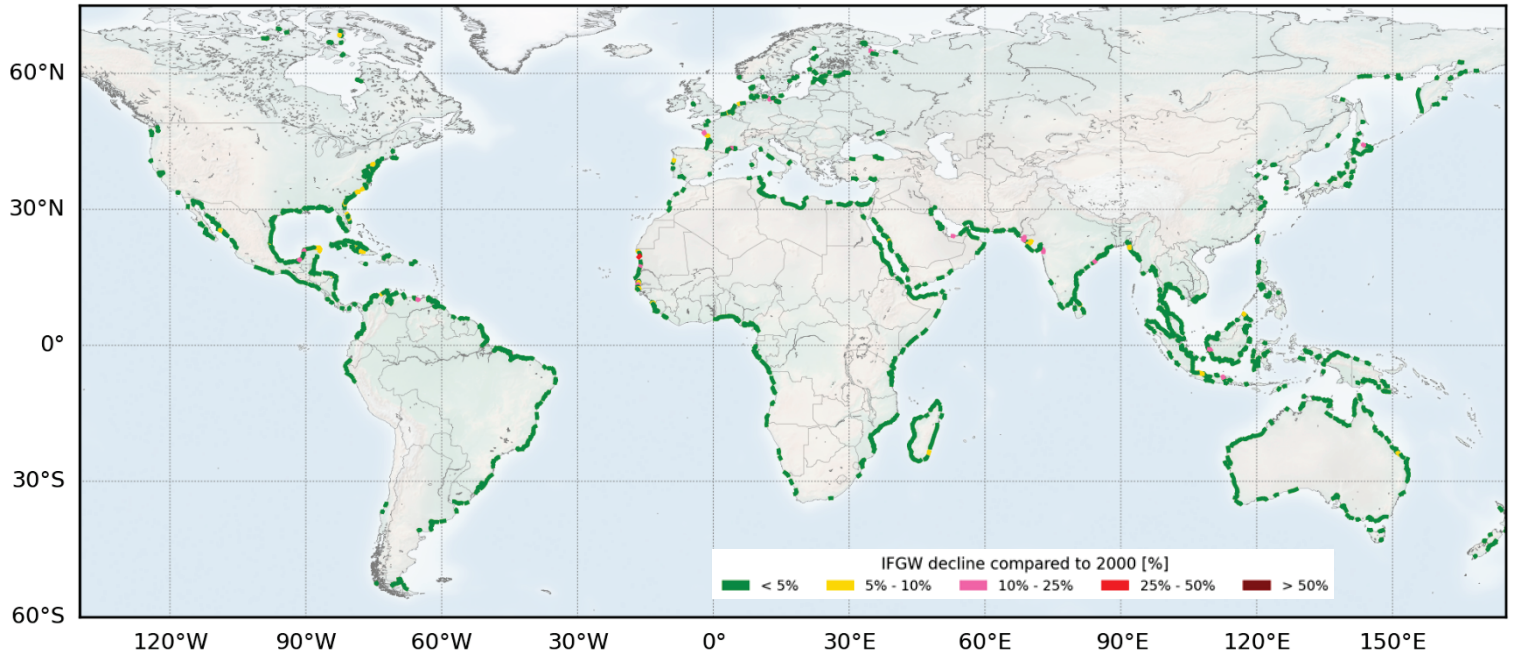

Figure D-22 Difference in inland fresh groundwater volume (IFGV) expressed as percentage IFGV in year 2200 and sea level rise for RCP 2.6 scenario compared to situation in year 2000. Results are averaged over the three different DEM inputs used in our modelling study.

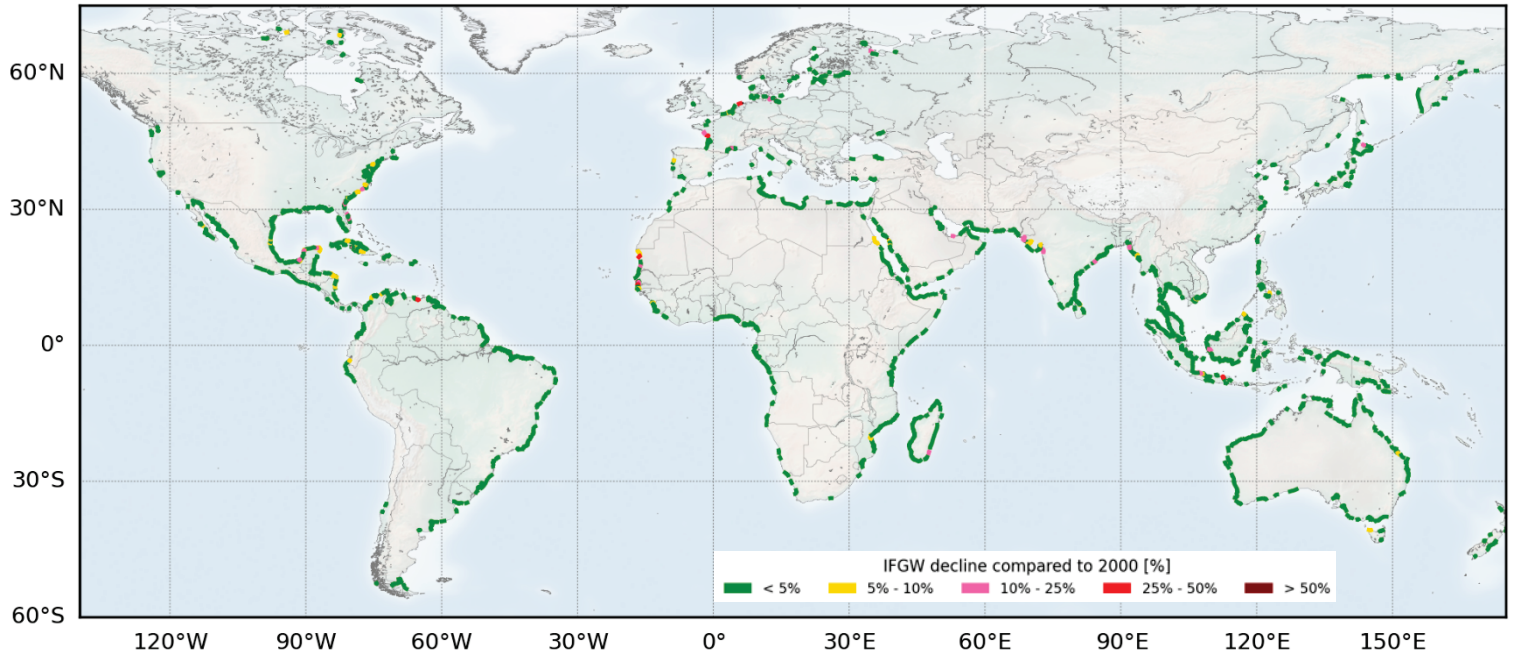

Figure D-23 Difference in inland fresh groundwater volume (IFGV) expressed as percentage IFGV in year 2300 and sea level rise for RCP 2.6 scenario compared to situation in year 2000. Results are averaged over the three different DEM inputs used in our modelling study.

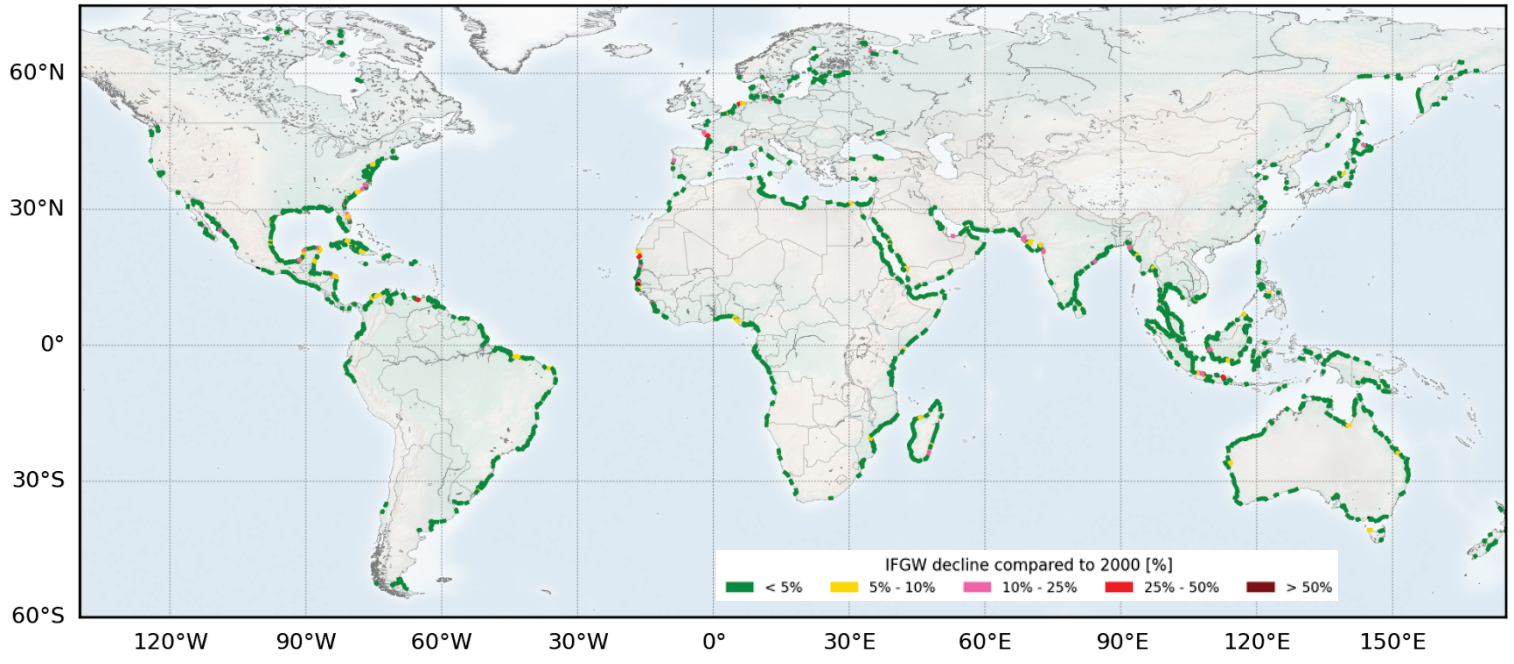

Figure D-24 Difference in inland fresh groundwater volume (IFGV) expressed as percentage IFGV in year 2050 and sea level rise for RCP 4.5 scenario compared to situation in year 2000. Results are averaged over the three different DEM inputs used in our modelling study.

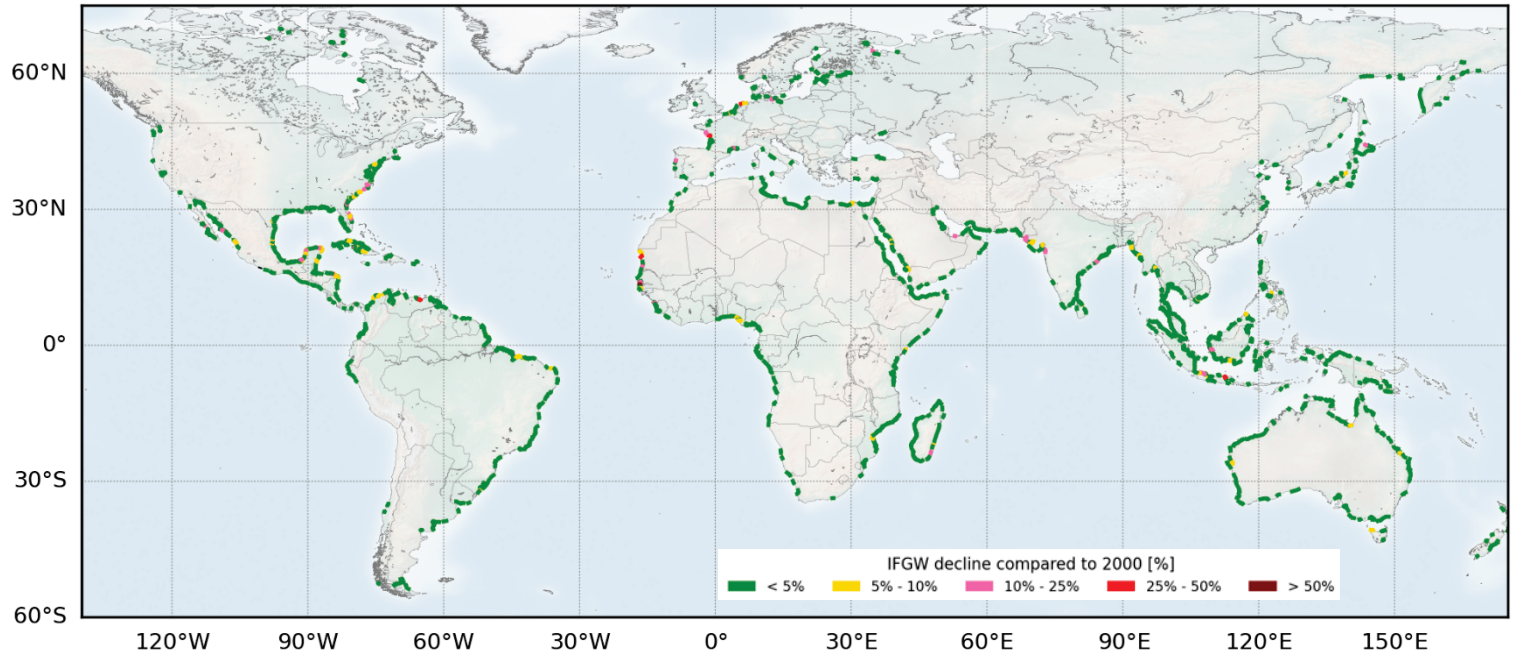

Figure D-25 Difference in inland fresh groundwater volume (IFGV) expressed as percentage IFGV in year 2100 and sea level rise for RCP 4.5 scenario compared to situation in year 2000. Results are averaged over the three different DEM inputs used in our modelling study.

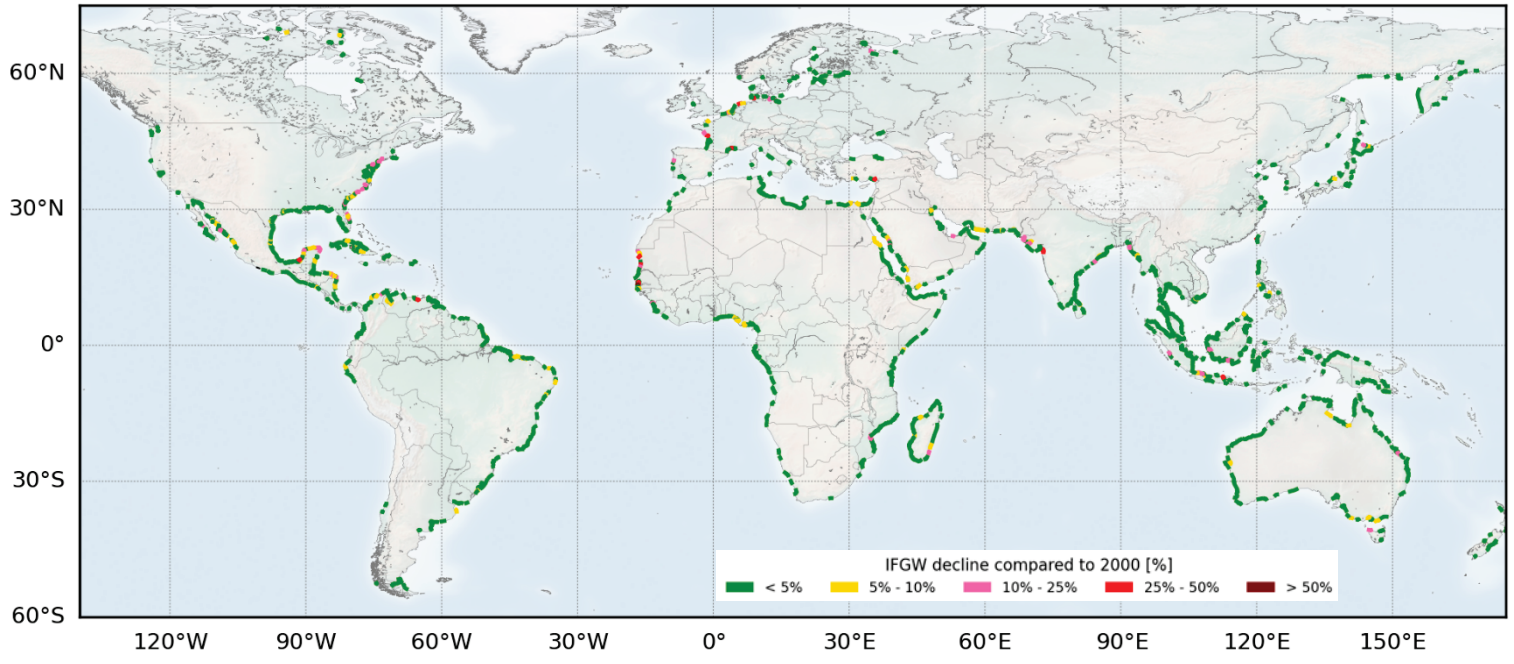

Figure D-26 Difference in inland fresh groundwater volume (IFGV) expressed as percentage IFGV in year 2200 and sea level rise for RCP 4.5 scenario compared to situation in year 2000. Results are averaged over the three different DEM inputs used in our modelling study.

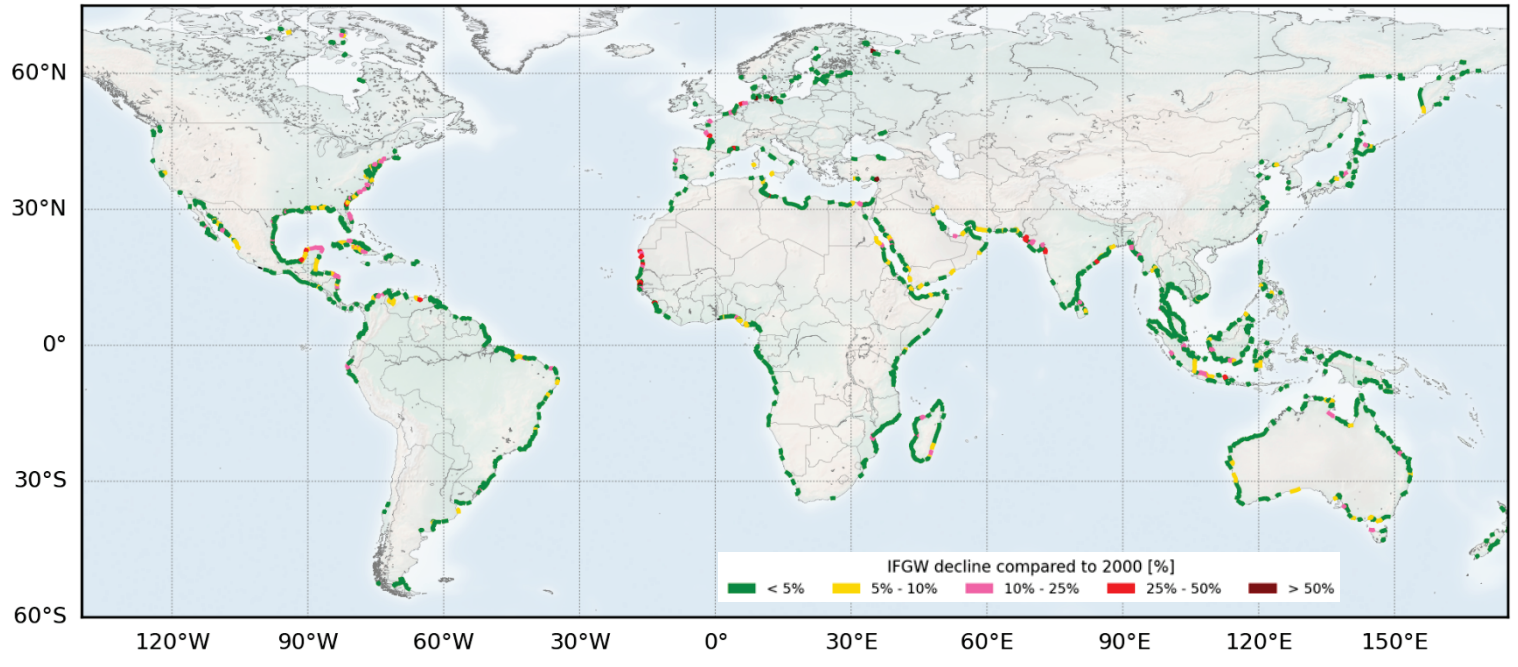

Figure D-27 Difference in inland fresh groundwater volume (IFGV) expressed as percentage IFGV in year 2300 and sea level rise for RCP 4.5 scenario compared to situation in year 2000. Results are averaged over the three different DEM inputs used in our modelling study.

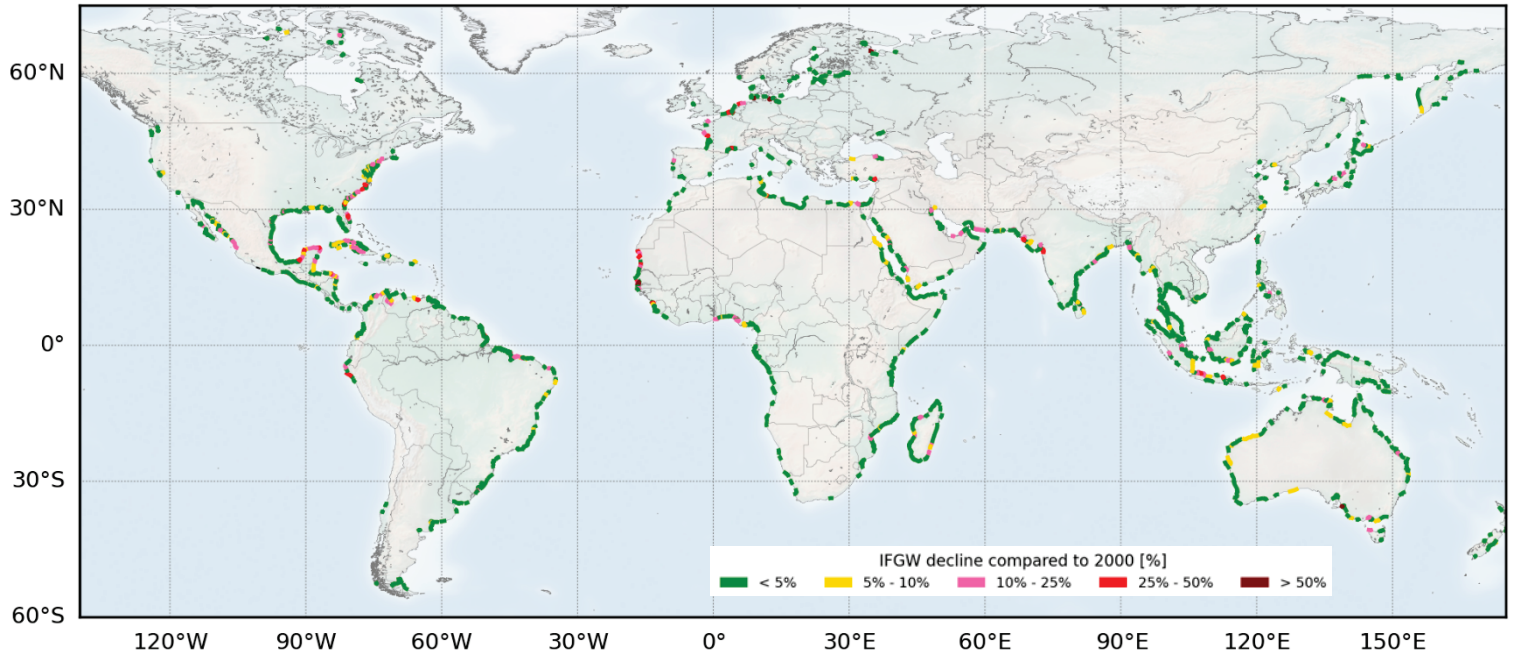

Figure D-28 Difference in inland fresh groundwater volume (IFGV) expressed as percentage IFGV in year 2050 and sea level rise for RCP 8.5 scenario compared to situation in year 2000. Results are averaged over the three different DEM inputs used in our modelling study.

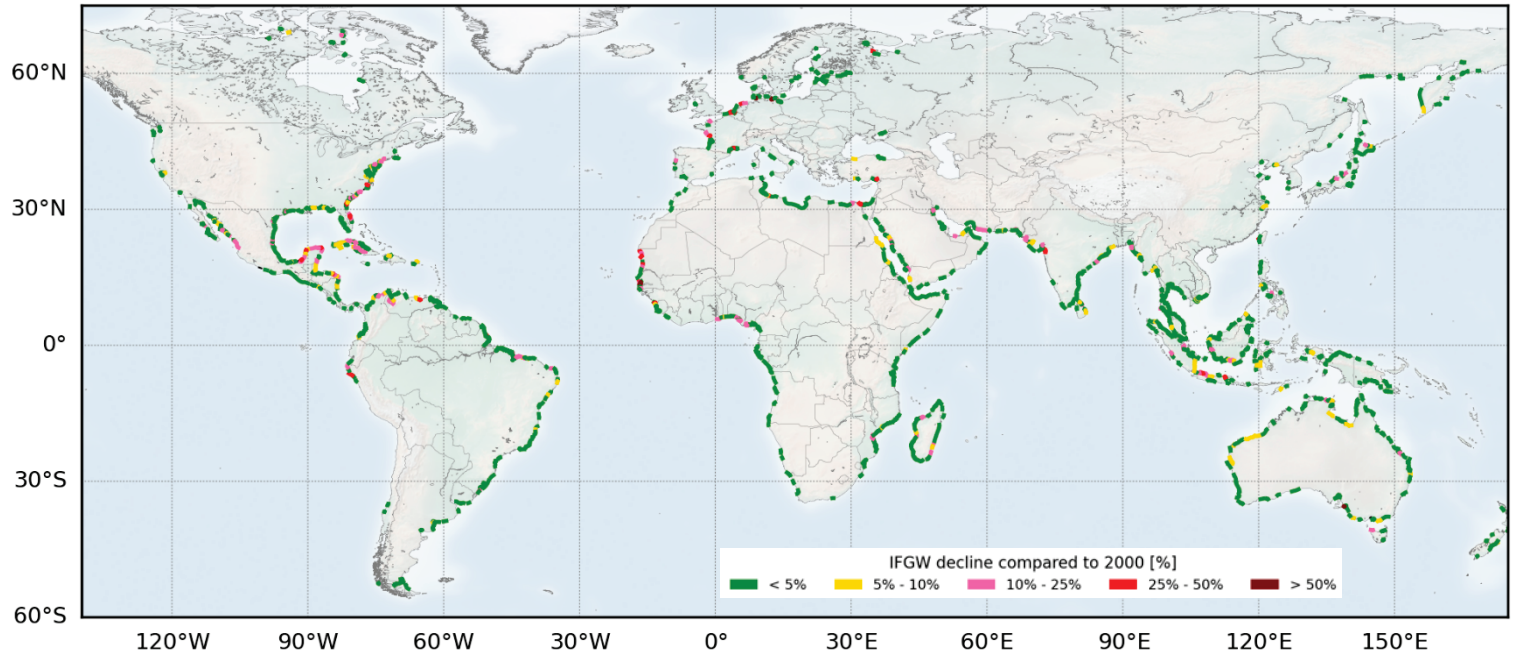

Figure D-29 Difference in inland fresh groundwater volume (IFGV) expressed as percentage IFGV in year 2100 and sea level rise for RCP 8.5 scenario compared to situation in year 2000. Results are averaged over the three different DEM inputs used in our modelling study.

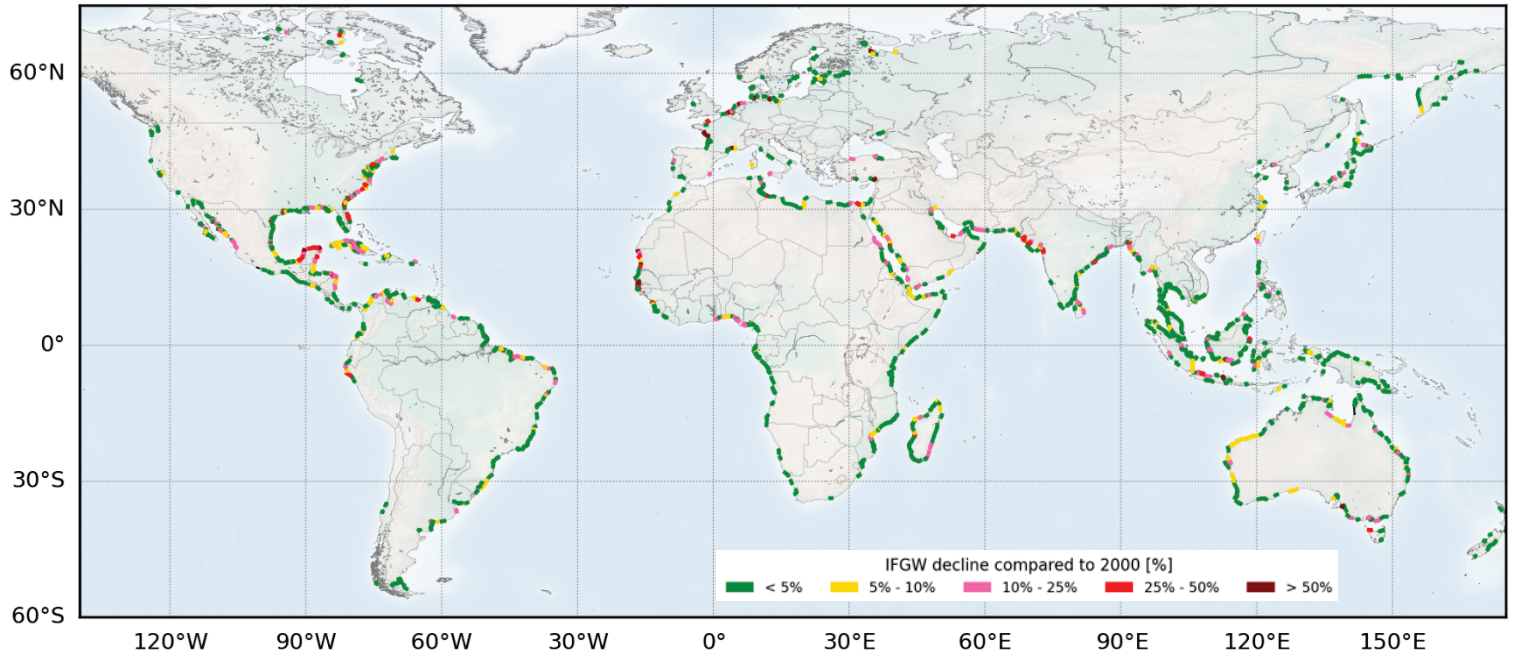

Figure D-30 Difference in inland fresh groundwater volume (IFGV) expressed as percentage IFGV in year 2200 and sea level rise for RCP 8.5 scenario compared to situation in year 2000. Results are averaged over the three different DEM inputs used in our modelling study.

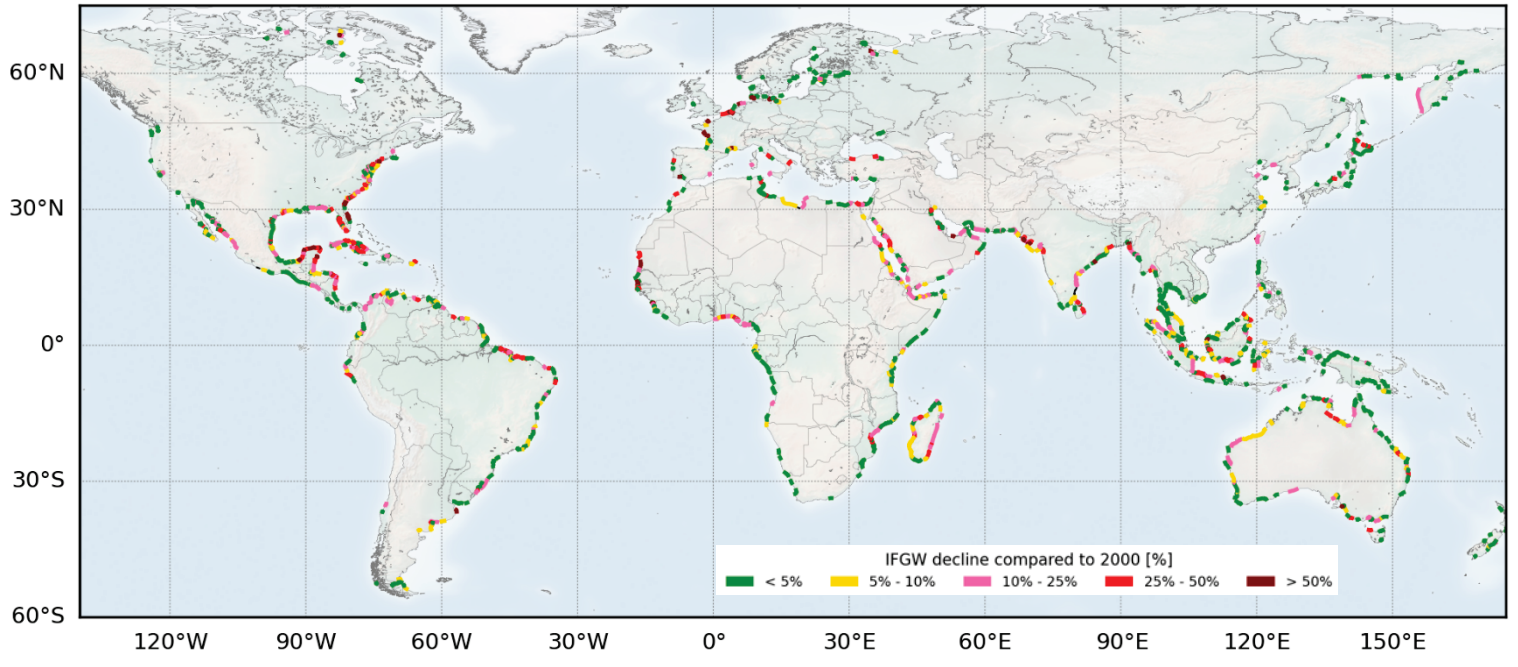

Figure D-31 Difference in inland fresh groundwater volume (IFGV) expressed as percentage IFGV in year 2300 and sea level rise for RCP 8.5 scenario compared to situation in year 2000. Results are averaged over the three different DEM inputs used in our modelling study.

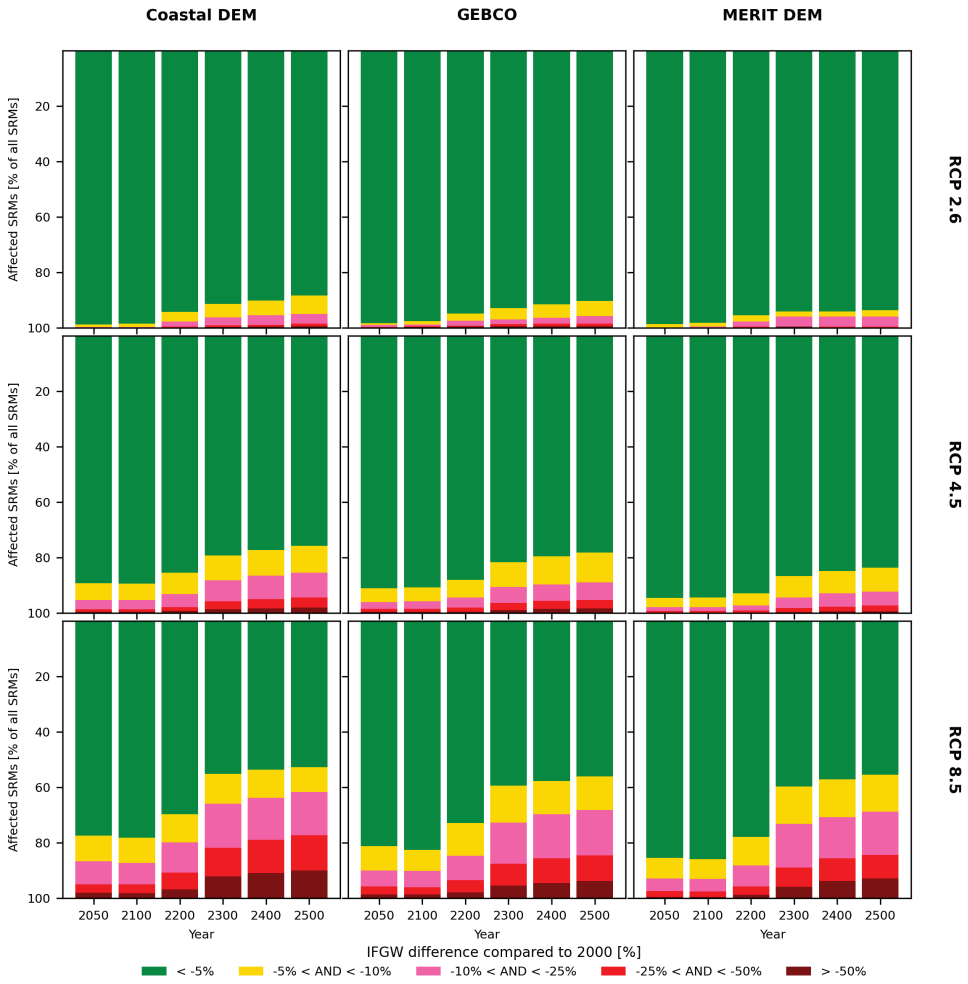

Figure D-32 Fraction of affected SRMs (all SRMs) in time for the three different RCP scenarios considered in this study and the three DEM groundwater model inputs.

Bibliography

Amado, L., 2013. Reservoir Exploration and Appraisal. Gulf Professional Publishing. https://doi.org/https://doi.org/10.1016/C2009-0-30581-4

Amir, N., Kafri, U., Herut, B., Shalev, E., 2013. Numerical Simulation of Submarine Groundwater Flow in the Coastal Aquifer at the Palmahim Area , the Mediterranean Coast of Israel 4005–4020. https://doi.org/10.1007/s11269-013-0392-2

Bakari, S.S., Aagaard, P., Vogt, R.D., Ruden, F., Brennwald, M.S., Johansen, I., Gulliksen, S., 2012. Groundwater residence time and paleorecharge conditions in the deep confined aquifers of the coastal watershed , South-East Tanzania. J. Hydrol. 466–467, 127–140. https://doi.org/10.1016/j.jhydrol.2012.08.016

Bakker, M., Post, V., Langevin, C.D., Hughes, J.D., White, J.T., Starn, J.J., Fienen, M.N., 2016. Scripting MODFLOW Model Development Using Python and FloPy. Groundwater 54, 733–739. https://doi.org/10.1111/gwat.12413

Bakker, M., Schaars, F., Hughes, J.D., Langevin, C.D., Dausman, A.M., 2013. Documentation of the Seawater Intrusion (SWI2) Package for MODFLOW. U.S. Geol. Surv. Tech. Methods 6-A46 47.

Bear, J., Dagan, G., 1964. Some exact solutions of interface problems by means of the hodograph method. Geophys. Res. 69, 1563–1572.

Becker, M., Papa, F., Karpytchev, M., Delebecque, C., Krien, Y., Khan, J.U., Ballu, V., Durand, F., Le Cozannet, G., Islam, A.K.M.S., Calmant, S., Shum, C.K., 2020. Water level changes, subsidence, and sea level rise in the Ganges-Brahmaputra-Meghna delta. Proc. Natl. Acad. Sci. U. S. A. 117, 1867–1876. https://doi.org/10.1073/pnas.1912921117

Bertoni, C., Lofi, J., Micallef, A., Moe, H., 2020. Seismic reflection methods in offshore groundwater research. Geosci. 10, 1–34. https://doi.org/10.3390/geosciences10080299

Bierkens, M.F.P., Bell, V.A., Burek, P., Chaney, N., Condon, L.E., David, C.H., de Roo, A., Döll, P., Drost, N., Famiglietti, J.S., Flörke, M., Gochis, D.J., Houser, P., Hut, R., Keune, J., Kollet, S., Maxwell, R.M., Reager, J.T., Samaniego, L., Sudicky, E., Sutanudjaja, E.H., Van de Giesen, N., Winsemius, H., Wood, E.F., 2015. Hyper-resolution global hydrological modelling: what is next? Hydrol. Process. 29, 310–320. https://doi.org/10.1002/hyp.10391

Bouwer, L.M., Jonkman, S.N., 2018. Global mortality from storm surges is decreasing. Environ. Res. Lett. 13. https://doi.org/10.1088/1748-9326/aa98a3

Bridge, J.S., 2009. Rivers and Floodplains: Forms, Processes, and Sedimentary Record. Wiley-Blackwell.

Burnett, W.C., Aggarwal, P.K., Aureli, A., Bokuniewicz, H., Cable, J.E., Charette, M.A., Kontar, E., Krupa, S., Kulkarni, K.M., Loveless, A., Moore, W.S., Oberdorfer, J.A., Oliveira, J., Ozyurt, N., Povinec, P., Privitera, A.M.G., Rajar, R., Ramessur, R.T., Scholten, J., Stieglitz, T., Taniguchi, M., Turner, J. V., 2006. Quantifying submarine groundwater discharge in the coastal zone via multiple methods. Sci. Total Environ. 367, 498–543. https://doi.org/10.1016/j.scitotenv.2006.05.009

Cardenas, M.B., Bennett, P.C., Zamora, P.B., Befus, K.M., Rodolfo, R.S., Cabria, H.B., Lapus, M.R., 2015. Devastation of aquifers from tsunami-like storm surge by Supertyphoon Haiyan. Geophys. Res. Lett. 2844–2851. https://doi.org/10.1002/2015GL063418.Received

Carrard, N., Foster, T., Willetts, J., 2020. Correction: Groundwater as a source of drinking water in southeast asia and the pacific: A multi-country review of current reliance and resource concerns. [Water (2019), 11, (1605)] doi: 10.3390/w11081605. Water (Switzerland) 12. https://doi.org/10.3390/w12010298

Carretero, S., Rapaglia, J., Bokuniewicz, H., Kruse, E., 2013. Impact of sea-level rise on saltwater intrusion length into the coastal aquifer, Partido de La Costa, Argentina. Cont. Shelf Res. 61–62, 62–70. https://doi.org/10.1016/j.csr.2013.04.029

Cattaneo, A., Steel, R.J., 2003. Transgressive deposits: A review of their variability. Earth-Science Rev. 62, 187–228. https://doi.org/10.1016/S0012-8252(02)00134-4

Charlier, R.H., Chaineux, M.C.P., Morcos, S., 2005. Panorama of the history of coastal protection. J. Coast. Res. 21, 79–111. https://doi.org/10.2112/03561.1

Chaumillon, E., Bertin, X., Fortunato, A.B., Bajo, M., Schneider, J.L., Dezileau, L., Walsh, J.P., Michelot, A., Chauveau, E., Créach, A., Hénaff, A., Sauzeau, T., Waeles, B., Gervais, B., Jan, G., Baumann, J., Breilh, J.F., Pedreros, R., 2017. Storm-induced marine flooding: Lessons from a multidisciplinary approach. Earth-Science Rev. 165, 151–184. https://doi.org/10.1016/j.earscirev.2016.12.005

Chen, Z., Auler, A.S., Bakalowicz, M., Drew, D., Griger, F., Hartmann, J., Jiang, G., Moosdorf, N., Richts, A., Stevanovic, Z., Veni, G., Goldscheider, N., 2017. The World Karst Aquifer Mapping project: concept, mapping procedure and map of Europe. Hydrogeol. J. 25, 771–785. https://doi.org/10.1007/s10040-016-1519-3

Chui, T.F.M., Terry, J.P., 2015. Groundwater salinisation on atoll islands after storm-surge flooding: Modelling the influence of central topographic depressions. Water Environ. J. 29, 430–438. https://doi.org/10.1111/wej.12116

CIESIN, 2017. Center for International Earth Science Information Network (CIESIN), Columbia University. 2018. Documentation for the Gridded Population of the World, Version 4 (GPWv4), Revision 11 Data Sets. [WWW Document]. NASA Socioecon. Data Appl. Cent. (SEDAC), Palisades, NY. URL https://doi.org/10.7927/H45Q4T5F (accessed 5.30.18).

Cobaner, M., Yurtal, R., Dogan, A., Motz, L.H., 2012. Three dimensional simulation of seawater intrusion in coastal aquifers: A case study in the Goksu Deltaic Plain. J. Hydrol. 464–465, 262–280. https://doi.org/10.1016/j.jhydrol.2012.07.022

Coffin, M.F., Gahagan, L.M., Lawver, L.A., n.d. Present-day Plate Boundary Digital Data Compilation. UTIG Tech. Rep. No. 1998.

Cohen, D., Person, M., Wang, P., Gable, C.W., Hutchinson, D., Marksamer, A., Dugan, B., Kooi, H., Groen, K., Lizarralde, D., Evans, R.L., Day-lewis, F.D., Jr, J.W.L., Lane Jr., J.W., Jr, J.W.L., 2010. Origin and Extent of Fresh Paleowaters on the Atlantic Continental Shelf , USA. Groundwater 48, 143–158. https://doi.org/10.1111/j.1745-6584.2009.00627.x

Cohen, K.M., Lobo, F.J.P., 2013. Continental shelf drowned landscapes: Submerged geomorphological and sedimentary record of the youngest cycles. Geomorphology 203, 1–5. https://doi.org/10.1016/j.geomorph.2013.09.006

Cooper, H.H., 1964. Sea water in coastal aquifers. US Government Printing Office.

Costa, P.D. La, Carretero, S., Rapaglia, J., Bokuniewicz, H., Kruse, E., 2013. Impact of sea-level rise on saltwater intrusion length into the coastal. Cont. Shelf Res. 61–62, 62–70. https://doi.org/10.1016/j.csr.2013.04.029

Custodio, E., 2002. Aquifer overexploitation: what does it mean? Hydrogeol. J. 10, 254–277. https://doi.org/10.1007/s10040-002-0188-6

Dagan, G., Bear, J., 1968. Solving the problem of local interface upconing in a coastal aquifer by the method of small perturbations, Journal of Hydraulic Research. https://doi.org/10.1080/00221686809500218

Dagan, G., Fiori, A., Jankovic, I., 2013. Upscaling of flow in heterogeneous porous formations: Critical examination and issues of principle. Adv. Water Resour. 51, 67–85. https://doi.org/10.1016/j.advwatres.2011.12.017

Daliakopoulos, I.N., Tsanis, I.K., Koutroulis, A., Kourgialas, N.N., Varouchakis, A.E., Karatzas, G.P., Ritsema, C.J., 2016. The threat of soil salinity: A European scale review. Sci. Total Environ. 573, 727–739. https://doi.org/https://doi.org/10.1016/j.scitotenv.2016.08.177

De Graaf, I., Van Beek, R.L.P.H., Gleeson, T., Moosdorf, N., Schmitz, O., Sutanudjaja, E.H., Bierkens, M.F.P., 2017. A global-scale two-layer transient groundwater model: Development and application to groundwater depletion. Adv. Water Resour. 102, 53–67. https://doi.org/10.1016/j.advwatres.2017.01.011

De Graaf, I.E.M., Sutanudjaja, E.H., van Beek, L.P.H., Bierkens, M.F.P., 2015. A high-resolution global-scale groundwater model. Hydrol. Earth Syst. Sci. 19, 823–837. https://doi.org/10.5194/hess-19-823-2015

De Lange, W.J., Prinsen, G.F., Hoogewoud, J.C., Veldhuizen, A.A., Verkaik, J., Oude Essink, G.H.P., van Walsum, P.E.V., Delsman, J.R., Hunink, J.C., Massop, H.T.L., Kroon, T., 2014. An operational, multi-scale, multi-model system for consensus-based, integrated water management and policy analysis: The Netherlands Hydrological Instrument. Environ. Model. Softw. 59, 98–108. https://doi.org/10.1016/j.envsoft.2014.05.009

Delsman, J.R., Hu-a-ng, K.R.M., Vos, P.C., de Louw, P.G.B., Oude Essink, G.H.P., Stuyfzand, P.J., Bierkens, M.F.P., 2014. Paleo-modeling of coastal saltwater intrusion during the Holocene: an application to the Netherlands. Hydrol. Earth Syst. Sci. 18, 3891–3905. https://doi.org/10.5194/hess-18-3891-2014

Delsman, J.R., Hu-a-ng, K.R.M., Vos, P.C., De Louw, P.G.B., Oude Essink, G.H.P., Stuyfzand, P.J., Bierkens, M.F.P., 2013. Palaeo-modeling of coastal salt water intrusion during the Holocene: an application to the Netherlands. Hydrol. Earth Syst. Sci. Discuss. 10, 13707–13742. https://doi.org/10.5194/hessd-10-13707-2013

Diersch, H.-J.G., 2013. FEFLOW: finite element modeling of flow, mass and heat transport in porous and fractured media. Springer Science & Business Media.

Dillon, P., Stuyfzand, P., Grischek, T., Lluria, M., Pyne, R.D.G., Jain, R.C., Bear, J., Schwarz, J., Wang, W., Fernandez, E., Stefan, C., Pettenati, M., van der Gun, J., Sprenger, C., Massmann, G., Scanlon, B.R., Xanke, J., Jokela, P., Zheng, Y., Rossetto, R., Shamrukh, M., Pavelic, P., Murray, E., Ross, A., Bonilla Valverde, J.P., Palma Nava, A., Ansems, N., Posavec, K., Ha, K., Martin, R., Sapiano, M., 2019. Sixty years of global progress in managed aquifer recharge. Hydrogeol. J. 27, 1–30. https://doi.org/10.1007/s10040-018-1841-z

Döll, P., 2009. Vulnerability to the impact of climate change on renewable groundwater resources: a global-scale assessment. Environ. Res. Lett. 4, 035006. https://doi.org/10.1088/1748-9326/4/3/035006

Drabbe, J., Ghyben, B.W., 1888. Nota in verband met de voorgenomen putboring nabij, Amsterdam. Tijdschr. Van K. Inst. Van Ingenieurs 5, 8–22.

Du Commun, J., 1828. On the cause of fresh water springs, fountains, etc. Am. J. Sci. Arts 14, 174.

Dutkiewicz, A., Müller, R.D., O'Callaghan, S., Jónasson, H., 2015. Census of seafloor sediments in the world's ocean. Geology 43, 795–798. https://doi.org/10.1130/G36883.1

Ehlers, J., Gibbard, P.L., 2004. Quaternary Glaciations Extent and Chronology, Volume 2. ed. Developments in Quaternary Sciences.

Engelen, J. Van, Oude Essink, G.H.P., Kooi, H., Bierkens, M.F.P., 2018. On the origins of hypersaline groundwater in the Nile Delta aquifer. J. Hydrol. 560, 301–317. https://doi.org/10.1016/j.jhydrol.2018.03.029

Engelen, J. Van, Verkaik, J., King, J., Nofal, E.R., Bierkens, M.F.P., Oude Essink, G.H.., 2019. A three-dimensional palaeohydrogeological reconstruction of the groundwater salinity distribution in the Nile Delta Aquifer 5175–5198.

Fan, Y., 2013. Global Patterns of Groundwater Table Depth Global Patterns of Groundwater Table Depth. https://doi.org/10.1126/science.1229881

Fan, Y., Miguez-Macho, G., Jobbágy, E.G., Jackson, R.B., Otero-Casal, C., 2017. Hydrologic regulation of plant rooting depth. Proc. Natl. Acad. Sci. 114, 201712381. https://doi.org/10.1073/pnas.1712381114

Faneca Sànchez, M., Bashar, K., Janssen, G.M.C.M., Vogels, M., Snel, J., Zhou, Y., Stuurman, R., Oude

Essink, G.H.P., 2015. SWIBANGLA : Managing salt water intrusion impacts in coastal groundwater systems of Bangladesh 153.

Faneca Šanchez, M., Gunnink, J.L., Van Baaren, E.S., Oude Essink, G.H.P., Siemon, B., Auken, E., Elderhorst, W., De Louw, P.G.B., 2012. Modelling climate change effects on a dutch coastal groundwater system using airborne electromagnetic measurements. Hydrol. Earth Syst. Sci. 16, 4499–4516. https://doi.org/10.5194/hess-16-4499-2012

Ferguson, G., Gleeson, T., 2012. Vulnerability of coastal aquifers to groundwater use and climate change. Nat. Clim. Chang. 2, 342–345. https://doi.org/10.1038/nclimate1413

Feseker, T., 2007. Numerical studies on saltwater intrusion in a coastal aquifer in northwestern Germany. Hydrogeol. J. 15, 267–279. https://doi.org/10.1007/s10040-006-0151-z

Feuerstein, G., Kak, S., Frawley, D., 2005. The search of the cradle of civilization: new light on ancient India. Motilal Banarsidass Publisher.

Fick, S.E., Hijmans, R.J., 2017. WorldClim 2: new 1-km spatial resolution climate surfaces for global land areas. Int. J. Climatol. 37, 4302–4315. https://doi.org/10.1002/joc.5086

Fleitmann, D., Burns, S.J., Mudelsee, M., Neff, U., Kramers, J., Mangini, A., Matter, A., 2003. Holocene Forcing of the Indian Monsoon Recorded in a Stalagmite from Southern Oman. Science (80-.). 300, 1737–1739.

Gardner, L.R., 2009. Assessing the effect of climate change on mean annual runoff. J. Hydrol. 379, 351–359. https://doi.org/10.1016/j.jhydrol.2009.10.021

Geldern, R. Van, Hayashi, T., Böttcher, M.E., Mottl, M.J., Barth, J.A.C., Stadler, S., 2013. Stable isotope geochemistry of pore waters and marine sediments from the New Jersey shelf : Methane formation and fl uid origin 96–112. https://doi.org/10.1130/GES00859.1

Gelhar, L.W., Welty, C., Rehfeldt, K.R., 1992. A critical review of data on field-scale dispersion in aquifers. Water Resour. Res. 28, 1955–1974. https://doi.org/10.1029/92WR00607

Ghaffour, N., Missimer, T.M., Amy, G.L., 2013. Technical review and evaluation of the economics of water desalination : Current and future challenges for better water supply sustainability. Desalination 309, 197–207. https://doi.org/10.1016/j.desal.2012.10.015

Ghassemi, F., Jakeman, A., Jacobson, G., 1990. Mathematical modelling of sea water intrusion, Nauru Island. Hydrol. Process. 4, 269–281. https://doi.org/https://doi.org/10.1002/hyp.3360040307

Gingerich, S.B., Voss, C.I., 2005. Three-dimensional variable-density flow simulation of a coastal aquifer in southern Oahu, Hawaii, USA. Hydrogeol. J. 13, 436–450. https://doi.org/10.1007/s10040-004-0371-z

Gingerich, S.B., Voss, C.I., Johnson, A.G., 2017. Seawater-flooding events and impact on freshwater lenses of low-lying islands: controlling factors, basic management and mitigation. J. Hydrol. https://doi.org/10.1016/j.jhydrol.2017.03.001

Giosan, L., Syvitski, J., Constantinescu, S., Day, J., 2014. Protect the world's deltas. Nature 516, 31–33. https://doi.org/10.1038/516031a

Gleeson, T., Befus, K.M., Jasechko, S., Luijendijk, E., Cardenas, M.B., 2015. The global volume and distribution of modern groundwater. Nat. Geosci. https://doi.org/10.1038/NGEO2590

Gleeson, T., Luijendijk, E., Mcdonnell, J.J., Taylor, R.G., Wada, Y., 2017. Global aquifers dominated by fossil groundwaters but wells vulnerable to modern contamination. Nat. Geosci. 10, 425–430. https://doi.org/10.1038/NGEO2943

Gleeson, T., Moosdorf, N., Hartmann, J., Van Beek, L.P.H., 2014. A glimpse beneath earth's surface: GLobal HYdrogeology MaPS (GLHYMPS) of permeability and porosity. Geophys. Res. Lett. 41, 3891–3898. https://doi.org/10.1002/2014GL059856

Goldewijk, K.K., Beusen, A., Doelman, J., Stehfest, E., 2017. Anthropogenic land use estimates for the Holocene - HYDE 3.2. Earth Syst. Sci. Data 9, 927–953. https://doi.org/10.5194/essd-9-927-2017

Gossel, W., Sefelnasr, A., Wycisk, P., 2010. Modelling of paleo-saltwater intrusion in the northern

part of the Nubian Aquifer System, Northeast Africa. Hydrogeol. J. 18, 1447–1463. https://doi.org/10.1007/s10040-010-0597-x

Grant, K.M., Rohling, E.J., Bar-Matthews, M., Ayalon, A., Medina-Elizalde, M., Ramsey, C.B., Satow, C., Roberts, A.P., 2012. Rapid coupling between ice volume and polar temperature over the past 150,000 years. Nature 491, 744–747. https://doi.org/10.1038/nature11593

Groen, J., Velstra, J., Meesters, A.G.C.A., 2000. Salinization processes in paleowaters in coastal sediments of Suriname : evidence from d 37 Cl analysis and diffusion modelling. J. Hydrol. 234, 1–20.

Guo, W., Langevin, C.D., 2002. User's Guide to SEAWAT: A Computer Program For Simulation of Three-Dimensional Variable-Density Ground-Water Flow: Techniques of Water-Resources Investigations 6-A7.

Gustafson, C., Key, K., Evans, R.L., 2019. Aquifer systems extending far offshore on the U.S. Atlantic margin. Sci. Rep. 1–10. https://doi.org/10.1038/s41598-019-44611-7

H.-O. Pörtner, Roberts, D.C., Masson-Delmotte, V., Zhai, P., Tignor, M., Poloczanska, E., Mintenbeck, K., Alegría, A., Nicolai, M., Okem, A., Petzold, J., Rama, B., (eds.), N.M.W., 2019. The Ocean and Cryosphere in a Changing Climate. A Special Report of the Intergovernmental Panel on Climate Change. Intergov. Panel Clim. Chang. 1–765.

Haakon, T., Fridtjof, B., 2012. Submarine Groundwater : A New Concept for the Supply of Drinking Water. Water Resour. Manag. 1015–1026. https://doi.org/10.1007/s11269-011-9806-1

Hanebuth, T.J., Stattegger, K., Saito, Y., 2002. The stratigraphic architecture of the central Sunda Shelf (SE Asia) recorded by shallow-seismic surveying. Geo-Marine Lett. 22, 86–94. https://doi.org/10.1007/s00367-002-0102-1

Haroon, A., Lippert, K., Mogilatov, V., Tezkan, B., 2018. First application of the marine differential electric dipole for groundwater investigations: A case study from Bat Yam, Israel. Geophysics 83, B59–B76. https://doi.org/10.1190/geo2017-0162.1

Harris, I., Jones, P.D., Osborn, T.J., Lister, D.H., 2014. Updated high-resolution grids of monthly climatic observations - the CRU TS3.10 Dataset. Int. J. Climatol. 34, 623–642. https://doi.org/10.1002/joc.3711

Hartmann, J., Moosdorf, N., 2012. The new global lithological map database GLiM: A representation of rock properties at the Earth surface. Geochemistry, Geophys. Geosystems 13, 1–37. https://doi.org/10.1029/2012GC004370

Hathaway, J.C., Poag, C.W., Valentine, P.C., Miller, R.E., Schultz, D.M., Manheim, F.T., Kohout, F.A., Bothner, M.H., Sangrey, D.A., 1979. U.S. geological survey core drilling on the Atlantic shelf. Science (80-.). 206, 515–527. https://doi.org/10.1126/science.206.4418.515

Hayes, M.O., 1966. Marine Geology -Elsevier Publishing Company, Amsterdam -Printed in The Netherlands RELATIONSHIP BETWEEN COASTAL CLIMATE AND BOTTOM SEDIMENT TYPE ON THE INNER CONTINENTAL SHELF 5, 111–132.

Head, M.J., Gibbard, P.L., 2005. Early-Middle Pleistocene transitions: the land-ocean evidence. Geological Society of London. https://doi.org/10.1144/GSL.SP.2005.247

Hempel, S., Frieler, K., Warszawski, L., Schewe, J., Piontek, F., 2013. A trend-preserving bias correction – The ISI-MIP approach. Earth Syst. Dyn. 4, 219–236. https://doi.org/10.5194/esd-4-219-2013

Hengl, T., De Jesus, J.M., MacMillan, R.A., Batjes, N.H., Heuvelink, G.B.M., Ribeiro, E., Samuel-Rosa, A., Kempen, B., Leenaars, J.G.B., Walsh, M.G., Gonzalez, M.R., 2014. SoilGrids1km - Global soil information based on automated mapping. PLoS One 9. https://doi.org/10.1371/journal.pone.0105992

Henriksen, H.J., Troldborg, L., Nyegaard, P., Sonnenborg, T.O., Refsgaard, J.C., Madsen, B., 2003. Methodology for construction, calibration and validation of a national hydrological model for Denmark. J. Hydrol. 280, 52–71. https://doi.org/10.1016/S0022-1694(03)00186-0

Herbert, E.R., Boon, P., Burgin, A.J., Neubauer, S.C., Franklin, R.B., Ardón, M., Hopfensperger, K.N., Lamers, L.P.M., Gell, P., 2015. A global perspective on wetland salinization: ecological consequences of a growing threat to freshwater wetlands. Ecosphere 6, art206. https://doi.org/https://doi.org/10.1890/ES14-00534.1

Herrera-García, G., Ezquerro, P., Tomas, R., Béjar-Pizarro, M., López-Vinielles, J., Rossi, M., Mateos, R.M., Carreón-Freyre, D., Lambert, J., Teatini, P., Cabral-Cano, E., Erkens, G., Galloway, D., Hung, W.C., Kakar, N., Sneed, M., Tosi, L., Wang, H., Ye, S., 2021. Mapping the global threat of land subsidence. Science (80-.). 371, 34–36. https://doi.org/10.1126/science.abb8549

Herzberg, A., 1901. Die wasserversorgung einiger Nordseebader. J. Gasbeleucht. Wasserversorg. 44, 842–844.

Hijmans, R.J., Cameron, S.E., Parra, J.L., Jones, P.G., Jarvis, A., 2005. Very high resolution interpolated climate surfaces for global land areas. Int. J. Climatol. 25, 1965–1978. https://doi.org/10.1002/joc.1276

Horn, M., 2020. AAPG, Giant oil and gas fields of the world [WWW Document]. URL https://worldmap.harvard.edu/data/geonode:giant_oil_and_gas_fields_of_the_world_co_yxz

Huang, P., Chiu, Y., 2018. A Simulation-Optimization Model for Seawater Intrusion Management at Pingtung Coastal. Water 1–28. https://doi.org/10.3390/w10030251

Huizer, S., Luijendijk, A.P., Bierkens, M.F.P., Oude Essink, G.H.P., 2019. Global potential for the growth of fresh groundwater resources with large beach nourishments. Sci. Rep. 9, 1–14. https://doi.org/10.1038/s41598-019-48382-z

Huizer, S., Oude Essink, G.H.P., Bierkens, M.F.P., 2016. Fresh groundwater resources in a large sand replenishment. Hydrol. Earth Syst. Sci. 20, 3149–3166. https://doi.org/10.5194/hess-20-3149-2016

Huscroft, J., Gleeson, T., Hartmann, J., Börker, J., 2018. Compiling and Mapping Global Permeability of the Unconsolidated and Consolidated Earth: GLobal HYdrogeology MaPS 2.0 (GLHYMPS 2.0). Geophys. Res. Lett. 45, 1897–1904. https://doi.org/10.1002/2017GL075860

Ingebritsen, S.E., Galloway, D.L., 2014. Coastal subsidence and relative sea level rise. Environ. Res. Lett. 9. https://doi.org/10.1088/1748-9326/9/9/091002

Jasechko, S., Perrone, D., Seybold, H., Fan, Y., Kirchner, J.W., 2020. Groundwater level observations in 250,000 coastal US wells reveal scope of potential seawater intrusion. Nat. Commun. 11, 1–9. https://doi.org/10.1038/s41467-020-17038-2

Jiao, J.J., Shi, L., Kuang, X., 2015. Reconstructed chloride concentration pro fi les below the seabed in Hong Kong (China) and their implications for offshore groundwater resources 277–286. https://doi.org/10.1007/s10040-014-1201-6

Jones, E., Qadir, M., Vliet, M.T.H. Van, Smakhtin, V., Kang, S., 2019. The state of desalination and brine production : A global outlook. Sci. Total Environ. 657, 1343–1356. https://doi.org/10.1016/j.scitotenv.2018.12.076

Karner, G.D., Watts, A.B., 1982. On isostasy at Atlantic-type continental margins. J. Geophys. Res. 87, 2923–2948. https://doi.org/10.1029/JB087iB04p02923

Ketabchi, H., Mahmoodzadeh, D., Ataie-Ashtiani, B., Simmons, C.T., 2016. Sea-level rise impacts on seawater intrusion in coastal aquifers: Review and integration. J. Hydrol. 535, 235–255. https://doi.org/10.1016/j.jhydrol.2016.01.083

Ketabchi, H., Mahmoodzadeh, D., Ataie-ashtiani, B., Werner, A.D., Simmons, C.T., 2014. Sea-level rise impact on fresh groundwater lenses in two-layer small islands. Hydrol. Process. 28, 5938–5953. https://doi.org/10.1002/hyp.10059

Khan, M.R., Voss, C.I., Yu, W., Michael, H.A., 2014. Water Resources Management in the Ganges Basin: A Comparison of Three Strategies for Conjunctive Use of Groundwater and Surface Water. Water Resour. Manag. 28, 1235–1250. https://doi.org/10.1007/s11269-014-0537-y

Kirezci, E., Young, I.R., Ranasinghe, R., Muis, S., Nicholls, R.J., Lincke, D., Hinkel, J., 2020. Projections of global-scale extreme sea levels and resulting episodic coastal flooding over the 21st Century. Sci. Rep. 10, 1–12. https://doi.org/10.1038/s41598-020-67736-6

Knight, A.C., Werner, A.D., Irvine, D.J., 2019. Combined geophysical and analytical methods to estimate offshore freshwater extent. J. Hydrol. 576, 529–540. https://doi.org/10.1016/j.jhydrol.2019.06.059

Knight, A.C., Werner, A.D., Morgan, L.K., 2018. The onshore influence of offshore fresh groundwater. J. Hydrol. 561, 724–736. https://doi.org/10.1016/j.jhydrol.2018.03.028

Konikow, L.F., 2011. The Secret to Successful Solute-Transport Modeling. Groundwater 49, 144–159. https://doi.org/https://doi.org/10.1111/j.1745-6584.2010.00764.x

Konikow, L.F., Bredehoeft, J.D., 1992. Ground-water models cannot be validated. Adv. Water Resour. 15, 75–83. https://doi.org/https://doi.org/10.1016/0309-1708(92)90033-X

Kooi, H., Groen, J., 2003. Geological processes and the management of groundwater resources in coastal areas. Netherlands J. Geosci. 82, 31–40.

Kooi, H., Groen, J., 2001. Offshore continuation of coastal groundwater systems; predictions using sharp-interface approximations and variable-density flow modelling. J. Hydrol. 246, 19–35. https://doi.org/10.1016/S0022-1694(01)00354-7

Kooi, H., Groen, J., Leijnse, a., 2000. Modes of seawater intrusion during transgressions. Water Resour. Res. 36, 3581–3589. https://doi.org/10.1029/2000WR900243

Kulp, S.A., Strauss, B.H., 2019. New elevation data triple estimates of global vulnerability to sea-level rise and coastal floodin. Nat. Commun. 10. https://doi.org/10.1038/s41467-019-12808-z

Kummu, M., Taka, M., Guillaume, J.H.A., 2018. Gridded global datasets for Gross Domestic Product and Human Development Index over 1990-2015. Sci. Data 5, 1–15. https://doi.org/10.1038/sdata.2018.4

Lambeck, K., Rouby, H., Purcell, A., Sun, Y., Sambridge, M., 2014a. Sea level and global ice volumes from the Last Glacial Maximum to the Holocene. Proc. Natl. Acad. Sci. U. S. A. 111, 15296–303. https://doi.org/10.1073/pnas.1411762111

Lambeck, K., Rouby, H., Purcell, A., Sun, Y., Sambridge, M., 2014b. Sea level and global ice volumes from the Last Glacial Maximum to the Holocene. Proc. Natl. Acad. Sci. 111, 15296–15303. https://doi.org/10.1073/pnas.1411762111

Langevin, C.D., Guo, W., 2006. MODFLOW/MT3DMS-based simulation of variable-density ground water flow and transport. Ground Water 44, 339–351. https://doi.org/10.1111/j.1745-6584.2005.00156.x

Langevin, C.D., Thorne, D.T.J., Dausman, A.M., Sukop, M.C., Guo, W., 2008. SEAWAT version 4: A computer program for simulation of multi-species solute and heat transport. U.S. Geol. Surv. Tech. Methods B. 6 39.

Larsen, F., Tran, L.V., Hoang, H. Van, Tran, L.T., Christiansen, A.V., Pham, N.Q., 2017. Groundwater salinity influenced by Holocene seawater trapped in incised valleys in the Red River delta plain. Nat. Geosci. 10. https://doi.org/10.1038/NGEO2938

Laruelle, G.G., Dürr, H.H., Lauerwald, R., Hartmann, J., Slomp, C.P., Goossens, N., Regnier, P.A.G., 2013. Global multi-scale segmentation of continental and coastal waters from the watersheds to the continental margins. Hydrol. Earth Syst. Sci. 17, 2029–2051. https://doi.org/10.5194/hess-17-2029-2013

Lev-Yadun, S., Gopher, A., Abbo, S., 2000. The cradle of agriculture. Science (80-.). 288, 1602--1603.

Levi, E., Goldman, M., Tibor, G., Herut, B., 2018. Delineation of Subsea Freshwater Extension by Marine Geoelectromagnetic Soundings (SE Mediterranean Sea). Water Resour. Manag. 3765–3779.

Lone, A., Fousiya, A.A., Shah, R., Achyuthan, H., 2018. Reconstruction of Paleoclimate and Environmental Fluctuations Since the Early Holocene Period Using Organic Matter and C:N

Proxy Records: A Review. J. Geol. Soc. India 91, 209–214. https://doi.org/10.1007/s12594-018-0837-6

Lorenz, E., 2000. The butterfly effect. World Sci. Ser. Nonlinear Sci. Ser. A 39, 91–94.

Maathuis, H., Mak, W., Adi, S., 2000. Groundwater: Past Achievements and Future Challenges. Balkema.

Mabrouk, M., Jonoski, A., Essink, G.H.P.O., Uhlenbrook, S., 2019. Assessing the fresh-saline groundwater distribution in the Nile delta aquifer using a 3D variable-density groundwater flow model. Water (Switzerland) 11. https://doi.org/10.3390/w11091946

Mabrouk, M., Jonoski, A., Oude Essink, G.H.P., Uhlenbrook, S., 2018. Impacts of Sea Level Rise and Groundwater Extraction Scenarios on Fresh Groundwater Resources. Water 10. https://doi.org/10.3390/w10111690

Mahmoodzadeh, D., Karamouz, M., 2019. Seawater intrusion in heterogeneous coastal aquifers under flooding events. J. Hydrol. 568, 1118–1130. https://doi.org/10.1016/j.jhydrol.2018.11.012

Masson-Delmotte, V., Zhai, P., Pörtner, H.O., Roberts, D., Skea, J., Shukla, P.R., Pirani, A., Moufouma-Okia, W., Péan, C., Pidcock, R., Connors, S., Matthews, J.B.R., Chen, Y., Zhou, X., Gomis, M.I., Lonnoy, E., Maycock, T., Tignor, M., Waterfield (eds.), T., 2018. IPCC, 2018: Summary for Policymakers. In: Global warming of 1.5°C. An IPCC Special Report on the impacts of global warming of 1.5°C above pre-industrial levels and related global greenhouse gas emission pathways, in the context of strengthening the global.

McDonald, M.G., Harbaugh, A.W., 1988. A modular three-dimensional finite-difference ground-water flow model, Techniques of Water-Resources Investigations. https://doi.org/10.3133/twri06A1

Meisler, H., Leahy, P.P., Knobel, L.L., 1984. Effect of Eustatic Sea-Level Changes on Saltwater-Freshwater in the Northern Atlantic Coastal Plain. USGS Water Supply Pap. 2255.

Merkens, J.L., Reimann, L., Hinkel, J., Vafeidis, A.T., 2016. Gridded population projections for the coastal zone under the Shared Socioeconomic Pathways. Glob. Planet. Change 145, 57–66. https://doi.org/10.1016/j.gloplacha.2016.08.009

Meybeck, M., Dürr, H.H., Vörösmarty, C.J., 2006. Global coastal segmentation and its river catchment contributors: A new look at land-ocean linkage. Global Biogeochem. Cycles 20, 1–15. https://doi.org/10.1029/2005GB002540

Meyer, R., Engesgaard, P., Sonnenborg, T.O., 2019. Origin and Dynamics of Saltwater Intrusion in a Regional Aquifer: Combining 3-D Saltwater Modeling With Geophysical and Geochemical Data. Water Resour. Res. 55, 1792–1813. https://doi.org/https://doi.org/10.1029/2018WR023624

Miall, A.D., 2014. Fluvial depositional systems. Springer Berlin Heidelberg. https://doi.org/10.1007/978-3-319-00666-6

Micallef, A., 2020. Global database of offshore freshened groundwater records. https://doi.org/10.5281/ZENODO.4247833

Micallef, A., Mountjoy, J.J., Schwalenberg, K., Jegen, M., Bradley, W.A., Woelz, S., Gerring, P., Luebben, N., Spatola, D., Otero, D.C., Mueller, C., 2018. How Offshore Groundwater Shapes the Seafloor. Earth Sp. Sci. News 99, 1–8. https://doi.org/10.1029/2018EO090691

Micallef, A., Person, M., Berndt, C., Bertoni, C., Cohen, D., Dugan, B., Evans, R., Haroon, A., Hensen, C., Jegen, M., Key, K., Kooi, H., Liebetrau, V., Lofi, J., Mailloux, B.J., Martin-Nagle, R., Michael, H.A., Müller, T., Schmidt, M., Schwalenberg, K., Trembath-Reichert, E., Weymer, B., Zhang, Y., Thomas, A.T., 2021. Offshore Freshened Groundwater in Continental Margins. Rev. Geophys. 59, 1–54. https://doi.org/10.1029/2020rg000706

Michael, H.A., Post, V.E.A., Wilson, A.M., Werner, A.D., 2017. Science, society, and the coastal groundwater squeeze. Water Resour. Res. 53, 2610–2617. https://doi.org/doi.org/10.1002/2017WR020851

Michael, H.A., Russoniello, C.J., Byron, L.A., 2013. Global assessment of vulnerability to sea-level rise in topography-limited and recharge-limited coastal groundwater systems. Water Resour. Res.

49, 2228–2240. https://doi.org/10.1002/wrcr.20213

Michael, H.A., Scott, K.C., Koneshloo, M., Yu, X., Khan, M.R., Li, K., 2016. Geologic influence on groundwater salinity drives large seawater circulation through the continental shelf. Geophys. Res. Lett. 43, 10,782-10,791. https://doi.org/10.1002/2016GL070863

Michael, H.A., Voss, C.I., 2009. Estimation of regional-scale groundwater flow properties in the Bengal Basin of India and Bangladesh. Hydrogeol. J. 17, 1329–1346. https://doi.org/10.1007/s10040-009-0443-1

Minderhoud, P.S.J., Coumou, L., Erkens, G., Middelkoop, H., Stouthamer, E., 2019. Mekong delta much lower than previously assumed in sea-level rise impact assessments. Nat. Commun. 10, 1–13. https://doi.org/10.1038/s41467-019-11602-1

Minderhoud, P.S.J., Erkens, G., Pham, V.H., Bui, V.T., Erban, L., Kooi, H., Stouthamer, E., 2017. Impacts of 25 years of groundwater extraction on subsidence in the Mekong delta, Vietnam. Environ. Res. Lett. 12, 064006. https://doi.org/10.1088/1748-9326/aa7146

Mohan, C., Western, A.W., Wei, Y., Saft, M., 2018. Predicting groundwater recharge for varying land cover and climate conditions – a global meta-study. Hydrol. Earth Syst. Sci. 2689–2703. https://doi.org/10.5194/hess-22-2689-2018

Montzka, C., Herbst, M., Weihermüller, L., Verhoef, A., Vereecken, H., 2017. A global data set of soil hydraulic properties and sub-grid variability of soil water retention and hydraulic conductivity curves. Earth Syst. Sci. Data Discuss. 1–25. https://doi.org/10.5194/essd-2017-13

Moosdorf, N., Oehler, T., 2017. Societal use of fresh submarine groundwater discharge: An overlooked water resource. Earth-Science Rev. 171, 338–348. https://doi.org/10.1016/j.earscirev.2017.06.006

Morgan, L.K., Werner, A.D., Patterson, A.E., 2018. A conceptual study of offshore fresh groundwater behaviour in the Perth Basin (Australia): Modern salinity trends in a prehistoric context. J. Hydrol. Reg. Stud. 19, 318–334. https://doi.org/10.1016/j.ejrh.2018.10.002

Muis, S., Verlaan, M., Winsemius, H.C., Aerts, J.C.J.H., Ward, P.J., 2016. A global reanalysis of storm surges and extreme sea levels. Nat. Commun. 7, 51–69. https://doi.org/10.1038/ncomms11969

Muller, R.D., Sdrolias, M., Gaina, C., Roest, W.R., 2008. Age, spreading rates, and spreading asymmetry of the world's ocean crust 1–19. https://doi.org/10.1029/2007GC001743

Murowchick, R., 1994. Cradles of civilization: China. Norman: University of Oklahoma Press.

Nam, S. Il, Stein, R., Grobe, H., Hubberten, H., 1995. Late Quaternary glacial-interglacial changes in sediment composition at the East Greenland continental margin and their paleoceanographic implications. Mar. Geol. 122, 243–262. https://doi.org/10.1016/0025-3227(94)00070-2

Nations, U., 2017. World Population Prospects: The 2017 Revision, Key Findings and Advance Tables (No. ESA/P/WP/248).

Natural Earth [WWW Document], 2017. URL http://www.naturalearthdata.com/downloads/10m-physical-vectors (accessed 7.21.17).

Neumann, B., Vafeidis, A.T., Zimmermann, J., Nicholls, R.J., 2015. Future coastal population growth and exposure to sea-level rise and coastal flooding - A global assessment. PLoS One 10. https://doi.org/10.1371/journal.pone.0118571

Nicholls, R.J., Cazenave, A., 2010. Sea-level rise and its impact on coastal zones. Science 328, 1517–1520. https://doi.org/10.1126/science.1185782

Nicholls, R.J., Lincke, D., Hinkel, J., Brown, S., Vafeidis, A.T., Meyssignac, B., Hanson, S.E., Merkens, J.L., Fang, J., 2021. A global analysis of subsidence, relative sea-level change and coastal flood exposure. Nat. Clim. Chang. https://doi.org/10.1038/s41558-021-00993-z

Nofal, E.R., Amer, M.A., El-didy, S.M., Fekry, A.M., 2016. Delineation and modeling of seawater intrusion into the Nile Delta Aquifer : A new perspective. Water Sci. 29, 156–166. https://doi.org/10.1016/j.wsj.2015.11.003

NTSG, 2019. MODIS Global Evapotranspiration Project (MOD16) [WWW Document]. URL

http://www.ntsg.umt.edu/project/modis/mod16.php (accessed 7.24.19).

Oteri, A.U., 1988. Electric log interpretation for the evaluation of salt water intrusion in the eastern Niger Delta. Hydrol. Sci. J. 33, 19–30. https://doi.org/10.1080/02626668809491219

Oude Essink, G.H.P., 2001. Saltwater intrusion in 3D large-scale aquifers: A Dutch case. Phys. Chem. Earth, Part B Hydrol. Ocean. Atmos. 26, 337–344. https://doi.org/10.1016/S1464-1909(01)00016-8

Oude Essink, G.H.P., Baaren, E.S. Van, Louw, P.G.B. De, Van Baaren, E.S., De Louw, P.G.B.B., 2010. Effects of climate change on coastal groundwater systems: A modeling study in the Netherlands. Water Resour. Res. 46, 1–16. https://doi.org/10.1029/2009WR008719

Paldor, A., Aharonov, E., Katz, O., 2020. Thermo-haline circulations in subsea confined aquifers produce saline, steady-state deep submarine groundwater discharge. J. Hydrol. 580, 124276. https://doi.org/https://doi.org/10.1016/j.jhydrol.2019.124276

Paleologos, E.K., Farouk, S., Nahyan, M.T. Al, 2018. Water resource management towards a sustainable water budget in the United Arab Emirates. IOP Conf. Ser. Earth Environ. Sci. 191. https://doi.org/10.1088/1755-1315/191/1/012007

Pauw, P.S., van der Zee, S.E.A.T.M., Leijnse, A., Delsman, J.R., De Louw, P.G.B., De Lange, W.J., Oude Essink, G.H.P., 2014. Low-Resolution Modeling of Dense Drainage Networks in Confining Layers. Ground Water 1–11. https://doi.org/10.1111/gwat.12273

Pauw, P.S., van der Zee, S.E.A.T.M., Leijnse, A., Oude Essink, G.H.P., 2015. Saltwater Upconing Due to Cyclic Pumping by Horizontal Wells in Freshwater Lenses. Groundwater n/a-n/a. https://doi.org/10.1111/gwat.12382

Pelletier, J.D., Broxton, P.D., Hazenberg, P., Zeng, X., Troch, P.A., Niu, G.-Y., Williams, Z., Brunke, M.A., Gochis, D., 2016. A gridded global data set of soil, intact regolith, and sedimentary deposit thicknesses for regional and global land surface modeling. J. Adv. Model. Earth Syst. 8, 41–65. https://doi.org/10.1002/2015MS000526

Perriquet, M., Leonardi, V., Henry, T., Jourde, H., 2014. Saltwater wedge variation in a non-anthropogenic coastal karst aquifer influenced by a strong tidal range (Burren, Ireland). J. Hydrol. 519, 2350–2365. https://doi.org/10.1016/j.jhydrol.2014.10.006

Person, M., Dugan, B., Swenson, J.B., Urbano, L., Library, L., Street, W., York, N., York, N., Stott, C., Willett, M., 2003. Pleistocene hydrogeology of the Atlantic continental shelf , New England 1324–1343.

Person, M., Marksamer, A., Dugan, B., Sauer, P.E., Brown, K., Bish, D., Licht, K.J., Willett, M., 2012. Use of a vertical δ 18 O pro fi le to constrain hydraulic properties and recharge rates across a glacio-lacustrine unit , Nantucket Island ,. Hydrogeol. J. 20, 325–336. https://doi.org/10.1007/s10040-011-0795-1

Person, M., Wilson, J.L., Morrow, N., Post, V.E.A., 2017. Continental-shelf freshwater water resources and improved oil recovery by low-salinity water flooding. Am. Assoc. Pet. Geol. Bull. 101, 1–18. https://doi.org/10.1306/05241615143

Pham, V.H., Van Geer, F.C., Bui Tran, V., Dubelaar, W., Oude Essink, G.H.P., 2019. Paleo-hydrogeological reconstruction of the fresh-saline groundwater distribution in the Vietnamese Mekong Delta since the late Pleistocene. J. Hydrol. Reg. Stud. 23, 100594. https://doi.org/10.1016/j.ejrh.2019.100594

Pillans, B., Chappell, J., Naish, T.R., 1998. A review of the Milankovitch climatic beat: Template for Plio-Pleistocene sea-level changes and sequence stratigraphy. Sediment. Geol. 122, 5–21. https://doi.org/10.1016/S0037-0738(98)00095-5

Pirazzoli, P.A., 1997. Sea-Level Changes: The Last 20,000 Years. Wiley.

Pitman, M.G., Läuchli, A., 2002. Global Impact of Salinity and Agricultural Ecosystems, in: Läuchli, A., Lüttge, U. (Eds.), Salinity: Environment - Plants - Molecules. Springer Netherlands, Dordrecht, pp. 3–20. https://doi.org/10.1007/0-306-48155-3_1

Pollard, D., Deconto, R.M., 2016. Contribution of Antarctica to past and future sea-level rise. Nature 531, 591–597. https://doi.org/10.1038/nature17145

Post, V.E.A., Eichholz, M., Brentführer, R., 2018a. Groundwater management in coastal zones, Global Issues in Water Policy. Bundesanstalt für Geowissenschaften und Rohstoffe (BGR), Hannover, Germany. https://doi.org/10.1007/978-3-030-61931-2_8

Post, V.E.A., Groen, J., Kooi, H., Person, M., Ge, S., Edmunds, W.M., 2013. Offshore fresh groundwater reserves as a global phenomenon. Nature 504, 71–78. https://doi.org/10.1038/nature12858

Post, V.E.A., Houben, G.J., Van Engelen, J., 2018b. What is the Ghijben-Herzberg principle and who formulated it? Hydrogeol. J. 26, 1801–1807. https://doi.org/10.1007/s10040-018-1796-0

Post, V.E.A., Oude Essink, G.H.P., Szymkiewicz, A., Bakker, M., Houben, G., Custodio, E., Voss, C., 2018c. Celebrating 50 years of SWIMs (Salt Water Intrusion Meetings). Hydrogeol. J. 26, 1767–1770. https://doi.org/10.1007/s10040-018-1800-8

Pranzini, G., 2002. Groundwater salinization in Versilia (Italy), in: 17th Salt Water Intrusion Meeting, Delft, The Netherlands, 6–10 May 2002.

Prudhomme, C., Giuntoli, I., Robinson, E.L., Clark, D.B., Arnell, N.W., Dankers, R., Fekete, B.M., Franssen, W., Gerten, D., Gosling, S.N., Hagemann, S., Hannah, D.M., Kim, H., Masaki, Y., Satoh, Y., Stacke, T., Wada, Y., Wisser, D., 2014. Hydrological droughts in the 21st century, hotspots and uncertainties from a global multimodel ensemble experiment. Proc. Natl. Acad. Sci. U. S. A. 111, 3262–3267. https://doi.org/10.1073/pnas.1222473110

Qadir, M., Quillérou, E., Nangia, V., Murtaza, G., Singh, M., Thomas, R.J., Drechsel, P., Noble, A.D., 2014. Economics of salt-induced land degradation and restoration. Nat. Resour. Forum 38, 282–295. https://doi.org/https://doi.org/10.1111/1477-8947.12054

Rahman, M.M., Penny, G., Mondal, M.S., Zaman, M.H., Kryston, A., Salehin, M., Nahar, Q., Islam, M.S., Bolster, D., Tank, J.L., Müller, M.F., 2019. Salinization in large river deltas: Drivers, impacts and socio-hydrological feedbacks. Water Secur. 6, 100024. https://doi.org/https://doi.org/10.1016/j.wasec.2019.100024

Ranjan, P., Kazama, S., Sawamoto, M., Sana, A., 2009. Global scale evaluation of coastal fresh groundwater resources. Ocean Coast. Manag. 52, 197–206. https://doi.org/10.1016/j.ocecoaman.2008.09.006

Rasmussen, P., Sonnenborg, T.O., Goncear, G., Hinsby, K., 2013. Assessing impacts of climate change, sea level rise, and drainage canals on saltwater intrusion to coastal aquifer. Hydrol. Earth Syst. Sci. 17, 421–443. https://doi.org/10.5194/hess-17-421-2013

Reijenstein, H.M., Posamentier, H.W., Bhattacharya, J.P., 2011. Seismic geomorphobgy and high-resolution seismic stratigraphy of inner-shelf fluvial, estuarine, deltaic, and marine sequences, Gulf of Thailand. Am. Assoc. Pet. Geol. Bull. 95, 1959–1990. https://doi.org/10.1306/03151110134

Reynolds, D.J., Steckler, M.S., Coakley, B.J., 1991. The role of the sediment load in sequence stratigraphy: the influence of flexural isostasy and compaction. J. Geophys. Res. 96, 6931–6949. https://doi.org/10.1029/90JB01914

Rodriguez, E., Morris, C., Belz, J., 2006. An assessment of the SRTM topographic products. Photogramm. Eng. Remote Sensing 72, 249–260. https://doi.org/0099-1112/06/7203–0249/$3.00/0

Sanford, W.E., Konikow, L.F., 1985. A two-constituent solute-transport model for ground water having variable density. US Department of the Interior, Geological Survey.

Sefelnasr, A., Sherif, M., 2014. Impacts of Seawater Rise on Seawater Intrusion in the Nile Delta Aquifer, Egypt. Groundwater 52, 264–276. https://doi.org/10.1111/gwat.12058

Shangguan, W., Hengl, T., Mendes de Jesus, J., Yuan, H., Dai, Y., 2017. Mapping the global depth to bedrock for land surface modeling. J. Adv. Model. Earth Syst. 9, 65–88. https://doi.org/10.1002/2016MS000686

Shemer, H., Semiat, R., 2017. Sustainable RO desalination – Energy demand and environmental impact. Desalination 424, 10–16. https://doi.org/10.1016/j.desal.2017.09.021

Shiklomanov, I.A., 1993. World Water Resources, A new appraisal and assessment for the 21st century.

Small, C., Nicholls, R.J., 2003. A global analysis of human settlement in coastal zones. J. Coast. Res. 19, 584–599.

Smith, D.E., Harrison, S., Firth, C.R., Jordan, J.T., 2011. The early Holocene sea level rise. Quat. Sci. Rev. 30, 1846–1860. https://doi.org/10.1016/j.quascirev.2011.04.019

Solórzano-Rivas, S.C., Werner, A.D., 2018. On the representation of subsea aquitards in models of offshore fresh groundwater. Adv. Water Resour. 112, 283–294. https://doi.org/10.1016/j.advwatres.2017.11.025

Sprenger, C., Hartog, N., Hernández, M., Vilanova, E., Grützmacher, G., Scheibler, F., Hannappel, S., 2017. Inventory of managed aquifer recharge sites in Europe: historical development, current situation and perspectives. Hydrogeol. J. 25, 1909–1922. https://doi.org/10.1007/s10040-017-1554-8

Stone, A., Lanzoni, M., Smedley, P., 2019. Groundwater Resources, in: Simon J. Dadson Dustin E. Garrick Edmund C. Penning-Rowsell Jim W. Hall Rob Hope Jocelyne Hughes (Ed.), Water Science, Policy, and Management: A Global Challenge. Wiley. https://doi.org/10.1002/9781119520627.ch3

Strack, O.D.L., 1976. A single-potential solution for regional interface problems in coastal aquifers. Water Resour. Res. 12, 1165–1174. https://doi.org/10.1029/WR012i006p01165

Sutanudjaja, E.H., Beek, R. Van, Wanders, N., Wada, Y., Bosmans, J.H.C., Drost, N., Ent, R.J. Van Der, Graaf, I.E.M. De, Hoch, J.M., Jong, K. De, Karssenberg, D., 2018. PCR-GLOBWB 2 : a 5 arcmin global hydrological and water resources model. Geosci. Model Dev. 08, 2429–2453. https://doi.org/10.5194/gmd-11-2429-2018

Syvitski, J.P., Peckham, S.D., Hilberman, R., Mulder, T., 2003. Predicting the terrestrial flux of sediment to the global ocean: a planetary perspective. Sediment. Geol. 162, 5–24.

Syvitski, J.P.M., Kettner, A.J., Overeem, I., Hutton, E.W.H., Hannon, M.T., Brakenridge, G.R., Day, J., Vörösmarty, C., Saito, Y., Giosan, L., Nicholls, R.J., 2009. Sinking deltas due to human activites. Nat. Geosci. 2, 681–686. https://doi.org/10.1038/ngeo629

Taniguchi, M., Burnett, W.C., Cable, J.E., Turner, J. V., 2002. Investigation of submarine groundwater discharge. Hydrol. Process. 16, 2115–2129. https://doi.org/10.1002/hyp.1145

Tardif, R., Hakim, G.J., Perkins, W.A., Horlick, K.A., Erb, M.P., Emile-Geay, J., Anderson, D.M., Steig, E.J., Noone, D., 2019. Last Millennium Reanalysis with an expanded proxy database and seasonal proxy modeling. Clim. Past 15, 1251–1273. https://doi.org/10.5194/cp-15-1251-2019

Taylor, R.G., 2012. Ground water and climate change. Nat. Clim. Chang. 3, 322–329. https://doi.org/10.1038/NCLIMATE1744

Terry, J.P., Chui, T.F.M., 2012. Evaluating the fate of freshwater lenses on atoll islands after eustatic sea-level rise and cyclone-driven inundation: A modelling approach. Glob. Planet. Change 88–89, 76–84. https://doi.org/10.1016/j.gloplacha.2012.03.008

Tessler, Z.D., Vörösmarty, C.J., Grossberg, M., Gladkova, I., Aizenman, H., Syvitski, J.P.M., Foufoula-Georgiou, E., 2015. Profiling risk and sustainability in coastal deltas of the world. Science (80-.). 349, 638–643.

Thomas, A.T., Reiche, S., Riedel, M., Clauser, C., 2019. The fate of submarine fresh groundwater reservoirs at the New Jersey shelf , USA. Hydrogeol. J. https://doi.org/https://doi.org/10.1007/s10040-019-01997-y

Thorslund, J., van Vliet, M.T.H., 2020. A global dataset of surface water and groundwater salinity measurements from 1980–2019. Sci. Data 7, 1–11. https://doi.org/10.1038/s41597-020-0562-z

Trabelsi, R., Zouari, K., Kammoun, S., Trigui, M.R., 2020. Recharge and paleo-recharge of

groundwater in different basins in Tunisia. Quat. Int. 547, 152–165. https://doi.org/https://doi.org/10.1016/j.quaint.2019.04.026

Trapp Jr., H., Horn, M.A., Trapp, H.J., Horn, M.A., 1997. Ground Water Atlas of the United States: Segment 11, Delaware, Maryland, New Jersey, North Carolina, Pennsylvania, Virginia, West Virginia, Hydrologic Atlas.

UNESCO, 2015. The United Nations world water development report 2015: water for a sustainable world. UNESCO Publishing, Paris.

Været, L., Leijnse, A., Cuamba, F., Haldorsen, S., 2012. Holocene dynamics of the salt-fresh groundwater interface under a sand island, Inhaca, Mozambique. Quat. Int. 257, 74–82. https://doi.org/10.1016/j.quaint.2011.11.020

Van Camp, M., Mtoni, Y., Mjemah, I.C., Bakundukize, C., Walraevens, K., 2014. Investigating seawater intrusion due to groundwater pumping with schematic model simulations: The example of the Dar es Salaam coastal aquifer in Tanzania. J. African Earth Sci. 96, 71–78. https://doi.org/10.1016/j.jafrearsci.2014.02.012

Van Weert, F., J., Gun, Van der, J., Reckman, J., 2008. World-wide overview of saline and brackish groundwater at shallow and intermediate depths. Int. Groundw. Resour. Assess. Cent. Rep. GP 20, 1, 87 pp.

Van Weert, F., Van der Gun, J., Reckman, J., 2009. Global Overview of Saline Groundwater Occurrence and Genesis. Igrac 26–27.

Vandenbohede, A., Lebbe, L., 2006. Occurrence of salt water above fresh water in dynamic equilibrium in a coastal groundwater flow system near De Panne, Belgium. Hydrogeol. J. 14, 462–472. https://doi.org/10.1007/s10040-005-0446-5

Varma, S., Michael, K., 2011. Impact of multi-purpose aquifer utilisation on a variable-density groundwater flow system in the Gippsland Basin, Australia. Hydrogeol. J. https://doi.org/10.1007/s10040-011-0800-8

Verkaik, J., Sutanudjaja, E., Essink, G.O., Lin, H.X., Bierkens, M., 2019. Parallel global hydrology and water resources PCR-GLOBWB-MODFLOW model at hyper-resolution scale (1 km): first results., in: Geophysical Research Abstracts.

Voss, C.I., 1984. A finite-element simulation model for saturated-unsaturated, fluid-density-dependent ground-water flow with energy transport or chemically-reactive single-species solute transport. Water Resour. Investig. Rep. 84, 4369.

Voss, C.I., Souza, W.R., 1987. Variable density flow and solute transport simulation of regional aquifers containing a narrow freshwater-saltwater transition zone. Water Resour. Res. 23, 1851–1866. https://doi.org/https://doi.org/10.1029/WR023i010p01851

Vousdoukas, M.I., Voukouvalas, E., Annunziato, A., Giardino, A., Feyen, L., 2016. Projections of extreme storm surge levels along Europe. Clim. Dyn. 47, 3171–3190. https://doi.org/10.1007/s00382-016-3019-5

Wada, Y., Bierkens, M.F.P., 2014. Sustainability of global water use: Past reconstruction and future projections. Environ. Res. Lett. 9. https://doi.org/10.1088/1748-9326/9/10/104003

Waelbroeck, C., Labeyrie, L., Michel, E., Duplessy, J.C., McManus, J.F., Lambeck, K., Balbon, E., Labracheri, M., 2002. Sea-level and deep water temperature changes derived from benthic foraminifera isotopic records. Quat. Sci. Rev. 21, 295–305.

Wahl, T., 2017. Sea-level rise and storm surges, relationship status: complicated. Environ. Res. Lett. 12.

Walsh, J.P., Nittrouer, C.A., 2009. Understanding fine-grained river-sediment dispersal on continental margins. Mar. Geol. 263, 34–45. https://doi.org/10.1016/j.margeo.2009.03.016

Warner, K., Hamza, M., Oliver-Smith, A., Renaud, F., Julca, A., 2010. Climate change, environmental degradation and migration. Nat. Hazards 55, 689–715.

Weatherall, P., Marks, K.M., Jakobsson, M., Schmitt, T., Tani, S., Arndt, J.E., Rovere, M., Chayes, D.,

Ferrini, V., Wigley, R., 2015. A new digital bathymetric model of the world's oceans. Earth Sp. Sci. 2, 331–345. https://doi.org/10.1002/2015EA000107

Werner, A.D., Bakker, M., Post, V.E. a, Vandenbohede, A., Lu, C., Ataie-Ashtiani, B., Simmons, C.T., Barry, D. a., 2013. Seawater intrusion processes, investigation and management: Recent advances and future challenges. Adv. Water Resour. 51, 3–26. https://doi.org/10.1016/j.advwatres.2012.03.004

Werner, A.D., Simmons, C.T., 2009. Impact of sea-level rise on sea water intrusion in coastal aquifers. Ground Water 47, 197–204. https://doi.org/10.1111/j.1745-6584.2008.00535.x

Werner, A.D., Ward, J.D., Morgan, L.K., Simmons, C.T., Robinson, N.I., Teubner, M.D., 2012. Vulnerability indicators of sea water intrusion. Ground Water 50, 48–58. https://doi.org/10.1111/j.1745-6584.2011.00817.x

Whittaker, J.M., Goncharov, A., Williams, S.E., M??ller, R.D., Leitchenkov, G., 2013. Global sediment thickness data set updated for the Australian-Antarctic Southern Ocean. Geochemistry, Geophys. Geosystems 14, 3297–3305. https://doi.org/10.1002/ggge.20181

Wicke, B., Smeets, E., Dornburg, V., Global, S., Vashev, B., 2011. The global technical and economic potential of bioenergy from salt-affected soils. Energy Environ. Sci. View. https://doi.org/10.1039/C1EE01029H

World Health Organization, 2017. Guidelines for drinking-water quality: fourth edition incorporating the first addendum.

Wu, W.Y., Lo, M.H., Wada, Y., Famiglietti, J.S., Reager, J.T., Yeh, P.J.F., Ducharne, A., Yang, Z.L., 2020. Divergent effects of climate change on future groundwater availability in key mid-latitude aquifers. Nat. Commun. 11, 1–9. https://doi.org/10.1038/s41467-020-17581-y

Wu, Z., Li, J., Li, S., Shang, J., Jin, X., 2017. A new method to identify the foot of continental slope based on an integrated profile analysis. Mar. Geophys. Res. 38, 199–207. https://doi.org/10.1007/s11001-016-9273-4

Xiao, H., Wang, D., Medeiros, S.C., Hagen, S.C., Hall, C.R., 2018. Assessing sea-level rise impact on saltwater intrusion into the root zone of a geo-typical area in coastal east-central Florida. Sci. Total Environ. 630, 211–221. https://doi.org/https://doi.org/10.1016/j.scitotenv.2018.02.184

Yamanaka, T., Shimada, J., Tsujimura, M., Lorphensri, O., Mikita, M., Hagihara, A., Onodera, S., 2011. Tracing a confined groundwater flow system under the pressure of excessive groundwater use in the lower central plain, Thailand. Hydrol. Process. 25, 2654–2664. https://doi.org/10.1002/hyp.8007

Yamazaki, D., Ikeshima, D., Tawatari, R., Yamaguchi, T., O'Loughlin, F., Neal, J.C., Sampson, C.C., Kanae, S., Bates, P.D., 2017. A high-accuracy map of global terrain elevations. Geophys. Res. Lett. 5844–5853. https://doi.org/10.1002/2017GL072874

Yang, J., Graf, T., Herold, M., Ptak, T., 2013. Modelling the effects of tides and storm surges on coastal aquifers using a coupled surface–subsurface approach. J. Contam. Hydrol. 149, 61–75. https://doi.org/10.1016/j.jconhyd.2013.03.002

Yang, J., Zhang, H., Yu, X., Graf, T., Michael, H.A., 2018. Impact of hydrogeological factors on groundwater salinization due to ocean- surge inundation. Adv. Water Resour. 111, 423–434. https://doi.org/10.1016/j.advwatres.2017.11.017

Yechieli, Y., Shalev, E., Wollman, S., Kiro, Y., Kafri, U., 2010. Response of the Mediterranean and Dead Sea coastal aquifers to sea level variations. Water Resour. Res. 46, 1–11. https://doi.org/10.1029/2009WR008708

Yu, X., Michael, H.A., 2019. Offshore Pumping Impacts Onshore Groundwater Resources and Land Subsidence Geophysical Research Letters. Geophys. Res. Lett. 2553–2562. https://doi.org/10.1029/2019GL081910

Yu, X., Yang, J., Graf, T., Koneshloo, M., O'Neal, M.A., Michael, H.A., 2016. Impact of topography on groundwater salinization due to ocean surge inundation. Water Resour. Res. 52, 5794–5812. https://doi.org/10.1002/ 2016WR018814

Zamrsky, D., Karssenberg, M.E., Cohen, K.M., Bierkens, M.F.P., Oude Essink, G.H.P., 2020. Geological Heterogeneity of Coastal Unconsolidated Groundwater Systems Worldwide and Its Influence on Offshore Fresh Groundwater Occurrence. Front. Earth Sci. 7, 1–23. https://doi.org/10.3389/feart.2019.00339

Zamrsky, D., Oude Essink, G.H.P., Bierkens, M.F.P., 2018. Estimating the thickness of unconsolidated coastal aquifers along the global coastline. Earth Syst. Sci. data 1–19. https://doi.org/10.1594/PANGAEA.880771

Zech, A., Attinger, S., Bellin, A., Cvetkovic, V., Dietrich, P., Fiori, A., Teutsch, G., Dagan, G., 2019. A Critical Analysis of Transverse Dispersivity Field Data. Groundwater 57, 632–639. https://doi.org/10.1111/gwat.12838

Zech, A., Attinger, S., Cvetkovic, V., Dagan, G., Dietrich, P., Fiori, A., Rubin, Y., Teutsch, G., 2015. Is unique scaling of aquifer macrodispersivity supported by field data? Water Resour. Res. 7662–7679. https://doi.org/10.1002/2015WR017200.A

Zhang, Z., Zou, L., Cui, R., Wang, L., 2011. Study of the storage conditions of submarine freshwater resources and the submarine freshwater resources at north of Zhoushan sea area. Mar. Sci. Bull 30, 47–52.

Zheng, C., Wang, P., 1998. MT3DMS: A modular three-dimensional multispeces transport model for simulation of advection, dispersion, and chemical reactions of contaminants in groundwater systems. Technical report, Waterways Experiment Station, US Army Corps of Engineers. A Modul. three-dimensional multi-species … 239.

Zhou, Y., Sawyer, A.H., David, C.H., Famiglietti, J.S., 2019. Fresh Submarine Groundwater Discharge to the Near-Global Coast. Geophys. Res. Lett. 46, 5855–5863. https://doi.org/10.1029/2019GL082749

Acknowledgements

It is a well-known fact that finishing a PhD thesis is never an easy task and is often accompanied by stressful moments, self-doubting situations and sometimes even runaway ideas. To successfully navigate these treacherous waters and safely reach the PhD harbor is a team achievement. This text is dedicated to all the people and animals that helped me across the finish line in the past few years. I hope to not forget anyone but if in some case you read this thesis and feel left out, I sincerely apologize.

First of all, I would like to thank my supervisors Marc and Gu for giving me an opportunity to conduct a PhD research under their wings and to guide me through with so much support, both professional and psychological. I was lucky enough that we share a similar sense of humor which made my life much easier and enjoyable during the last few years. During these years I was also lucky to be part of a very special and academically brilliant group of young promising scientists hidden away in a large corner room of the Physical geography department, internally known as the "man cave", thank you for all the silly humor and moments of pure laughter during all these years. I would also like to thank all the Physical geography department staff for all the help, support, inspiration and fun coffee corner conversations (especially every second Monday). Same goes to all the wonderful people from the Water Nexus projects, I thoroughly enjoyed all our general assemblies, both in academical and social aspect.

The biggest thanks of all goes to my parents for always believing in me and pushing me in the right direction, even though I always thought I was deciding by myself I now realize how smart they were in their ways. They gave me absolute freedom to follow my interests and study what I like which wasn't possible for my parents when they were my age. I hope that this thesis will give them a sense of pride and fulfillment as it is as much their achievement as it is mine. Without their overall support and motivation, I would never make it this far. I would also like to thank my sister for always being so successful, smart and internationally oriented, showing me the way forward the same way as when we were kids. Hope she doesn't mind that I am now officially the first PhD in the family, but if you decide to get one on your own someday, I offer my support.

Friends are the family you choose and I consider myself extremely lucky to have had so many friends around to share all the high and low points during the past years. My friends from Wageningen and Firehouse are an integral part of my life and the fact that even after our student years I still live together with some of them shows how close we will stay forever. Thanks for always being there for me and keeping the same dark humor as always. My current and former housemates (except one) made sure I never fell to deep into self-isolation and never became a full-scale hermit. Thank you for all the deep talks, common dinners, house improvement projects and social gatherings during all those years. The proof of how fruitful this cohabitation was is a bond between two very close friends that met at my birthday party and are now thinking about buying a house and starting a family together; true miracles can happen during a PhD project. I thank the two of you for being

such great friends and always making me feel smarter when I am around you. A special thanks goes to Lara that was always there to provide mental support, go for a walk and keeping me safe.

When I was a small kid growing up in Czech Republic, I never dreamt about becoming a scientist. Instead, I wanted to be a professional ice hockey player and win the Olympic games and play in the NHL. Everyone who has ever seen me play ice hockey would say that I have more talent in academia than on the ice. However, luckily, I still got to live my childhood dream while doing my PhD. This is thanks to the amazing student team Utrecht Buccaneers that took me in at age 30 and making me the oldest rookie to ever join the team. I would like to thank all the teammates I had the honor to play with during the past years, for all the fun on and off the ice. You really make me feel younger even though you always remind me how slow and old I am. Becoming a Buccaneer was one of the happiest moments of my life and I will forever be grateful for the chance I was given to become one.

About the author

Daniel was born on the 19th September 1986 in Prague, Czechoslovakia, just a few months after the catastrophic Chernobyl explosion. Some super hero movie influenced minds might think that this gave him a scientific super power giving him an edge during his PhD research. However, there is no direct scientific evidence supporting this claim so it has to be assumed that the grounds for Daniel's scientific career were laid during his still relatively young life. After spending his early years in Prague, he then started his early nomadic period, regularly moving between Bulgaria and Czech Republic. Finally landing at a Czech high school at age 16, Daniel got on to a shaky start and his teenage brain led him to believe that he would be better off learning a craft than pursuing higher education. After a brief parental motivational speech Daniel decided to keep his student status and started his bachelor studies in landscape engineering at the Czech University of Life Sciences in Prague. After successfully finishing his bachelor studies, Daniel decided to follow a master program in environmental modelling. This decision, coupled with an urge to move to another country once again, brought him to Wageningen University through the Erasmus exchange program. Eventually, Daniel extended his stay at Wageningen where he finished his master studies in hydrology and quantitative water management. As part of the master program, Daniel got an opportunity to work at Deltares under the supervision of Gu Oude Essink, assessing the impacts of tsunami waves on global coastal groundwater salinization. Despite the promising outcome of this one-year long internship, the results were never published, a decision that would come to haunt him during the next years. After graduation, Daniel landed his first adult job at DHI office in Prague as a consultant. However, after a little more than a year Daniel got an opportunity to start his PhD research at Utrecht University as part of a large NWO Water Nexus project, bringing together a significant number of Dutch academic institutions, private entities and research centers. The final outcome of this research is presented in this thesis. In near future Daniel will continue his academic journey at Utrecht University as a postdoc.

Scientific publications

Zamrsky, D., Karssenberg, M.E., Cohen, K.M., Bierkens, M.F., Oude Essink, G.H.P., 2020. Geological Heterogeneity of Coastal Unconsolidated Groundwater Systems Worldwide and Its Influence on Offshore Fresh Groundwater Occurrence. Front. Earth Sci. 7, 1–23. https://doi.org/10.3389/feart.2019.00339

Zamrsky, D., Oude Essink, G.H.P., Bierkens, M.F.P., 2018. Estimating the thickness of unconsolidated coastal aquifers along the global coastline. Earth Syst. Sci. data 1–19. https://doi.org/10.1594/PANGAEA.880771

Zamrsky D., Oude Essink G.H.P., Sutanudjaja E.H., van Beek L.P.H. (Rens), Bierkens M.F.P., 2021. Offshore fresh groundwater in coastal unconsolidated sediment systems as a potential fresh water source in the 21st century. Environmental Research Letters, *Submitted*

Zamrsky D., Oude Essink G.H.P., Bierkens M.F.P., 2021. Global impact of sea level rise on coastal fresh groundwater resources. *In preparation*

Conference proceedings

Oude Essink G.H.P., Faneca Sànchez M., Zamrsky, D. "Global Quick Scan of the Vulnerability of Groundwater systems to Tsunamis". In EGU General Assembly Conference Abstracts (p. 14480), May, 2014, Vienna, Austria

Zamrsky, D., Oude Essink G.H.P., Bierkens M.F.P. "Global Analysis of Fresh Groundwater Resources in Coastal Zones with Respect to Future Risks" In: 24th Salt Water Intrusion Meeting and the 4th Asia-Pacific Coastal Aquifer Management Meeting, 4 –8 July 2016, Cairns, Australia. Ed. by Adrian D. Werner. Cairns, p. 136-137.

Zamrsky, D., Oude Essink G.H.P., Bierkens M.F.P. "On aquifer thicknesses and geological complexity affecting fresh/salt groundwater distribution". In EGU General Assembly Conference Abstracts (p. 13677), April, 2017, Vienna, Austria

Zamrsky D., Oude Essink G.H.P., Bierkens M.F.P. "Estimating characteristic times of regional groundwater systems along the global coastline with regard to past sea level fluctuations and sediment accumulation patterns" In: 25th Salt Water Intrusion Meeting, 17-22 June 2018, Gdansk, Poland, pp. 360–361.

Bierkens M. F.P., King J. A., van Engelen J., Verkaik J., Zamrsky D., Oude Essink G.H.P. "Estimating regional to global fresh-brackish-salt groundwater occurrence to support future projections". In EGU General Assembly Conference Abstracts (p. 1835), 2020, May, Vienna, Austria